Neural Plasticity

Maladaptive Plasticity and Neuropathic Pain

Guest Editors: Xiang-Yao Li, You Wan, Shao-Jun Tang, Yun Guan, Feng Wei, and Daqing Ma

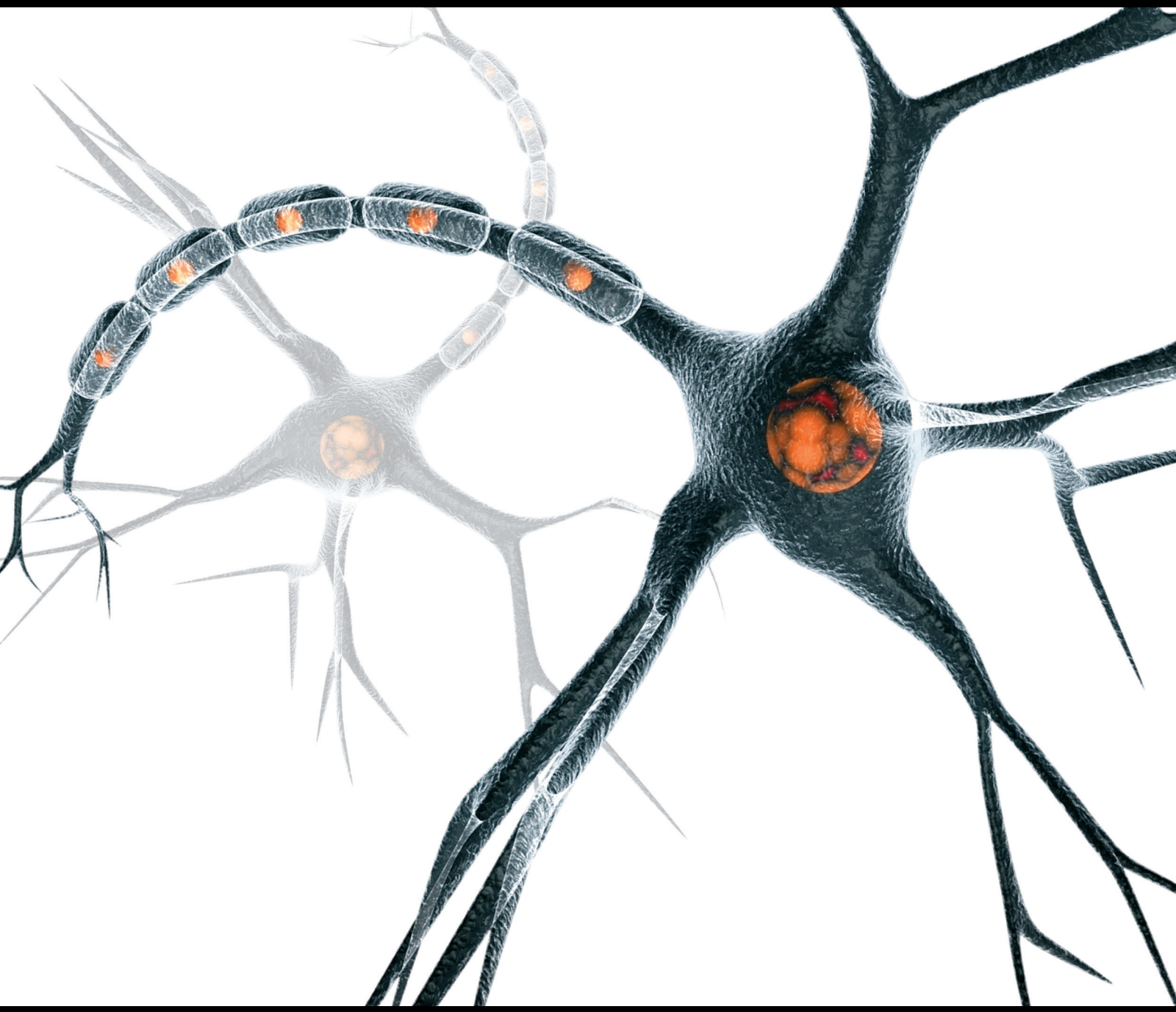

Maladaptive Plasticity and Neuropathic Pain

Neural Plasticity

Maladaptive Plasticity and Neuropathic Pain

Guest Editors: Xiang-Yao Li, You Wan, Shao-Jun Tang, Yun Guan, Feng Wei, and Daqing Ma

Editorial Board

Contents

Hindawi Publishing Corporation
Neural Plasticity
Volume 2016, Article ID 4842159, 2 pages
http://dx.doi.org/10.1155/2016/4842159

Editorial

Maladaptive Plasticity and Neuropathic Pain

Xiang-Yao Li,[1] You Wan,[2] Shao-Jun Tang,[3] Yun Guan,[4] Feng Wei,[5] and Daqing Ma[6]

[1]*Institute of Neuroscience and Collaborative Innovation Center for Brain Science, School of Medicine, Zhejiang University, Hangzhou, Zhejiang 310058, China*
[2]*Department of Neurobiology, School of Basic Medical Sciences, Peking University Health Science Center, Beijing 100191, China*
[3]*Department of Neuroscience and Cell Biology, University of Texas Medical Branch, Galveston, TX 77555, USA*
[4]*Department of Anesthesiology and Critical Care Medicine, School of Medicine, Johns Hopkins University, Baltimore, MD 21205, USA*
[5]*Department of Neural and Pain Sciences, Dental School, Program in Neuroscience, University of Maryland, 650 W. Baltimore Street, Baltimore, MD 21201, USA*
[6]*Anaesthetics, Pain Medicine and Intensive Care, Department of Surgery and Cancer, Faculty of Medicine, Imperial College London, Chelsea & Westminster Hospital, London SW10 9NH, UK*

Correspondence should be addressed to Xiang-Yao Li; leexiangyao@gmail.com

Received 27 October 2015; Accepted 28 October 2015

The neuropathic pain is caused by the injury or damage on the sensory nervous system; its pathological manifestations include allodynia, hyperalgesia, and spontaneous pain. About 4–8% of people in our society are suffering from this disease. The maladaptive plasticity refers to the plasticity in the nervous system that leads to a disruption of the function and may be considered as a disease state [1]. Emerging evidences from both human patients and animal models showed that maladaptive plastic changes happened along the sensory pathways, from the peripheral to central nervous system, which may contribute to the generation, development, and maintenance of neuropathic pain. The current special issue focused on the molecular mechanism underlying maladaptive plasticity along sensory pathways; different laboratories around the world investigated the maladaptive change in different signaling pathways at different levels; the contributions in this area will highlight the pain managements in the future.

The transient receptor potential cation channel subfamily V member 1 (TRPV1) is the first identified member of TRPV proteins. TRPV1 can be activated by high temperature or specific chemical stimuli. The activation of TRPV1 in the terminal of nociceptive primary afferents conveys noxious information to the spinal cord and superspinal regions. Recent studies also identified critical roles of TRPV1 in the central regions of pain pathway in pain regulation. In the current issue, T. Jian et al. report that TRPV1 in dorsal root ganglia (DRG) modulates histamine H4 receptor-mediated itch. This finding will extend our understanding of the mechanisms of histamine-induced itch and the interaction of the itch and pain. S.-I. Choi et al. review recent studies on TRPV1-regulated pain, especially pathological pain, and suggest that TRPV1 contributes to pain maintenance. The new data may have revealed novel insights into the roles of spinal cord TRPV1 in regulating spinal plasticity, which may identify a new target for modulating pathological pain.

Low back pain affects a large number of patients. Deformation of DRGs and their nerve roots is implicated in the pathogenesis. W.-J. Han et al. evaluate the analgesic effects of a novel synthesized nitronyl (NIT) nitroxide radicals on radicular low back pain in a rat model generated by chronic DRG compression. The authors report a significant analgesic effect of this agent, probably due to its antioxidation and anti-inflammation effects. Y-.B. Xie et al. describe a new rat animal model of human low back pain, by chronic compression of multiple DRGs on one side of lumber. This rat model develops spontaneous pain, cold allodynia, and hyperalgesia. Activating transcription factor 3 (ATF3) and CGRP are upregulated in bilateral DRG neurons and may contribute to the expression of DRG compression-induced pain.

Matrix metalloproteinases (MMPs) play important roles in nociception and allodynia. Q. Wang et al. report a critical role of Extracellular Matrix Metalloproteinase Inducer (EMMPRIN)/OX47, a key regulator of MMP activities, in

neuropathic pain development. Their studies show that SNL leads to OX47 upregulation in ipsilateral DRG and that downregulation of OX47 attenuates SNL-induced mechanical allodynia.

Gate-control theory of pain proposed by Melzack and Wall (1965) explains the regulation of noxious information transmission in the spinal substantia gelatinosa. F. J. R. Peláez and S. Taniguchi have revisited this theory from the perspective of NMDA receptor-mediated synaptic plasticity and intrinsic plasticity, and the Melzack and Wall circuit was slightly modified by using strictly excitatory nociceptive afferences and was further tested at different pain conditions.

Spinal microglia play critical roles in the developments of chronic pain. A. Jurga et al. report the contribution of TLR2 and TLR4 to neuropathic pain in a chronic constriction injury (CCI) model. They describe a time-dependent upregulation of TLR2, TLR4, MyD88, and TRIF mRNA and protein. In addition, blockade of TLR2 and TLR4 impairs the expression of pain behaviors and opioid analgesia. These findings support TLR2 and TLR4 as putative targets for developing therapeutic approaches.

J. Wang et al. report the involvements of mammalian target of rapamycin (mTOR) in the RVM, a key relay region for the descending pathway, in regulation of neuropathic pain. They show that phosphorylated mTOR protein increases mainly in RVM serotonergic spinally projecting neurons in the spared nerve injury (SNI) model. Infusion of rapamycin decreases both excitatory synaptic transmission and intrinsic excitability of serotonergic neurons, which may underlie the analgesic effects. These findings suggest a novel mechanism by which mTOR inhibitor causes analgesia.

The anterior cingulate cortex (ACC) is a heterogeneous brain region and is involved in regulation of pain, emotion, and sex attraction. Z.-X. Zuo et al. report that nerve ligation leads to AChE upregulation in the ACC. They have tested the analgesic effects of huperzine A, an alkaloid isolated from a Chinese club-moss, on evoked pain and spontaneous pain, and reported a significant analgesic effect on evoked pain but not spontaneous pain, indicating a specific role of AChE in regulation of evoked pain.

We are pleased to introduce this special issue that focuses on the maladaptive plasticity in the pain pathway, in both PNS and CNS. It is becoming clear that pain-related maladaptive changes can occur at a cellular level such as alteration of synaptic transmission and at a molecular level such as the dysregulation of various signaling pathways. The studies collected in this issue will help elucidate the pathogenic mechanism of neuropathic pain and facilitate the development of novel strategies for the pain treatments.

Acknowledgments

We would like to thank all authors and reviewers for their essential contribution to this special issue.

Xiang-Yao Li
You Wan
Shao-Jun Tang
Yun Guan
Feng Wei
Daqing Ma

References

[1] C. J. Woolf, "Recent advances in the pathophysiology of acute pain," *British Journal of Anaesthesia*, vol. 63, no. 2, pp. 139–146, 1989.

Hindawi Publishing Corporation
Neural Plasticity
Volume 2016, Article ID 5954890, 10 pages
http://dx.doi.org/10.1155/2016/5954890

Review Article

Emerging Role of Spinal Cord TRPV1 in Pain Exacerbation

Seung-In Choi,[1,2] Ji Yeon Lim,[1,2] Sungjae Yoo,[1,2] Hyun Kim,[1,3] and Sun Wook Hwang[1,2]

[1]*Department of Biomedical Sciences, Korea University College of Medicine, Seoul 136-705, Republic of Korea*
[2]*Department of Physiology, Korea University College of Medicine, Seoul 136-705, Republic of Korea*
[3]*Department of Anatomy, Korea University College of Medicine, Seoul 136-705, Republic of Korea*

Correspondence should be addressed to Hyun Kim; bkcloud18@gmail.com and Sun Wook Hwang; sunhwang@korea.ac.kr

Received 23 May 2015; Revised 20 July 2015; Accepted 12 August 2015

Academic Editor: You Wan

TRPV1 is well known as a sensor ion channel that transduces a potentially harmful environment into electrical depolarization of the peripheral terminal of the nociceptive primary afferents. Although TRPV1 is also expressed in central regions of the nervous system, its roles in the area remain unclear. A series of recent reports on the spinal cord synapses have provided evidence that TRPV1 plays an important role in synaptic transmission in the pain pathway. Particularly, in pathologic pain states, TRPV1 in the central terminal of sensory neurons and interneurons is suggested to commonly contribute to pain exacerbation. These observations may lead to insights regarding novel synaptic mechanisms revealing veiled roles of spinal cord TRPV1 and may offer another opportunity to modulate pathological pain by controlling TRPV1. In this review, we introduce historical perspectives of this view and details of the recent promising results. We also focus on extended issues and unsolved problems to fully understand the role of TRPV1 in pathological pain. Together with recent findings, further efforts for fine analysis of TRPV1's plastic roles in pain synapses at different levels in the central nervous system will promote a better understanding of pathologic pain mechanisms and assist in developing novel analgesic strategies.

1. Introduction

Transient receptor potential vanilloid subtype 1 (TRPV1) is a well-known pain-mediating ion channel expressed in sensory neurons including dorsal root ganglionic (DRG) neurons, trigeminal ganglionic (TG) neurons, and vagal neurons. In response to various harmful stimuli, TRPV1 pore opens and cationic flux through the pore into the nerve terminal causes electrical depolarization which may lead to action potential generation. When propagated and transmitted into the brain, the signals finally result in the perception of pain. Because of its extreme polymodality compared to other known peripheral sensor molecules that allows TRPV1 to cover a large spectrum of pain qualities from chemical through thermal ones and of its famous activator capsaicin which has been traditionally utilized for pain research even before TRPV1 discovery, TRPV1 has garnered a great deal of attention as a peripheral pain-modulating target. Topical application of a TRPV1 modulator is currently the mainstream for TRPV1-targeting analgesic strategies while systemic approaches have been dropped due to a potential for hyperthermic adverse effect because body temperature regulation is perturbed by antagonism of vagal TRPV1.

Although the initial report about TRPV1 finding suggested that it is specifically expressed in sensory neurons, its wider distribution in various regions including certain regions of the central nervous system (CNS) and nonnervous tissues has been surmised (for review, [1]). Using rodent and human brains, Mezey et al. verified the existence of TRPV1 protein and mRNA in the spinal cord, amygdala, medial and lateral habenula, hippocampus, striatum, hypothalamus, centromedian and paraventricular thalamic nuclei, substantia nigra, reticular formation, locus coeruleus, cerebellum, inferior olive, and certain cortical areas [2]. Soon after, Valtschanoff et al., focusing on the spinal cord, showed that both presynaptic (from the central terminal of sensory neurons) and postsynaptic regions (from the dendrites of spinal cord dorsal horn neurons) exhibit TRPV1 positivity, especially in the superficial laminae I and II, which are the first relaying stations in the pain sensory pathway [3]. Using

dorsal rhizotomy, they were able to histologically show that postsynaptic TRPV1 expression levels were highly dependent on the presence of peripheral inputs, indicating that spinal cord TRPV1 expression and function may be dynamically controlled by sensory states. Since that time, CNS and spinal cord expression of TRPV1 have been persistently confirmed [4, 5]. These results suggested that TRPV1 may play a role in the central areas and in this review we more focus on pain transmission in the spinal cord.

2. TRPV1 Expression in Neuropathic Pain Models

Altered expression of a protein depending on disease states often implies its importance in disease progression. Upregulation of TRPV1 in DRG or TG neurons under a proinflammatory state has been reported [6–9]. Differential regulation of TRPV1 expression occurs in neuropathic pain states. At the scale of whole DRG neuronal collection, including both damaged and undamaged neurons, the amount of TRPV1 was reduced in many different neuropathy models including those of sciatic nerve axotomy [10], partial nerve ligation [11], chronic constriction injury (CCI) [12], spinal nerve ligation [13], and diabetic neuropathy [14, 15]. The loss of total TRPV1 expression appears to be at least partially due to the degeneration of damaged TRPV1-positive DRG neurons. Interestingly, in the spinal cord dorsal horn, TRPV1 is upregulated in a CCI neuropathic pain model [16]. When looking at uninjured DRG neurons, higher TRPV1 expression was detected even in the neurons at different spinal levels from that for damaged ones [11, 17]. Different from the peripheral neuropathy models mentioned above, in the spinal cord injury models, an increase in TRPV1 proteins or mRNAs was consistently detected in the DRG [18–20]. The molecular and cellular mechanisms for such increased TRPV1 expressions in undamaged neurons in diverse injury models remain undetermined and we dealt with those in "Unsolved Issues" below. Briefly, the uninjured DRG neurons may be affected by inflammatory processes, for example, via increased secretion of inflammatory mediators such as nerve growth factor (NGF) from recruited immune components around adjacent damaged DRG or spinal cord regions. Indirect synaptic mechanisms via collaterals or descending circuits also likely participate in TRPV1 upregulation in DRGs at different spinal levels. The results of elevated TRPV1 levels indicate that peripheral TRPV1 expression can be controlled upon injury conditions and that increased amplification of pain signals may involve upregulation of TRPV1, which might serve as a potential leverage for therapeutic modulation.

3. Insights from Spinal TRPV1 Antagonism

Besides expression results, outcomes from pharmacological manipulation of spinal cord TRPV1 activity have also consistently emphasized its crucial role in pain transmission and therapeutic advantages. In particular, industrial field hypothesized that selective antagonism to spinal TRPV1 could be one option for avoiding adverse malignant hyperthermia since CNS TRPV1 seems to be free from the hyperthermic mechanism [21, 22]. Kanai et al. of Pfizer Japan not only demonstrated increased TRPV1 levels in the spinal cord of CCI rats but also produced a promising analgesic result from intrathecal administrations of the TRPV1 antagonist BCTC [16]. In the hundreds of nanomolar range, mechanical allodynia and calcitonin gene-related peptide-like immunoreactivity and substance P-like immunoreactivity were attenuated in the spinal cord from the CCI-injured rats [16]. Researchers at Abbott Labs used three different inflammatory pain models with complete Freund's adjuvant, capsaicin, and sodium monoiodoacetate injections. Their CNS-penetrable version, A-784168, more effectively blocked pain than a less penetrable A-795614, despite being similar in terms of *in vitro* profiles for TRPV1 antagonism [23]. Watabiki et al. at Astellas Pharma demonstrated that mechanical allodynia in their mouse spinal nerve ligation (SNL) model was alleviated by intrathecal injection of either of BCTC or their own TRPV1 antagonist AS1928370 [24]. A little later, the paradigm was also confirmed in the academic field. Wu et al. demonstrated that TRPV1 antagonism using intrathecal AMG9810 reversed mechanical and thermal hypersensitivities in a contusive spinal cord injury model [20]. Spinal TRPV1 knockdown with antisense oligonucleotide produced similar results. In fact, approaches with agonists have provided a similar insight. Two research groups independently demonstrated that intrathecal agonist (capsaicin or 9-hydroxyoctadecadienoic acid) injections induced mechanical allodynia [25, 26]. Since TRPV1 is not a mechanosensitive ion channel and thus TRPV1 in the periphery has no role in mediating mechanical phenotypes, the mechanical hypersensitivity is purely due to central TRPV1 activity on transmission. An agonist was used for the opposite purpose [27, 28]. Intrathecal injections of resiniferatoxin (RTX), a potent TRPV1 agonist, deactivated voltage-dependent components or ablated TRPV1-positive neuronal terminals [29–31]. Interestingly, in a carrageenan-induced inflammation model, the thermal threshold but not the mechanical threshold was normalized with this strategy [27, 28]. Although the model involved an agonistic challenge, body temperatures of the treated animals were largely unaffected. Collectively, the results from expression dynamics and pain pharmacology commonly raise the importance of the existence of spinal cord TRPV1. In turn, several groups have begun to explore the next question: how, differently from peripheral TRPV1, spinal TRPV1 intervenes pain transmission in pathologic states.

4. Proposed Nociceptive Roles of TRPV1 in the Spinal Cord

Spinal synaptic plasticity is a central concept that accounts for pathologic transition from a normal acute pain to a chronically morbid one [32]. Both long-term potentiation and depression (LTP and LTD) paradigms and technical progress for brain slice electrophysiology from learning and memory research mostly using the hippocampal area were imported to the pain field. Those concept and technology have contributed to the understanding of the pathological

pain transmission in the spinal cord and to finding painkilling targets: ionotropic and metabotropic glutamate receptors, N-type and T-type voltage-gated Ca^{2+} channels, upstream and downstream signaling molecules of the nitric oxide synthesis pathway, calcium/calmodulin-dependent kinases, neuropeptides and their receptors, and so forth [33]. For validating the spinal TRPV1 mechanism, this advantage has begun to be utilized. In this context, three important aspects of the roles of spinal TRPV1 have been reported in recent years [26, 34, 35]. The discussions about the detailed results follow.

4.1. Presynaptic TRPV1: Excitatory. Gone through simple traditional observations where spontaneous excitatory postsynaptic currents (sEPSCs) were facilitated by the presynaptic actions of capsaicin to understand the circuitry under normal conditions [36, 37], researchers became interested in TRPV1's role in pathologic states. Xu et al. found that TRPV1 in the central terminal of DRG neurons plays an important role in exaggerating pain in an inflammatory state during their analyses of the effects of endogenous proresolving lipids [34]. When they recorded the lamina II neurons of transverse slices of the murine lumbar spinal cord with a patch clamp technique, sEPSCs were increased upon tumor necrosis factor-α (TNF-α) exposure. Because the frequency but not the amplitude of EPSCs was increased, TNF-α seemed to elevate glutamate release by acting at presynaptic terminals. This perfusion with TNF-α *ex vivo* may represent an inflammatory or neuropathic pain state *in vivo*. Simultaneous treatment of capsazepine reversed this TNF-α effect: the changes were limited to numbers of sEPSC frequencies. Consequently, the results of this study provide multiple implications: the primary action site of the acute TNF-α effect is presynaptic sensory neurons; TRPV1 had been presumed to be a major effector of TNF-α action, at least in the periphery [38, 39], and the results confirmed it and extended to the central terminals; regarding capsazepine-affected parameters, TRPV1-mediated mechanism may be more important in presynapses. Despite being out of the scope of this review, resolvin E1, a potent endogenous proresolving lipid, appears to disturb the presynaptic signaling between TNF-α and TRPV1 via its G-protein-coupled receptor (GPCR) activation, as a part of its painkilling mechanisms [40–42].

4.2. Presynaptic TRPV1: Receiving Descending Excitatory Input. More recently, the Wei and Dong labs revisited the presynaptic role of TRPV1 from the viewpoint of descending excitatory modulation when they tried to explain secondary hyperalgesia that occurs from neighboring but uninjured receptive field under neuropathic conditions [35]. They developed a knock-in mouse line in which the expression of GCaMP3 encoding a Ca^{2+} indicator protein is driven by the promoter of Pirt (phosphoinositide-interacting regulator of transient receptor potential channels), a pan-DRG/TG marker [43]. With this mouse model, changes in intracellular Ca^{2+} levels in cell bodies and peripheral and central terminals can be discerned in DRG and TG neurons, even under *ex vivo* conditions surrounded by other tissue types or buried in complex synaptic circuits. They also created a cheek mechanical hyperalgesia model using CCI of the infraorbital nerve, which is the major branch of the maxillary (V2) TG nerve. Accordingly, the trigeminal subnucleus caudalis (Vc), which is analogous to the spinal dorsal horn in terms of the sensory synaptic circuit, was observed for presynaptic TRPV1 functions.

Although only V2 TG nerve had undergone the CCI procedure, heightened pain sensitivities occurred in the cheek, jaw, and ear, the latter two of which are mandibular (V3) TG nerve territories. When intracellular Ca^{2+} fluorescence level due to GCaMP3 was analyzed as a surrogate measure for excitability, both V2 and V3 central terminals in Vc exhibited larger Ca^{2+} increases than under normal conditions. Furthermore, these elevated sensitivities were commonly observed in terminals from superficial through deep laminae, suggesting that not only injured but also adjacent undamaged nerve fibers became hyperactive and that this situation consequently led to secondary hyperalgesia and allodynia. Based on their previous observations, Wei and Dong's group hypothesized that the rostral ventromedial medulla (RVM) in the brainstem relays 5-hydroxytryptamine (5-HT, serotonin) dependent excitatory input to uninjured nerves [44, 45]. Indeed, 5-HT immunoreactivity was elevated near the GCaMP3-positive central sensory terminals of Vc. Moreover, antagonistic manipulations including treatment using the 5-HT3 receptor antagonist in Vc or 5-HT depletion in RVM using RNA interference against its biosynthesis alleviated both hyperactivity of TRPV1-mediated Ca^{2+} signals and hypersensitive behaviors. Since 5-HT receptor-mediated TRPV1 facilitation was confirmed in the central presynaptic terminals, the descending excitatory axons from RVM seem to constitute axoaxonal contacts. Collectively, TRPV1 in the presynapse of sensory neurons that covers the undamaged regions participates in secondary pain amplification through a descending facilitation mechanism (Figure 1).

4.3. Postsynaptic TRPV1: Disinhibiting Secondary Projection. Previous positive results of the spinal cord expressions of TRPV1 strongly implicated a functional role of TRPV1 in the spinal postsynaptic neurons [2–4]. The Oh lab focused on the spinal cord inhibitory synapse regarding the role of TRPV1. In fact, loss of GABAergic or glycinergic inhibitory control in the spinal synaptic network has long been proposed as a cause of central pain sensitization [46–48]. Different from sEPSCs, evoked EPSCs have been reported to decrease after capsaicin perfusion [49, 50]. TRPV1 activation acutely induced increases in frequency in spontaneous inhibitory postsynaptic currents (sIPSCs) in the dorsal horn neurons via GABAergic or glycinergic connections [51, 52]. Oh's group hypothesized that TRPV1 plays a role in the pathologic condition. As mentioned, intrathecal injection of capsaicin elicits mechanical allodynia [26]. Notably, in a mouse model with ablation of TRPV1-positive DRG neurons, a significant proportion of mechanical hypersensitivity remained following intrathecal capsaicin administration, indicating that postsynaptic TRPV1 also contributes to the pain state. Indeed, TRPV1 expression and agonist-dependent activation

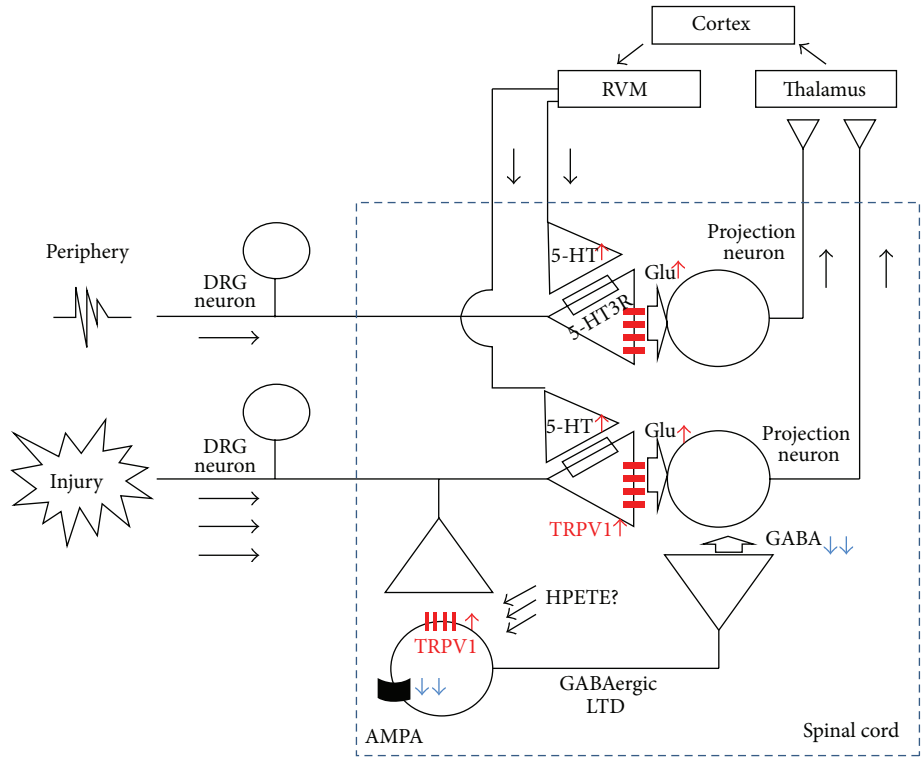

Figure 1: Schematic representation of the role of TRPV1 for pain exacerbation in the spinal cord pre- and postsynapses.

in postsynaptic dorsal horn neurons were verified, and over 75% of GABAergic interneurons were TRPV1-positive whereas ~75% of non-GABAergic postsynaptic neurons were TRPV1-negative. Surprisingly, in their EPSC profiling of the GABAergic neurons in response to electrical stimulation of the dorsal root entry zone, LTD occurred after postsynapse-specific TRPV1 activation. TRPV1 activation-induced LTD was dependent on an increase in the intracellular Ca^{2+} concentration and the reduction of alpha-amino-3-hydroxy-5-methyl-4-isoxazolepropionic acid (AMPA) receptor activities, similar to other typical LTD processes. Accordingly, LTD caused less excitability and reduced GABA release of the GABAergic interneurons, and therefore the secondary projection neurons (spinothalamic tract neurons in this study) received less inhibitory input, resulting in enhanced relay of pain signals to higher brain areas (Figure 1). The analgesic effects of spinal TRPV1 antagonism in mice CCI model were successfully repeated without malignant hyperthermia, but the authors proposed a novel mechanism engaging LTD of TRPV1-positive inhibitory neurons. How this postsynaptic TRPV1 is tonically stimulated under pathologic conditions remains to be elucidated.

5. Unsolved Issues

Because the studies on the contribution of TRPV1 to the transmission of spinal pain circuit are relatively in their early stage, much of biological information is still unavailable. Here, we focus on several important issues as follows.

5.1. Changes in Spinal TRPV1 Expression under Pathologic Conditions. Detailing how dynamically the spinal TRPV1 expression alters depending on the pathologic process may provide more sophisticated explanation of spinal pain mechanisms and help fine-tuning analgesic strategies. As mentioned above, a promising result from TRPV1 expression in the spinal cord has been demonstrated by Kanai et al. [16]. In their CCI rat model, TRPV1 expression of the ipsilateral superficial dorsal horns was gradually elevated for two weeks. This expression location indicates an increase in TRPV1 in the presynaptic terminals by neuropathic insult, supporting the enhanced capsaicin sensitivity of the central terminals in the novel trigeminal CCI neuropathy model [35]. Preceding Kanai et al.'s observation, there were several other similar observations in inflammatory pain model. Tohda et al. detected elevated TRPV1 levels in the dorsal horn presynaptic regions in a carrageenan-inflammation model [53]. In a relatively chronic inflammation model using complete Freund's adjuvant, despite a statistically ambiguous elevation on days from 1 to 2 after injection, over 50% increased TRPV1 levels were maintained for 1 to 3 weeks [6, 8]. After 3 weeks, the expression normalized. The increase may depend on the mediator effect including NGF, which is similar to well-known mechanisms for increases in TRPV1 expression of the peripheral terminals [9]. Therefore, the heightened contribution of presynaptic TRPV1 to pain amplification is predictable. However, information on TRPV1 dynamics of interneurons or projection neurons in the presence or absence of injury is still lacking.

5.2. Internal Signaling Cascades. Although TRPV1 is known as a major heat sensor in the body, its thermosensory functions and related thermoregulatory feedback mechanisms are unlikely to be exerted in the spinal cord because this region only experiences a limited range of temperatures, close to the core body temperature. Evidence mentioned above suggests that pharmacological antagonism for TRPV1 in the spinal cord does not cause thermal effects. However, that situation leads to another question: What conditions else activate TRPV1 there? Inflammatory peptides including TNF-α, which was tested by Xu et al. [34], and neurotransmitters such as 5-HT, which proved to be a descending modulator, may utilize TRPV1 for a downstream effector. For the TNF-α-TRPV1 signaling axis, hypotheses of prostaglandin production for increased TRPV1 activity and extracellular signal-regulated kinase (ERK) activation for elevated TRPV1 expression were raised by studies on DRG neurons [38, 54]. Extracellular prostaglandins are known to enhance TRPV1 sensitivity via phosphorylation by protein kinase A or C through their G-protein-coupled receptor-mediated signaling [55], but it remains elusive whether this paracrine signaling cascade also works for TNF-α axis. Even if this prostaglandin-mediated mechanism is true, the mechanism can only sensitize but not activate TRPV1. By this sensitization, heat threshold for TRPV1 activation might descend around the core body temperature. In addition, while only ERK itself has been shown to participate, there has not been sufficient clarification of the further downstream signal in this pathway. Moreover, it also needs to be explored in the presynapse whether the releases of neurotransmitter vesicles are facilitated simply by increased intracellular Ca^{2+} ions through TRPV1 opening-induced depolarization, or other unknown molecular downstream signals are involved.

5.3. Interactions with Other Ion Channel Components. The 5-HT3 receptor is a major receptor that receives descending excitatory input from RVM [35]. Interestingly, 5-HT3 receptor is a cation channel that may be functionally redundant regarding the TRPV1 outcome to depolarize the presynaptic area. Whether these two cation channels are additive or otherwise functionally or physically coupled for a synergistic action, as shown in recently published observations at the peripheral terminals about TRPV1-TRPA1 and TRPV1-anoctamin cooperation [56, 57], requires further examination.

Transient receptor potential ankyrin subtype 1 (TRPA1) is comparable to TRPV1 in terms of the importance of covering pain modalities and transductory roles to initiate nociceptor depolarization in the periphery [58]. If both TRP channels share central locations of their expressions, their redundancy, cooperativity, or compensation in the roles in synaptic transmission could not be ignorable. Indeed, the presynaptic facilitative role of TRPA1 in the spinal cord has been addressed [59]. The effects of antagonistic challenges against spinal TRPA1 function were examined and the treatment displayed analgesic outcomes in diverse pain models including SNL, rapid eye movement sleep deprivation, capsaicin-paw injection, formalin-paw injection, and diabetic neuropathy [60–62]. It was further demonstrated that the pain-facilitating effect of descending excitatory inputs from RVM stimulation or spinal cord 5-HT3 receptor activation was all blunted by TRPA1 antagonism [62]. Unlike TRPV1, the analgesic mechanism does not seem to employ the postsynaptic GABAergic disinhibition mechanism [62], which seems to be inconsistent when comparing the earlier and the most recent observations that spinal TRPA1 activation facilitates not only the frequency and amplitude of sEPSCs but also those of sIPSCs [59, 63].

5.4. Contribution of Endogenous TRPV1 Activators? As mentioned, Kim et al. [26] proposed that TRPV1 activation induces LTD in GABAergic interneurons. However, they only conducted external capsaicin administration for TRPV1 activation. Although this can form analgesic proof of concept from a therapeutic viewpoint, it is still poorly understood why the GABAergic neurons need to express TRPV1 regarding their ordinary transmission and what naturally stimulates TRPV1 in neuropathic conditions. Regarding the polymodality of TRPV1, the heat does not seem to be the only candidate. Kim et al. suggested that 12(S)-hydroperoxyeicosatetraenoic acid (12(S)-HPETE) may be a natural TRPV1 activator candidate. Gibson et al. [64] demonstrated that anterograde metabotropic glutamate receptor activation results in postsynaptic 12(S)-HPETE production and that this lipoxygenase metabolite retrogradely diffuses and activates presynaptic TRPV1, causing LTD in the hippocampal CA1 synapses. Application of this paradigm to the spinal cord may narrow down the candidate mechanisms to a GPCR-lipoxygenase cascade but measurement of which substances in the spinal cord are a major metabolite is still required, for example, hepoxilins and hydroxyoctadecadienoic acids [25, 42, 65, 66]. TRPA1 also has a wide spectrum for sensing endogenous reactive substances the levels of which are frequently elevated under injury conditions in tissues or within active synapses. Those are reactive oxygen and nitrogen species and lipid peroxidation products that are known to covalently bind and activate TRPA1 [58, 67]. Generation of these pathologic substances in the spinal cord may facilitate TRPA1-mediated transmission. Normalizing imbalanced local production of atypical excitatory substances for TRP channels by developing specific enzyme inhibitors might be another analgesic strategy to utilize the central TRP channel-mediated synaptic mechanism.

6. Extended Questions

Stemming from the recent accomplishments in spinal TRPV1 research, unexplored mechanisms connecting newly uncovered TRPV1's roles and related hypotheses are being raised.

6.1. Antagonism by Local Gene Editing. Like pharmacological approaches, gene editing strategies often promote understanding of a mechanism and also offer therapeutic insight. A series of studies using local RNA interference techniques have given new lines of firm evidence for the roles of TRPV1 in pathologic pain progress and also for its action in the spinal

cord [68–70]. As tools to improve the efficiency of interfering gene delivery and to lessen safety concerns are being developed, expectancy about future utility of gene editing therapies for chronic pain modulation is currently forming [71, 72]. In the last year, Hirai et al. showed that intrathecal administration of adenoassociated virus serotype 9 (AAV9) vector carrying short-hairpin RNA (shRNA) against TRPV1 resulted in long-term suppression of thermal hyperalgesia in a mouse spared nerve injury model [73]. Viral delivery may confer long-term stable generation of shRNA and limited exposure to immune protection mechanisms outside of the CNS region may help time scale of the effect further since shRNAs in themselves have tough permeability to blood brain barrier (BBB). The confinedness by intrathecal injection may also reduce potential adverse effects from nontarget tissues. Interestingly, despite spinal targeting, only thermal hyperalgesia, not mechanical or cold allodynia, was blunted, which typically occurs in DRG-specific TRPV1 impairment. Conversely, the parameters of shRNA abundance and TRPV1 mRNA reduction were significantly better in the spinal cord than in the DRGs. Differential translational compensation or the presence of TRPV1 isotypes free from the target sequence may be conceivable regarding the broad analgesic spectrum of the above circuit research.

6.2. Glial Involvement. Since TRPV1 expression is absent in glial components, it is not likely that the effects of pharmacological modulations of spinal TRPV1 have a direct link to glial contributions. However, in a follow-up study of Kim et al. [35], the Wei lab demonstrated indirect participation of TRPV1 [74]. Although they did not measure TRPV1 activity, Guo et al. repeated presynaptic stimulation by mimicking activation of the descending 5-HT pathway, which subsequently activated microglia and astrocytes. By showing pharmacological and histological evidence, they suggested that fractalkine released from the presynapses stimulates microglia and then interleukin-18 from activated microglia boosts astrocyte function, from which released interleukin-1β finally enhances excitability of the dorsal horn neurons by inducing phosphorylation of an N-methyl-D-aspartate receptor subunit. It is currently unexplored whether the presynaptic TRPV1 activation is linked with this process.

6.3. NO Other Plastic Players? Nitric oxide (NO) is of general importance as a retrograde signal for modifying brain synaptic strength. In pain synapses, postsynaptic NO plays a central role for presynaptic activation of the guanylyl cyclase-cyclic guanosine monophosphate- (cGMP-) protein kinase G pathway [75, 76]. Interestingly, TRPV1 activity seems to be tolerant of PKG action or even downregulated by PKG [77, 78]. Not only direct PKG action, but also effects of known substrates of PKG, for example, inositol trisphosphate receptor and myosin light-chain kinase, appear to be independent of the amplification of TRPV1 activity. Calcium/calmodulin-dependent protein kinase II (CAMKII) plays a crucial role in AMPA receptor facilitation in the postsynapse. It has been reported that phosphorylation of TRPV1 of DRG neurons by CAMKII is important for maintaining its sensitivity to ligands, which can be explored regarding the postsynaptic paradigm [79]. μ-opioid receptor-induced LTP in the spinal cord appears to occur in TRPV1-positive presynapses and it might be a future issue whether changes in TRPV1 activity in the central terminal are practically involved in opioid signaling [80].

6.4. Central Adverse Effects? Two of many reasons why peripheral TRPV1 has received much attention from industry in the decade since its gene discovery seem to be its polymodality integrating painful inputs with diverse qualities and its peripheral location. For the latter, a central advantage of targeting peripheral TRPV1 is that its ligand avoids the adverse effects of the CNS when it is designed to be BBB-impenetrable. However, assuming that the aim is CNS administration and considering the novel nociceptive roles of TRPV1 in the spinal circuit, one may need to conceive similar adverse situation as already observed or predicted for other CNS analgesic candidates because the target is possibly expressed in other central regions and may have differential actions.

As mentioned above, the bulbospinal circuit receives descending input from periaqueductal gray (PAG) and confers descending excitatory inputs as well as inhibitory ones [35, 81]. Earlier, McGaraughty et al. demonstrated that TRPV1 activation of dorsal PAG gave a hyperalgesic phase via the RVM circuit [82]. However, in ventrolateral PAG (VL-PAG), the neighboring region, it has been suggested that when μ-opioid receptor is simultaneously activated TRPV1 activation contributes to facilitation of glutamatergic interneuronal activity, which offers GABAergic inhibition of descending excitatory ON cells in the RVM circuit, leading to a reduction of nociceptive transmission in the spinal cord [83]. Decreased evoked IPSCs, increased miniature IPSCs and EPSCs, and contribution of the cannabinoid receptor have also been proposed by a different intra-PAG recording study [84]. Because this circuit was examined only under acute pain conditions, the analgesic aspect of TRPV1 action in VL-PAG needs to be further addressed for pathologic pain conditions.

Exploring the mechanism of analgesic effects of acetaminophen, researchers have found out that TRPV1 activation in the central nervous system is involved [85, 86]. When acetaminophen is systemically administered, its metabolites are formed in the brain by the action of fatty acid amide hydrolases. Those appear to directly activate brain TRPV1, leading to analgesia in formalin-induced pain and acute thermal or mechanical pain. Antagonism by intracerebroventricular injection of an antagonist and virtual localization of the drug using methylene blue injection argue that supraspinal TRPV1, but not spinal cord TRPV1, may participate in the central analgesic action. Interestingly, some of electrophilic and toxic metabolites produced during the acetaminophen metabolism, different from the metabolites that activate TRPV1, were reported to activate spinal presynaptic TRPA1, resulting in acute antinociception via subsequent inactivation of adjacent presynaptic voltage-gated Na^+ and Ca^{2+} channels [87].

Other adverse situations due to the potential presence of TRPV1 in CNS regions might be possible. For example,

whether inadvertent diffusion of an antagonist in the ventricular regions may enable access to untargeted areas and affect other brain functions including memory or mood needs to be carefully evaluated [64, 88, 89].

6.5. Agonistic Challenge as a Therapeutic Strategy? Whether TRPV1 activation can gain a therapeutic advantage is conceivable. Specific delivery of local anesthetics to TRPV1-positive nociceptor is being considered as a novel analgesic strategy [90, 91]. Some membrane-impermeable hydrophilic derivatives of lidocaine species are able to permeate into neurons through dilated TRPV1 pore when TRPV1 is activated and once inside, they can block voltage-gated Na^+ channels, with or without their permeant blockade of TRPV1 itself. TRPV1-negative neurons should be inert to the blocking effects of these drugs since the drugs can be admitted only through TRPV1, which may allow avoidance of common adverse effects of the local anesthetics including numbness and motor defects via interfering nonpain pathways. Such approaches of specific application may be taken into consideration in the future for modulation of spinal cord TRPV1.

Among TRPV1-targeting pain therapies, only topical capsaicin treatment is currently available in clinics. The rationale is based on the functional incapacitation of the peripheral sensory terminals by agonist-induced TRPV1 desensitization and mitochondrial permeability transition which leads to terminal ablation [79, 92]. The same mechanism might be possible in the spinal region: analgesia via defunctionalization of TRPV1-specific pre- and postsynapses by agonist-induced effects. However, as mentioned, intrathecal administration of TRPV1 agonists resulted in some pain phenotypes in animal studies [25, 26]. This appears to be predictable because it is an unavoidable side effect that topical capsaicin application in its early treatment stage evokes pain via initial TRPV1 activation in humans. One possible option to overcome this hurdle is currently thought to be a substitution by a nonpungent capsaicin analogue free from the initial pain induction [93]. Although such a class of TRPV1 agonists were recently developed, they have not been thoroughly tested regarding their analgesic effects.

7. Conclusion

In the early stage, more attention was given to the sensory involvement of TRPV1 in the peripheral terminal of the nociceptor neurons to harmful environments and to its contribution to neurogenic inflammation [94, 95]. However, revisiting traditional capsaicin pharmacology, assessments regarding TRPV1 expression patterns and their dynamics in diverse neural regions have provided clues of other nociceptive roles for TRPV1. Particularly, recent accumulation of knowledge on TRPV1 functions in the spinal presynaptic and postsynaptic locations connecting to exacerbation mechanisms for neuropathic pain has begun to address its roles in the central nervous system. This heightened understanding and new hypotheses also appear to raise the possibility of developing new proof of concept targeting spinal TRPV1. Such attempts for new approaches could be extended to other CNS locations and other polymodal TRP channels such as TRPA1. Further analyses regarding the role of TRPV1 in plastic changes for pain synapses at the individual level including supraspinal circuits will shed light on the collective contribution to exacerbation of pathologic pain and its analgesic utility.

Conflict of Interests

The authors declare no conflict of interests.

Authors' Contribution

Seung-In Choi and Ji Yeon Lim contributed equally to this work.

Acknowledgment

This work was supported by grants from the National Research Foundation of Korea (2013R1A1A2073123).

References

[1] E. S. Fernandes, M. A. Fernandes, and J. E. Keeble, "The functions of TRPA1 and TRPV1: moving away from sensory nerves," *British Journal of Pharmacology*, vol. 166, no. 2, pp. 510–521, 2012.

[2] É. Mezey, Z. E. Tóth, D. N. Cortright et al., "Distribution of mRNA for vanilloid receptor subtype 1 (VR1), and VR1- like immunoreactivity, in the central nervous system of the rat and human," *Proceedings of the National Academy of Sciences of the United States of America*, vol. 97, no. 7, pp. 3655–3660, 2000.

[3] J. G. Valtschanoff, A. Rustioni, A. Guo, and S. J. Hwang, "Vanilloid receptor VR1 is both presynaptic and postsynaptic in the superficial laminae of the rat dorsal horn," *Journal of Comparative Neurology*, vol. 436, no. 2, pp. 225–235, 2001.

[4] J. C. Roberts, J. B. Davis, and C. D. Benham, "[3H]Resiniferatoxin autoradiography in the CNS of wild-type and TRPV1 null mice defines TRPV1 (VR-1) protein distribution," *Brain Research*, vol. 995, no. 2, pp. 176–183, 2004.

[5] L. Cristino, L. de Petrocellis, G. Pryce, D. Baker, V. Guglielmotti, and V. Di Marzo, "Immunohistochemical localization of cannabinoid type 1 and vanilloid transient receptor potential vanilloid type 1 receptors in the mouse brain," *Neuroscience*, vol. 139, no. 4, pp. 1405–1415, 2006.

[6] R.-R. Ji, T. A. Samad, S.-X. Jin, R. Schmoll, and C. J. Woolf, "p38 MAPK activation by NGF in primary sensory neurons after inflammation increases TRPV1 levels and maintains heat hyperalgesia," *Neuron*, vol. 36, no. 1, pp. 57–68, 2002.

[7] N. M. Breese, A. C. George, L. E. Pauers, and C. L. Stucky, "Peripheral inflammation selectively increases TRPV1 function in IB4-positive sensory neurons from adult mouse," *Pain*, vol. 115, no. 1-2, pp. 37–49, 2005.

[8] H. Luo, J. Cheng, J.-S. Man, and Y. Wan, "Change of vanilloid receptor 1 expression in dorsal root ganglion and spinal dorsal horn during inflammatory nociception induced by complete Freund's adjuvant in rats," *NeuroReport*, vol. 15, no. 4, pp. 655–658, 2004.

[9] A. T. Stein, C. A. Ufret-Vincenty, L. Hua, L. F. Santana, and S. E. Gordon, "Phosphoinositide 3-kinase binds to TRPV1 and mediates NGF-stimulated TRPV1 trafficking to the plasma

membrane," *Journal of General Physiology*, vol. 128, no. 5, pp. 509–522, 2006.

[10] G. J. Michael and J. V. Priestley, "Differential expression of the mRNA for the vanilloid receptor subtype 1 in cells of the adult rat dorsal root and nodose ganglia and its downregulation by axotomy," *Journal of Neuroscience*, vol. 19, no. 5, pp. 1844–1854, 1999.

[11] L. J. Hudson, S. Bevan, G. Wotherspoon, C. Gentry, A. Fox, and J. Winter, "VR1 protein expression increases in undamaged DRG neurons after partial nerve injury," *European Journal of Neuroscience*, vol. 13, no. 11, pp. 2105–2114, 2001.

[12] M. Schäfers, L. S. Sorkin, C. Geis, and V. I. Shubayev, "Spinal nerve ligation induces transient upregulation of tumor necrosis factor receptors 1 and 2 in injured and adjacent uninjured dorsal root ganglia in the rat," *Neuroscience Letters*, vol. 347, no. 3, pp. 179–182, 2003.

[13] M. Schäfers, C. Geis, C. I. Svensson, Z. D. Luo, and C. Sommer, "Selective increase of tumour necrosis factor-alpha in injured and spared myelinated primary afferents after chronic constrictive injury of rat sciatic nerve," *European Journal of Neuroscience*, vol. 17, no. 4, pp. 791–804, 2003.

[14] G. Lauria, M. Morbin, R. Lombardi et al., "Expression of capsaicin receptor immunoreactivity in human peripheral nervous system and in painful neuropathies," *Journal of the Peripheral Nervous System*, vol. 11, no. 3, pp. 262–271, 2006.

[15] P. Facer, M. A. Casula, G. D. Smith et al., "Differential expression of the capsaicin receptor TRPV1 and related novel receptors TRPV3, TRPV4 and TRPM8 in normal human tissues and changes in traumatic and diabetic neuropathy," *BMC Neurology*, vol. 7, article 11, 2007.

[16] Y. Kanai, E. Nakazato, A. Fujiuchi, T. Hara, and A. Imai, "Involvement of an increased spinal TRPV1 sensitization through its up-regulation in mechanical allodynia of CCI rats," *Neuropharmacology*, vol. 49, no. 7, pp. 977–984, 2005.

[17] T. Fukuoka, A. Tokunaga, T. Tachibana, Y. Dai, H. Yamanaka, and K. Noguchi, "VR1, but not P2X3, increases in the spared L4 DRG in rats with L5 spinal nerve ligation," *Pain*, vol. 99, no. 1-2, pp. 111–120, 2002.

[18] Y. Zhou, Y. Wang, M. Abdelhady, M. S. Mourad, and M. M. Hassouna, "Change of vanilloid receptor 1 following neuromodulation in rats with spinal cord injury," *Journal of Surgical Research*, vol. 107, no. 1, pp. 140–144, 2002.

[19] L. M. Ramer, A. P. van Stolk, J. A. Inskip, M. S. Ramer, and A. Krassioukov, "Plasticity of TRPV1-expressing sensory neurons mediating autonomic dysreflexia following spinal cord injury," *Frontiers in Physiology*, vol. 3, article 257, 2012.

[20] Z. Wu, Q. Yang, R. J. Crook, R. G. O'Neil, and E. T. Walters, "TRPV1 channels make major contributions to behavioral hypersensitivity and spontaneous activity in nociceptors after spinal cord injury," *Pain*, vol. 154, no. 10, pp. 2130–2141, 2013.

[21] N. R. Gavva, A. W. Bannon, S. Surapaneni et al., "The vanilloid receptor TRPV1 is tonically activated in vivo and involved in body temperature regulation," *The Journal of Neuroscience*, vol. 27, no. 13, pp. 3366–3374, 2007.

[22] S. McGaraughty, J. A. Segreti, R. M. Fryer, B. S. Brown, C. R. Faltynek, and P. R. Kym, "Antagonism of TRPV1 receptors indirectly modulates activity of thermoregulatory neurons in the medial preoptic area of rats," *Brain Research*, vol. 1268, pp. 58–67, 2009.

[23] M. Cui, P. Honore, C. Zhong et al., "TRPV1 receptors in the CNS play a key role in broad-spectrum analgesia of TRPV1 antagonists," *Journal of Neuroscience*, vol. 26, no. 37, pp. 9385–9393, 2006.

[24] T. Watabiki, T. Kiso, M. Tsukamoto, T. Aoki, and N. Matsuoka, "Intrathecal administration of AS1928370, a transient receptor potential vanilloid 1 antagonist, attenuates mechanical allodynia in a mouse model of neuropathic pain," *Biological and Pharmaceutical Bulletin*, vol. 34, no. 7, pp. 1105–1108, 2011.

[25] A. M. Patwardhan, P. E. Scotland, A. N. Akopian, and K. M. Hargreaves, "Activation of TRPV1 in the spinal cord by oxidized linoleic acid metabolites contributes to inflammatory hyperalgesia," *Proceedings of the National Academy of Sciences of the United States of America*, vol. 106, no. 44, pp. 18820–18824, 2009.

[26] Y. H. Kim, S. K. Back, A. J. Davies et al., "TRPV1 in GABAergic interneurons mediates neuropathic mechanical allodynia and disinhibition of the nociceptive circuitry in the spinal cord," *Neuron*, vol. 74, no. 4, pp. 640–647, 2012.

[27] J. A. Jeffry, S.-Q. Yu, P. Sikand, A. Parihar, M. S. Evans, and L. S. Premkumar, "Selective targeting of TRPV1 expressing sensory nerve terminals in the spinal cord for long lasting analgesia," *PLoS ONE*, vol. 4, no. 9, Article ID e7021, 2009.

[28] M. Bishnoi, C. A. Bosgraaf, and L. S. Premkumar, "Preservation of acute pain and efferent functions following intrathecal resiniferatoxin-induced analgesia in rats," *The Journal of Pain*, vol. 12, no. 9, pp. 991–1003, 2011.

[29] T. L. Yaksh, D. H. Farb, S. E. Leeman, and T. M. Jessell, "Intrathecal capsaicin depletes substance P in the rat spinal cord and produces prolonged thermal analgesia," *Science*, vol. 206, no. 4417, pp. 481–483, 1979.

[30] J. I. Nagy, P. C. Emson, and L. L. Iversen, "A re-evaluation of the neurochemical and antinociceptive effects of intrathecal capsaicin in the rat," *Brain Research*, vol. 211, no. 2, pp. 497–502, 1981.

[31] K. Kusudo, H. Ikeda, and K. Murase, "Depression of presynaptic excitation by the activation of vanilloid receptor 1 in the rat spinal dorsal horn revealed by optical imaging," *Molecular Pain*, vol. 2, article 8, 2006.

[32] C. Luo, T. Kuner, and R. Kuner, "Synaptic plasticity in pathological pain," *Trends in Neurosciences*, vol. 37, no. 6, pp. 343–355, 2014.

[33] R.-R. Ji, T. Kohno, K. A. Moore, and C. J. Woolf, "Central sensitization and LTP: do pain and memory share similar mechanisms?" *Trends in Neurosciences*, vol. 26, no. 12, pp. 696–705, 2003.

[34] Z.-Z. Xu, L. Zhang, T. Liu et al., "Resolvins RvE1 and RvD1 attenuate inflammatory pain via central and peripheral actions," *Nature Medicine*, vol. 16, no. 5, pp. 592–597, 2010.

[35] Y. S. Kim, Y. Chu, L. Han et al., "Central terminal sensitization of TRPV1 by descending serotonergic facilitation modulates chronic pain," *Neuron*, vol. 81, no. 4, pp. 873–887, 2014.

[36] K. Yang, E. Kumamoto, H. Furue, and M. Yoshimura, "Capsaicin facilitates excitatory but not inhibitory synaptic transmission in substantia gelatinosa of the rat spinal cord," *Neuroscience Letters*, vol. 255, no. 3, pp. 135–138, 1998.

[37] T. Nakatsuka, H. Furue, M. Yoshimura, and J. G. Gu, "Activation of central terminal vanilloid receptor-1 receptors and alpha beta-methylene-ATP-sensitive P2X receptors reveals a converged synaptic activity onto the deep dorsal horn neurons of the spinal cord," *The Journal of Neuroscience*, vol. 22, no. 4, pp. 1228–1237, 2002.

[38] G. D. Nicol, J. C. Lopshire, and C. M. Pafford, "Tumor necrosis factor enhances the capsaicin sensitivity of rat sensory neurons," *Journal of Neuroscience*, vol. 17, no. 3, pp. 975–982, 1997.

[39] X. Jin and R. W. Gereau IV, "Acute p38-mediated modulation of tetrodotoxin-resistant sodium channels in mouse sensory neurons by tumor necrosis factor-α," *Journal of Neuroscience*, vol. 26, no. 1, pp. 246–255, 2006.

[40] R.-R. Ji, Z.-Z. Xu, G. Strichartz, and C. N. Serhan, "Emerging roles of resolvins in the resolution of inflammation and pain," *Trends in Neurosciences*, vol. 34, no. 11, pp. 599–609, 2011.

[41] S. Yoo, J. Y. Lim, and S. W. Hwang, "Resolvins: endogenously-generated potent painkilling substances and their therapeutic perspectives," *Current Neuropharmacology*, vol. 11, no. 6, pp. 664–676, 2013.

[42] S. Yoo, J. Y. Lim, and S. W. Hwang, "Sensory TRP channel interactions with endogenous lipids and their biological outcomes," *Molecules*, vol. 19, no. 4, pp. 4708–4744, 2014.

[43] K. N. Patel, Q. Liu, S. Meeker, B. J. Undem, and X. Dong, "Pirt, a TRPV1 modulator, is required for histamine-dependent and -independent itch," *PLoS ONE*, vol. 6, no. 5, Article ID e20559, 2011.

[44] F. Wei, W. Guo, S. Zou, K. Ren, and R. Dubner, "Supraspinal glial-neuronal interactions contribute to descending pain facilitation," *Journal of Neuroscience*, vol. 28, no. 42, pp. 10482–10495, 2008.

[45] M. Okubo, A. Castro, W. Guo et al., "Transition to persistent orofacial pain after nerve injury involves supraspinal serotonin mechanisms," *The Journal of Neuroscience*, vol. 33, no. 12, pp. 5152–5161, 2013.

[46] T. L. Yaksh, "Behavioral and autonomic correlates of the tactile evoked allodynia produced by spinal glycine inhibition: effects of modulatory receptor systems and excitatory amino acid antagonists," *Pain*, vol. 37, no. 1, pp. 111–123, 1989.

[47] L. Sivilotti and C. J. Woolf, "The contribution of GABAA and glycine receptors to central sensitization: disinhibition and touch-evoked allodynia in the spinal cord," *Journal of Neurophysiology*, vol. 72, no. 1, pp. 169–179, 1994.

[48] K. A. Moore, T. Kohno, L. A. Karchewski, J. Scholz, H. Baba, and C. J. Woolf, "Partial peripheral nerve injury promotes a selective loss of GABAergic inhibition in the superficial dorsal horn of the spinal cord," *The Journal of Neuroscience*, vol. 22, no. 15, pp. 6724–6731, 2002.

[49] K. Yang, E. Kumamoto, H. Furue, Y.-Q. Li, and M. Yoshimura, "Action of capsaicin on dorsal root-evoked synaptic transmission to substantia gelatinosa neurons in adult rat spinal cord slices," *Brain Research*, vol. 830, no. 2, pp. 268–273, 1999.

[50] M. L. Baccei, R. Bardoni, and M. Fitzgerald, "Development of nociceptive synaptic inputs to the neonatal rat dorsal horn: glutamate release by capsaicin and menthol," *The Journal of Physiology*, vol. 549, no. 1, pp. 231–242, 2003.

[51] F. Ferrini, C. Salio, A. M. Vergnano, and A. Merighi, "Vanilloid receptor-1 (TRPV1)-dependent activation of inhibitory neurotransmission in spinal substantia gelatinosa neurons of mouse," *Pain*, vol. 129, no. 1-2, pp. 195–209, 2007.

[52] F. Ferrini, C. Salio, L. Lossi, G. Gambino, and A. Merighi, "Modulation of inhibitory neurotransmission by the vanilloid receptor type 1 (TRPV1) in organotypically cultured mouse substantia gelatinosa neurons," *Pain*, vol. 150, no. 1, pp. 128–140, 2010.

[53] C. Tohda, M. Sasaki, T. Konemur, T. Sasamura, M. Itoh, and Y. Kuraishi, "Axonal transport of VR1 capsaicin receptor mRNA in primary afferents and its participation in inflammation-induced increase in capsaicin sensitivity," *Journal of Neurochemistry*, vol. 76, no. 6, pp. 1628–1635, 2001.

[54] S. Hensellek, P. Brell, H.-G. Schaible, R. Bräuer, and G. Segond von Banchet, "The cytokine TNFα increases the proportion of DRG neurones expressing the TRPV1 receptor via the TNFR1 receptor and ERK activation," *Molecular and Cellular Neuroscience*, vol. 36, no. 3, pp. 381–391, 2007.

[55] T. Moriyama, T. Higashi, K. Togashi et al., "Sensitization of TRPV1 by EP_1 and IP reveals peripheral nociceptive mechanism of prostaglandins," *Molecular Pain*, vol. 1, article 3, 2005.

[56] H.-J. Weng, K. Patel, N. Jeske et al., "Tmem100 is a regulator of TRPA1-TRPV1 complex and contributes to persistent pain," *Neuron*, vol. 85, no. 4, pp. 833–846, 2015.

[57] Y. Takayama, D. Uta, H. Furue, and M. Tominaga, "Pain-enhancing mechanism through interaction between TRPV1 and anoctamin 1 in sensory neurons," *Proceedings of the National Academy of Sciences*, vol. 112, no. 16, pp. 5213–5218, 2015.

[58] S. Kim and S. W. Hwang, "Emerging roles of TRPA1 in sensation of oxidative stress and its implications in defense and danger," *Archives of Pharmacal Research*, vol. 36, no. 7, pp. 783–791, 2013.

[59] M. Kosugi, T. Nakatsuka, T. Fujita, Y. Kuroda, and E. Kumamoto, "Activation of TRPA1 channel facilitates excitatory synaptic transmission in substantia gelatinosa neurons of the adult rat spinal cord," *Journal of Neuroscience*, vol. 27, no. 16, pp. 4443–4451, 2007.

[60] H. Wei, H. Chapman, M. Saarnilehto, K. Kuokkanen, A. Koivisto, and A. Pertovaara, "Roles of cutaneous versus spinal TRPA1 channels in mechanical hypersensitivity in the diabetic or mustard oil-treated non-diabetic rat," *Neuropharmacology*, vol. 58, no. 3, pp. 578–584, 2010.

[61] A. Pertovaara and A. Koivisto, "TRPA1 ion channel in the spinal dorsal horn as a therapeutic target in central pain hypersensitivity and cutaneous neurogenic inflammation," *European Journal of Pharmacology*, vol. 666, no. 1–3, pp. 1–4, 2011.

[62] H. Wei, A. Koivisto, M. Saarnilehto et al., "Spinal transient receptor potential ankyrin 1 channel contributes to central pain hypersensitivity in various pathophysiological conditions in the rat," *Pain*, vol. 152, no. 3, pp. 582–591, 2011.

[63] M. Yamanaka, W. Taniguchi, N. Nishio et al., "In vivo patch-clamp analysis of the antinociceptive actions of TRPA1 activation in the spinal dorsal horn," *Molecular Pain*, vol. 11, no. 1, p. 20, 2015.

[64] H. E. Gibson, J. G. Edwards, R. S. Page, M. J. Van Hook, and J. A. Kauer, "TRPV1 channels mediate long-term depression at synapses on hippocampal interneurons," *Neuron*, vol. 57, no. 5, pp. 746–759, 2008.

[65] A. M. Gregus, S. Doolen, D. S. Dumlao et al., "Spinal 12-lipoxygenase-derived hepoxilin A3 contributes to inflammatory hyperalgesia via activation of TRPV1 and TRPA1 receptors," *Proceedings of the National Academy of Sciences of the United States of America*, vol. 109, no. 17, pp. 6721–6726, 2012.

[66] S. W. Hwang, H. Cho, J. Kwak et al., "Direct activation of capsaicin receptors by products of lipoxygenases: endogenous capsaicin-like substances," *Proceedings of the National Academy of Sciences of the United States of America*, vol. 97, no. 11, pp. 6155–6160, 2000.

[67] S.-I. Choi, S. Yoo, J. Y. Lim, and S. W. Hwang, "Are sensory TRP channels biological alarms for lipid peroxidation?" *International Journal of Molecular Sciences*, vol. 15, no. 9, pp. 16430–16457, 2014.

[68] T. Christoph, A. Grünweller, J. Mika et al., "Silencing of vanilloid receptor TRPV1 by RNAi reduces neuropathic and visceral pain in vivo," *Biochemical and Biophysical Research Communications*, vol. 350, no. 1, pp. 238–243, 2006.

[69] T. Christoph, G. Bahrenberg, J. De Vry et al., "Investigation of TRPV1 loss-of-function phenotypes in transgenic shRNA expressing and knockout mice," *Molecular and Cellular Neuroscience*, vol. 37, no. 3, pp. 579–589, 2008.

[70] S. Kasama, M. Kawakubo, T. Suzuki, T. Nishizawa, A. Ishida, and J. Nakayama, "RNA interference-mediated knock-down of transient receptor potential vanilloid 1 prevents forepaw inflammatory hyperalgesia in rat," *European Journal of Neuroscience*, vol. 25, no. 10, pp. 2956–2963, 2007.

[71] P. H. Tan, L. C. Yang, and R. R. Ji, "Therapeutic potential of RNA interference in pain medicine," *The Open Pain Journal*, vol. 2, no. 1, pp. 57–63, 2009.

[72] T. Hirai, M. Enomoto, A. Machida et al., "Intrathecal shRNA-AAV9 inhibits target protein expression in the spinal cord and dorsal root ganglia of adult mice," *Human Gene Therapy Methods*, vol. 23, no. 2, pp. 119–127, 2012.

[73] T. Hirai, M. Enomoto, H. Kaburagi et al., "Intrathecal AAV serotype 9-mediated delivery of shRNA against TRPV1 attenuates thermal hyperalgesia in a mouse model of peripheral nerve injury," *Molecular Therapy*, vol. 22, no. 2, pp. 409–419, 2014.

[74] W. Guo, K. Miyoshi, R. Dubner et al., "Spinal 5-HT_3 receptors mediate descending facilitation and contribute to behavioral hypersensitivity via a reciprocal neuron-glial signaling cascade," *Molecular Pain*, vol. 10, article 35, 2014.

[75] R. Kuner, "Spinal excitatory mechanisms of pathological pain," *Pain*, vol. 156, supplement 1, pp. S11–S17, 2015.

[76] C. Luo, V. Gangadharan, K. K. Bali et al., "Presynaptically localized cyclic GMP-dependent protein kinase 1 is a key determinant of spinal synaptic potentiation and pain hypersensitivity," *PLoS Biology*, vol. 10, no. 3, Article ID e1001283, 2012.

[77] L. Loo, A. J. Shepherd, A. D. Mickle et al., "The C-type natriuretic peptide induces thermal hyperalgesia through a noncanonical G$\beta\gamma$-dependent modulation of TRPV1 channel," *Journal of Neuroscience*, vol. 32, no. 35, pp. 11942–11955, 2012.

[78] Y. Jin, J. Kim, and J. Kwak, "Activation of the cGMP/protein kinase G pathway by nitric oxide can decrease TRPV1 activity in cultured rat dorsal root ganglion neurons," *Korean Journal of Physiology and Pharmacology*, vol. 16, no. 3, pp. 211–217, 2012.

[79] J. Jung, J. S. Shin, S. Y. Lee et al., "Phosphorylation of vanilloid receptor 1 by Ca^{2+}/calmodulin-dependent kinase II regulates its vanilloid binding," *The Journal of Biological Chemistry*, vol. 279, no. 8, pp. 7048–7054, 2004.

[80] H.-Y. Zhou, S.-R. Chen, H. Chen, and H.-L. Pan, "Opioid-induced long-term potentiation in the spinal cord is a presynaptic event," *Journal of Neuroscience*, vol. 30, no. 12, pp. 4460–4466, 2010.

[81] L. M. Mendell, "Computational functions of neurons and circuits signaling injury: relationship to pain behavior," *Proceedings of the National Academy of Sciences of the United States of America*, vol. 108, supplement 3, pp. 15596–15601, 2011.

[82] S. McGaraughty, K. L. Chu, R. S. Bitner et al., "Capsaicin infused into the PAG affects rat tail flick responses to noxious heat and alters neuronal firing in the RVM," *Journal of Neurophysiology*, vol. 90, no. 4, pp. 2702–2710, 2003.

[83] S. Maione, K. Starowicz, L. Cristino et al., "Functional interaction between TRPV1 and mu-opioid receptors in the descending antinociceptive pathway activates glutamate transmission and induces analgesia," *Journal of Neurophysiology*, vol. 101, no. 5, pp. 2411–2422, 2009.

[84] H.-T. Liao, H.-J. Lee, Y.-C. Ho, and L.-C. Chiou, "Capsaicin in the periaqueductal gray induces analgesia via metabotropic glutamate receptor-mediated endocannabinoid retrograde disinhibition," *British Journal of Pharmacology*, vol. 163, no. 2, pp. 330–345, 2011.

[85] C. Mallet, D. A. Barrière, A. Ermund et al., "TRPV1 in brain is involved in acetaminophen-induced antinociception," *PLoS ONE*, vol. 5, no. 9, Article ID e12748, pp. 1–11, 2010.

[86] D. A. Barrière, C. Mallet, A. Blomgren et al., "Fatty acid amide hydrolase-dependent generation of antinociceptive drug metabolites acting on TRPV1 in the brain," *PLoS ONE*, vol. 8, no. 8, Article ID e70690, 2013.

[87] D. A. Andersson, C. Gentry, L. Alenmyr et al., "TRPA1 mediates spinal antinociception induced by acetaminophen and the cannabinoid delta(9)-tetrahydrocannabiorcol," *Nature Communications*, vol. 2, no. 1, article no. 551, 2011.

[88] I. J. You, Y. H. Jung, M. J. Kim et al., "Alterations in the emotional and memory behavioral phenotypes of transient receptor potential vanilloid type 1-deficient mice are mediated by changes in expression of 5-HT_{1A}, $GABAA_A$, and NMDA receptors," *Neuropharmacology*, vol. 62, no. 2, pp. 1034–1043, 2012.

[89] T. E. Brown, A. M. Chirila, B. R. Schrank, and J. A. Kauer, "Loss of interneuron LTD and attenuated pyramidal cell LTP in Trpv1 and Trpv3 KO mice," *Hippocampus*, vol. 23, no. 8, pp. 662–671, 2013.

[90] A. M. Binshtok, B. P. Bean, and C. J. Woolf, "Inhibition of nociceptors by TRPV1-mediated entry of impermeant sodium channel blockers," *Nature*, vol. 449, no. 7162, pp. 607–610, 2007.

[91] M. Puopolo, A. M. Binshtok, G.-L. Yao, S. B. Oh, C. J. Woolf, and B. P. Bean, "Permeation and block of TRPV1 channels by the cationic lidocaine derivative QX-314," *Journal of Neurophysiology*, vol. 109, no. 7, pp. 1704–1712, 2013.

[92] C. Y. Shin, J. Shin, B.-M. Kim et al., "Essential role of mitochondrial permeability transition in vanilloid receptor 1-dependent cell death of sensory neurons," *Molecular and Cellular Neuroscience*, vol. 24, no. 1, pp. 57–68, 2003.

[93] T. Iida, T. Moriyama, K. Kobata et al., "TRPV1 activation and induction of nociceptive response by a non-pungent capsaicin-like compound, capsiate," *Neuropharmacology*, vol. 44, no. 7, pp. 958–967, 2003.

[94] S. W. Hwang and U. Oh, "Current concepts of nociception: nociceptive molecular sensors in sensory neurons," *Current Opinion in Anaesthesiology*, vol. 20, no. 5, pp. 427–434, 2007.

[95] M. J. Caterina, A. Leffler, A. B. Malmberg et al., "Impaired nociception and pain sensation in mice lacking the capsaicin receptor," *Science*, vol. 288, no. 5464, pp. 306–313, 2000.

Hindawi Publishing Corporation
Neural Plasticity
Volume 2016, Article ID 5238730, 12 pages
http://dx.doi.org/10.1155/2016/5238730

Research Article

Blockade of Toll-Like Receptors (TLR2, TLR4) Attenuates Pain and Potentiates Buprenorphine Analgesia in a Rat Neuropathic Pain Model

Agnieszka M. Jurga, Ewelina Rojewska, Anna Piotrowska, Wioletta Makuch, Dominika Pilat, Barbara Przewlocka, and Joanna Mika

Department of Pain Pharmacology, Institute of Pharmacology, Polish Academy of Sciences, 31-343 Krakow, Poland

Correspondence should be addressed to Joanna Mika; joasia272@onet.eu

Received 7 May 2015; Revised 7 September 2015; Accepted 20 September 2015

Academic Editor: Shao-Jun Tang

Accumulating evidence indicates that microglial TLR2 and TLR4 play a significant role in nociception. Experiments were conducted to evaluate the contribution of TLR2 and TLR4 and their adaptor molecules to neuropathy and their ability to amplify opioid effectiveness. Behavioral tests (von Frey's and cold plate) and biochemical (Western blot and qRT-PCR) analysis of spinal cord and DRG tissue were conducted after chronic constriction injury (CCI) to the sciatic nerve. Repeated intrathecal administration of *LPS-RS* (TLR2 and TLR4 antagonist) and *LPS-RS Ultrapure* (TLR4 antagonist) attenuated allodynia and hyperalgesia. Biochemical analysis revealed time-dependent upregulation of mRNA and/or protein levels of TLR2 and TLR4 and MyD88 and TRIF adaptor molecules, which was paralleled by an increase in IBA-1/CD40-positive cells under neuropathy. *LPS-RS* and *LPS-RS Ultrapure* similarly influenced opioid analgesia by enhancing the effectiveness of buprenorphine but not morphine. Summing up, in light of their upregulation over the course of pain, both TLR2 and TLR4 may indeed play a significant role in neuropathy, which could be linked to the observed activation of IBA-1/CD40-positive cells. Blockade of TLR2 and TLR4 produced analgesia and enhanced buprenorphine's effectiveness, which suggests that they may be a putative target for future pharmacological pain relief tools, especially for opioid rotation, when the effect of morphine is tolerated.

1. Introduction

Neuropathic pain may appear as a consequence of mechanical nerve injury, the progression of cancer, multiple sclerosis, stroke, and so forth [1, 2]. The currently used analgesics, especially opioid drugs, are not fully effective in reducing chronic pain symptoms [1, 2]; however, the broad range of receptors and signal transduction pathways that could be involved in this process provides a wealth of research opportunities. The current evidence shows that spinal microglia are critically involved in the development and maintenance of neuropathic pain, with a pivotal role of two members of the Toll-like receptor (TLR) family, TLR2 and TLR4 [3, 4]. In the central nervous system, TLR2 and TLR4 are expressed predominantly on glial cells, and for neuropathy, the most relevant expression is on microglia [3, 5].

Direct stimulation of TLRs with exogenous ligands, for example, TLR4 by lipopolysaccharide (LPS), can provoke pain [6]. What is more, induced hypersensitivity is reported to be decreased in TLR2 or TLR4 deficient mice [3, 4]. Most of the proalgesic actions of TLRs are believed to be connected with the detection of pain by sensory neurons in response to local peripheral inflammation [7]. Regarding neuropathic pain, it has been proposed that neuronal damage can lead to the release of proinflammatory factors, for example, saturated fatty acids (SFAs), which activate spinal microglia via the TLR4/NF-kB signaling pathway [8, 9]. Despite numerous studies, the exact functional meaning of both TLR2 and TLR4

for pain as well as the possible differences between them in neuropathic pain remains to be elucidated.

LPS-RS (lipopolysaccharide from *Rhodobacter sphaeroides*) is a potent antagonist of TLR2 and TLR4, whereas *LPS-RS Ultrapure* specifically antagonizes TLR4. *LPS-RS* is reported to attenuate hypersensitivity in various neuropathic pain animal models, for example, the Sprague-Dawley rat *paclitaxel*-related chemotherapy-induced peripheral neuropathy (CIPN) model, the cancer-induced bone pain (CIBP) model in Wistar rats, the inflammatory arthritis pain model in *C57Bl/6* mice, and the nerve injury-induced model in Sprague-Dawley rats [10–13]. To our knowledge, *LPS-RS Ultrapure*, a highly specific TLR4 antagonist, has not been used in experiments on animals to date.

What is more, TLR2 or TLR4 deficient animals with induced neuropathy are more resistant to pain [4]. It has been shown that TLR4 activation is mediated by dimerization of adapter proteins such as MyD88 (myeloid differentiation primary response gene 88) or TRIF (TIR-domain-containing adapter-inducing interferon-β), but TLR2 uses only MyD88 [14]. Current studies report changes in the protein levels of TLR4 as well as of the MyD88 and TRIF adaptor molecules in pain models (*paclitaxel*-induced neuropathic pain [12] and cancer-induced bone pain [11, 12]); however, as far as we know, their protein levels of TLR4 as well as of the MyD88 and TRIF adaptor molecules have not been studied in neuropathic pain induced by CCI to the sciatic nerve in Wistar rats. Such experiments seem to be important because, in the case of TLR2 and TLR4 regulation, they may show some new mechanisms, which are essential for neuropathic pain development. Recently, it has been shown that TLR2 and TLR4 antagonism produces an analgesic effect in behavioral tests in cancer pain models [11, 12].

Opioid analgesics are commonly used for the treatment of neuropathic pain; however, as has already been mentioned, their efficacy is not satisfactory in comparison to their side effects [15]. In the CNS, microglia play a crucial role in the maintenance of neuronal homeostasis and produce immune factors, which are believed to play an essential role in pain development [16]. It has been shown that, in mice genetically lacking TLR2 or TLR4, microglial activation is markedly decreased, with a parallel reduction of neuropathic pain symptoms [3, 4]. Moreover, it has been reported that antagonism of TLR4 in healthy rats attenuates the development of morphine tolerance [17–20]; therefore, we found it interesting to study how/if TLR2/4 antagonists influence opioid effectiveness in a rat model of neuropathic pain.

Using qRT-PCR and Western blot, we have measured mRNA and protein changes of glial cell markers, TLRs (TLR4 and TLR2), and adaptor molecules (MyD88 and TRIF) in the spinal cord and DRG tissue on the 2nd, 7th, and 14th days after chronic constriction injury of the sciatic nerve in rats. We found it interesting to investigate how *LPS-RS Ultrapure* (a highly specific TLR4 antagonist) and *LPS-RS* (an antagonist of both TLR4 and TLR2) influence neuropathic pain symptoms, such as allodynia and hyperalgesia, which develop after CCI. Another important question which arose is whether these two antagonists of TLRs, *LPS-RS*, and *LPS-RS Ultrapure* might improve the effectiveness of opioids, such as morphine and buprenorphine, in a neuropathic pain model.

2. Materials and Methods

2.1. Animals. Male Wistar rats (290–330 g) from Charles River (Hamburg, Germany) were housed in cages that were lined with sawdust under a standard 12/12 h light/dark cycle (lights on at 06:00 A.M.), with food and water available *ad libitum*. Care was taken to reduce the number of animals used, and all experiments were performed according to the recommendations of IASP [21] and the NIH Guide for the Care and Use of Laboratory Animals and were approved by the local Bioethics Committee (Krakow, Poland).

2.2. Catheter Implantation. Rats were prepared for intrathecal (*i.th.*) injection by implanting catheters according to the method of Yaksh and Rudy [22] under pentobarbital (60 mg/kg; *i.p.*) anesthesia. The intrathecal polyethylene catheter (PE 10, Intramedic; Clay Adams, Parsippany, NJ) was sterilized by immersion in 70% (v/v) ethanol and precisely flushed with sterile water before insertion. Rats were placed on a stereotaxic table (David Kopf Instruments, Tujunga, CA), and an incision was made in the atlantooccipital membrane. The catheter (7.8 cm of its length) was carefully introduced into the subarachnoid space at the rostral level of the lumbar enlargement of the spinal cord (L4-L5), flushed slowly with 10 μL of sterile water, and the tip was tightened. After catheter implantation, the rats were monitored for physical impairments and allowed to recover for a minimum of 1 week before the actual experiment. Animals with visible motor deficits were excluded from further study.

2.3. Chronic Constriction Injury (CCI). CCI was produced in rats according to Bennett and Xie [23] under sodium pentobarbital anesthesia (60 mg/kg; *i.p.*). The *biceps femoris* and the *gluteus superficialis* were separated for right sciatic nerve exposure. Four ligatures (4/0 silk) were tied loosely around the nerve distal to the sciatic notch with 1 mm spacing until they elicited a brief twitch in the respective hind limb. Surgery caused long-lasting neuropathic pain symptoms, such as allodynia and hyperalgesia, in all of the rats.

2.4. Drug Administration. *LPS-RS* (a TLR4 and TLR2 antagonist derived from *R. sphaeroides*; InvivoGen, Toulouse, France) and *LPS-RS Ultrapure* (a TLR4-specific antagonist derived from *R. sphaeroides*; InvivoGen, Toulouse, France) were administered at a dose chosen based on the available literature and our preliminary study [10–13, 24]. *LPS-RS* [20 μg/5 μL; dissolved in water for injection], *LPS-RS Ultrapure* [20 μg/5 μL; dissolved in water for injection], and vehicle (water for injection) were administered by *i.th.* injection once per day for 9 days (CCI surgery was defined as day 0; substances were administered from day −1 until day 7). The vehicle group received injections (5 μL of water for injection) according to the same schedule. The *i.th.* injections were performed using a 50 μL Hamilton syringe with a 30 1/2-gauge needle; 5 μL was injected per animal, followed by 10 μL of sterile water.

2.5. Behavioral Tests. Two behavioral tests, von Frey's and cold plate, were performed at two time points: on 2nd and

7th days after CCI. The tests were conducted in time courses, including the 1st and 3rd hour after the morning drug or vehicle injection.

2.5.1. Mechanical Allodynia (von Frey's Test). Allodynia was measured in rats subjected to CCI by the use of an automatic von Frey apparatus (Dynamic Plantar Aesthesiometer; Cat. number 37400, Ugo Basile, Italy). The rats were placed in plastic cages with a wire net floor and left for a while to acclimate. The von Frey filament was applied to the midplantar surface of the CCI-exposed ipsilateral and contralateral hind paw, and measurements were taken automatically with a cut-off at 26 g [25].

2.5.2. Thermal Hyperalgesia (Cold Plate Test). Hyperalgesia was assessed using the cold plate test (Cold/Hot Plate Analgesia Meter; number 05044, Columbus Instruments, USA) as has been described previously [25, 26]. The temperature of the cold plate was maintained at 5°C, and the cut-off latency was 30 s. The rats were placed on the cold plate, and the time until the hind paw was lifted was recorded. The injured paw was the first to react in every case and after animal reaction the animal is taken away from the cage due to minimalized the painful stimulation.

2.6. Biochemical Tests

2.6.1. qRT-PCR Analysis of Gene Expression. Ipsilateral dorsal rat spinal cords (L4–L6) were collected on 2nd, 7th, and 14th days after injury. Total RNA was extracted according to the method described by Chomczynski and Sacchi [27] using TRIzol reagent (Life Technologies, Carlsbad, CA, USA) as previously described [28]. RNA concentration was measured using a NanoDrop ND-1000 Spectrometer. Reverse transcription was performed on 1000 ng of total RNA using Omniscript reverse transcriptase (Qiagen Inc., Venlo, Netherlands) at 37°C for 60 minutes. cDNA was diluted 1 : 10 with H_2O. qRT-PCR was performed using Assay-On-Demand TaqMan probes according to the manufacturer's protocol (Applied Biosystems, Carlsbad, CA, USA) and run on a Real-Time PCR iCycler (Bio-Rad, Hercules, CA, USA). Rn01527838_g1 (*Hprt*), Rn00569848_m1 (*Tlr4*), Rn02133647_m1 (*Tlr2*), Rn01640049_m1 (*MyD88*), Rn02082474_s1 (*Ticam2*), and Rn01423590_m1 (*CD40*) were used as TaqMan primers and probes. Because of disability to design starters based on rat *Trif* sequence, we have used *Ticam2* dedicated primer which, analogically to *Trif*, is connected only to TLR4 and not to TLR2 downstream signaling. The expression of HPRT (a housekeeping gene) was quantified to control for variation in cDNA amounts across groups. Cycle threshold values were calculated automatically by iCycler IQ 3.0 software with the default parameters. RNA abundance was calculated as $2^{-(\text{threshold cycle})}$.

2.6.2. Western Blot Analysis. Ipsilateral dorsal lumbar (L4–L6) spinal cord and dorsal root ganglia (DRG) were collected immediately after decapitation on 2nd, 7th, and 14th days after CCI. Tissue was stored at −80°C until processing, which was described previously [28]. Blots were incubated overnight at 4°C with primary antibodies: anti-IBA-1 (rabbit anti-rat, 1 : 1000, Proteintech, Chicago IL, USA), anti-TLR2 (rabbit anti-rat, 1 : 2000, Novus Biological, Littleton CO, USA), anti-TLR4 (rabbit anti-rat, 1 : 1000, Proteintech, Chicago IL, USA), anti-MyD88 (rabbit anti-rat, 1 : 1000, Abcam, Cambridge, UK), and anti-TRIF (rabbit anti-rat, 1 : 500, Novus Biologicals, Littleton CO, USA) and for 1 h at RT with a corresponding secondary polyclonal HRP antibody (goat anti-rabbit IgG, 1 : 5000, Bio-Rad, Hercules, CA, USA). Both primary and secondary antibodies were diluted in solutions from *SignalBoost Immunoreaction Enhancer Kit* (Merck Millipore, Darmstadt, Germany). Immunocomplexes were detected using *Clarity Western ECL Substrate* (BioRad, Hercules, CA, USA) and visualized using a Fujifilm LAS-4000 fluoroimager system. The blots were stripped using *Restore Western Blot Stripping Buffer* (ThermoScientific, Waltham, MA, USA) for 15 minutes at RT and reprobed with an antibody against GAPDH (mouse anti-rabbit, 1 : 5000, Merck Millipore, Darmstadt, Germany) as a loading control.

2.7. Data Analysis. The behavioral data are presented as the mean ± SEM of 10–25 rats per group. Tests were performed on four groups: *INTACT*, *2d CCI*: 2 days after injury, *7d CCI*: 7 days after injury, and *14d CCI*: 14 days after injury. Intergroup differences were statistically evaluated by ANOVA followed by Bonferroni's *post hoc* test. Significance was defined as $^{***}p < 0.001$, indicating a significant difference versus the INTACT group. $^{+}p < 0.05$, $^{++}p < 0.01$, and $^{+++}p < 0.001$ indicate significant differences compared with vehicle-treated CCI-exposed rats; $^{\#\#}p < 0.01$ and $^{\#\#\#}p < 0.001$ indicate a significant difference compared with LPS-RS- or LPS-RS Ultrapure-treated CCI-exposed rats; $^{\wedge}p < 0.05$, $^{\wedge\wedge}p < 0.01$, and $^{\wedge\wedge\wedge}p < 0.001$ indicate differences between opioid-treated CCI-exposed groups.

The qRT-PCR analyses from the tissue were performed in four groups: *INTACT*, *2d CCI*: tissue collected 2 days after injury, *7d CCI*: tissue collected 7 days after injury, and *14d CCI*: tissue collected 14 days after injury. The results from 6–8 animals are presented as fold changes compared with the INTACT rats. The qRT-PCR data are presented as the mean ± SEM and represent the normalized averages that were derived from the threshold qRT-PCR cycles from four to eight samples for each group. Intergroup differences were analyzed using ANOVAs followed by Bonferroni's multiple comparison tests. $^{*}p < 0.05$, $^{***}p < 0.01$, and $^{***}p < 0.001$ indicate significant differences versus INTACT animals.

The protein analyses were performed using the Western blot method. Analysis of the tissue was performed in four groups: *INTACT*, *2d CCI*: tissue collected 2 days after injury, *7d CCI*: tissue collected 7 days after injury, and *14d CCI*: tissue collected 14 days after injury. The results are presented as fold changes compared to the INTACT group. The data are presented as the mean ± SEM and represent the normalized averages derived from analyses of 4–7 samples for each group performed with the Multi Gauge analysis program. Intergroup differences were analyzed using ANOVA followed by Bonferroni's multiple comparison tests. $^{*}p < 0.05$, $^{***}p < 0.01$, and $^{***}p < 0.001$ indicate significant differences versus INTACT animals.

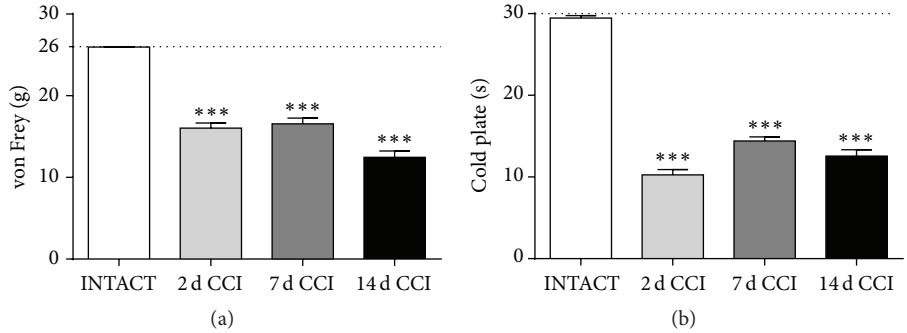

Figure 1: Levels of allodynia ((a); von Frey's test) and hyperalgesia ((b); cold plate test) measured on 2nd, 7th, and 14th days after chronic constriction injury (CCI) in rats. The data are presented as the mean ± SEM (11–25 rats per group). Intergroup differences were analyzed using one-way ANOVA followed by Bonferroni's multiple comparisons test. *** $p < 0.001$ indicates a significant difference versus the INTACT group.

3. Results

3.1. Development of Allodynia and Hyperalgesia due to Neuropathic Pain Development, as Measured on the 2nd, 7th, and 14th Days after CCI. We observed that mechanical allodynia (von Frey's test) lasted from the 2nd day after injury constantly through the 7th day, reaching a maximum of two weeks after CCI (Figure 1(a)). Thermal hyperalgesia (cold plate test) turned out to be the strongest on day 2 after surgery, which is probably the result of early-stage inflammatory pain, which is silenced until days 7 and 14, when pain is constant and still strong (Figure 1(b)). There was no change as measured at the contralateral paw (25.94 ± 0.6 g) in von Frey test in CCI-exposed rats versus INTACT animals (25.96 ± 0.045 g).

3.2. Changes in CD40, TLR2, TLR4, MyD88, and TICAM2 mRNA Levels, as Measured on the 2nd, 7th, and 14th Days after CCI. Expression of the marker for CD40-positive cells in the spinal cord had already risen by 237% on 2nd day. Very strong changes, 184% and 135%, were still measured on 7th and 14th days, respectively, after CCI (Figure 2(a)). Weak (21%) upregulation of CD40 was observed on 2nd day in the DRG, the strongest change (44%) on 7th day, and a slight decrease to 32% upregulation on 14th day after CCI (Figure 2(b)).

In contrast, significant changes in TLR2 mRNA were not observed on 2nd day in the spinal cord or DRG. However, a very strong increase in TLR2 mRNA levels was detected on 7th and 14th days, 87% and 122%, respectively, in the spinal cord (Figure 2(c)) and 46% and 28% in the DRG (Figure 2(d)).

The very strong 81% upregulation of TLR4 expression was observed on 2nd day and lasted at a high level (108% of control) until 14th day after CCI in the spinal cord (Figure 2(e)). Changes in the DRG tissue were less pronounced; the strongest change was 26% on 2nd day, which slowly diminished to 22% on 14th day after CCI (Figure 2(f)).

Upregulation of MyD88 expression (99%) was observed until 2nd day, with a peak (127%) on 7th day and lasting at the high level of 97% until 14th day after CCI in the spinal cord (Figure 2(g)). Similar results were obtained in the DRG: the 128% upregulation started on 2nd day, diminished to 67% upregulation on 7th day and to 58% on 14th day after CCI (Figure 2(h)). Significant changes in TICAM2 expression were detected in the spinal cord: 46%, 112%, and 89%, as measured on 2nd, 7th, and 14th days after CCI, respectively (Figure 2(i)). We did not detect any changes in TICAM2 expression in the DRG tissue (Figure 2(j)).

3.3. Changes in IBA-1, TLR2, TLR4, MyD88, and TRIF Protein Levels, as Measured on the 2nd, 7th, and 14th Day after CCI. The 88% increase in IBA-1-positive cells was already observed on day 2 in the spinal cord. Even stronger upregulation of 302% was measured on day 7, which slowly decreased to 141% on day 14 after CCI (Figure 3(a)). In the DRG, we did not observe any significant changes in IBA-1 protein after CCI (Figure 3(b)).

The pattern of TLR2 protein level changes showed an increase of 16% and 27% 7 and 14 days after CCI in the spinal cord (Figure 3(c)); in the DRG, additional (48%) upregulation was already observed on day 2, which lasted at a high level (43%) until the 14th day (Figure 3(d)).

Changes in TLR4 protein levels were not observed on day 2 in either the spinal cord or the DRG. However, 28% upregulation was detected on day 7 in the spinal cord and was constant (21%) until day 14 (Figure 3(e)). Similar regulation was observed in the DRG: rises of 29% and 34% on days 7 and 14 after CCI (Figure 3(f)).

An increase in MyD88 protein was already observed in the spinal cord on day 2, with a peak on day 7 (93%); then expression slowly diminished with time, reaching an increase of 38% (Figure 3(g)). In the DRG, 20% upregulation was observed only on day 2 after CCI (Figure 3(h)). Changes in TRIF protein level were not detected in the spinal cord (Figure 3(i)); however, 38% upregulation was detected on day 2 in the DRG (Figure 3(j)).

We have not observed significant changes in IBA-1, TLR2, TLR4, MyD88, and TRIF protein levels on the contralateral side of the spinal cord and DRG (Table 1).

3.4. LPS-RS and LPS-RS Ultrapure Administration Attenuated Allodynia and Hyperalgesia, as Measured 2 and 7 Days after

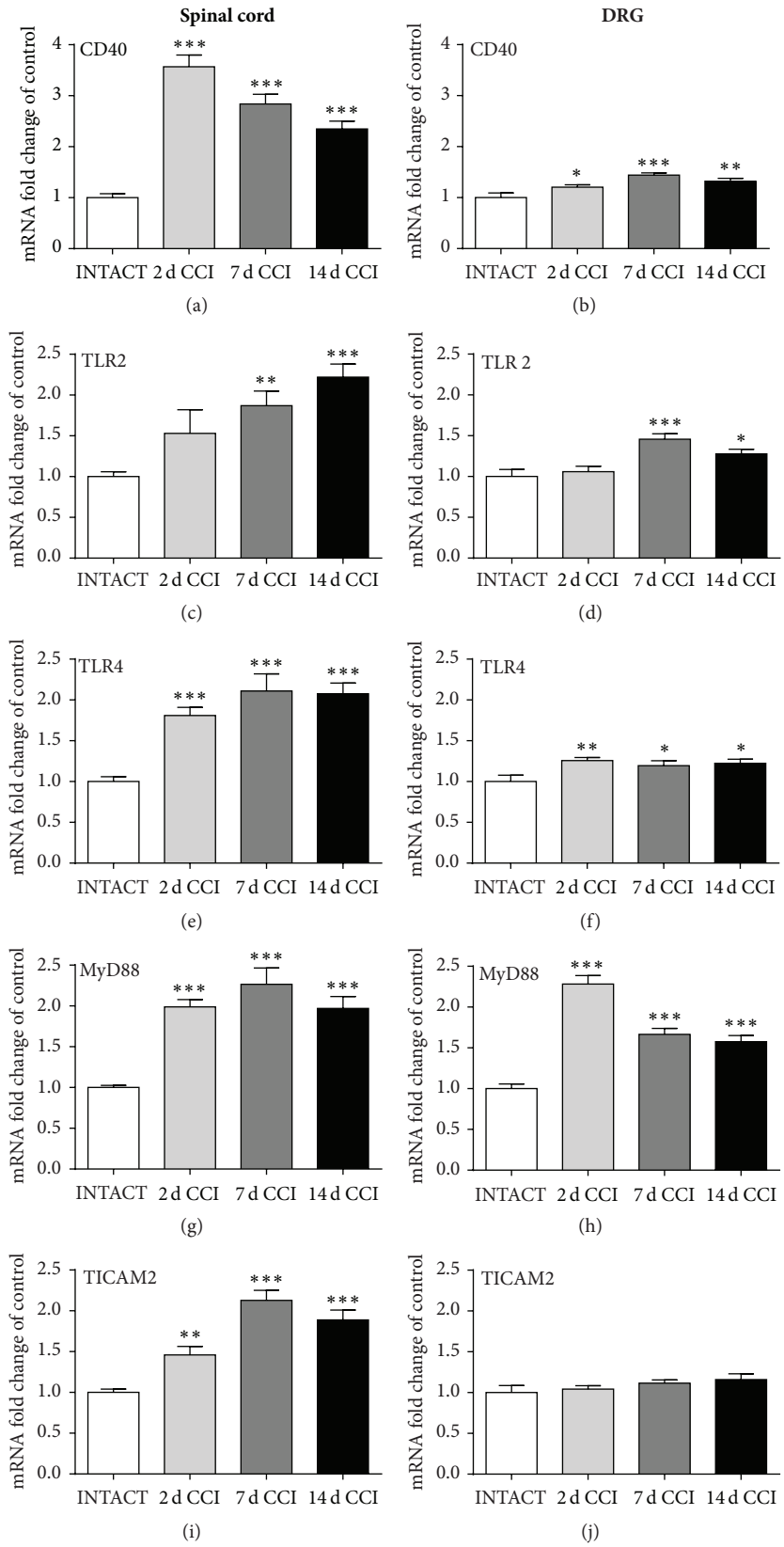

Figure 2: Quantitative real-time PCR analysis of *CD40* (a, b), *TLR2* (c, d), *TLR4* (e, f), *MyD88* (g, h), and *TICAM2* (i, j) mRNA levels in the ipsilateral dorsal lumbar spinal cord (a, c, e, g, and i) and DRG (b, d, f, h, and j) tissue on 2nd, 7th, and 14th days after chronic constriction injury (CCI) in rats. The data are presented as the mean ± SEM, which represent normalized averages derived from the threshold cycles obtained in qRT-PCR from 6–8 samples per group. Intergroup differences were analyzed using one-way ANOVA followed by Bonferroni's multiple comparisons test. $^{*}p < 0.05$, $^{**}p < 0.01$, and $^{***}p < 0.001$ indicate significant differences versus the INTACT group.

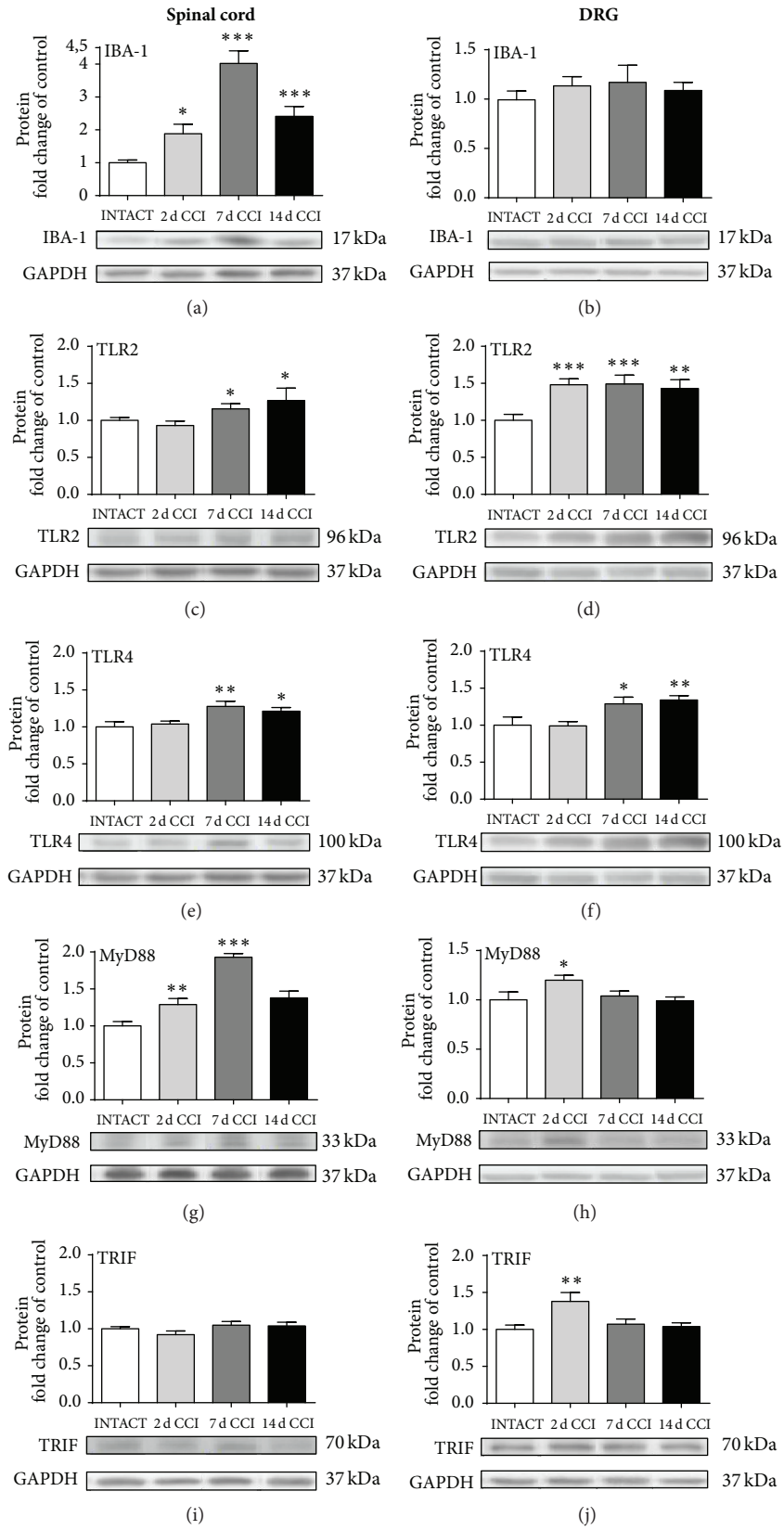

Figure 3: Western blot analysis of IBA-1 (a, b), TLR2 (c, d), TLR4 (e, f), MyD88 (g, h), and TRIF (i, j) protein levels in the ipsilateral dorsal lumbar spinal cord (a, c, e, g, and i) and DRG (b, d, f, h, and j) tissue on 2nd, 7th, and 14th days after chronic constriction injury (CCI) in rats. The data are presented as the mean ± SEM of 4–7 samples per group. Intergroup differences were analyzed using one-way ANOVA followed by Bonferroni's multiple comparisons test. $^{*}p < 0.05$, $^{**}p < 0.01$, and $^{***}p < 0.001$ indicate significant differences versus the INTACT group.

Table 1: Western blot analysis of IBA-1, TLR2, TLR4, MyD88, and TRIF protein levels in the contralateral dorsal lumbar spinal cord and DRG tissue on 7th day after chronic constriction injury (CCI) in rats. The results are not statistically significant and are presented as the mean ± SEM of 4–7 samples per group (see also Figure 4).

Protein level	7th day after CCI Dorsal lumbar section, contralateral side			
	INTACT		Vehicle-CCI	
Spinal cord	IBA-1	1.00 ± 0.07	IBA-1	1.12 ± 0.19
	TLR2	1.00 ± 0.13	TLR2	1.17 ± 0.08
	TLR4	1.00 ± 0.06	TLR4	1.11 ± 0.13
	MyD88	1.00 ± 0.05	MyD88	1.09 ± 0.06
	TRIF	1.00 ± 0.04	TRIF	0.99 ± 0.06
DRG	IBA-1	1.00 ± 0.10	IBA-1	1.02 ± 0.08
	TLR2	1.00 ± 0.08	TLR2	0.81 ± 0.11
	TLR4	1.00 ± 0.16	TLR4	0.98 ± 0.07
	MyD88	1.00 ± 0.11	MyD88	0.98 ± 0.05
	TRIF	1.00 ± 0.03	TRIF	1.00 ± 0.08

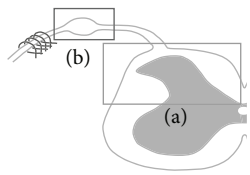

Figure 4: (a) Spinal cord and (b) DRG.

CCI. All of the vehicle-treated, CCI-exposed rats revealed neuropathic pain symptoms after surgery. Strong allodynia was measured on days 2 and 7 after injury by von Frey's test (Figures 5(a) and 5(b)), and thermal hyperalgesia was measured by cold plate test (Figures 5(c) and 5(d)). Repeated administration of both drugs: *LPS-RS* and *LPS-RS Ultrapure* [20 μg/5 μL; i.th.], was effective in reducing hypersensitivity, as measured one and three hours after drug administration on days 2 and 7 after injury (Figures 5(a)–5(d)).

3.5. Chronic LPS-RS or LPS-RS Ultrapure Treatment Influences the Analgesic Effects of Single Buprenorphine but Not Morphine Administration, as Measured on Day 7 after CCI. Repeated intrathecal administration of *LPS-RS* and *LPS-RS Ultrapure* [20 μg/5 μL *i.th.;* both] as well as single intrathecal injection of morphine or buprenorphine [2.5 μg/5 μL, *i.th.;* both] on day 7 following CCI attenuated neuropathic pain symptoms in the rats (Figure 6). The analgesic effects of morphine or buprenorphine alone were similar to those of *LPS-RS* and *LPS-RS Ultrapure*, as measured 30 minutes after injection. The morphine/drug combination (2.5 μg of morphine 30 minutes after the administration of *LPS-RS* and *LPS-RS Ultrapure*) did not lead to a more effective analgesic effect in either the von Frey test (Figure 6(a)) or the cold plate test (Figure 6(c)). Interestingly, the buprenorphine/drug combination (2.5 μg of buprenorphine 30 minutes after the administration of *LPS-RS* and *LPS-RS Ultrapure*) led to an enhancement of the effectiveness of the opioid, as measured by von Frey's test (Figure 6(b)) and cold plate test (Figure 6(d)). The effect of buprenorphine was close to cut-off in the injured rats when combined with *LPS-RS* and *LPS-RS Ultrapure*.

4. Discussion

Our experiments have completed the data that was already available from different models regarding the contribution of TLR2 and TLR4 in the modulation of neuropathic pain. We show that, under chronic pain conditions, there are time-dependent changes in both the mRNA and protein levels of TLR2 and TLR4 as well as their adaptor molecules (MyD88 and TRIF/TICAM2), which appears parallel to the activation of macrophages/microglial cells. The TLR antagonists *LPS-RS* (TLR2 and TLR4) and *LPS-RS Ultrapure* (TLR4) similarly diminished pain behavior after CCI, suggesting a greater contribution of TLR4 in neuropathy, at least in the rat nerve injury-induced neuropathic pain model. Moreover, this pharmacological interference enhanced buprenorphine's but not morphine's antiallodynic and antihyperalgesic properties under conditions of neuropathic pain.

Existing research therapies against pain seem to have limited effectiveness, partly because they target mainly neurons and do not influence microglial activation. Therefore, in light of our results and available preclinical reports, an exciting alternative of targeting microglial activation is becoming one of the first steps in diminishing the progression of neuropathic pain. Understanding the relationship between microglia and TLRs may help in developing new targets for drugs. Solid evidence indicates the critical involvement of microglia in neuropathy, reinforcing the idea that these cells not only are a structural support for neurons but also contribute significantly to their function [16, 26, 29, 30]. The signals that induce microglial activation in response to nerve injury remain incompletely clarified. Among the various receptors expressed on microglia, the Toll-like family, especially subtypes 2 and 4, are a possible answer to that problem because they act as a link between microglial activation and nerve injury and play a crucial role in the development of neuropathic pain symptoms [31, 32].

Our studies were performed using the neuropathic pain model developed by Bennett and Xie [23]. We observed that mechanical allodynia and thermal hyperalgesia develop as soon as 2 days after sciatic nerve injury. Our qRT-PCR analysis revealed simultaneous upregulation in TLR4 expression in the lumbar (L4–L6) dorsal spinal cord and DRG, which was significant until day 14 after CCI in the Wistar rats. Similar results were observed by Wu et al. [33] in Sprague-Dawley rats at the spinal level on day 7 and by other laboratories in diabetic mouse models [34, 35]. Our results showed the enhanced expression of TLR2 in the spinal cord and DRG on days 7 and 14 after CCI. Similar results were obtained by others using a mouse CCI model [36]. MyD88 mRNA levels remained elevated throughout the whole time course in the spinal cord and DRG. There are no corresponding data for neuropathic pain; however, similar results were obtained in the Sprague-Dawley rat model of irritable bowel

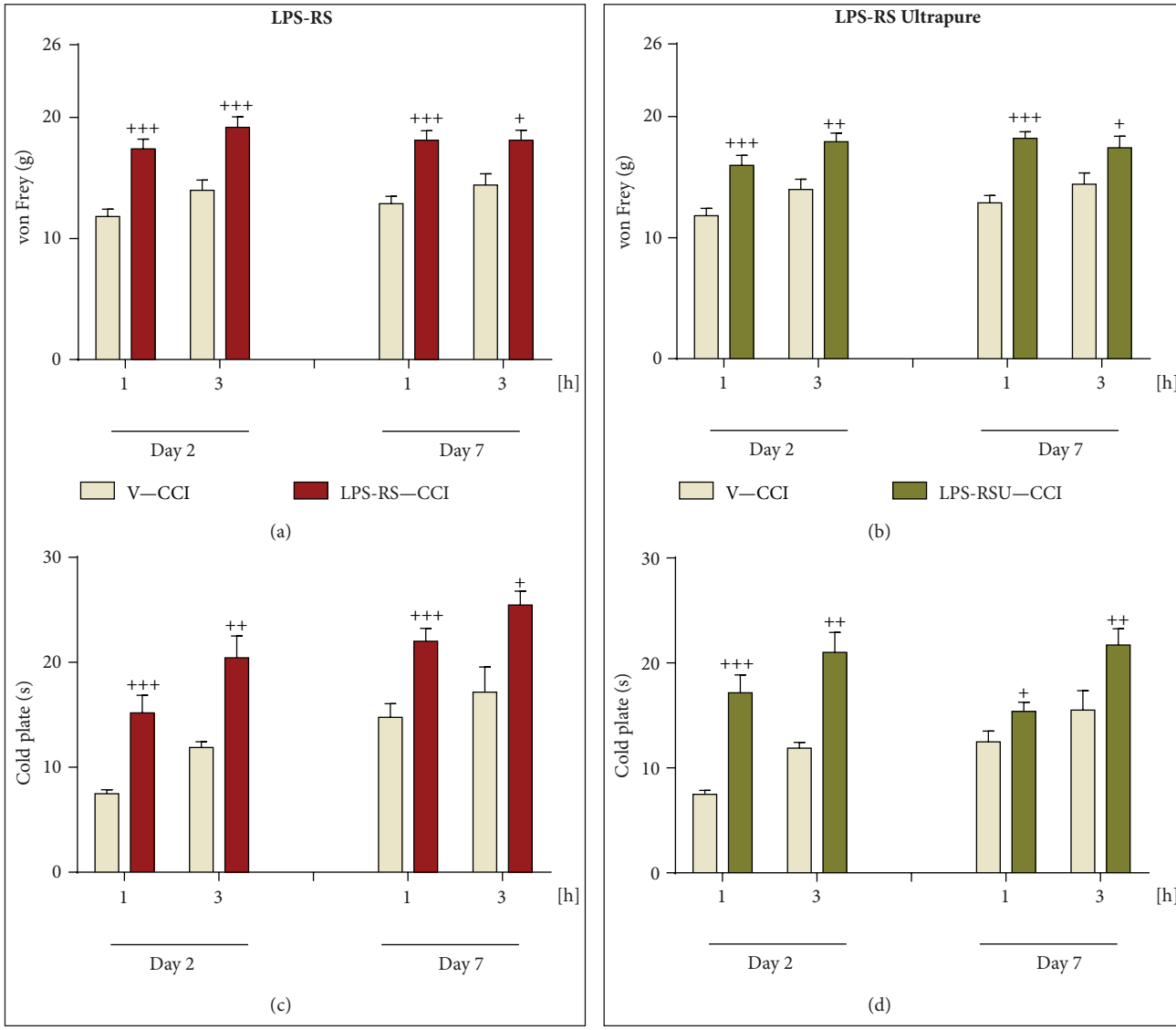

Figure 5: The influence of once daily, repeated intrathecal administration of vehicle ("V", sterile water), *LPS-RS* [20 μg/5 μL], or *LPS-RS Ultrapure* ["LPS-RSU", 20 μg/5 μL] on pain behavior, as measured by von Frey's test (mechanical allodynia; (a), (b)) and the cold plate test (thermal hyperalgesia; (c), (d)), 1 and 3 hours after drug administration on 2nd and 7th days after chronic constriction injury (CCI) to the sciatic nerve. The data are presented as the mean ± SEM (10–25 rats per group). Intergroup differences were analyzed using one-way ANOVA followed by Bonferroni's multiple comparisons test. $^{+}p < 0.05$, $^{++}p < 0.01$, and $^{+++}p < 0.001$ indicate significant differences compared with the vehicle-treated, CCI-exposed rat group (V-CCI).

syndrome (IBS) hypersensitivity [37]. TICAM2 expression was significantly enhanced in the spinal cord, with a peak on day 7 after surgery; however, in contrast to the protein results, there was no difference from baseline detected in the DRG. There are no data available regarding TICAM2 or TRIF regulation in chronic pain states.

As we have shown, the qRT-PCR analysis of TLR2, TLR4, and MyD88 [34, 35, 37] expression was carried out by several laboratories, although changes in their protein levels are poorly examined under neuropathic pain conditions. To date, the only published data available regarding protein levels of TLR4 and its signaling molecules in neuropathy were provided by Li et al. [12] in a paclitaxel-related chemotherapy-induced peripheral neuropathy model. We have shown using Western blot analysis in the CCI model that TLR4 protein levels are upregulated in the spinal cord on days 7 and 14 after CCI. Similar spinal regulation was published recently in the CIPN model by Li's group, who reported significant upregulation of TLR4 protein levels in parallel to pain development, as measured in the CIPN Sprague-Dawley rat model [11]. In the DRG, however, the changes are quite opposite because elevation is observed during the early stages of neuropathy development and in our model, from day 7, when neuropathic pain has already developed. We are the first to report that

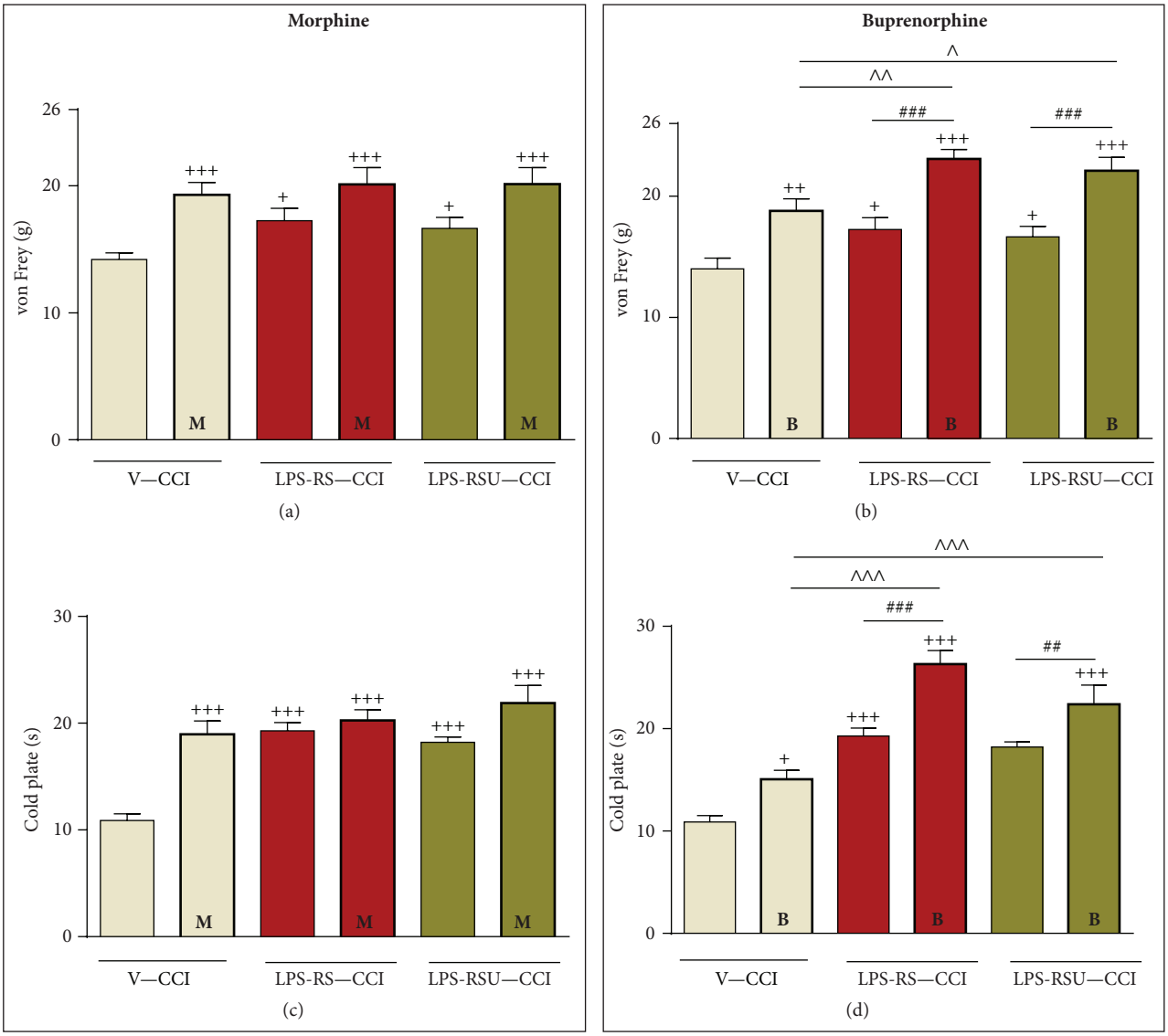

Figure 6: The influence of a single intrathecal administration of vehicle ("V", sterile water), *LPS-RS* [20 μg/5 μL], or *LPS-RS Ultrapure* ["LPS-RSU" 20 μg/5 μL] on morphine ("M", 2.5 μg/5 μL; (a), (c)) or buprenorphine ("B", 2.5 μg/5 μL; (b), (d)) analgesia, as measured by von Frey's test (mechanical allodynia; (a), (b)) and the cold plate test (thermal hyperalgesia; (c), (d)) 7 days after chronic constriction injury (CCI). The data are presented as the mean ± SEM. Intergroup differences were analyzed using one-way ANOVA followed by Bonferroni's multiple comparisons test. $^{+}p < 0.05$, $^{++}p < 0.01$, and $^{+++}p < 0.001$ indicate significant differences compared with the vehicle-treated, CCI-exposed rats (V-CCI); $^{\#}p < 0.05$, $^{\#\#}p < 0.01$, and $^{\#\#\#}p < 0.001$ indicate significant differences between the *LPS-RS* and *LPS-RS Ultrapure* treated CCI-exposed groups after additional vehicle administration comparing to additional morphine or buprenorphine treated CCI-exposed groups; $^{\wedge}p < 0.05$, $^{\wedge\wedge}p < 0.01$, and $^{\wedge\wedge\wedge}p < 0.001$ indicate significant differences between vehicle-treated CCI-exposed groups after morphine or buprenorphine treatment and *LPS-RS/LPS-RSU* opioid treated CCI-exposed groups.

TLR2 protein levels, similar to TLR4 protein levels, are also upregulated in the lumbar spinal cord during the second week of pain development. The importance of TLR2 was already suggested by Shi et al. [36], who reported that, in TLR2 KO mice, nerve injury-induced thermal hyperalgesia was completely abolished. This finding is contrary to that observed in wild-type mice, in which mechanical allodynia was partially reduced. Shi et al. suggested that TLR2 is necessary for the development of neuropathic pain and that its contribution is more important in thermal hypersensitivity than in mechanical allodynia. In our experiment, TLR2 and TLR4 were also upregulated in DRG tissue at all of the time points measured after CCI-induced neuropathy. This implies that the only change that can be observed in the DRG occurs at the beginning of neuropathy progression, so it can be assumed that the response of TLR4 to the injury state in the DRG is faster than that of TLR2. However, a distinction between the possible contributions of these two receptors to neuropathic pain cannot be ascertained based on the depicted results, and this issue needs future study. We

decided to investigate the changes in the levels of the MyD88 and TRIF adaptor molecules to verify if there is difference between TLR2 (connected to MyD88) and TLR4 (connected to both MyD88 and TRIF) activation. Our data suggest that CCI induced a strong and gradual increase in MyD88 protein until day 7, with a slight, though not significant, reduction on the 14th day. Other results reported in the CIPN model showed no significant changes in spinal MyD88 protein [12]. In the DRG, as we believe, both our results and the results of Li et al. [12] are consistent and show an increase in MyD88 in the early stage (on the 2nd day) of neuropathy development. The results obtained in our experiments indicate no spinal changes in TRIF protein over the whole time course and a short-term rise in the DRG in the early stage of neuropathy development (on the 2nd day), which is in agreement with the results obtained by Li et al. [12]. Our results suggest that, in the spinal cord, MyD88 (TLR2 and TLR4) is activated but TRIF (TLR4) is not. Because the biochemical studies did not allow us to differentiate the role of these two receptors in neuropathic pain, we employed pharmacological studies using a TLR4-specific antagonist (*LPS-RS Ultrapure*) and for comparison a TLR4- and TRL2-specific antagonist (*LPS-RS*). By our experiments, we have shown that, surprisingly, both substances similarly diminished the thermal hyperalgesia and tactile allodynia in our model of neuropathic pain.

Our results obtained after *LPS-RS* administration are in agreement with those reported using different animal models, showing its beneficial effects in other models, for example, the Sprague-Dawley rat paclitaxel-induced neuropathy model [12], the Wistar rat cancer-induced bone pain model [11], the *C57Bl/6* mouse inflammatory arthritis pain model [10], and the Sprague-Dawley rat nerve injury-induced model [13]. Our results also show that chronic intrathecal administration of *LPS-RS* diminished neuropathic pain induced by mechanical nerve injury. To date, there have not been any reports that *LPS-RS Ultrapure* has any influence on the maintenance of neuropathic pain in any model; thus, we are the first to report that specific antagonism of TLR4 is enough to produce an analgesic effect. Taking this into consideration, we assumed that antagonism of both TLR2 and TLR4 by *LPS-RS* would have diminished more of the neuropathic pain symptoms than antagonism of only TLR4 by the specific antagonist *LPS-RS Ultrapure*. However, our data suggest that TLR4 makes a greater contribution to neuropathy development and maintenance, at least in the rat nerve injury-induced neuropathic pain model.

Because it has been already published that antagonism of TLR4 enhances morphine analgesia in various contexts, our results seem to shed light on the extremely important passage through this theory. Namely, our data indicate that both *LPS-RS* and *LPS-RS Ultrapure* enhance the effectiveness of buprenorphine but not morphine. Most of the studies in INTACT animals reported to date refer to the attenuation of morphine tolerance by TLR4 antagonism in both rat and mouse models [18–20]. In 2013, Eidson and Murphy [17] reported a complex study using the CFA model in male Sprague-Dawley rats, which showed that cumulative doses of morphine along with a single systemic (*s.c.*) injection of (+)-naloxone resulted in the enhancement of opioid analgesia. Moreover, TLR4 antagonism directly in the PAG showed a similar effect, but, without morphine, there was no analgesia reported [17]. Although many hypotheses have been proposed to date [38], no strict evidence has been published demonstrating that TLR4 antagonism *in vivo* could actually be effective alone and moreover enhance opioid effectiveness under neuropathic pain conditions. Although there are works suggesting that TLR4 antagonism potentiates the analgesic efficacy of morphine, the studies were performed in INTACT animals, not in a neuropathic pain model (so in the absence of pain) [39, 40]. Knowing that a single, acute injection of an effective dose [2.5 μg; *i.th.*] of morphine or buprenorphine attenuates hypersensitivity in neuropathic rats, here, we report that although the TLR4 antagonists actually enhanced buprenorphine's analgesic effect, in contrast, the effect of morphine was not enhanced. Morphine suppresses neuropathic pain via opioid receptors, while buprenorphine also activates nociceptin/orphanin FQ peptide (NOP) receptors [41]. Preliminary data published to date suggests there is a link between TLR4 activation by an exogenous ligand (LPS) and NOP upregulation because they indicate that antagonism of TLR4 also attenuates the enhancement of NOP levels [42]. To test this hypothesis, we conducted a biochemical experiment in which we compared levels of NOP protein in groups treated with LPS-RS/LPS-RS Ultrapure/vehicle to levels in INTACT animals. We observed significant elevation of nociceptin receptor expression after injury (vehicle-treated) and attenuation of this effect after drug treatment (*data not shown*). Our observation that the effect of buprenorphine can be enhanced (in contrast to morphine) by antagonism of TLR2 or TLR4 needs further evaluation because it could explain the possibility of buprenorphine opioid rotation after the development of morphine tolerance.

5. Conclusion

Under conditions of neuropathic pain, we have measured upregulation of CD40, TLR2, TLR4, MyD88, and TICAM2 mRNA in the spinal cord and/or DRG using qRT-PCR method. The Western blot technique revealed upregulation of IBA-1, TLR2, TLR4, MyD88, and TRIF protein levels in the spinal cord and/or DRG. Our data suggest that both TLR2 and TLR4 may play a significant role in neuropathic pain, in light of their upregulation over the course of chronic pain, which could be linked to the activation of microglia and other IBA-1/CD40-positive cells that was also observed. Blockade of TLR2 and TLR4 produced analgesia and moreover enhanced the effectiveness of buprenorphine. The graphical abstract of our main results is available in the Supporting Information. Understanding the link between microglia and TLRs may help in developing new targets for pharmacotherapy. Depicted results may have great importance and possible clinical implications in neuropathy therapies in human due to their high conservatism of TLRs between species.

Conflict of Interests

The authors declare no conflict of interests.

Acknowledgments

This study is supported by The National Science Centre, Poland Grants OPUS NCN 2011/03/B/NZ4/00042 and Harmonia 5 2013/10/M/NZ4/00261. Agnieszka M. Jurga is a holder of a KNOW scholarship sponsored by the Ministry of Science and Higher Education, Republic of Poland.

References

[1] R. H. Dworkin, D. C. Turk, N. P. Katz et al., "Evidence-based clinical trial design for chronic pain pharmacotherapy: a blueprint for ACTION," *Pain*, vol. 152, no. 3, supplement, pp. S107–S115, 2011.

[2] E. Kalso, J. E. Edwards, R. A. Moore, and H. J. McQuay, "Opioids in chronic non-cancer pain: systematic review of efficacy and safety," *Pain*, vol. 112, no. 3, pp. 372–380, 2004.

[3] D. Kim, M. A. Kim, I.-H. Cho et al., "A critical role of toll-like receptor 2 in nerve injury-induced spinal cord glial cell activation and pain hypersensitivity," *The Journal of Biological Chemistry*, vol. 282, no. 20, pp. 14975–14983, 2007.

[4] F. Y. Tanga, N. Nutile-McMenemy, and J. A. DeLeo, "The CNS role of Toll-like receptor 4 in innate neuroimmunity and painful neuropathy," *Proceedings of the National Academy of Sciences of the United States of America*, vol. 102, no. 16, pp. 5856–5861, 2005.

[5] K. Miyake, "Innate immune sensing of pathogens and danger signals by cell surface Toll-like receptors," *Seminars in Immunology*, vol. 19, no. 1, pp. 3–10, 2007.

[6] R. E. Sorge, M. L. LaCroix-Fralish, A. H. Tuttle et al., "Spinal cord Toll-like receptor 4 mediates inflammatory and neuropathic hypersensitivity in male but not female mice," *The Journal of Neuroscience*, vol. 31, no. 43, pp. 15450–15454, 2011.

[7] T. Liu, Y.-J. Gao, and R.-R. Ji, "Emerging role of Toll-like receptors in the control of pain and itch," *Neuroscience Bulletin*, vol. 28, no. 2, pp. 131–144, 2012.

[8] D. Hwang, "Modulation of the expression of cyclooxygenase-2 by fatty acids mediated through toll-like receptor 4-derived signaling pathways," *The FASEB Journal*, vol. 15, no. 14, pp. 2556–2564, 2001.

[9] J. Y. Lee, K. H. Sohn, S. H. Rhee, and D. Hwang, "Saturated fatty acids, but not unsaturated fatty acids, induce the expression of cyclooxygenase-2 mediated through Toll-like receptor 4," *The Journal of Biological Chemistry*, vol. 276, no. 20, pp. 16683–16689, 2001.

[10] C. A. Christianson, D. S. Dumlao, J. A. Stokes et al., "Spinal TLR4 mediates the transition to a persistent mechanical hypersensitivity after the resolution of inflammation in serum-transferred arthritis," *Pain*, vol. 152, no. 12, pp. 2881–2891, 2011.

[11] X. Li, X.-W. Wang, X.-M. Feng, W.-J. Zhou, Y.-Q. Wang, and Q.-L. Mao-Ying, "Stage-dependent anti-allodynic effects of intrathecal Toll-like receptor 4 antagonists in a rat model of cancer induced bone pain," *The Journal of Physiological Sciences*, vol. 63, no. 3, pp. 203–209, 2013.

[12] Y. Li, H. Zhang, H. Zhang, A. K. Kosturakis, A. B. Jawad, and P. M. Dougherty, "Toll-like receptor 4 signaling contributes to paclitaxel-induced peripheral neuropathy," *The Journal of Pain*, vol. 15, no. 7, pp. 712–725, 2014.

[13] M. R. Hutchinson, Y. Zhang, K. Brown et al., "Non-stereoselective reversal of neuropathic pain by naloxone and naltrexone: involvement of toll-like receptor 4 (TLR4)," *European Journal of Neuroscience*, vol. 28, no. 1, pp. 20–29, 2008.

[14] K. A. Kigerl, J. P. D. R. Vaccari, W. D. Dietrich, P. G. Popovich, and R. W. Keane, "Pattern recognition receptors and central nervous system repair," *Experimental Neurology*, vol. 258, pp. 5–16, 2014.

[15] R. Przewlocki and B. Przewlocka, "Opioids in neuropathic pain," *Current Pharmaceutical Design*, vol. 11, no. 23, pp. 3013–3025, 2005.

[16] J. Mika, M. Zychowska, K. Popiolek-Barczyk, E. Rojewska, and B. Przewlocka, "Importance of glial activation in neuropathic pain," *European Journal of Pharmacology*, vol. 716, no. 1–3, pp. 106–119, 2013.

[17] L. N. Eidson and A. Z. Murphy, "Blockade of Toll-like receptor 4 attenuates morphine tolerance and facilitates the pain relieving properties of morphine," *The Journal of Neuroscience*, vol. 33, no. 40, pp. 15952–15963, 2013.

[18] L. Bai, C. Zhai, K. Han et al., "Toll-like receptor 4-mediated nuclear factor-κB activation in spinal cord contributes to chronic morphine-induced analgesic tolerance and hyperalgesia in rats," *Neuroscience Bulletin*, vol. 30, no. 6, pp. 936–948, 2014.

[19] J. L. Johnson, P. E. Rolan, M. E. Johnson et al., "Codeine-induced hyperalgesia and allodynia: investigating the role of glial activation," *Translational Psychiatry*, vol. 4, no. 11, article e482, 2014.

[20] T. A. Mattioli, H. Leduc-Pessah, G. Skelhorne-Gross et al., "Toll-like receptor 4 mutant and null mice retain morphine-induced tolerance, hyperalgesia, and physical dependence," *PLoS ONE*, vol. 9, no. 5, Article ID e97361, 2014.

[21] M. Zimmermann, "Ethical guidelines for investigations of experimental pain in conscious animals," *Pain*, vol. 16, no. 2, pp. 109–110, 1983.

[22] T. L. Yaksh and T. A. Rudy, "Analgesia mediated by a direct spinal action of narcotics," *Science*, vol. 192, no. 4246, pp. 1357–1358, 1976.

[23] G. J. Bennett and Y.-K. Xie, "A peripheral mononeuropathy in rat that produces disorders of pain sensation like those seen in man," *Pain*, vol. 33, no. 1, pp. 87–107, 1988.

[24] S. S. Lewis, M. R. Hutchinson, N. Rezvani et al., "Evidence that intrathecal morphine-3-glucuronide may cause pain enhancement via toll-like receptor 4/MD-2 and interleukin-1β," *Neuroscience*, vol. 165, no. 2, pp. 569–583, 2010.

[25] W. Makuch, J. Mika, E. Rojewska, M. Zychowska, and B. Przewlocka, "Effects of selective and non-selective inhibitors of nitric oxide synthase on morphine- and endomorphin-1-induced analgesia in acute and neuropathic pain in rats," *Neuropharmacology*, vol. 75, pp. 445–457, 2013.

[26] J. Mika, M. Osikowicz, W. Makuch, and B. Przewlocka, "Minocycline and pentoxifylline attenuate allodynia and hyperalgesia and potentiate the effects of morphine in rat and mouse models of neuropathic pain," *European Journal of Pharmacology*, vol. 560, no. 2-3, pp. 142–149, 2007.

[27] P. Chomczynski and N. Sacchi, "Single-step method of RNA isolation by acid guanidinium thiocyanate-phenol-chloroform extraction," *Analytical Biochemistry*, vol. 162, no. 1, pp. 156–159, 1987.

[28] E. Rojewska, K. Popiolek-Barczyk, A. M. Jurga, W. Makuch, B. Przewlocka, and J. Mika, "Involvement of pro- and antinociceptive factors in minocycline analgesia in rat neuropathic pain model," *Journal of Neuroimmunology*, vol. 277, no. 1-2, pp. 57–66, 2014.

[29] I. Bettoni, F. Comelli, C. Rossini et al., "Glial TLR4 receptor as new target to treat neuropathic pain: efficacy of a new receptor

antagonist in a model of peripheral nerve injury in mice," *Glia*, vol. 56, no. 12, pp. 1312–1319, 2008.

[30] J. Mika, "Modulation of microglia can attenuate neuropathic pain symptoms and enhance morphine effectiveness," *Pharmacological Reports*, vol. 60, no. 3, pp. 297–307, 2008.

[31] J. H. Hayward and S. J. Lee, "A decade of research on TLR2 discovering its pivotal role in glial activation and neuroinflammation in neurodegenerative diseases," *Experimental Neurobiology*, vol. 23, no. 2, pp. 138–147, 2014.

[32] S. Lehnardt, L. Massillon, P. Follett et al., "Activation of innate immunity in the CNS triggers neurodegeneration through a Toll-like receptor 4-dependent pathway," *Proceedings of the National Academy of Sciences of the United States of America*, vol. 100, no. 14, pp. 8514–8519, 2003.

[33] F.-X. Wu, J.-J. Bian, X.-R. Miao et al., "Intrathecal siRNA against Toll-like receptor 4 reduces nociception in a rat model of neuropathic pain," *International Journal of Medical Sciences*, vol. 7, no. 5, pp. 251–259, 2010.

[34] J.-E. Yan, W. Yuan, X. Lou, and T. Zhu, "Streptozotocin-induced diabetic hyperalgesia in rats is associated with upregulation of toll-like receptor 4 expression," *Neuroscience Letters*, vol. 526, no. 1, pp. 54–58, 2012.

[35] Y. P. Zhang, C. Y. Song, Y. Yuan et al., "Diabetic neuropathic pain development in type 2 diabetic mouse model and the prophylactic and therapeutic effects of coenzyme Q10," *Neurobiology of Disease*, vol. 58, pp. 169–178, 2013.

[36] X. Q. Shi, H. Zekki, and J. Zhang, "The role of TLR2 in nerve injury-induced neuropathic pain is essentially mediated through macrophages in peripheral inflammatory response," *GLIA*, vol. 59, no. 2, pp. 231–241, 2011.

[37] Z.-Y. Chen, X.-W. Zhang, L. Yu et al., "Spinal toll-like receptor 4-mediated signalling pathway contributes to visceral hypersensitivity induced by neonatal colonic irritation in rats," *European Journal of Pain*, vol. 19, no. 2, pp. 176–186, 2015.

[38] L. R. Watkins, M. R. Hutchinson, K. C. Rice, and S. F. Maier, "The "Toll" of opioid-induced glial activation: improving the clinical efficacy of opioids by targeting glia," *Trends in Pharmacological Sciences*, vol. 30, no. 11, pp. 581–591, 2009.

[39] M. R. Hutchinson, Y. Zhang, M. Shridhar et al., "Evidence that opioids may have toll-like receptor 4 and MD-2 effects," *Brain, Behavior, and Immunity*, vol. 24, no. 1, pp. 83–95, 2010.

[40] S. S. Lewis, M. R. Hutchinson, Y. Zhang et al., "Glucuronic acid and the ethanol metabolite ethyl-glucuronide cause toll-like receptor 4 activation and enhanced pain," *Brain, Behavior, and Immunity*, vol. 30, pp. 24–32, 2013.

[41] T. Takahashi, K. Okubo, S. Kojima et al., "Antihyperalgesic effect of buprenorphine involves nociceptin/orphanin FQ peptide-receptor activation in rats with spinal nerve injury-induced neuropathy," *Journal of Pharmacological Sciences*, vol. 122, no. 1, pp. 51–54, 2013.

[42] C. Acosta and A. Davies, "Bacterial lipopolysaccharide regulates nociceptin expression in sensory neurons," *Journal of Neuroscience Research*, vol. 86, no. 5, pp. 1077–1086, 2008.

Hindawi Publishing Corporation
Neural Plasticity
Volume 2016, Article ID 2130901, 16 pages
http://dx.doi.org/10.1155/2016/2130901

Research Article

Bilateral Neuropathy of Primary Sensory Neurons by the Chronic Compression of Multiple Unilateral DRGs

Ya-Bin Xie,[1,2] Huan Zhao,[1,2] Ying Wang,[1] Kai Song,[1] Ming Zhang,[1] Fan-Cheng Meng,[1] Yu-Jie Yang,[1] Yang-Song He,[1] Fang Kuang,[1] Si-Wei You,[1] Hao-Jun You,[3] and Hui Xu[1,2]

[1]*Department of Neurobiology and Collaborative Innovation Center for Brain Science, School of Basic Medicine, Fourth Military Medical University, Xi'an 710032, China*
[2]*Center for Neuron and Disease, Frontier Institutes of Life Science and of Science and Technology, Xi'an Jiaotong University, Xi'an 710049, China*
[3]*Center for Biomedical Research on Pain (CBRP), College of Medicine, Xi'an Jiaotong University, Xi'an 710061, China*

Correspondence should be addressed to Hui Xu; xubz@fmmu.edu.cn

Received 14 February 2015; Revised 18 June 2015; Accepted 30 July 2015

Academic Editor: Feng Wei

To mimic multilevel nerve root compression and intervertebral foramina stenosis in human, we established a new animal model of the chronic compression of unilateral multiple lumbar DRGs (mCCD) in the rat. A higher occurrence of signs of spontaneous pain behaviors, such as wet-dog shaking and spontaneous hind paw shrinking behaviors, was firstly observed from day 1 onward. In the meantime, the unilateral mCCD rat exhibited significant bilateral hind paw mechanical and cold allodynia and hyperalgesia, as well as a thermal preference to 30°C plate between 30 and 35°C. The expression of activating transcription factor 3 (ATF3) was significantly increased in the ipsilateral and contralateral all-sized DRG neurons after the mCCD. And the expression of CGRP was significantly increased in the ipsilateral and contralateral large- and medium-sized DRG neurons. ATF3 and CGRP expressions correlated to evoked pain hypersensitivities such as mechanical and cold allodynia on postoperative day 1. The results suggested that bilateral neuropathy of primary sensory neurons might contribute to bilateral hypersensitivity in the mCCD rat.

1. Introduction

Mounting evidence suggests a possible cause of low back pain and radicular pain is the mechanical deformation of the dorsal root ganglion (DRG) and its nerve roots, resulting from spinal stenosis, radiculopathies, and tumors [1]. The chronic compression of a single DRG (CCD) model mimics low back pain and radicular pain syndromes in the rat, for example, significant unilateral mechanical and heat hyperalgesia [2, 3]. However, whether CCD model exhibits spontaneous pain and cold allodynia remains unknown. Multilevel lumbosacral radiculopathies are more common than single level radiculopathies in clinic, and patients with back disorders typically exhibit multilevel nerve root compression and intervertebral foramina stenosis. In this study, the rat model of the chronic compression of unilateral multiple DRGs (mCCD) of lumbar levels 3–5 was modified. And spontaneous pain and evoked pain hypersensitivities were examined in the mCCD model. Numerous studies have shown that activating transcription factor 3 (ATF3) could be used as a neuronal marker of nerve injury [4, 5], whereas calcitonin gene-related peptide (CGRP) is a marker of nociceptive information transmission in the DRG and spinal cord [6]. Possible molecular mechanisms contributing to spontaneous pain and evoked hypersensitivities were investigated by examining plastic changes in the expression of ATF3 and CGRP in the bilateral DRGs in the mCCD rat.

2. Materials and Methods

2.1. Animals. Two-month-old male Sprague-Dawley rats (180–250 g) were obtained from the Fourth Military Medical University animal center and were maintained under standard laboratory conditions (12/12-hour light/dark cycle, 22 ± 2°C, food and water ad libitum). All animals were allowed to adapt to laboratory conditions for at least one week

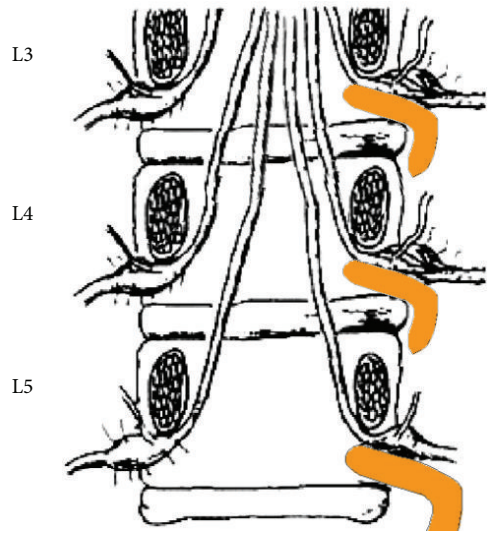

Figure 1: Schematic diagram of the compression of the DRG in the mCCD model.

and were subjected to mechanical paw withdrawal threshold tests before surgery. Rats with von Frey filament mechanical thresholds between 8 and 15 grams of force were chosen and randomly divided into three groups (control, sham and mCCD groups). All procedures were in strict accordance with the guidelines established by the Fourth Military Medical University Animal Care Committee. All efforts were made to minimize animal suffering and to reduce the number of animals used.

2.2. Surgical Procedures. Rats were deeply anesthetized with an intraperitoneal (i.p.) injection of sodium pentobarbital (50 mg/kg body weight). All manipulations were done on the left side of the spinal column. Special care was paid to prevent infection and to minimize the influence of inflammation. The hair of the rats' lower back was shaved and the skin was sterilized with 0.5% chlorhexidine and covered with clean gauze. Sterile surgical instruments were used. With the rats in a prone position, an incision was made along the midline of the back at the L2 and L6 spinal level. Following separation of the paraspinal muscles from the transverse process, the L3–L5 intervertebral foramina were exposed. L-shaped rods made of hollow stainless steel (4 mm in length and 0.5–0.8 mm in diameter) were carefully inserted into the L3, L4, and L5 foramina to compress the DRGs (Figure 1). In some cases, a sham surgery group of rats, the surgical procedure was identical to that for the chronic compression group, except that the stainless steel rods were not inserted into the intervertebral foramina. At the end of each study, mCCD animals were deeply anesthetized with intraperitoneal sodium pentobarbital and were dissected to verify that the compression were done at the right levels. The damage of the spinal cord at the spinal canal was examined by tracing the root to the L3–L5 DRGs after a vast dissection. Animals that had a lesion at the wrong level were excluded from the study.

2.3. Spontaneous Pain. Prior to testing, rats were adapted to the plastic testing chambers for at least one week (1 h per day). All tests took place between 4:00 PM and 6:00 PM, and the testing area was dimly lit to limit stress or anxiety. During behavioral assays, the experimenter was blind to the experimental treatment.

Analysis of spontaneous behavior was performed after surgery on days 1, 3, 5, 7, 14, 21, 28, and 35. All behavioral observations were performed in a low illuminated soundproof room. A sound-attenuated clear Perspex testing cage (25 × 25 × 40 cm) was fitted with a camera to record video for offline behavioral analysis. Rats were videotaped from below for 3 to 4 hours at every time point, from which 150 minutes were analyzed. Video recording started 30 minutes after the rats were placed in a cage to allow the animals to adapt to the testing conditions. A trained observer viewed the video recordings and counted the number and scored the magnitude of classified pain behaviors. The observer was trained to provide a similar rating performance (at the 95% confidence limit) of each behavior. "Wet-dog shaking" (WDS) was a behavior that resembles a wet dog that is shaking to remove water from the fur [7]. These behaviors were recorded as the number of incidences during 10-minute observation windows and summed to provide a total number of observed wet-dog shaking behaviors. Spontaneous paw shrinking behavior was recorded as the number of incidents of shrinking bilateral toes. Behaviors were recorded as number of incidences during the 10-minute observation time by using a counter, and then the total numbers of WDS and spontaneous hind paw shrinking behaviors were calculated among 150 minutes.

2.4. Mechanical Paw Withdrawal Threshold. Paw withdrawal thresholds to mechanical stimulation were assessed as described [8] using von Frey filaments (Stoelting Corporation, USA). Animals were placed in plastic cages with a wire mesh floor. To test for the tactile threshold required to evoke withdrawal of the stimulated paw, von Frey filaments with different bending forces (2–15.0 g) were applied perpendicularly to the plantar part of the hind paw in an ascending order. Each filament was applied 5 times to its minimum bending force, and a paw withdrawal threshold was defined as three positive responses. To avoid potential tissue damage, the cut-off threshold was assigned as 15.0 g-force.

2.5. Thermal Paw Withdrawal Latency. Paw withdrawal latency (PWL) to thermal stimulation was determined with a commercially available thermal Plantar Test Meter (Stoelting Corporation, USA). Rats were placed in clear plastic chambers on the top of a glass surface. The temperature of the surface was maintained at 30°C. The stimulus current of the infrared light radiant heat stimulus was maintained at 4.9 amperes while a 24-second cut-off was used to limit possible tissue damage. The time from the start of the light beam to the lifting of the paw from the glass plate (i.e., PWL) was measured. To ensure consistency, the radiant heat stimulus was always applied to the midplantar surface of the hind paw.

2.6. Cold Allodynia. Cold sensitivity to innocuous cold stimulation was tested by the acetone test. In brief, rats were placed in transparent plastic cages with small holes in the bottom and habituated to the test chamber for at least 30 min before the measurements. Acetone (50 μL) was gently sprayed onto the plantar surface of the hind paw using a 1 mL syringe with a blunt tip needle. A brisk foot withdrawal response after an acetone spray was considered a positive response, and the responses were graded on a four-point scale: 0, no response; 1, brisk withdrawal or flick of the paw; 2, repeated flicking of the paw; and 3, repeated flicking and licking of the paw [9]. The acetone spray was applied five times with an interval of 5 min between each application. The frequency of foot withdrawal was expressed as a percentage: (number of trials accompanied by brisk foot withdrawal) × 100/(number of total trials). Acetone response scores were the average of the graded points from the five acetone spray trials.

2.7. Thermal Preference Task. The thermal preference task involves two temperature-regulated aluminum plates (the same as described above) that are placed end to end and separated by a piece of Plexiglass with a hole cut in it for the rat to walk through. The entire area is enclosed in a Plexiglass box (30 cm × 13 cm × 16 cm), creating two compartments whose temperatures can be independently adjusted. Thermal preference trials were 300 s and the rat was allowed to freely move back and forth between the two compartments for the entire trial. Stimulus temperatures for thermal preference testing were set at 25 and 30°C, 30 and 35°C, and 35 and 40°C, respectively. Training for the thermal preference task occurred over a four-day period with the floor plates set at 20°C for the first four trials. This allowed the rats to acclimate to the test chamber, while exploring freely from compartment to compartment and learning that the floor on each side had a different temperature. The amount of time spent on the different temperature side was recorded, respectively. A rat was considered to have crossed over when all four feet were in the new compartment.

2.8. Immunocytochemical Staining and Cell Counts. After the defined survival time, rats in the control (which were not treated before the surgery of the mCCD) and mCCD groups were euthanized under deep anesthesia (sodium pentobarbital, 50 mg/kg) and perfused transcardially with 0.9% saline and 4% paraformaldehyde in 0.1 M PBS (pH 7.4). The L3–L5 DRGs were removed and postfixed in the same fixative for 2 hr and then placed in 20% sucrose until they sank. The entire DRGs were cut on a cryostat into serial coronal sections at 14 μm, with the first of every six sections being mounted on poly-L-lysine-coated slides and prepared for CGRP or ATF3 immunostaining.

Sections were blocked with 3% donkey serum in 0.3% Triton X-100 for 1 hr at room temperature (RT) and then incubated with rabbit anti-CGRP (1 : 1000, Sigma, USA) for 18 hr or rabbit anti-ATF3 (1 : 100, Santa Cruz Biotechnology, USA) overnight at RT. These sections were washed and incubated with fluorescently labeled goat anti-rabbit IgG (Alexa Fluor 594, Invitrogen, Life Technologies Corp., USA) for 4 hr at RT. The specificity of immunolabeling was verified by controls in which the primary antibody was omitted. Immunocytochemical double-labeling was conducted to determine the types of the cells that express CGRP or ATF3. For double- or triple-staining, the sections were incubated at RT for 18 hr in a cocktail solution containing different combinations of the following antibodies: rabbit anti-ATF3 antibody (1 : 250; Molecular Probes Inc., USA), mouse anti-neurofilament protein NF200 antibody (marker for neurons with myelinated axons; 1 : 1000; Millipore, USA), and/or mouse anti-peripherin antibody (marker for small neurons; 1 : 800, Sigma). After multiple washes in PBS, the sections were incubated at room temperature for 4 hr with fluorescently labeled goat anti-mouse IgG (Alexa Fluor 488, FITC; 1 : 500; Molecular Probes Inc., for the NF200) and/or fluorescently labeled goat anti-rabbit IgG (Alexa Fluor 594, Texas Red; 1 : 800; Molecular Probes Inc., for the ATF3), and all the sections were finally incubated at room temperature for 15 minutes with Hoechst 33342 nucleic acid stain (1 : 1000, Sigma). Sections were mounted on gelatinized slides and coverslipped.

Every sixth section throughout the DRG was processed for immunocytochemistry. All positive cells in the DRG were counted in each section at 400x magnification, omitting cells in the outermost focal plane. The total number of positive cells per section was determined and multiplied by 6 to obtain the total number of cells per DRG. The number of Hoechst-positive cells was regarded as total DRG cells in one section. For quantification of ATF3 positive, CGRP positive, and ATF3/NF200, ATF3/peripherin, CGRP/NF200, and CGRP/peripherin double-labeled cells, immunofluorescence images were obtained under a BX51 fluorescence microscope (Olympus, Japan). The percentage of ATF3 or CGRP positive cells per section was the number of ATF3 or CGRP positive cells divided by the number of Hoechst-positive cells. The percentage of double-staining of ATF3 with NF200 or peripherin was calculated among NF200- or peripherin-positive neurons, respectively. Similarly, the percentage of double-staining of CGRP with NF200 or peripherin was calculated among NF200- or peripherin-positive neurons, respectively.

2.9. Statistical Analysis. All results were expressed as mean ± SEM. Statistical analyses of pain behaviors were performed with a repeated measures analysis of variance (RM ANOVA). The difference of pain behaviors between bilateral sides was analyzed with one-way ANOVA followed by Bonferroni multiple comparison *post hoc* tests. General linear model was used on data in Figure 2(d). Immunocytochemical data in Figures 5(b), 6(b), 7(b), and 8(c)–8(e) were analyzed with general linear model followed by Bonferroni multiple comparison *post hoc* test. Linear regression analysis was performed on data in the Supplementary Figures in Supplementary Material available online at http://dx.doi.org/10.1155/2016/2130901. Data management and statistical analyses were performed using SPSS (v14.0). Statistical significance was set at $P < 0.05$.

3. Results

3.1. Spontaneous Pains. During the period of behavioral testing of up to five weeks, a total of 95 rats with the chronic

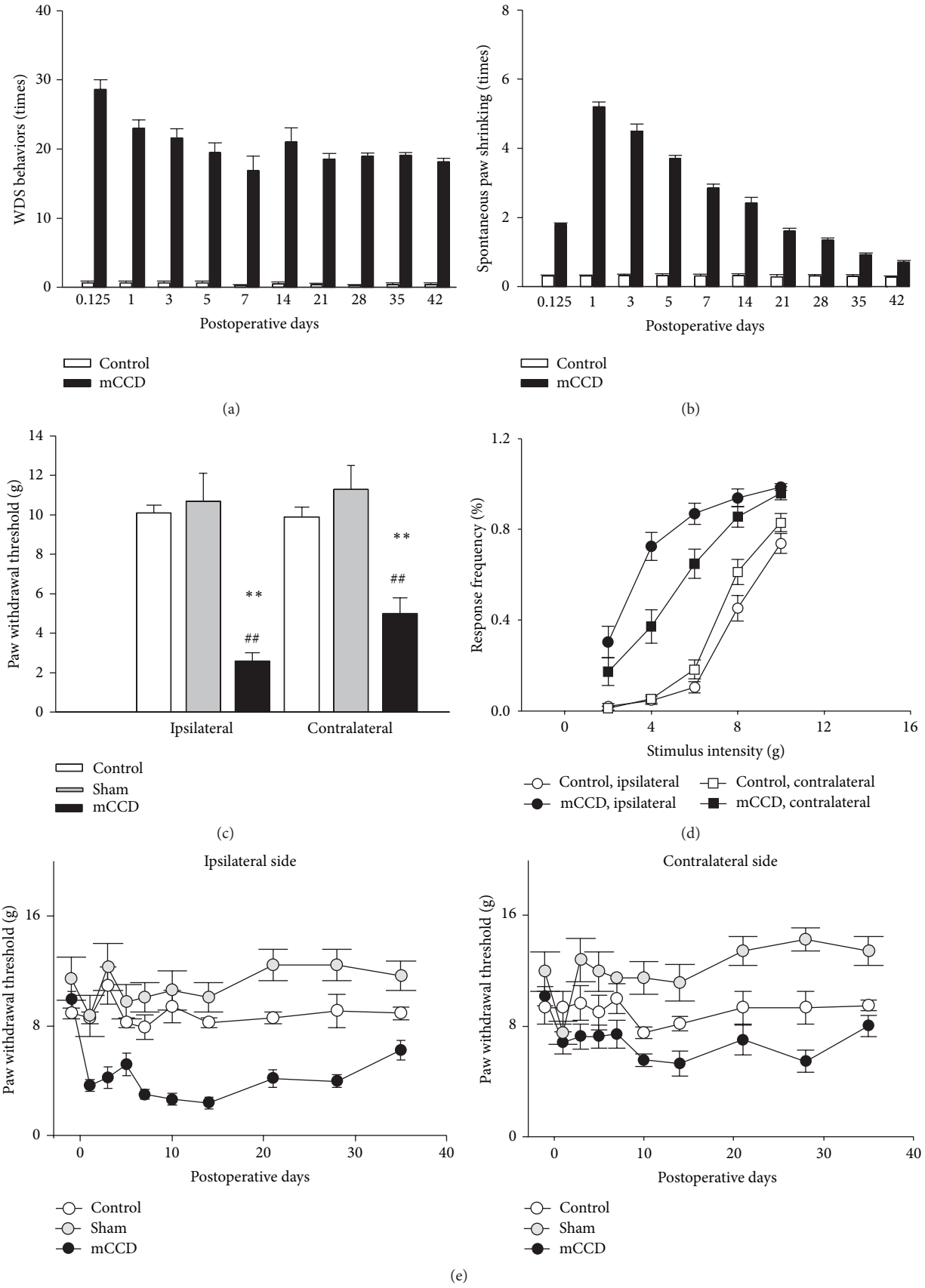

Figure 2: Continued.

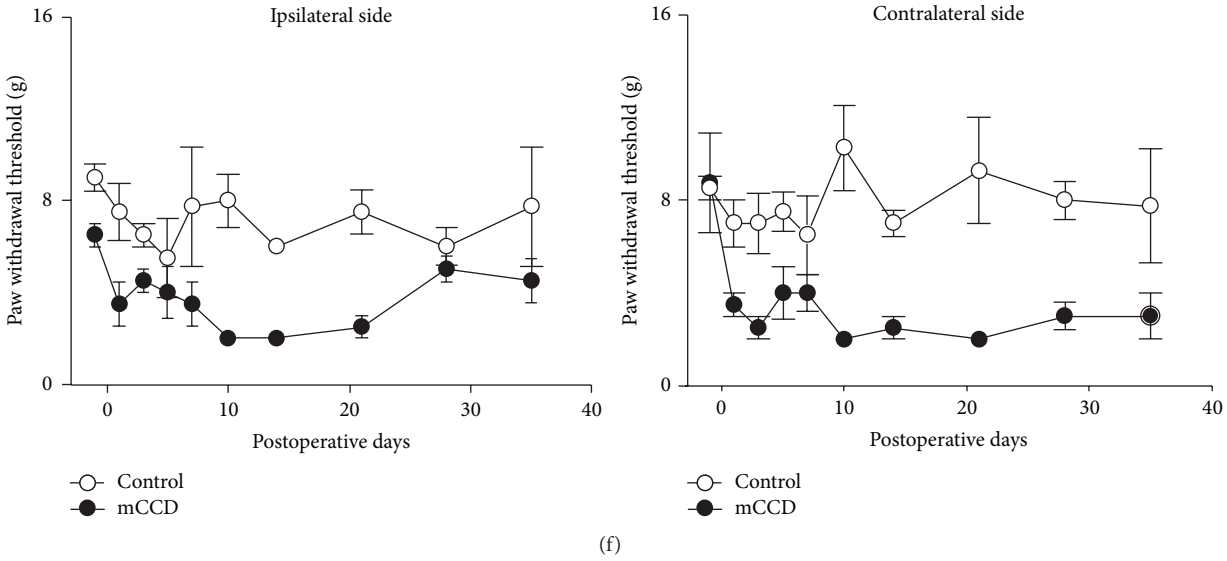

Figure 2: Behaviors of spontaneous pain, mechanical allodynia, and hyperalgesia recorded in mCCD rats. (a) The increase of the number of "wet-dog shaking" (WDS) behaviors at different time points after the mCCD (RM ANOVA, $P < 0.01$). (b) The increase of the number of shrinking bilateral hind paws at different time points after the mCCD (RM ANOVA, $P < 0.01$). (c) Hind paw withdrawal thresholds were markedly decreased bilaterally after the chronic compression ($n = 29$) compared to those of control ($n = 35$) and sham groups ($n = 6$) (on 10th postoperative day, one-way ANOVA followed by Bonferroni tests, $^{**}P$s < 0.01 compared to those of control group, $^{\#\#}P$s < 0.01 compared to those of sham group). (d) Stimulus response curves of ipsilateral and contralateral hind paws to von Frey filaments. Following the chronic compression of multiple DRGs ($n = 10$), the stimulus response curves of both hind paws were markedly shifted to the left compared to those of the control group ($n = 6$) (general line model, all Ps < 0.05), and there was an obvious significant increase in the response frequency to 2.0 and 6.0 g von Frey filaments (nonnoxious mechanical stimuli) of both the ipsilateral and contralateral sides (Bonferroni test, Ps < 0.01). There was also a significant increase in the response to 8.0 and 10.0 g von Frey filaments (which were noxious mechanical stimuli) bilaterally (Bonferroni test, Ps < 0.01). (e) The time course of ipsilateral and contralateral hind paw mechanical withdrawal thresholds after chronic compression of multiple DRGs (mCCD group: $n = 29$; control group: $n = 35$; sham group: $n = 6$). The ipsilateral hind paw withdrawal thresholds were decreased significantly below baseline on the 1st postoperative day and remained low throughout the entire testing period (RM ANOVA, Ps < 0.01). Contralateral mechanical thresholds were similarly decreased to a lesser extent on the 1st postoperative day, reached their lowest peak during the 10th to 14th postoperative day (RM ANOVA, Ps < 0.05), and recovered to basal levels thereafter. (f) Bilateral mechanical hypersensitization occurred in bilateral forepaws in the mCCD rat (mCCD group: $n = 4$; control group: $n = 4$; RM ANOVA, Ps < 0.05).

compression of multiple DRGs, 6 sham rats, and 80 control naive rats without any surgery appeared in good health. Rats were awake within several minutes after anesthesia was terminated and responsive an hour later. They gained weight during the test period and were well groomed and exhibited no self-inflicted wounds. Three hours after the compression of multiple DRGs, rats exhibited a marked guarding behavior of leaning to the healthy side to minimize weight bearing of the injured hind paw. This phenomenon lasted throughout the observation period (the longest period was 42 days) of the present study. Videotape analysis confirmed that the incidence of wet-dog shaking (WDS) was significantly increased on postoperative days 1, 3, 5, 7, 14, 21, 28, 35, and 42, respectively, compared to those of normal control rats (mCCD group: $n = 8$; control group: $n = 8$; Figure 2(a), RM ANOVA, $P < 0.01$). Moreover, spontaneous lifting of bilateral feet was increased for mCCD rats at all time points and statistically significantly different to those of normal rats at day 1 to day 42 compared to those of normal control rats (mCCD group: $n = 8$; control group: $n = 8$; Figure 2(b), RM ANOVA, $P < 0.01$). No rats in any groups exhibited the autotomy that could occur after nerve transection.

3.2. Bilateral Mechanical Allodynia and Hyperalgesia. Withdrawal thresholds to mechanical stimulation of the plantar surface of the hind paws were examined in mCCD rats ($n = 29$) on days 1, 3, 5, 7, 10, 14, 21, 28, and 35, postoperatively, and in normal control animals ($n = 35$). This increase in mechanical sensitivity was reflected in the large bilateral decrease in the hind paw withdrawal thresholds (defined as the minimum bending force required to elicit 50% response incidence) after the mCCD (Figure 2(c), ipsilateral: 4.0 ± 0.4 g; contralateral: 6.0 ± 0.5 g, day 10 compared to those of the control and sham groups) (Figure 2(c), control group: ipsilateral side, one-way ANOVA followed by Bonferroni test, $P < 0.01$, contralateral side, one-way ANOVA followed by Bonferroni test, $P < 0.01$; sham group: ipsilateral side, one-way ANOVA followed by Bonferroni test, $P < 0.01$, contralateral side, one-way ANOVA followed by Bonferroni test, $P < 0.01$). In control animals ($n = 35$), hind paw mechanical withdrawal thresholds were 9.7 ± 0.4 g (left side) and 9.9 ± 0.5 g (right side), and there was no significant difference between sides (Figure 2(c), one-way ANOVA followed by Bonferroni test, $P > 0.05$). Similarly, hind paw mechanical withdrawal thresholds were 10.7 ± 1.4 g

(left side) and 11.3 ± 1.2 g (right side), and there was no significant difference between sides (Figure 2(c), one-way ANOVA followed by Bonferroni test, $P > 0.05$). The mean incidence of left and right hind paw withdrawal responses to von Frey filament stimulation increased monotonically with increases in bending force within the range of 2.0 to 10.0 g (Figure 2(d)). There were statistically significant interactions between every two factors of sides, groups, and intensities (general line model, all Ps < 0.05). There was no significant difference in the mechanical sensitivity between hind paws preoperatively (Figure 2(d), Bonferroni test, $P > 0.05$). Following the chronic compression of multiple DRGs, the stimulus response curves of both the left (ipsilateral) and right (contralateral) hind paws were markedly shifted to the left compared to those of the control group (Figure 2(d), day 10, Bonferroni test, Ps < 0.05). The increase in mechanical sensitivity was significant for 2.0 and 6.0 g von Frey filaments (nonnoxious mechanical stimuli) bilaterally (Figure 2(d), Bonferroni test, Ps < 0.01). Moreover, the increase in the response frequency was significant for 8.0 and 10.0 g von Frey filaments (which were noxious mechanical stimuli) as well, for both the ipsilateral and contralateral sides (Figure 2(d), Bonferroni test, Ps < 0.01). The time course of mechanical withdrawal thresholds of the ipsilateral and contralateral hind paws following the mCCD was shown in Figure 2(e). Following the mCCD, the withdrawal thresholds of the ipsilateral hind paw decreased significantly on the 1st postoperative day and remained below baseline throughout the entire testing period (Figure 2(e), RM ANOVA, $P < 0.01$). The contralateral mechanical thresholds decreased but to a lesser extent starting on the 1st postoperative day. Contralateral mechanical sensitivity peaked 10 to 14 days postoperatively and subsequently recovered to the basal preoperative levels by day 35 (Figure 2(e), RM ANOVA, $P < 0.05$). There was also significant difference between ipsilateral and contralateral mechanical sensitivity in the mCCD (one-way ANOVA followed by Bonferroni test, $P < 0.01$). In contrast, hind paw mechanical withdrawal thresholds did not significantly change in control rats throughout the testing period (Figure 2(e), RM ANOVA, $P > 0.05$). Similarly, the trend of bilateral mechanical hypersensitization occurred in bilateral forepaws in the mCCD rat (mCCD group: $n = 4$; control group: $n = 4$; Figure 2(f), RM ANOVA, $P < 0.05$).

3.3. Bilateral Thermal Hyperalgesia. Hind paw withdrawal latencies (PWLs) to radiant thermal stimulation were examined in normal and mCCD rats (on presurgical and testing/postoperative days 1, 3, 5, 7, 10, 14, and 21, resp.) and analyzed separately for each hind paw (Figure 3(a)). Before surgery, the mean latencies were 12.0 ± 0.4 s (left side, $n = 14$) and 11.9 ± 0.5 s (right side, $n = 14$), and no significant difference was observed between the 2 sides (one-way ANOVA followed by Bonferroni test, $P > 0.05$). Following the chronic compression of multiple DRGs, the ipsilateral hind paw withdrawal latencies were transiently decreased from postoperative day 1 to day 14 (RM ANOVA, $P < 0.001$) that subsequently recovered to the basal preoperative levels on postoperative day 21 compared to that of control rats. The contralateral hind paw thermal latencies exhibited a delayed decrease from postoperative day 3 and returned to the baseline on postoperative day 21. There was also a significant difference between ipsilateral and contralateral thermal sensitivity in the mCCD (one-way ANOVA followed by Bonferroni test, $P < 0.01$). In contrast, hind paw withdrawal latencies did not significantly change in control rats throughout the testing period ($n = 7$, RM ANOVAs, $P > 0.05$) and there were no significant differences between thermal withdrawal latencies of left and right hind paws in control rats (one-way ANOVA followed by Bonferroni test, $P > 0.05$). However, there were no significant differences in either ipsilateral or contralateral thermal sensitivity of forepaws in the mCCD on postoperative days 8 and 15 compared to those of control rats (mCCD group: $n = 4$; control group: $n = 4$; Figure 3(b), RM ANOVAs, Ps > 0.05).

3.4. Bilateral Cold Allodynia. Cold sensitivities of the ipsilateral and contralateral hind paws to acetone were tested prior to surgery and on day 10 after the mCCD. Before surgery, cold allodynic response scores of the hind paws to acetone were 0.8 ± 0.1 (left, $n = 16$) and 0.9 ± 0.1 (right, $n = 16$), and no significant difference existed between the left and right sides (Figure 3(c), one-way ANOVA followed by Bonferroni test, $P > 0.05$). Similarly, there was no significant difference in the cold allodynia response frequencies between the two hind paws (Figure 3(d), 0.5 ± 0.1 (left, $n = 16$) and 0.6 ± 0.1 (right, $n = 16$), one-way ANOVA followed by Bonferroni test, $P > 0.05$). After the chronic compression of multiple DRGs, both ipsilateral and contralateral response scores to acetone were markedly increased when compared with the control group (Figure 3(c), ipsilateral: 2.1 ± 0.1, $n = 16$, one-way ANOVA followed by Bonferroni test, $P < 0.01$; contralateral: 1.6 ± 0.2, $n = 16$, one-way ANOVA followed by Bonferroni test, $P < 0.01$). There was no significant difference between ipsilateral and contralateral response scores to acetone in mCCD rats. Similarly, allodynic response frequencies of both ipsilateral and contralateral hind paws were significantly increased in chronically compressed rats (Figure 3(d), ipsilateral: 0.9 ± 0.1, $n = 16$, one-way ANOVA followed by Bonferroni test, $P < 0.01$; contralateral: 0.8 ± 0.1, $n = 16$, one-way ANOVA followed by Bonferroni test, $P < 0.01$, compared to that of control group). There was no significant difference between ipsilateral and contralateral cold response scores and frequencies in the mCCD (one-way ANOVA followed by Bonferroni test, Ps > 0.05).

3.5. Thermal Preference to a Low-Temperature Plate between 30 and 35°Cs. On 25°C and 30°C plates, mCCD ($n = 3$) and control ($n = 4$) rats preferred staying on 30°C plates (Figure 4(a), repeated measures analysis of variance, $P < 0.01$). MCCD rats preferred spending significantly more time on the less hot (30°C) side of plate than control naive rats on 35°C plates (Figure 4(b), repeated measures analysis of variance, $P < 0.01$), whereas mCCD and control rats responded the same and preferred staying on 35°C plate on either 35°C or 40°C plates (Figure 4(c), repeated measures analysis of variance, $P < 0.01$). All these trends were not changed during the period of postoperative days 1 to 42.

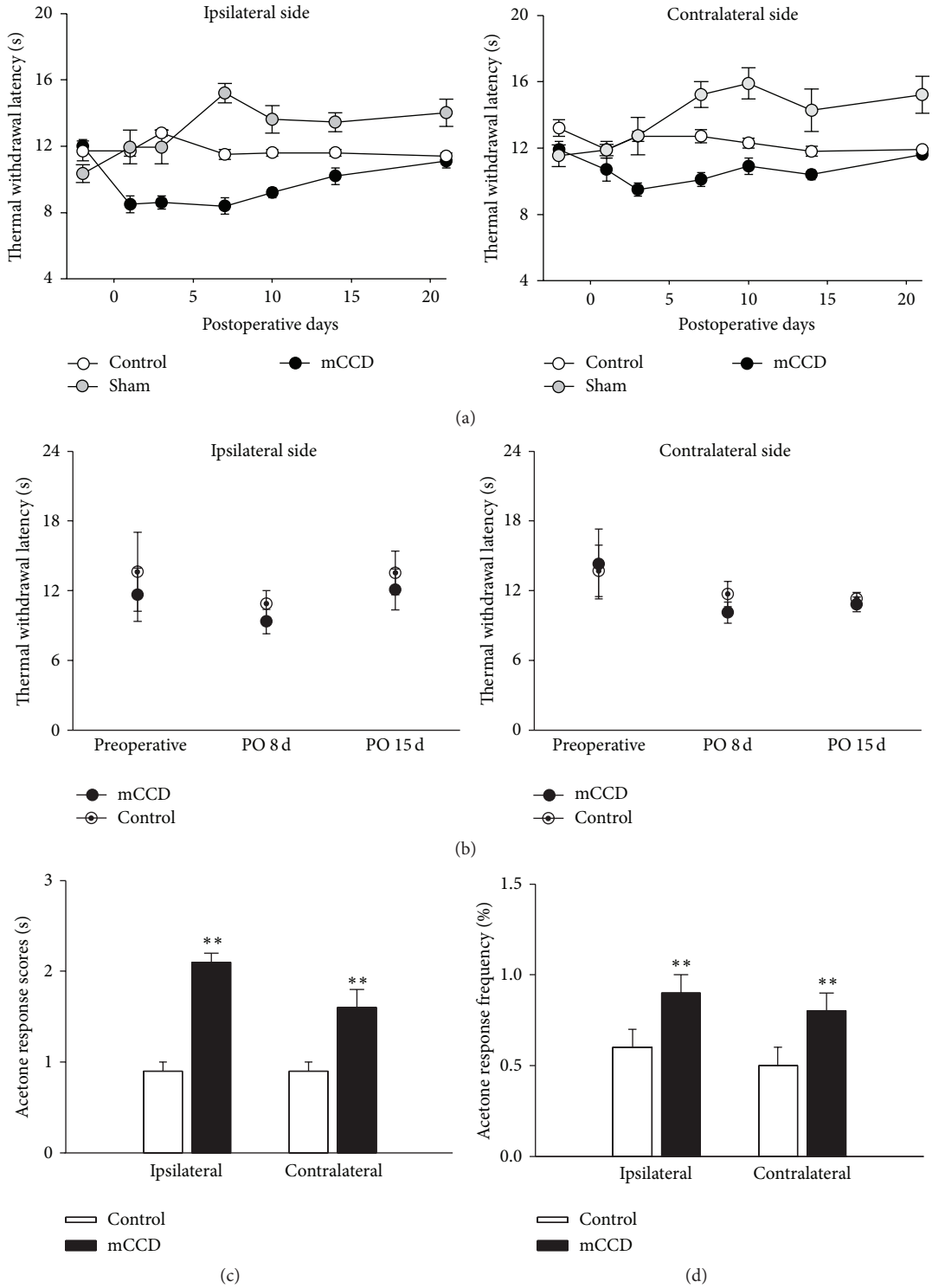

Figure 3: Thermal hyperalgesia and cold allodynic behaviors in the mCCD rat. (a) The time course of ipsilateral and contralateral hind paw withdrawal latencies to radiant thermal stimulation in mCCD ($n = 8$) and control rats ($n = 8$). Following the chronic compression of multiple DRGs, ipsilateral and contralateral hind paw withdrawal latencies were transiently decreased from the 1st postoperative day to postoperative day 21 compared to those of control groups (RM ANOVA, ipsilateral side: $P < 0.05$; contralateral side: $P < 0.05$). After 21 days, hind paw withdrawal latencies recovered to the baseline preoperative levels. (b) The time course of ipsilateral and contralateral forepaw withdrawal latencies to radiant thermal stimulation in mCCD ($n = 4$) and control rats ($n = 4$). No significant changes in either ipsilateral or contralateral forepaw withdrawal latencies in the mCCD rat (RM ANOVA, Ps > 0.05). (c) Response scores of the ipsilateral and contralateral hind paws to acetone in control ($n = 23$) and mCCD ($n = 16$) rats. Both ipsilateral and contralateral response scores to acetone increased after the chronic compression of multiple DRGs compared with the control group (one-way ANOVA followed by Bonferroni test, ipsilateral: $P < 0.001$; contralateral: $P < 0.01$). (d) Response frequencies of the ipsilateral and contralateral hind paws to acetone in control and mCCD rats. Cold allodynic response frequencies of both ipsilateral and contralateral hind paws were significantly increased in chronically compressed rats compared to that of the control group (one-way ANOVA followed by Bonferroni test, ipsilateral: $P < 0.01$; contralateral: $P < 0.01$).

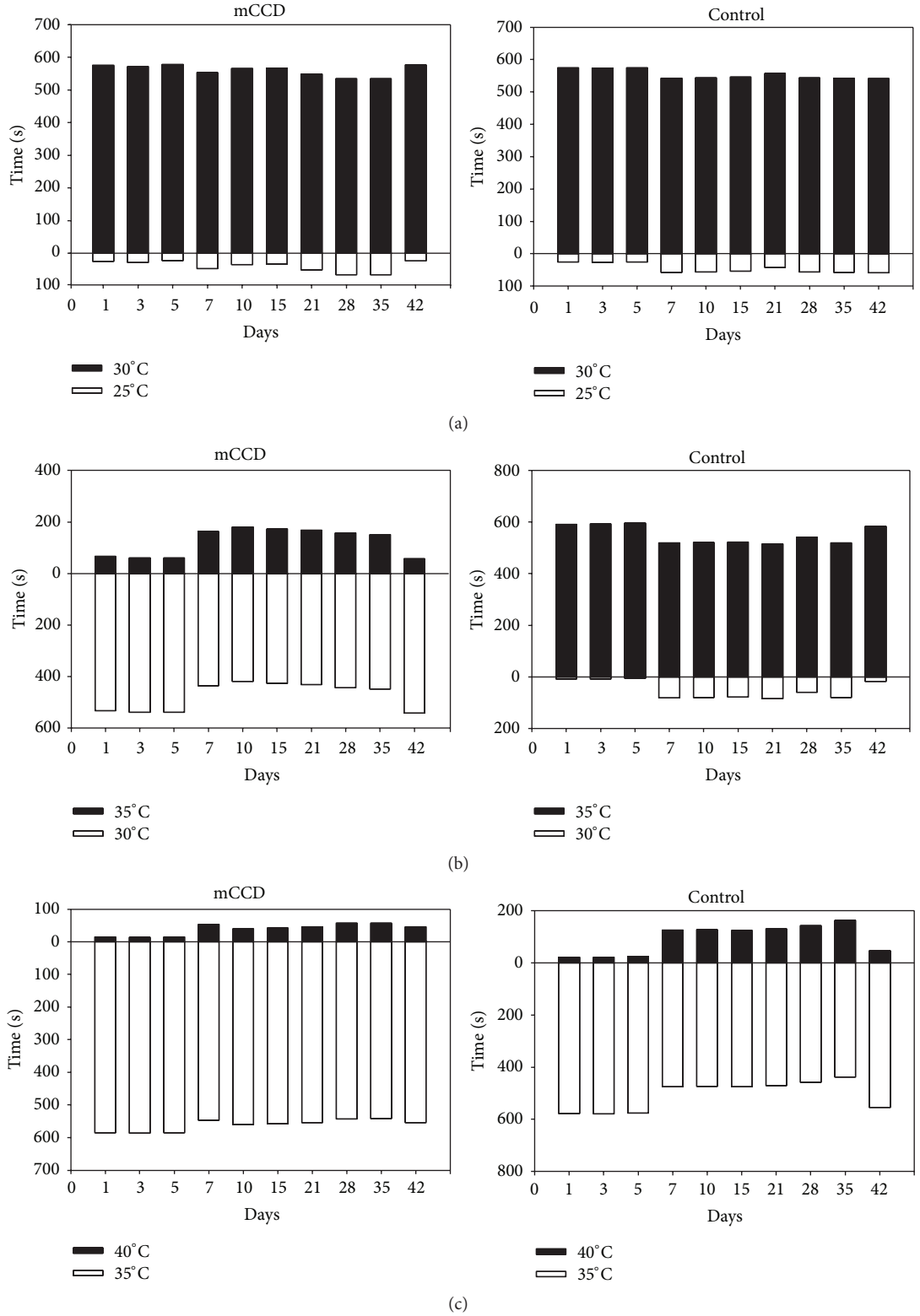

Figure 4: Decreased thermal preference to 30°C plate during the range of 30 and 35°C in mCCD rats. (a) Similar thermal preference of 30°C between control and mCCD rats to the temperature of 25 and 30°C (two-way ANOVA, $P < 0.01$). (b) Decreased thermal preference to 30°C of thermal preference in mCCD to the temperature of 30 and 35°C (two-way ANOVA, $P < 0.01$). (c) Similar thermal preference of 35°C between control and mCCD rats to the temperature of 35 and 40°C (two-way ANOVA, $P < 0.01$).

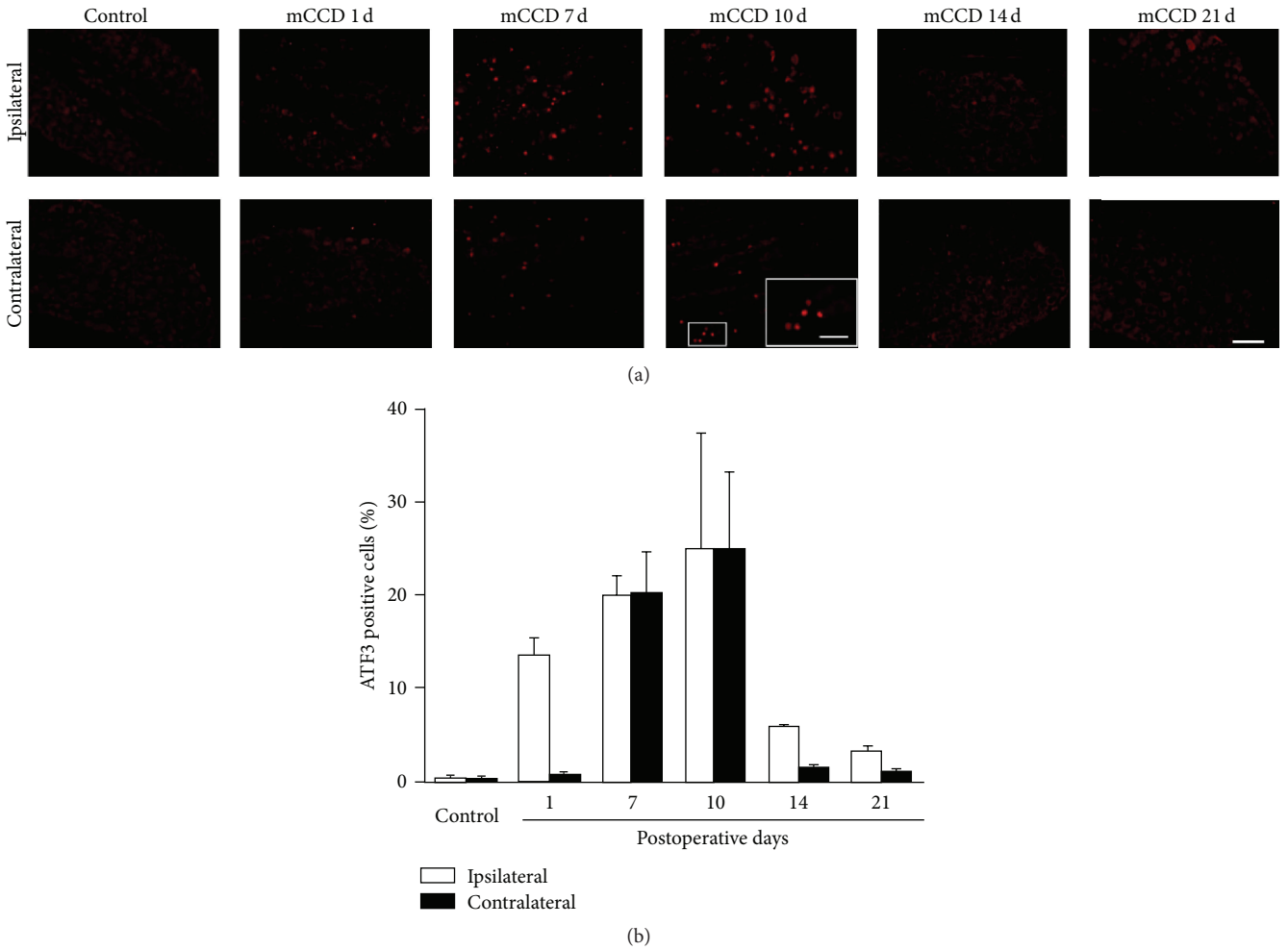

Figure 5: ATF3 expression was markedly increased in both ipsilateral and contralateral DRG neurons following the mCCD. (a) ATF3 expression in ipsilateral and contralateral DRGs in control and mCCD rats on 1st, 7th, 10th, 14th, and 21st postoperative days (inset: higher magnification, scale bar = 20 μm). (b) Percentage of ATF3 positive cells in ipsilateral and contralateral DRGs following the multiple DRG compression. Scale bar = 50 μm. Bonferroni test, Ps < 0.001, compared to the bilateral DRG neurons of control rats.

3.6. The ATF3 Expression in Ipsilateral and Contralateral DRGs. Following the mCCD, ATF3 expression was investigated in ipsilateral and contralateral DRGs postoperatively on days 1, 7, 10, 14, and 21. Before the surgery, in normal naive rats, which were not treated, ATF3 was investigated in L3–L5 DRGs at the starting day. There was hardly any expression of ATF3 in L3–L5 DRG neurons (Figure 4(a)). No significant difference in the expression of ATF3 was detected between the L3–L5 DRGs (data not shown). There were no statistically significant interactions between the factors of sides and days and the factors of sides and immunostaining markers (Figures 5–8, general line model, all Ps > 0.05); however, there were statistically significant interactions between the factors of immunostaining markers and days (Figures 5(a) and 5(b), general line model, $P < 0.001$). Following the mCCD, the expression of ATF3 markedly increased in both ipsilateral and contralateral L3–L5 DRG neurons on postoperative days 1, 7, 10, and 14 (Figures 5(a) and 5(b), Bonferroni tests, Ps < 0.001), and there was no statistical significance between the ATF3 expressions of the ipsilateral and contralateral DRGs (Figures 5(a) and 5(b), Bonferroni test, $P > 0.05$). For a side there was no difference in the expression of ATF3 among the L3, L4, and L5 DRGs (data not shown). A significant increase of ATF3 expression in bilateral DRG neurons gradually decreased to a low level on day 21 (Figures 5(a) and 5(b), Bonferroni tests, Ps > 0.05). There was a trend of delayed increase in ATF3 expression of contralateral DRGs compared to that of ipsilateral DRGs.

Immunostaining with NF200, to label large- and medium-sized DRG cells, and peripherin, to identify small-sized DRG neurons, was used to further investigate which cell types were expressing ATF3 following the mCCD. In normal control rats, there was little expression of ATF3 in large- and medium-sized DRG neurons in L3–L5 DRGs and no difference was detected in the ATF3 expression between sides (Figure 6, Bonferroni test, $P > 0.05$). Following the mCCD, the expression of ATF3 was markedly increased in ipsilateral large- and medium-sized DRG neurons (day 10, shown in Figure 6(a)) and reached a peak on day 10 and gradually decreased to a stable level till day 14 (Bonferroni

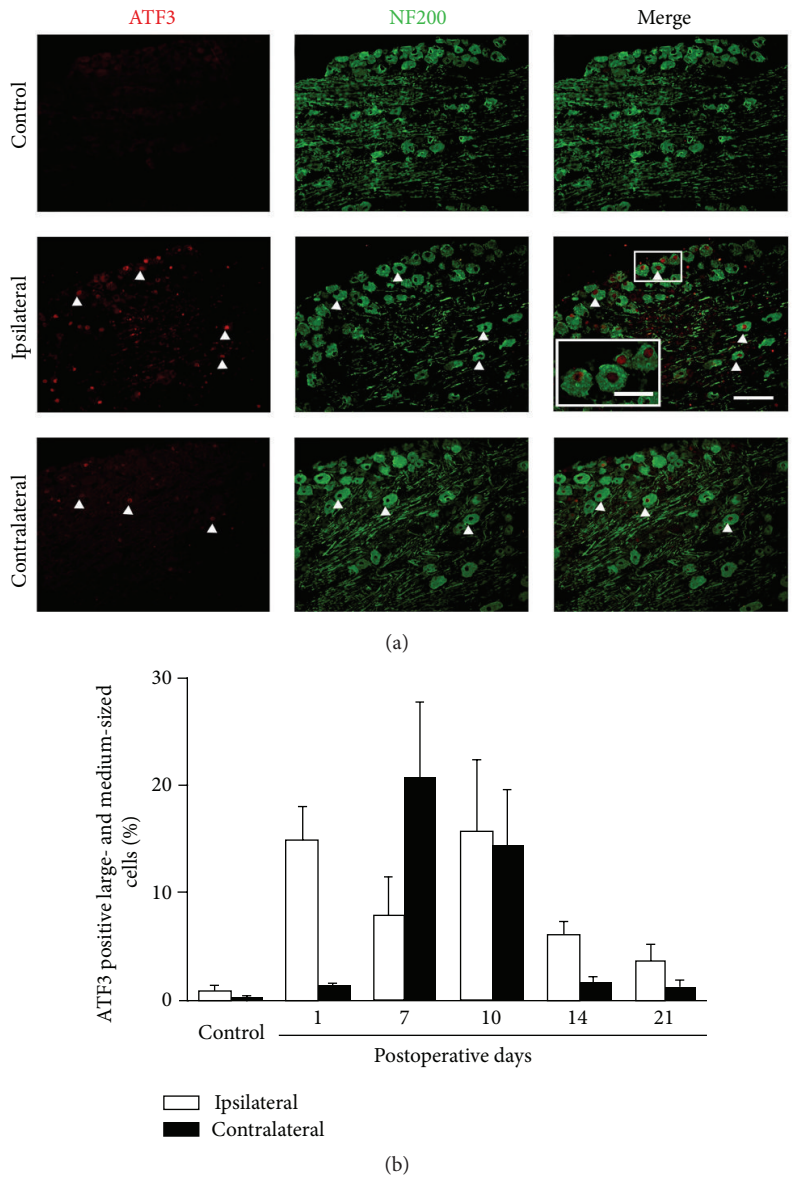

Figure 6: Increased ATF3 expressions in ipsilateral and contralateral large- and medium-sized DRG neurons following the mCCD. (a) ATF3 expression in ipsilateral large- and medium-sized DRG neurons of control rats. (b) ATF3 expression in ipsilateral large- and medium-sized DRG neurons at day 10 after mCCD surgery. C, ATF3 expression in contralateral large- and medium-sized DRG neurons at day 10 after mCCD surgery (inset: higher magnification, scale bar = 20 μm). D, Percentage of ATF3 positive cells in ipsilateral and contralateral large- and medium-sized DRG neurons in control and on the 1st, 7th, 10th, 14th, and 21st postoperative days. Scale bar = 50 μm (a–C). Bonferroni test, Ps < 0.001, compared to the bilateral DRG neurons of control rats.

test, $P < 0.001$). The expression of ATF3 was significantly increased in contralateral large- and medium-sized DRG neurons on day 7, reached the peak on day 10 (Bonferroni test, $P < 0.001$), and gradually decreased to a low level on day 21 (Bonferroni test, $P > 0.05$). A trend of delayed increase in contralateral large- and medium-sized and small-sized DRG neurons occurred compared to the expression of ipsilateral DRG neurons following the chronic compression of the DRGs.

In small-sized DRG cells, the expression of ATF3 was significantly increased in ipsilateral DRG neurons on day 1, reached a peak on day 7, and gradually decreased to a stable level till day 14 (Figure 7, Bonferroni test, $P < 0.001$), which then returned to basal levels on day 21 (Figure 7, Bonferroni test, $P > 0.05$). In the contralateral small-sized DRG neurons, the expression of ATF3 was markedly increased on day 7, was decreased on day 14 (Figure 7, Bonferroni test, $P < 0.001$), and was returned to basal levels by day 14 (Figure 7, Bonferroni test, $P > 0.05$).

3.7. The CGRP Expression in Ipsilateral and Contralateral DRGs. Following the mCCD, the expression of CGRP, a neuropeptide related to nociceptive information transmission, was investigated in ipsilateral and contralateral DRGs on

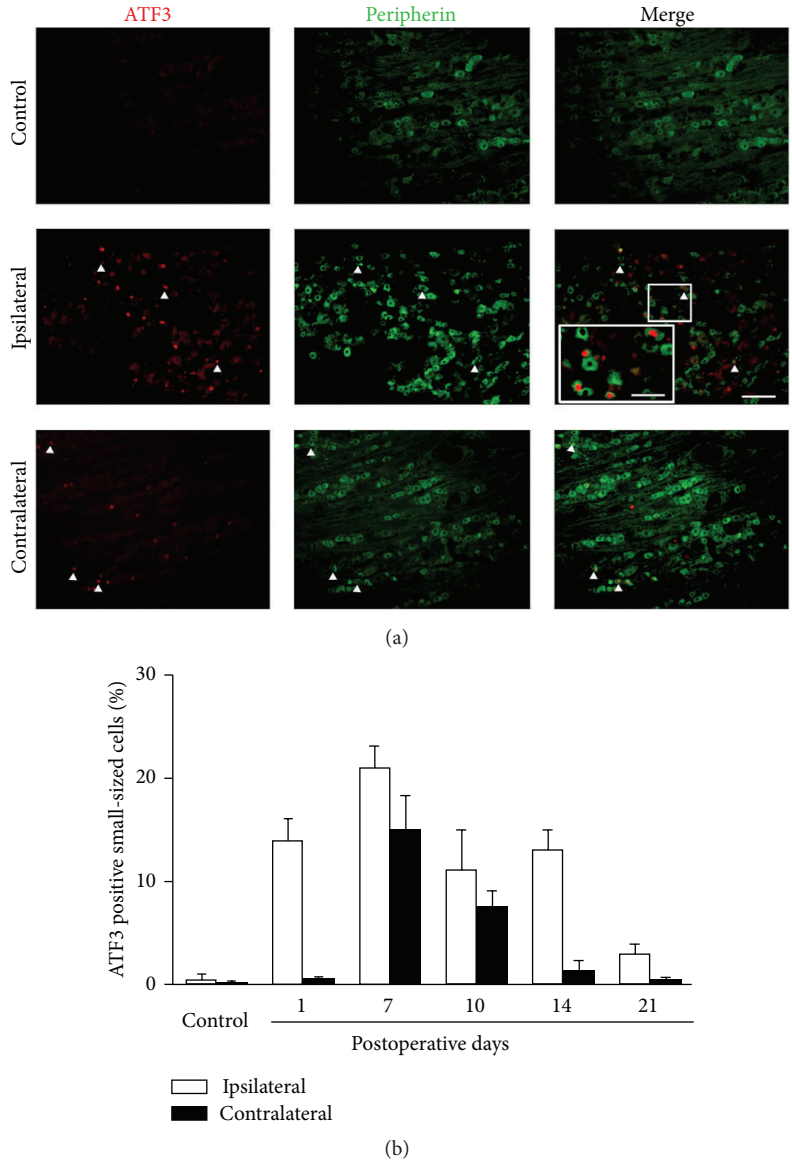

Figure 7: Increased ATF3 expressions in ipsilateral and contralateral small-sized DRG neurons following the mCCD. (a) ATF3 expression in ipsilateral small-sized DRG neurons of control rats. (b) ATF3 expression in ipsilateral small-sized DRG neurons at day 10 after mCCD surgery. C, ATF3 expression in contralateral small-sized DRG neurons at day 10 after mCCD surgery (inset: higher magnification, scale bar = 20 μm). D, The percentage of ATF3 positive cells in ipsilateral and contralateral small-sized DRG neurons in control and on the 1st, 7th, 10th, 14th, and 21st postoperative days. Scale bar = 50 μm (a–C). Bonferroni test, $P < 0.001$, compared to the bilateral DRG neurons of control rats.

postoperative days 1, 7, 10, 14, and 21. In normal control rats, 30% of the lumbar DRG neurons expressed CGRP (Figure 8). There was no marked difference in the CGRP expression between the L3–L5 DRG neurons (data not shown). Compared with the control group, the expression of CGRP significantly was increased in both ipsilateral and contralateral DRGs after the mCCD (Figure 8(c), Bonferroni test, $P < 0.05$). An increase of CGRP expression in ipsilateral DRG neurons occurred rapidly on postoperative day 1 and remained at a high level through day 21 (Bonferroni test, $P < 0.001$). A similar increase of CGRP expression in contralateral DRG neurons occurred on postoperative day 7 and remained at a high level till day 21 (Bonferroni test, $P < 0.001$).

Following the mCCD, the expression of CGRP was markedly increased (day 10, shown in Figure 8(a)) in bilateral large- and medium-sized DRG neurons and reached a peak on day 10 and gradually decreased to a stable level till day 21 (Bonferroni test, $P < 0.001$). A trend of decrease of CGRP expression in ipsilateral small-sized DRG neurons occurred rapidly on postoperative day 1 and remained at a low level through day 21 (Bonferroni test, $P < 0.001$). A trend of a delayed increase of CGRP expression in contralateral small-sized DRG neurons occurred on postoperative day 14 and remained at a high level till day 21 (Bonferroni test, $P < 0.001$).

The extent of neuronal injury was measured by the expression of ATF3 in the DRGs in order to investigate

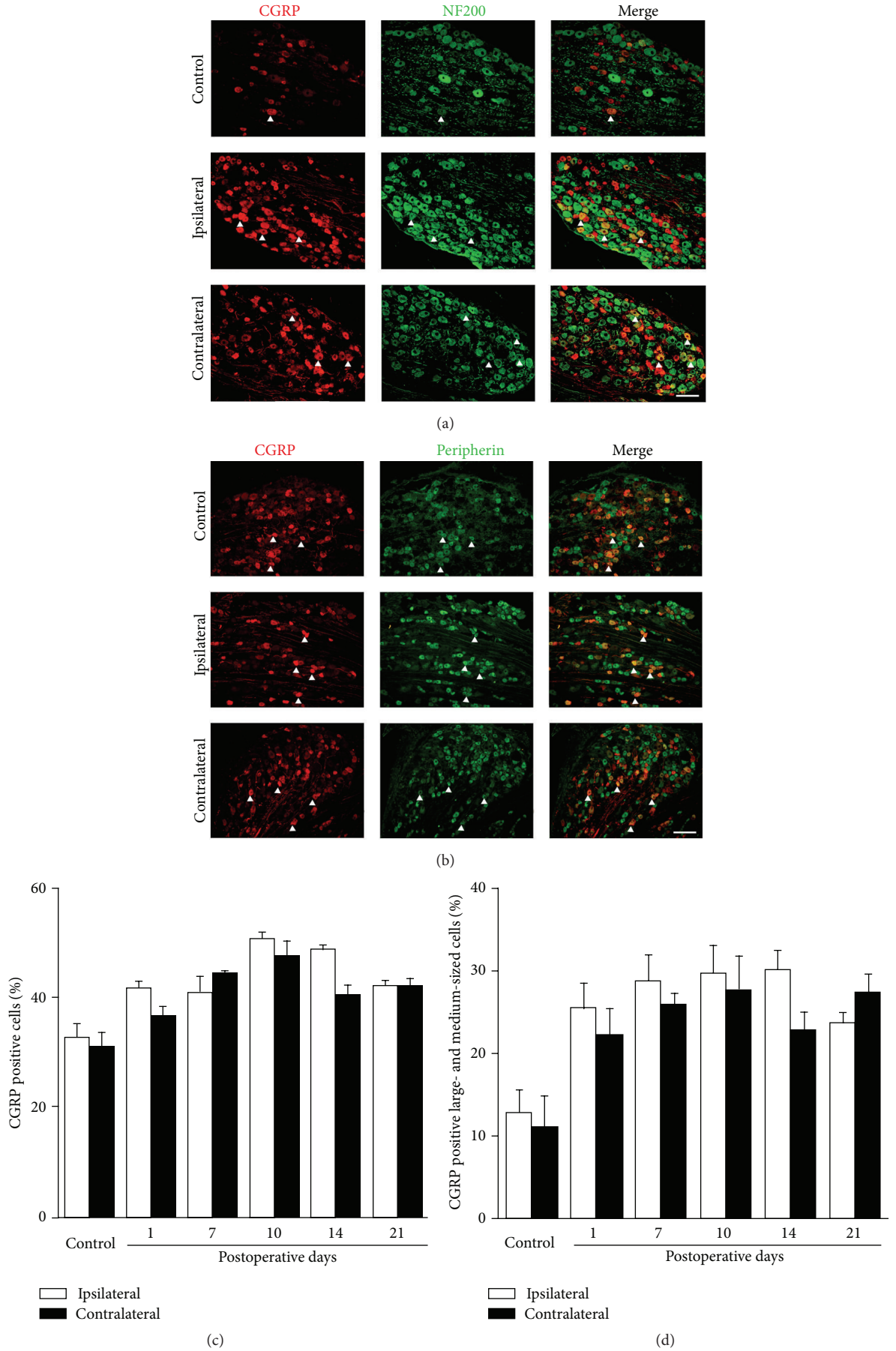

Figure 8: Continued.

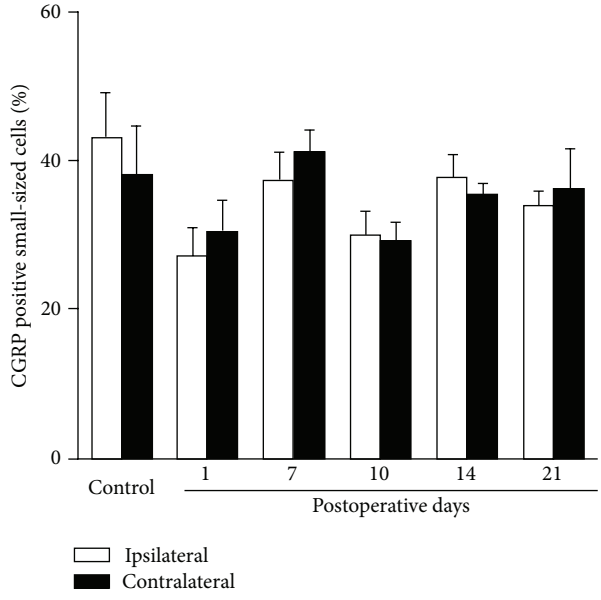

Figure 8: CGRP expression was significantly increased in large- and medium-sized neurons but not in small-sized neurons in ipsilateral and contralateral DRGs following the mCCD. (a) CGRP expression in ipsilateral large- and medium-sized DRG neurons in control and mCCD rats (on 10th postoperative day, inset: higher magnification, scale bar = 20 μm). (b) CGRP expression in ipsilateral small-sized DRG neurons in control and mCCD rats (on 10th postoperative day; inset: higher magnification, scale bar = 20 μm). (c) Percentage of CGRP positive cells in ipsilateral and contralateral DRGs following the multiple DRG compression on the 1st, 7th, 10th, 14th, and 21st postoperative day. (d) The percentage of CGRP positive cells in ipsilateral and contralateral large- and medium-sized DRG neurons was significantly increased following the chronic compression of DRGs. (e) The percentage of CGRP positive small-sized neurons in ipsilateral and contralateral DRGs was significantly increased following the chronic compression of DRGs. Scale bar = 50 μm (a-b). Bonferroni test, Ps < 0.001, compared to the bilateral DRG neurons of control rats.

the relationship of the expression of pain behaviors to neuronal injury after the mCCD ($n = 5$). Linear regression lines relating the extent of hypersensitive behaviors and the percentages of ATF3 positive DRG neurons were almost perfectly superimposed for the bilateral mechanical and cold allodynia (Supplementary Figures 1A and 1B, linear regression analysis, Ps < 0.05). The results indicated a strong influence of the number of damaged sensory neurons on the bilateral allodynic behaviors on 1st postoperative day (Supplementary Figure 1, $P < 0.05$). Similarly, significant correlations between the expression of CGRP in the DRGs and evoked pain hypersensitive behaviors were observed after the chronic compression of multiple DRGs. The extents of evoked pain hypersensitive behaviors (mechanical and cold allodynia) were positively correlated with the CGRP expression in both ipsilateral and contralateral DRG neurons ($n = 5$, Supplementary Figures 2A and 2B), indicating an influence of the number of sensory neurons conducting nociceptive information on evoked pain behaviors.

4. Discussion

Our study showed that mCCD rats exhibited spontaneous pain, contralateral mechanical allodynia, mechanical and thermal hyperalgesia, and cold allodynia similar to the ipsilateral hypersensitivity, as well as thermal allodynia. Moreover, the expression of ATF3 and CGRP was upregulated in ipsilateral and contralateral DRGs. The extent of evoked mechanical and cold allodynia was positively correlated with the upregulated expression of ATF3, a neural injury marker, and CGRP, a marker of nociceptive information transmission, in bilateral DRG neurons, respectively.

4.1. Behavioral Signs of Spontaneous Pain and Bilateral Hypersensitivities. Spontaneous pain is a very serious symptom in patients with neuropathic pain. One proposed biomarker of spontaneous pain is autotomy, a behavior frequently observed in rats with complete hind paw denervation or neuroma models [10, 11], but this rarely occurs in models of partial paw denervation, such as SNL and partially sciatic ligation [12, 13]. In the present study, there were marked and rapid increases of the numbers of wet-dog shaking and spontaneous hind paw shrinking behaviors following the mCCD, indicating that mCCD rats developed a rapid and lasting spontaneous pain in addition to the evoked pain behaviors, but without autotomy. This is the first time the spontaneous pain in the mCCD rat is reported. Our results showed that the increased change of bilateral spontaneous toe shrinking behavior lasted till postoperative day 42 and resembled the change of wet-dog shaking behavior after the mCCD. It is also suggested that bilateral spontaneous hind paw shrinking behaviors were able to be used to evaluate spontaneous pain of the rat.

It is interesting to note that the mCCD model displayed early and long-lasting contralateral mechanical allodynia and

hyperalgesia in addition to ipsilateral allodynia and hyperalgesia, which differs from the CCD model of a single DRG [2, 3], and the contralateral hypersensitivity occurred earlier and to a greater extent compared to the CCD model [14]. Moreover, the contralateral mechanical allodynia occurred not only in hind paws but also in forepaws, indicating that a supraspinal mechanism might be involved in the mCCD rat. In addition, contralateral mechanical allodynia and hyperalgesia were much less strong than ipsilateral evoked pain behaviors. Contralateral mechanical allodynia has been shown in animal models of neuropathic and inflammatory pain, including unilateral spinal nerve ligated rats [13, 15] and the spared nerve injury model [16]. Similarly, significant contralateral mechanical hyperalgesia and allodynia have been also reported in the ultraviolet- (UV-) B irradiated inflammation model [17]. Previous studies provided evidence that the duration and intensity of bilateral pain are dependent on the severity of the neural injury [18–20]. Our present data showed that significant increased expression of ATF3 was observed in all-sized neurons in the ipsilateral and contralateral DRGs in the mCCD rat. Increased ATF3 expression was more delayed in contralateral DRGs on postoperative day 7 compared to that of ipsilateral DRGs. This significant increased expression of ATF3 was observed in all-sized neurons in the ipsilateral and contralateral DRGs. Furthermore, there were significant correlations between ATF3 expression and evoked pain behaviors such as mechanical and cold allodynia on postoperative day 1. Our results suggested that both ipsilateral and contralateral neuronal damage in the periphery might contribute to bilateral mechanical and cold allodynia in the mCCD rat. Those results were consistent with contralateral neuropathology of the DRG in a rat model of noncompressive disc herniation [4]. This might be a reason that marked bilateral mechanical allodynia and hyperalgesia developed due to the extensive neuronal damage of ipsilateral and contralateral DRGs after the mCCD, while there were no or mild contralateral allodynia and hyperalgesia in the CCD model because of the single DRG affected.

The mCCD rat exhibited delayed and transient contralateral thermal hyperalgesia in the hind paws on postoperative day 3 that lasted up to 14 days, inconsistent with the results described after lumbar 5 ventral root transection of the rat lasting for a long period [21]. The phenomenon did not happen in the forepaws. This result indicated that peripheral or spinal mechanisms might contribute to contralateral heat hyperalgesia. In addition, bilateral cold allodynia occurs in the mCCD rat as well. Cold allodynia is one of the most common symptoms among sympathetic-maintained pain patients. Up till now, there were few animal models that display this phenomenon. Contralateral cold allodynia was shown for the L4 and L5 SNL model, but not for the L5 SNL model [9, 22]. This suggests contralateral cold allodynia possibly correlates with the extent of peripheral neuropathy. Our results also showed mCCD rats exhibited a decreased thermal preference. Taken together, the mCCD rat exhibits many characteristics of bilateral hypersensitivity including mechanical, cold, and thermal allodynia and thermal hyperalgesia as well.

4.2. Peripheral Mechanism of Contralateral Hypersensitivity. Previous studies demonstrated that hyperexcitability of DRG neurons was involved in the development or maintenance of chronic neuropathic pain [23]. Plastic changes of DRG neurons generate ectopic afferent signals to induce abnormal sensory processing and further bombard spinal or supraspinal structure to result in central sensitization in chronic pain condition. Our study showed that ATF3 expression was markedly and rapidly increased in the contralateral uncompressed DRG neurons from postoperative day 1. It is very likely that primary sensory neurons became hyperexcitable due to peripheral neuronal damage, in turn contributing to the development and maintenance of contralateral hypersensitivity in the mCCD rat. Injury signals might be generated and transmitted from injured DRG neurons to the blood stream via neurotrophic factors or directly to the spinal cord where retrograde signals might be generated and transmitted from the spinal cord to the contralateral DRGs. Target-derived trophic factors from injured and degenerated DRG neurons and axons may be acting on DRG neurons in the contralateral ganglion via blood circulation. Potential trophic factors include neurotrophic growth factor and neurotrophin 3 [24].

Increasing evidence demonstrates that glial cell activation may be involved in the development and maintenance of bilateral pain [25, 26]. Although it is reported that ATF3 expression was upregulated in satellite cells of the DRG after an injury to the sciatic nerve [27], it was not observed in the present study. It is likely that the expression of ATF3 in satellite cells is much weaker than that in sensory neurons. Our study showed that CGRP expression was markedly and rapidly increased in the contralateral large- and medium-sized DRG neurons only after the mCCD. CGRP has been regarded as a signaling molecule mediating the interactions between damaged neurons and surrounding glial cells, and it activates both astrocytes and microglia at the transcriptional level [28, 29]. Thus, CGRP might be involved in the process of bilateral pain through the activation of astrocytes and microglia. This activation might be mediated through calcium waves or oscillations spread within astroglial networks that could then promote new synaptic connections in the spinal cord [30]. If so, strong signals from injured DRGs transmitted to the ipsilateral spinal cord may also amplify calcium waves or oscillations of astrocytes that then activate the contralateral spinal cord and finally spread to uncompressed DRGs.

Ectopic spontaneous activity of injured DRG neurons is involved in glial activation and the development of pathological pain [5, 31, 32]. It seems likely that peripheral satellite glial cells might be activated by the spontaneous activity of compressed DRG neurons and that the activation of glial cells might further contribute to bilateral pain following the chronic compression of multiple DRGs. Activated glia release proinflammatory cytokines, such as IL-1, IL-6, and TNF-alpha, which lead to further activation of glia and act as a secondary stimulus [33].

It is still not known whether the signaling of bilateral hypersensitivity operates primarily at the nociceptor, spinal, thalamic, or cerebral cortical levels. One speculation is that

the signaling may be mediated via the commissure tracts in the spinal cord, where signaling via interneurons is aided by growth factors such as the brain-derived neurotrophic factor (BDNF) and neurotrophin 3 [34]. Another possibility is that substances may be released from injured sensory neurons which carry a "pain message" to the brain, which promote bilateral descending pain facilitating pathways [35]. Further studies are necessary to investigate the origins of contralateral hypersensitivity in the central and peripheral systems.

5. Conclusions

Our results showed a contralateral hypersensitivity by the chronic compression of multiple DRGs and neuropathic changes in contralateral primary sensory neurons that may be involved in the induction and the maintenance of contralateral hypersensitivity including tactile allodynia, thermal hyperalgesia, and cold allodynia. Understanding signaling mechanisms and pathogenesis underlying contralateral sensitization, specifically in the case of chronic low back pain, will have novel therapeutic targets for the management of treatment of pain. Based on our study, one potential treatment site may target at the level of uncompressed contralateral sensory neurons, which might have some success in treating intractable phantom pain.

Conflict of Interests

None of the authors of this paper have a financial interest related to this work.

Authors' Contribution

Ya-Bin Xie, Huan Zhao, and Ying Wang contributed equally to this work.

Acknowledgments

This work was supported by grants from the National Natural Science Foundation of China (nos. 30870830 and 31371120 to Dr. Hui Xu), Chinese National Key Project for Basic Research (2011CB504402 to Dr. Si-Wei You), and Ministry of Education Foundation for Returned Overseas Students (HG3503 to Dr. Hui Xu). The authors would like to thank Dr. W. W. for technical help in spontaneous pain testing and Dr. L. S. for statistical analysis of all data.

References

[1] C. A. Briggs and S. Chandraraj, "Variations in the lumbosacral ligament and associated changes in the lumbosacral region resulting in compression of the fifth dorsal root ganglion and spinal nerve," *Clinical Anatomy*, vol. 8, no. 5, pp. 339–346, 1995.

[2] S.-J. Hu and J.-L. Xing, "An experimental model for chronic compression of dorsal root ganglion produced by intervertebral foramen stenosis in the rat," *Pain*, vol. 77, no. 1, pp. 15–23, 1998.

[3] X.-J. Song, S.-J. Hu, K. W. Greenquist, J.-M. Zhang, and R. H. LaMotte, "Mechanical and thermal hyperalgesia and ectopic neuronal discharge after chronic compression of dorsal root ganglia," *Journal of Neurophysiology*, vol. 82, no. 6, pp. 3347–3358, 1999.

[4] Y. Li, C. Xi, M. Niu et al., "Contralateral neuropathology in dorsal root ganglia in a rat model of noncompressive disc herniation," *Neuroscience Letters*, vol. 493, no. 1-2, pp. 49–54, 2011.

[5] L. Liang, Z. Wang, N. Lü, J. Yang, Y. Zhang, and Z. Zhao, "Involvement of nerve injury and activation of peripheral glial cells in tetanic sciatic stimulation-induced persistent pain in rats," *Journal of Neuroscience Research*, vol. 88, no. 13, pp. 2899–2910, 2010.

[6] H.-G. Schaible, "On the role of tachykinins and calcitonin gene-related peptide in the spinal mechanisms of nociception and in the induction and maintenance of inflammation-evoked hyperexcitability in spinal cord neurons (with special reference to nociception in joints)," *Progress in Brain Research*, vol. 113, pp. 423–441, 1996.

[7] K. Olmarker, "Puncture of a lumbar intervertebral disc induces changes in spontaneous pain behavior: an experimental study in rats," *Spine*, vol. 33, no. 8, pp. 850–855, 2008.

[8] S. R. Chaplan, F. W. Bach, J. W. Pogrel, J. M. Chung, and T. L. Yaksh, "Quantitative assessment of tactile allodynia in the rat paw," *Journal of Neuroscience Methods*, vol. 53, no. 1, pp. 55–63, 1994.

[9] Y. Choi, Y. W. Yoon, H. S. Na, S. H. Kim, and J. M. Chung, "Behavioral signs of ongoing pain and cold allodynia in a rat model of neuropathic pain," *Pain*, vol. 59, no. 3, pp. 369–376, 1994.

[10] P. Koplovitch, A. Minert, and M. Devor, "Spontaneous pain in partial nerve injury models of neuropathy and the role of nociceptive sensory cover," *Experimental Neurology*, vol. 236, no. 1, pp. 103–111, 2012.

[11] P. D. Wall, M. Devor, R. Inbal et al., "Autotomy following peripheral nerve lesions: experimental anesthesia dolorosa," *Pain*, vol. 7, no. 2, pp. 103–113, 1979.

[12] Z. Seltzer, R. Dubner, and Y. Shir, "A novel behavioral model of neuropathic pain disorders produced in rats by partial sciatic nerve injury," *Pain*, vol. 43, no. 2, pp. 205–218, 1990.

[13] S. H. Kim and J. M. Chung, "An experimental model for peripheral neuropathy produced by segmental spinal nerve ligation in the rat," *Pain*, vol. 50, no. 3, pp. 355–363, 1992.

[14] J.-M. Zhang, H. Li, and S. J. Brull, "Perfusion of the mechanically compressed lumbar ganglion with lidocaine reduces mechanical hyperalgesia and allodynia in the rat," *Journal of Neurophysiology*, vol. 84, no. 2, pp. 798–805, 2000.

[15] F. Zhang, X. Feng, R. Dong et al., "Effects of clonidine on bilateral pain behaviors and inflammatory response in rats under the state of neuropathic pain," *Neuroscience Letters*, vol. 505, no. 3, pp. 254–259, 2011.

[16] G. Blackburn-Munro, N. Ibsen, and H. K. Erichsen, "A comparison of the anti-nociceptive effects of voltage-activated Na^+ channel blockers in the formalin test," *European Journal of Pharmacology*, vol. 445, no. 3, pp. 231–238, 2002.

[17] E. K. Davies, Y. Boyle, B. A. Chizh, B. M. Lumb, and J. C. Murrell, "Ultraviolet B-induced inflammation in the rat: a model of secondary hyperalgesia?" *Pain*, vol. 152, no. 12, pp. 2844–2851, 2011.

[18] Z.-T. Bai, T. Liu, Z.-F. Chai, X.-Y. Pang, and Y.-H. Ji, "Rat pain-related responses induced by experimental scorpion BmK sting," *European Journal of Pharmacology*, vol. 552, no. 1–3, pp. 67–77, 2006.

[19] Z.-T. Bai, T. Liu, X.-Y. Pang, F. Jiang, M. Cheng, and Y.-H. Ji, "Functional depletion of capsaicin-sensitive primary afferent fibers attenuates rat pain-related behaviors and paw edema induced by the venom of scorpion Buthus martensi Karch," *Neuroscience Research*, vol. 62, no. 2, pp. 78–85, 2008.

[20] R. D. Hubbard and B. A. Winkelstein, "Dorsal root compression produces myelinated axonal degeneration near the biomechanical thresholds for mechanical behavioral hypersensitivity," *Experimental Neurology*, vol. 212, no. 2, pp. 482–489, 2008.

[21] J.-T. Xu, W.-J. Xin, Y. Zang, C.-Y. Wu, and X.-G. Liu, "The role of tumor necrosis factor-alpha in the neuropathic pain induced by Lumbar 5 ventral root transection in rat," *Pain*, vol. 123, no. 3, pp. 306–321, 2006.

[22] M. J. Arguis, J. Perez, G. Martínez, M. Ubre, and C. Gomar, "Contralateral neuropathic pain following a surgical model of unilateral nerve injury in rats," *Regional Anesthesia and Pain Medicine*, vol. 33, no. 3, pp. 211–216, 2008.

[23] J. M. Chung and K. Chung, "Importance of hyperexcitability of DRG neurons in neuropathic pain," *Pain Practice*, vol. 2, no. 2, pp. 87–97, 2002.

[24] M. S. Ramer, S. W. N. Thompson, and S. B. McMahon, "Causes and consequences of sympathetic basket formation in dorsal root ganglia," *Pain*, vol. 82, supplement 6, pp. S111–S120, 1999.

[25] E. D. Milligan, C. Twining, M. Chacur et al., "Spinal glia and proinflammatory cytokines mediate mirror-image neuropathic pain in rats," *Journal of Neuroscience*, vol. 23, no. 3, pp. 1026–1040, 2003.

[26] D. Huang and B. Yu, "The mirror-image pain: an unclered phenomenon and its possible mechanism," *Neuroscience and Biobehavioral Reviews*, vol. 34, no. 4, pp. 528–532, 2010.

[27] P. Hu, A. L. Bembrick, K. A. Keay, and E. M. McLachlan, "Immune cell involvement in dorsal root ganglia and spinal cord after chronic constriction or transection of the rat sciatic nerve," *Brain, Behavior, and Immunity*, vol. 21, no. 5, pp. 599–616, 2007.

[28] R. J. Cady, J. R. Glenn, K. M. Smith, and P. L. Durham, "Calcitonin gene-related peptide promotes cellular changes in trigeminal neurons and glia implicated in peripheral and central sensitization," *Molecular Pain*, vol. 7, article 94, 2011.

[29] M. Reddington, J. Priller, J. Treichel, C. Haas, and G. W. Kreutzberg, "Astrocytes and microglia as potential targets for calcitonin gene related peptide in the central nervous system," *Canadian Journal of Physiology and Pharmacology*, vol. 73, no. 7, pp. 1047–1049, 1995.

[30] L. E. Spataro, E. M. Sloane, E. D. Milligan et al., "Spinal gap junctions: potential involvement in pain facilitation," *Journal of Pain*, vol. 5, no. 7, pp. 392–405, 2004.

[31] Y. H. Chung, C. M. Shin, M. J. Kim, E. Young Lee, G. Kim, and C. I. Cha, "Enhanced expression of p53 in reactive astrocytes following transient focal ischemia," *Neurological Research*, vol. 24, no. 3, pp. 324–328, 2002.

[32] W. Xie, J. A. Strong, and J.-M. Zhang, "Early blockade of injured primary sensory afferents reduces glial cell activation in two rat neuropathic pain models," *Neuroscience*, vol. 160, no. 4, pp. 847–857, 2009.

[33] C. Abbadie, S. Bhangoo, Y. De Koninck, M. Malcangio, S. Melik-Parsadaniantz, and F. A. White, "Chemokines and pain mechanisms," *Brain Research Reviews*, vol. 60, no. 1, pp. 125–134, 2009.

[34] M. Koltzenburg, "Neutralization of endogenous NGF prevents the sensitization of nociceptors supplying inflamed skin," *European Journal of Neuroscience*, vol. 11, no. 5, pp. 1698–1704, 1999.

[35] L. Becerra, S. Morris, S. Bazes et al., "Trigeminal neuropathic pain alters responses in CNS circuits to mechanical (brush) and thermal (cold and heat) stimuli," *Journal of Neuroscience*, vol. 26, no. 42, pp. 10646–10657, 2006.

Hindawi Publishing Corporation
Neural Plasticity
Volume 2016, Article ID 4131395, 14 pages
http://dx.doi.org/10.1155/2016/4131395

Research Article

The Gate Theory of Pain Revisited: Modeling Different Pain Conditions with a Parsimonious Neurocomputational Model

Francisco Javier Ropero Peláez[1] and Shirley Taniguchi[2]

[1]*Center of Mathematics, Computation and Cognition, Universidade Federal do ABC, 09210-180 Santo André, SP, Brazil*
[2]*Basic Sciences, Albert Einstein Hospital, 05521-200 Sao Paulo, SP, Brazil*

Correspondence should be addressed to Francisco Javier Ropero Peláez; francisco.pelaez@ufabc.edu.br

Received 16 May 2015; Accepted 19 August 2015

Academic Editor: You Wan

The gate control theory of pain proposed by Melzack and Wall in 1965 is revisited through two mechanisms of neuronal regulation: NMDA synaptic plasticity and intrinsic plasticity. The Melzack and Wall circuit was slightly modified by using strictly excitatory nociceptive afferents (in the original arrangement, nociceptive afferents were considered excitatory when they project to central transmission neurons and inhibitory when projecting to substantia gelatinosa). The results of our neurocomputational model are consistent with biological ones in that nociceptive signals are blocked on their way to the brain every time a tactile stimulus is given at the same locus where the pain was produced. In the computational model, the whole set of parameters, independently of their initialization, always converge to the correct values to allow the correct computation of the circuit. To test the model, other painful conditions were analyzed: phantom limb pain, wind-up and wind-down pain, breakthrough pain, and demyelinating syndromes like Guillain-Barré and multiple sclerosis.

1. Introduction

The gate control theory of pain developed by Melzack and Wall in 1965 [1] proposes that tiny neural networks distributed along the dorsal horn of the spinal cord are responsible for relieving the pain in a specific body location when an intense tactile stimulation is applied at the same place. We experience this phenomenon in our daily life when rubbing the spot where an injury has just occurred.

According to them, axons of first order afferent nociceptors and low-threshold afferent mechanoreceptors converge to the same neurons in the substantia gelatinosa (SG) in the dorsal horn of the spinal cord, where inhibitory interneurons block nociceptive signals on their way to the brain. Since mechanoreceptors are low-threshold and their axons are myelinated, they produce high-rate action potentials. In contrast, nociceptive stimuli are less intense (in the sense of transmission rate) because they are transmitted through non-myelinated axons. Figure 1(a) shows the neural arrangement proposed by Melzack and Wall.

According to Wall, the gate theory of pain is not a final version so that its details might be discussed and improved.

"That a gate control exists is no longer open to doubt but its functional role and its detailed mechanism remain open for speculation and for experiment" [2].

Other authors (see [3, 4]) detected some flaws in the theory emphasizing the necessity of reviewing the gate control theory.

One controversial detail of the model (see Figure 4 in [1]) is that afferent nociceptors produce an excitatory stimulus on first central transmission (CT) neurons and, simultaneously, an inhibitory stimulus on neurons in the SG. This fact seems to contradict the idea that axon terminals of excitatory neurons are all excitatory, and axon terminals of inhibitory neurons are all inhibitory. This neuron's specialization is due to the absence of any mechanism in axons for guiding excitatory neurotransmitters from their origin at the neuron's soma to some specific axon terminals, while diverting inhibitory neurotransmitters to other terminals. By considering this, we

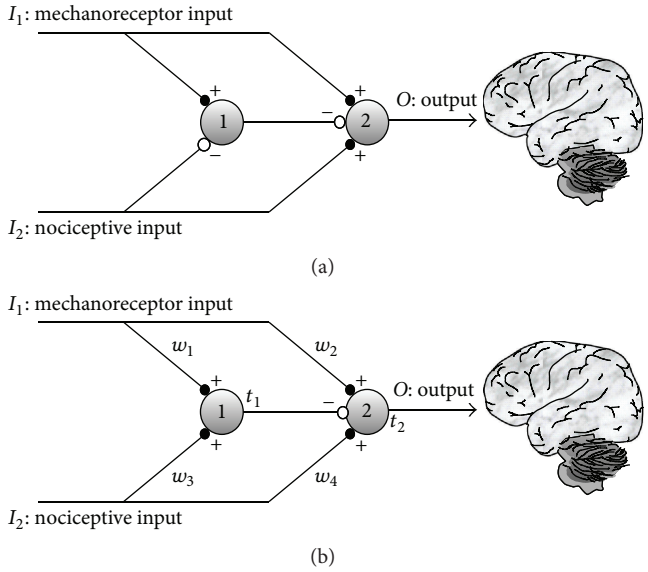

Figure 1: (a) The gate control mechanism proposed by Melzack and Wall in 1965. Both nociceptive and mechanoreceptors signals are projected to neurons in the substantia gelatinosa, represented by neuron 1, and towards the first central transmission neurons, represented by neuron 2. Mechanoreceptor signals are more intense (higher transmission rate) than nociceptive signals. Nociceptive signals inhibit neuron 1 (white dotted connection in figure) and, at the same time, produce excitation on neuron 2. (b) Current proposal: all nociceptive and mechanoreceptor axon terminals are excitatory. Synaptic weights (w_i) change according to NMDA plasticity. Firing thresholds, t_1 and t_2, of neurons 1 and 2 also vary according to intrinsic plasticity.

have decided to test whether it is possible to obtain the normal operation of the gate with only excitatory synapses from nociceptive neurons. Note that in this case the gate circuit (see Figure 1(b)) is completely symmetrical: the same type of arrangement is present in both the upper and the lower halves of the circuit. The only difference between these two halves is the type of signal arriving from mechanoreceptors (in the upper half of Figure 1(b)) that is more intense than the signal from nociceptors (in the lower half of Figure 1(b)) arrangement.

Considering these ideas, we implemented a computational model of the neural circuit shown in Figure 1(b) with only excitatory connections from nociceptive and mechanoreceptors inputs. We have tested the operation of the model with and without the property of firing threshold adaptation also called intrinsic plasticity [5–7] and with and without NMDA plasticity [8–10] in their synaptic inputs. For a review of plasticity in pain, see Woolf and Salter (2000) [11] and Todd (2010) [12]. We did not model plasticity in the inhibitory synapses located at the axon terminals of SG neurons because plasticity is usually absent in axon terminals of inhibitory neurons although several types of inhibitory plasticity have been recently described in the literature [13]. As it will be shown in the following sections, the model only operates similarly to the gate when a standard type of stimulation is applied and when both kinds of plasticity are taken into account: synaptic plasticity that modifies the synaptic weights (synaptic efficiencies) and intrinsic plasticity (adaptability of the firing threshold). We consider that a type of stimulation is "standard" or "conventional" when, in first place, the four binary combinations of inputs I_1I_2 (00, 01, 10, and 11) are sequentially or randomly presented to the gate circuit (note that "1" indicates presence of stimulus and "0" absence of stimulus). Besides, the standard type of stimulation should have another feature: mechanoreceptor stimuli should be more intense than the nociceptive stimuli. With this kind of "standard stimuli" and considering synaptic and intrinsic plasticity, synaptic weights and neurons' thresholds converge to very specific final stability values in which the normal behavior of the gate takes place. Once parameters are stabilized, the conventional behavior of the gate circuit is obtained; that is to say, pain is blocked in the gate when concomitant sensory and nociceptive stimuli are applied.

We are also going to demonstrate that when sensory and mechanoreceptor stimulation are not the standard ones, the final parameters' setpoint can be different and an anomalous pain condition can be produced. For example, in the case of demyelination of mechanoreceptor axons in multiple sclerosis [14] or in the Guillain-Barré syndrome [15], sensory and nociceptive stimuli can be similar in intensity so that, due to the symmetry of the circuit, the gate final setup can treat somatosensory stimuli as nociceptive, thereby relaying a pain sensation to the brain (CT neurons activation) in the presence of touch alone (mechanical allodynia). Another example of nonstandard combination of inputs to the gate is phantom pain sensed after a limb amputation in a specific spot of the nonexistent limb. Phantom pain spontaneously appears without stimulation. As it will be shown, such situation occurs because the final setup of parameters allows null stimuli to produce a CT neuron activation that is transmitted as a pain signal to the brain. Wind-up pain and wind-down pain will also be studied showing that stimuli intensity is determinant in the adjustment of gate circuit parameters. Finally, we study the case of breakthrough pain. It corresponds to a situation in which gate parameters cross an unstable equilibrium point before reaching the final equilibrium setup where a situation of intense pain prevails.

2. Methods

2.1. Configuration of Training Epochs. As it has been suggested in the Introduction, a critical aspect to reach a certain pain condition is the way sensory and nociceptive inputs are combined when they are input to the gate circuit. The four possible types of inputs combination are shown in Table 1(a) in which bit = 1 means presence and bit = 0 absence of input.

In neural networks literature, a training epoch is a set of input patterns that is repeatedly presented to a neural network. In our case, an epoch is the set of the four possible inputs combinations shown in Table 1(a) but with graded sensory and nociceptive inputs as in Table 1(b). In this case, Table 1(b) shows a specific type of epoch used to train the network in a standard way. Numerical values correspond to input neuron's firing probabilities and are arbitrarily selected to represent a stimulation regime. For example, in

Table 1: Configuration of a standard training epoch: (a) shows four binary combinations in terms of the presence/absence of certain nociceptive/mechanoreceptor input. (b) represents the same table in terms of afferent nociceptors and mechanoreceptors' firing probabilities. Taking into account that axons of afferent nociceptors are not myelinated, their firing probability is lower than in the case of afferent mechanoreceptors.

(a)

Nociceptive input	Mechanoreceptor input
0	0
0	1
1	0
1	1

(b)

Nociceptive input	Mechanoreceptor input
0	0
0	0.6
0.3	0
0.3	0.6

Table 2: Stimulus intensity and firing probability of sensory/nociceptive receptors. For the qualitative purposes of our research, we elaborate a table that arbitrarily associate a verbal expression describing the intensity of a sensory/nociceptive stimulus with a firing probability interval.

Verbal expression for stimulus intensity	Firing probability intervals in sensory/nociceptive receptors
Very intense	(0.8, 1]
Intense	(0.6, 0.8]
Medium	(0.4, 0.6]
Weak	(0.25, 0.4]
Very weak	[0, 0.20]

a standard stimulation regime, the firing probability from sensory (mechanoreceptor) inputs is higher than the firing probability of nociceptive ones.

Human subjects categorize the intensity of stimuli using verbal expressions like very intense, intense, medium, low, and so forth. It is reasonable to think that an intense stimulus produces a higher firing probability in sensory/nociceptive receptors than a medium stimulus. Given that, up to now, there is not a universal criterion for associating a verbal expression with a firing probability value; we have defined a preliminary scale for the qualitative purposes of the present research.

For translating the verbal expressions indicating the intensity of sensory/nociceptive inputs into firing probabilities, we arbitrarily elaborate Table 2.

With this kind of table, it is possible to translate into firing probabilities, a sentence like the following.

"During a standard kind of stimulation, sensory inputs are of medium to intense intensity being nociceptive inputs weak. In the case of a demyelinating syndrome, sensory inputs become weak. Dysesthesia might take place with a subsequent regime of stimulation with medium nociceptive inputs."

We will use this verbal description in Section 3.2.2 for studying demyelinating syndrome pain.

2.2. Neuron Model. Neurons used in the model belong to the very simplified rate-code neuron type: their outputs, O, representing their firing frequencies. In the rate-code output model, the probabilities of an action potential in the presynaptic and postsynaptic neurons are, respectively, written as I and O. The synaptic weight w relates I and the excitatory postsynaptic potential, E, at synapse j:

$$E_j = w_j I_j. \tag{1}$$

The postsynaptic action potential probability is given by a nonlinear (sigmoidal) function of neuron's net input: $O = f(\text{net})$. Such net input, Net, is obtained after summing the postsynaptic potentials of all synapses:

$$\text{net} = \sum_{j=1}^{n} E_j = \sum_{j=1}^{n} w_j I_j. \tag{2}$$

The sigmoidal function of neuron's activation yields the probability of an output action potential and is given in our simulations by

$$O = \frac{1}{1 + e^{-k(\text{net}+0.5-2s)}}, \tag{3}$$

where s is a parameter that contributes to modeling the neuron's firing threshold, t, where $t = 2s - 0.5$. k is a curve-compressing factor that was set to 50 for modeling a steep slope of the sigmoid function. The range of s is $0 < s < 1$. For $s = 0$, the sigmoid is completely shifted leftwards so that, for net $= 0$, $O = 1$. In the case $s = 1$, the sigmoid is completely shifted rightwards so that, for net $= 1$, the output value of the sigmoid is $O = 0$.

2.3. Adjustable Properties: Synaptic and Intrinsic Plasticity. We have demonstrated elsewhere [16] that NMDA plasticity (that, according to Woolf and Thompson [9] is present at SG neuron synapses) can be modeled through a probabilistic rule. Since we are utilizing rate-code neurons with outputs indicating a probability and not real binary outputs, we need to obtain at least a fictitious binary output for calculating the weight value, w, of NMDA synapses. The fictitious output of the presynaptic neuron (bit = 1 or bit = 0) is denoted by i (lowercase) and the postsynaptic fictitious output (bit = 1 or bit = 0) is denoted by o. Binary values i and o are randomly generated with probabilities I and O, respectively. With these binary values, the correlation among synaptic inputs and outputs is calculated by means of the probabilistic version of the so-called presynaptic rule, which is the conditional probability:

$$w = P\left(\frac{o}{i}\right) = \frac{n(o \cap i)}{n(i)}, \tag{4}$$

where $n()$ in the numerator counts the number of concurrent presynaptic and postsynaptic unitary binary outputs.

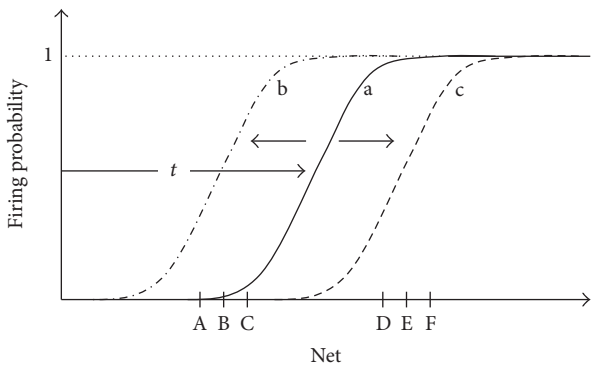

Figure 2: Intrinsic plasticity is the property of real neurons that allows the neuron's sigmoidal activation function to shift either leftwards or rightwards, so that the sigmoid is placed over intervals corresponding to the average net input of the neuron. (a) Initial position of the sigmoidal activation function. (b) If the values of net inputs of the neuron are low (as in case of inputs A, B, and C), the activation function shifts leftwards. (c) If net input values are high (as in D, E, and F), the sigmoid gradually shifts rightwards.

The apparent shortcoming of this probabilistic synaptic weight modeling is that the higher the weight the more correlated the presynaptic and postsynaptic neurons so that weights become higher. At the end, it seems that weight values have no other possibility rather than growing until they saturate, that is, turn into one.

Fortunately, neurons have another property that contributes to moderating the tendency of synaptic weights to increase until saturation. This property, called intrinsic plasticity [5, 6], either increments or decrements the neurons firing threshold so that the neuron is, respectively, less prone or more prone to fire in the future. Neurons in spinal cord laminae III–VI, that is, in deep dorsal horn, express intrinsic plasticity (see a comprehensive review in Sandkühler, 2009 [7]).

Rigorously, there is not a clear cut-edge defining a threshold that changes the neuron firing probability from zero to one. Instead of this, the transition is governed by the sigmoid function presented in (3) that is also depicted in Figure 2, in which the firing probability makes a gradual transition from zero to one. For us, the firing threshold will be defined as the value of net input that makes the neuron fire with probability equal to 0.5.

We have demonstrated elsewhere [16] that synaptic weights increment can be counterbalanced by the dynamic adjustment of the shift of the sigmoidal function so that the more the synaptic weights (and accordingly the net input value) grow, the more the shift grows. Thus, the steepest slope of the sigmoid tends to be placed over the average net input of the neuron (see Figure 2). Such dynamic adjustment makes synaptic weights stop increasing and stabilize in specific values.

The following equation modeling intrinsic plasticity calculates the shift parameter of the activation function, s, at time t in terms of the shift parameter and output probability of the neuron at time $t-1$:

$$s_t = \frac{\upsilon \cdot O_{t-1} + s_{t-1}}{\upsilon + 1}, \tag{5}$$

where υ is a small arbitrary factor that adjusts the shifting rate of the activation function.

As previously mentioned, parameter s allows the calculation of firing threshold, t, which is

$$t = 2s - 0.5. \tag{6}$$

Considering that the range of variable "net" after weight stabilization is in the $[0, 1]$ interval, the arbitrary election of this equation for modeling threshold, t, allows to have the sigmoid completely shifted rightwards with $s = 1$ and completely shifted to the left for $s = 0$.

In this paper, we show that the dynamic interactions between synaptic and intrinsic plasticity are the factors that allow the stabilization of parameters in the gate circuit. Once parameters are stabilized under either standard or altered modes of operation, they give rise to either normal or altered pain sensations.

2.4. Some Notes regarding Units, Scales, and Iterations. In this research, we use a phenomenological type of neuron modelling. We take into account that, at least in mammals, rate coding is the way neurons communicate with one another. In gate circuit models, the neuron's output O is a rate (3) value. Such rate can be expressed in the form of a probability ranging from zero to one. When $O = 1$, it means that the neuron fires every time it is possible. Probabilities are dimensionless measurements because they are obtained from the quotient of equal type of magnitudes (see (4)). For this reason, in the graphs of this paper, unit specification does not appear in the vertical axes representing neuron's output, O.

Synaptic weights are also calculated as conditional probabilities and are, therefore, dimensionless. For this reason, graphs representing weights do not have unit specifications in their axes. In a similar way, variables that are obtained as a combination of dimensionless variables are also dimensionless like the net input, net, and the shift parameter, s. When these variables appear in a graph, they are devoid of unit specifications.

A comparison with binary bits might help in the understanding of these ideas. A binary bit is a dimensionless magnitude that is either 1 or 0. For computers to work, binary 1 is arbitrarily associated with a certain voltage level that depends on the available technology. In TTL (transistor-transistor logic) technology, binary 1 is arbitrarily associated with a 5 volts' voltage level and binary 0 with a 0 volts' level. In a similar way, the net input value, that is dimensionless, is associated in real neurons with specific postsynaptic voltage levels.

Regarding time comparisons, computers use "iterations" to perform their instructions. An iteration is typically a sequence of tasks in a programming loop. In our model, the four possible combinations of sensory/nociceptive inputs that integrate an epoch are processed inside an iteration. When each combination of sensory/nociceptive inputs feeds the gate circuit neurons, their net inputs and outputs are calculated, and their firing thresholds and synaptic weights are altered. According to this, we can say that the real counterpart of an iteration in our computer model would be a period

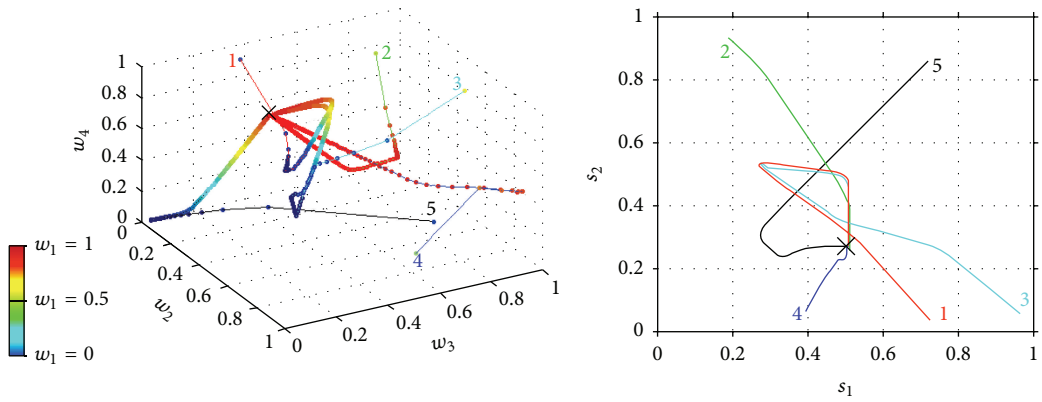

(a) (b)

I_1	I_2	O_1	O_2	O_3	O_4	O_5
0	0	0.1	0.1	0.1	0.1	0.1
0	0.3	1	1	1	1	1
0.6	0	0	0	0	0	0
0.6	0.3	0	0	0	0	0

(c)

Figure 3: Evolution of gate circuit parameters when considering both intrinsic and synaptic plasticity. Five program simulations (5 thin colored lines) are depicted, starting with different initial weights and shifts. (a) Evolution of weights: each coordinate (w_2, w_3, w_4) represents the set of synaptic weights in each iteration, with the color of the point representing the value of weight w_1. Along iterations, all lines converge to the same coordinate (w_1, w_2, w_3, w_4) = (1, 0, 0.5, 0.5). (b) After 5000 iterations, the shift parameters of the activation function of the SG neuron (s_1) and of the T neuron (s_2) also converge to a certain point (0.5, 0.27). (c) With the final set of weights and shift parameters, the probability of a CT neuron's firing is given by the table being I_1 the mechanoreceptor input probability and I_2 the nociceptive input probability.

of time in which all combinations of sensory/nociceptive stimulus are given to a subject with specific intensity degrees. In order to relate iterations, time windows, and evolution of patients with stimulation protocols, patterned experimental tests with real patients should be necessary.

3. Results

This section is devoted to analyzing the behavior of the gate circuit under standard (Section 3.1) and nonstandard (Section 3.2) types of stimulation.

In Section 3.1, we will show that the conventional gate operation is achieved once gate parameters (intrinsic and synaptic plasticity) stabilize after a dynamic transitory period. During this transitory period, a standard training epoch (depicted in Table 1(b)) is input to the gate, being the mechanoreceptor input higher than the nociceptor input. As it will be demonstrated, synaptic and intrinsic plasticity interact for allowing parameters stabilization and convergence because one type of plasticity counterbalances the other. Under such condition, the operation emerging from the circuit consists of pain only being elicited (CT neurons fire) when nociceptive signals are the only input to the circuit which is the conventional gate circuit operation.

At the end of Section 3.1, we will see that the adequate convergence of parameters does not take place when intrinsic plasticity or synaptic plasticity alone is taken into account. The interplay of both synaptic and intrinsic plasticity is necessary to create the conditions for the circuit to reach the set-point that makes the circuit respond in the conventional way.

In Section 3.2, we are going to study other pain conditions that result from anomalous training epochs given to the network, that is, (a) when mechanoreceptor input is equal to or lower than nociceptive input as in demyelinating syndromes, (b) when inputs are absent as in phantom pain, (c) when continuous weak sensory inputs produce an abrupt increment of pain sensation (wind-up pain), (d) when a continuous intense nociceptive input produces a temporary analgesia (wind-down pain), and (e) when an intense pain generates a transitory wind-down episode followed by break-through pain.

3.1. Standard Pain Responses due to Standard Stimulation Regime. As previously mentioned, in this section, we will study the evolution of synaptic weights, w_i, and shift parameters, s_i, when a standard type of stimulation is input to the gate circuit. The model uses intrinsic plasticity in SG and CT neurons and NMDA synaptic plasticity in excitatory synapses. In order to allow the conventional gate operation, the interplay

between intrinsic and synaptic plasticity is necessary for parameter stabilization and convergence. Equation (4) has been used for modeling weights modification and (5) was used to model the gradual shift of the activation function. Figure 3 shows five trajectories of weights (Figure 3(a)) and shifts (Figure 3(b)) corresponding to five different simulations (five colored lines with the same color numbers), each of them starting with different shifts and weight values. As we have four weights w_1, w_2, w_3, and w_4 (see location of each of these weights in Figure 1(b)), a four-dimensional coordinate system would be necessary for representing their evolution along iterations. We have managed to represent the trajectory of the four weights along 5000 iterations in a three-dimensional coordinate system (see Figure 3(a)) by representing the value of w_1 as a colored point over each trajectory. The color of each point corresponds to a color scale in which dark blue means $w_1 = 0$ and red means $w_1 = 1$. The values of w_2, w_3, and w_4 are represented in a conventional three-dimensional system. All weight values are dimensionless and range from 0 to 1 because they are obtained from a conditional probability equation (4).

Notice that the five weight trajectories converge to the same coordinate: $w_1 = 1$, $w_2 = 0$, and $w_3 = w_4 = 0.5$. Shift trajectories (Figure 3(b)) also converge to the final shifts values $s_1 = 0.5$ and $s_2 = 0.27$ that, according to (6), correspond to the firing thresholds: $t_1 = 0.51$ and $t_2 = 0.02$. This final coordinate is marked with "x" in Figures 3(a) and 3(b).

The table in Figure 3(c) is obtained at the final points of each colored trajectory. In the table's first row, the ith colored subindex of O_i refers to the same color trajectory. The table shows the output value, O_i, of the CT neuron when applying a standard epoch to the circuit using the final parameters of each of the ith trajectories. In this case, the final parameters in the five trajectories are equal, so that the output when applying a standard epoch to each of the five circuit configurations is the same. In this case, the outputs correspond to the standard or conventional *modus operandi* of the gate circuit in which the CT neuron is only active when only the nociceptive input is active. The output probability that is equal to 0.1 when inputs I_1 and I_2 are equal to zero depends on the value of the sigmoidal function in zero. If a more realistic approximation of the activation function was used, in which $f(0) = 0$, the output probability would certainly yield zero. Graph of Figure 4 also represents the output O of the gate circuit (i.e., the output of the CT neuron) similarly to table in Figure 3(c). The difference between the table and Figure 4 is that the table shows the response of the circuit at the final setpoint marked with "x" in Figure 3(a). Figure 4, instead, shows the response of the circuit along iterations for each combination of inputs (in this case, in a standard epoch). For example, the dark blue ribbon shows the output of CT neuron when both inputs are null ($I_1 = 0$ and $I_2 = 0$) from the very first iteration until iteration 150. The cyan ribbon represents the response of the circuit along iterations when only a sensory signal is given ($I_1 = 0.6$ and $I_2 = 0$).

We see that under these conditions there is no CT neuron's output (there is no pain signal from the gate circuit when a sensory input alone is given). The yellow ribbon

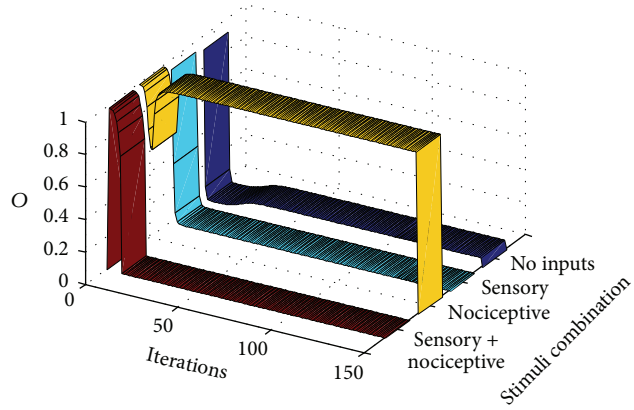

Figure 4: This graph shows the output, O, of the CT neuron in the gate circuit along computer iterations. It shows that the circuit quickly adapts, for eliciting standard gate outputs when standard pain and sensory signal are input to the circuit (a standard training epoch is given to the circuit in each iteration). Each ribbon represents the output of the circuit when a certain combination of inputs is introduced as input to the circuit. The dark blue ribbon yields the output (the CT neuron action potential probability) when no inputs are introduced. Cyan, yellow, and red ribbons yield the CT neuron output under conditions in which only sensory, nociceptive, or both inputs are, respectively, input to the gate circuit.

represents the output when only a nociceptive signal ($I_1 = 0$ and $I_2 = 0.3$) is input. In this case, the CT neuron's output quickly grows from the very first iterations so that a pain signal is only elicited by the gate circuit when a pure nociceptive input enters the gate. Finally, the flat dark red ribbon shows that no pain signal is elicited by the gate circuit along all iterations when both sensory and nociceptive input are simultaneously entering the circuit.

In summary, Figure 4 shows that the interplay between intrinsic and synaptic plasticity, together with the presentation of a standard type of input patterns, leads the gate circuit to the gate conventional *modus operandi*: when both sensory and nociceptive inputs are simultaneously input to the gate, CT neurons are silent. However, when nociceptive signals are input alone, they produce the CT neuron's output.

We performed other similar simulations, but only considering either intrinsic (Figure 5) or synaptic plasticity (Figure 6). As before, the five thin colored lines represent parameters evolution from five different initial conditions. It can be noticed that with only one type of plasticity there is no convergence of parameters and the gate circuit does not respond in a standard manner when a standard type of stimulation is applied.

3.2. Nonstandard Pain Responses due to Nonstandard Stimulation Regimes. In this section, we will show computer simulations that reveal how neuropathic pain evolves from a normal pain situation in terms of sensory/nociceptive stimulation. Our premise here is that the gate circuit is a kind of neural network that is trained (achieves different parameter configurations) depending on the type of external stimulation. For creating the initial standard conditions, the gate circuit is

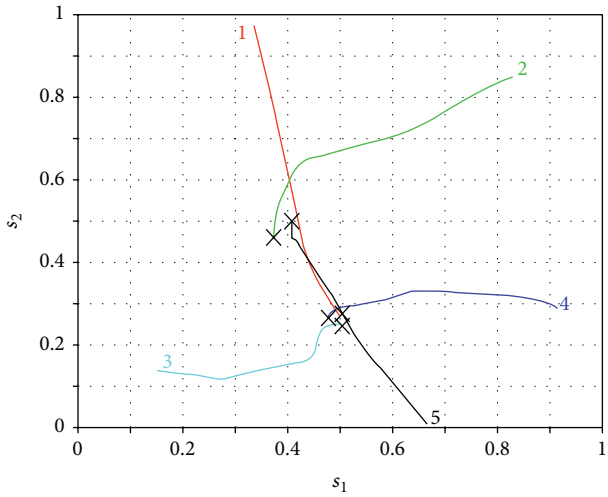

(a)

I_1	I_2	O_1	O_2	O_3	O_4	O_5
0	0	0.1	0	0	0.1	0
0	0.3	1	0.9	0.5	1	0
0.6	0	0	0.8	0	0	1
0.6	0.3	0	0.2	0	0	1

(b)

Figure 5: Evolution of gate circuit parameters with only intrinsic plasticity. (a) Evolution of the shift parameters of neurons 1 (SG) and 2 (CT) in five different simulations (different line colors). Crosses represent the values of shift parameters at the last iteration. (b) Truth table after each one of the simulations. Colors in the indexes refer to the same color curves in (a).

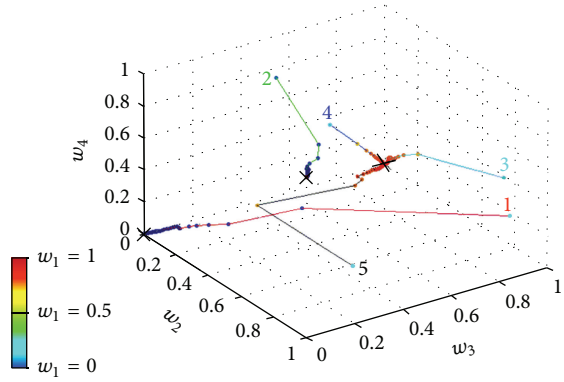

(a)

I_1	I_2	O_1	O_2	O_3	O_4	O_5
0	0	0	1	0	0	1
0	0.3	0	1	0	0	1
0.6	0	0	1	0	0	1
0.6	0.3	0	1	0	0	1

(b)

Figure 6: Evolution of gate circuit parameters with only synaptic plasticity. (a) Five computer simulations (five colors of narrow lines) representing synaptic weights evolution during 5000 iterations, once the shifts of activation functions are fixed. Because there are four weights and we have a 3D coordinates system, one of the coordinates, w_1, is measured by a scale of colors ranging from 0 to 1. A cross indicates last iteration. (b) Truth table for each one of the simulations.

trained with a standard set of sensory/nociceptive inputs (as in previous sections) during the first 50 computer iterations. In this way, at iteration 50, the gate circuit is programmed as in Section 3.1. From iteration 51 ahead, the circuit is exposed to an abnormal training epoch (abnormal set of sensory/nociceptive patterns), which depends on the type of syndrome being modeled. In this paper, we model different syndromes: phantom pain, demyelinating pain syndromes like multiple scleroses or Guillain-Barre syndrome, breakthrough pain, wind-up pain, and wind-down pain.

3.2.1. Phantom Pain Simulation. Let us start with the so called "*phantom pain*" [17] appearing in a nonexisting limb after amputation.

As it has been mentioned, the gate circuit is initially set to behave in a standard way by inputting a standard training "epoch" during its first 50 iterations. Once the circuit settles down, we model the amputation by zeroing both sensory and nociceptive inputs along the following 50 iterations (see Figure 7(a)). From iteration 101 to iteration 150, very subtle sensory and nociceptive inputs enter the circuit, simulating abnormal action potentials fired by neuromas (formed from injured nerve endings at the stump site). Figure 7(b) shows the CT neuron output, O, along the mentioned iterations for the different nociceptive and sensory combinations. We can see that, from iteration 101 ahead, two cases are possible depending on the stability point in which model parameters settle down. In graph (b), we notice that a CT neurons output (a pain signal) is produced when either a nociceptive input is present (yellow ribbon) or no inputs are present at all (dark blue ribbon). In graph (c), a pain sensation (CT neuron output) appears when there are no input signals at all (dark

Sensory stimulus (I_1)	Nociceptive stimulus (I_2)
0	0
0	0
0	0
0	0

(a)

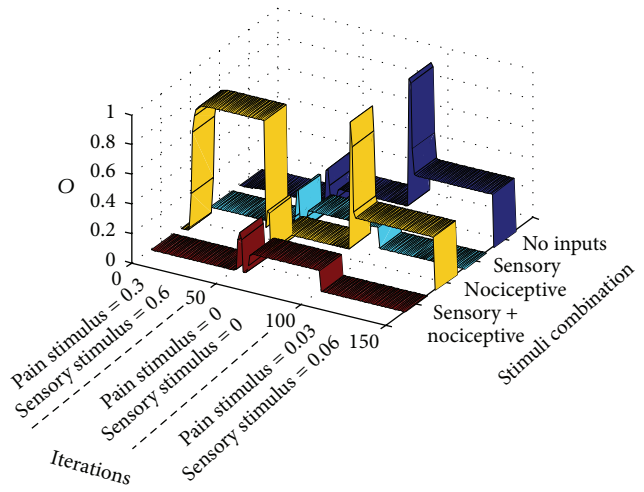

(b)

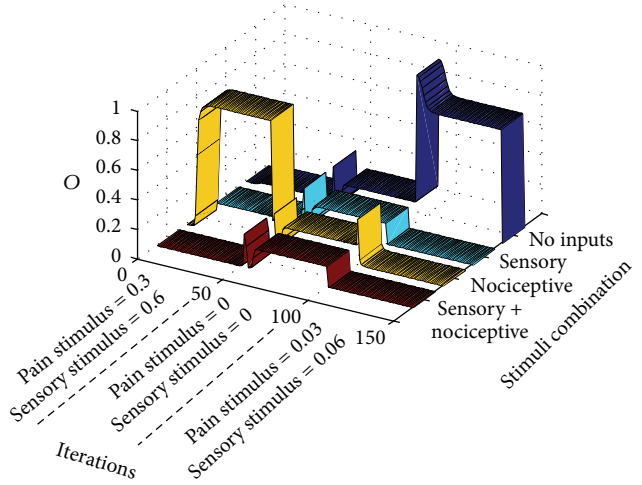

(c)

Figure 7: Modeling phantom limb pain: after presenting a standard training epoch to the gate model during 50 iterations, (a) a null training epoch is input to the gate along 50 more iterations in order to model the period after amputation. (b and c) After 100 iterations, very weak input signals are input to the gate model. Graphs correspond to two stability points. Both graphs show that pain signals are emitted from CT neurons in a situation in which there are no inputs to the gate in a condition known as dysesthesia (blue ribbon). Graph (b) shows a situation of a setpoint in which weak nociceptive inputs elicit a pain signal from CT neurons (yellow ribbon).

blue ribbon). Although the peripheric pain component due to neuromas is not difficult to accept, pain when no input at all is present at the gate is more difficult to understand. This case is consistent with clinical findings that demonstrate that phantom pain remains even when local anesthesia is applied to the stump. The general consensus trying to explain this last case is that phantom pain is a top-down phenomenon caused by maladaptive cortical plasticity. However, a recent article [18] has reopened the discussion regarding the peripheral versus central origin of phantom pain. The results of our computational model shows that the gate circuit cannot be understood anymore as a "gate" that allows/precludes nociceptive signals, but as a type of signal processor that either generates or does not generate a pain signal according to the input signals and to the gate internal parameters configuration. Instead of always mitigating pain, the gate circuit is also able to create pain (produce a CT output), even in the absence of sensorial and nociceptive stimuli. For a neuron to fire in the absence of stimuli, the only possibility is that it has incremented its excitability by lowering its firing threshold (according to intrinsic plasticity). In the case of our simulations, the CT neuron lowered its threshold to $t = -0.05$. The whole set of parameters for the case of Figure 7(c) is shown in Figure 12(b).

3.2.2. Demyelinating Syndrome Simulation. Let us model a *demyelinating syndrome* like multiple scleroses or Guillain-Barré syndrome that appears after 50 iterations of a standard pain situation. This case is also an example on how we translate a verbal expression like the one presented at the end of Section 2.1 for developing a stimulation protocol.

In this case, the demyelinating syndrome makes mechanoreceptors convey weaker signals to the gate circuit. Table in Figure 8(a) shows the training epoch used from

Sensory stimulus (I_1)	Nociceptive stimulus (I_2)
0	0
0.32	0
0	0.3
0.32	0.3

(a)

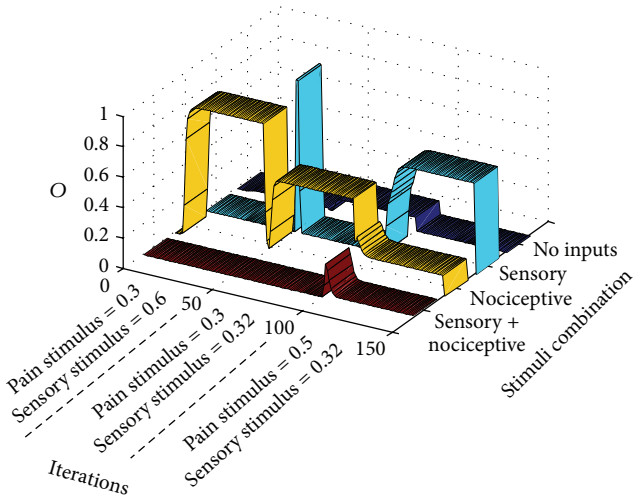

(b)

Figure 8: Modeling demyelinating syndromes: after 50 iterations with standard training epochs, signals from sensory receptors are weakened like in a demyelinating syndrome. Abnormal pain sensations only take place from iteration 100 with pain sensations when a sensory signal is input to the gate (dysesthesia).

iteration 50 to iteration 100. Notice that sensory stimuli are weaker than in the standard training epoch, almost similar to stimuli from nociceptive nonmyelinated fibers. Here, we see that dysesthesia appears from iteration 101, at the onset of some concomitant event generating more intense nociceptive signals (in this case, a new training epoch was applied with nociceptive stimuli rising from 0.3 to 0.5). In these new conditions, pain sensations appear with sensorial stimuli (cyan ribbon).

Although gate parameters usually converge to an equilibrium point like the previously described, other equilibrium points are possible in demyelinating syndromes. This fact is in accordance with the literature that mentions different types of pain associated with demyelinating diseases like the Guillain-Barré syndrome (see [19]) and multiple scleroses (see [20]).

3.2.3. Breakthrough Pain Simulation. Breakthrough pain [21] is defined as "a transitory exacerbation of pain experienced by the patient who has relatively stable and adequately controlled baseline (background) pain" [22].

In this case, after the preliminary standard setup during the first 50 iterations, the training epoch in Figure 9(a) is input to the gate circuit. After a few iterations, a wind-down phenomenon takes place in which nociceptive input signals (see yellow ribbon) produce decreasing pains sensations (CT neurons output). When pain sensations seem to be less intense, pain is triggered again when a moderate nociceptive stimulus is applied. Under the same circumstances, that is, intense nociceptive stimuli, other sequences are also possible. Nonstandard pain responses differ from the standard case in that in nonstandard cases there are usually secondary stability points in which pain responses are not so easy to predict.

3.2.4. Wind-Down Pain. In this case, we will analyze wind-down pain which also was a pain response that appeared in previous case. Wind-down pain is usually experienced when intense aversive nociceptive stimuli are constantly applied. We performed the computational model of this case by letting the circuit settle under standard conditions during the first 50 iterations. From iterations 50 to 100, the unique stimulus applied was an intense I_2 input in the nociceptive entrance.

In order to better understand the response of the circuit to the four combinations of inputs without altering parameters' setup at the end of the intense nociceptive input presentation, we block synaptic and intrinsic plasticity from iterations 100 to 150 (this "parameters freezing" procedure was not performed in previous cases). In this way, we tested the circuit with all the combination of nociceptive and mechanoreceptor inputs. As seen at the final "tail" of colored ribbons of Figure 10, there is a reduced response to any of the combinations. In cancer pain, this wind-down component can be masked by the concomitant usage of analgesics like morphine [23], so that pain relief is erroneously thought to be due to the pharmacological treatment rather than being derived from neural plasticity dynamics.

3.2.5. Wind-Up Pain. Wind-up pain is the pain response elicited when a constant sensory weak stimulus is input through mechanoreceptors. The consequence of this apparently innocuous procedure is that, in the long run, an intense pain appears in the subject. We have simulated the conditions of wind-up pain from standard conditions (Figure 11) by initially letting the circuit settle in a stable point along the 50 initial iterations. From iterations 50 to 100, the only stimulus is a weak (0.1) mechanoreceptor one. To test the circuit response immediately after the stimulation procedure, avoiding altering circuit parameters, we block plasticity from iterations 100 to 150 and introduce the four mechanoreceptor/nociceptive stimuli combinations. As it can be seen, there is an intense pain when no input is applied to the circuit. In

Table 3: Output of CT neuron, O_2, for each of the I_1, I_2 input pairs in the standard gate operation calculated from stability weights and thresholds represented in Figure 12(a): Net_1 is obtained applying (2). In this case Net_1 is calculated as $\text{Net}_1 = w_1 I_1 + w_3 I_2$ for each pair. Neuron 1 output, O_1, is equal to 1 when Net_1 is higher than its threshold, t_1. Net_2 is calculated having into account neuron 1 inhibitory output: $\text{Net}_2 = w_2 I_1 + w_4 I_2 - O_1$. Finally the pain signal relayed to the brain from neuron 2 is triggered when $\text{Net}_2 > t_2$.

I_1	I_2	w_1	w_3	Net_1	t_1	O_1	w_2	w_4	Net_2	t_2	O_2
0	**0**	1	0.5	0	0.51	0	0	0.5	0	0.02	**0**
0	**0.3**	1	0.5	0.15	0.51	0	0	0.5	0.15	0.02	**1**
0.6	**0**	1	0.5	0.6	0.51	1	0	0.5	−1	0.02	**0**
0.6	**0.3**	1	0.5	0.75	0.51	1	0	0.5	−0.85	0.02	**0**

Sensory stimulus (I_1)	Nociceptive stimulus (I_2)
0	0
0	1
0.6	0
0.6	1

(a)

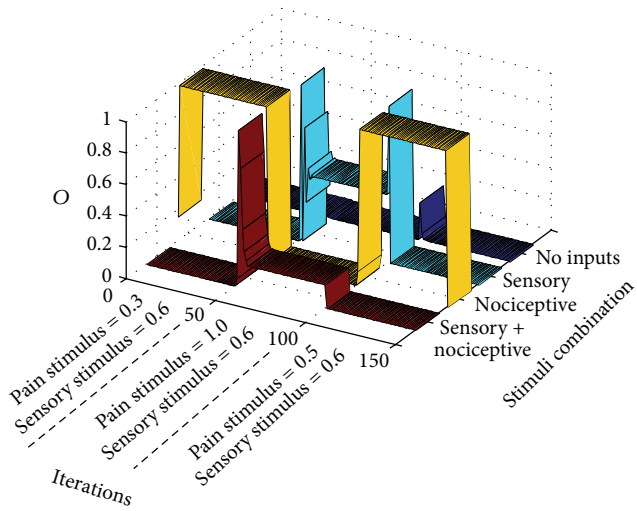

(b)

Figure 9: Modeling breakthrough pain: after 50 iterations with standard training epochs, an intense nociceptive stimulus is input to the gate. Initially, wind-down pain (yellow ribbon) takes place concomitantly with a mild episode of dysesthesia (cyan ribbon). After a period in which pain seems to be relieved, pain is again installed as in breakthrough pain.

this case, the pain that is actually felt by the subject undertaking repetitive weak sensory stimulation seems to be a type of dysesthesia that possibly comes up between repetitive sensorial stimuli.

4. Discussion

One of the objectives of this work is to highlight the dependence of pain responses on gate circuit parameters (synaptic weight and firing threshold values) and on the relative contribution of afferent mechanoreceptors and nociceptors.

Usually afferent mechanoreceptors have myelinated axons generating more intense responses than nociceptors. At the same time, sensory and nociceptive stimuli are usually delivered to the central nervous system according to a stimulation protocol (epoch) that is similar to the standard one presented in Section 2.1. Under these standard conditions, the synaptic weights and firing thresholds of the gate circuit evolve until settling in a stable point that allows the conventional operation of the circuit (see synaptic weight values, w, and firing threshold values, t, in Figure 12(a)).

This conventional operation means that when a mechanoreceptor's input alone is input to the gate circuit or when mechanoreceptor and nociceptive inputs are both input to the circuit, no pain (CT neuron response) is relayed. Table 3 helps in calculating the output of the circuit, O_2, for each of the $I_1 I_2$ combinations of sensory/nociceptive inputs under standard conditions.

Table 3 uses the final weights and neuron's firing thresholds shown in Figure 12(a). For calculating the output of neuron 1, O_1, the computer program applies the sigmoidal activation function of (3) to its net input (see (2)). As our sigmoid is very similar to a step function, it is also possible to obtain O_1 by simply comparing Net_1 with threshold t_1. If the net input of neuron 1 is higher than its threshold, neuron 1 output is 1, which is almost the same result of applying the sigmoid to Net_1. For calculating the final response of neuron 2, it is necessary to introduce the inhibitory contribution of SG neuron, as follows: $\text{Net}_2 = w_2 I_1 + w_4 I_2 - O_1$. The final output, O_2, results from applying the sigmoidal function to Net_2, that is roughly the same result as checking whether Net_2 is higher than threshold t_2, as explained.

A similar table might be elaborated for testing the response of the circuit after settling in a nonstandard set of parameters (see Figures 12(b), 12(c), 12(d), 12(e), and 12(f)). Nonstandard parameters make the gate circuit behave in nonstandard ways like in phantom limb pain, pain in demyelinating syndromes, breakthrough pain, and wind-down and

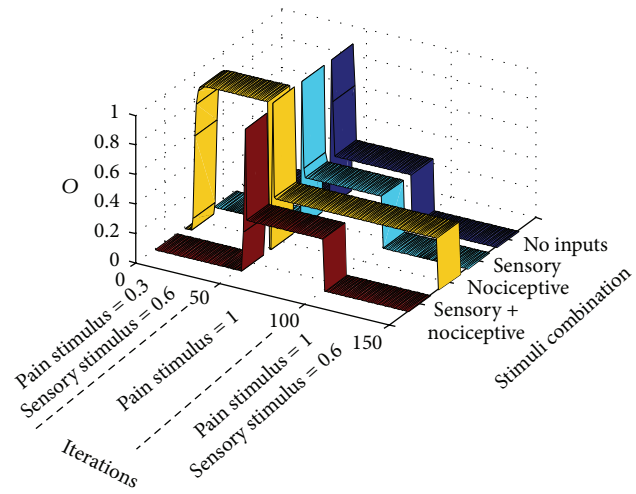

Figure 10: Modeling wind-down pain: after 50 iterations of standard training epochs, signals from nociceptive receptors become very intense. From iterations 50 to 100, the gate circuit, instead of receiving different stimuli like in previous cases, receives an intense nociceptive stimulus of value 1. For testing pain responses to other types of stimuli during the phase of intense nociceptive stimulation, all types of plasticity (synaptic and intrinsic) are blocked from iterations 100 to 150 (this procedure was not done in previous examples). As seen, after a long intense pain stimulation, the circuit becomes less responsive to all types of stimuli.

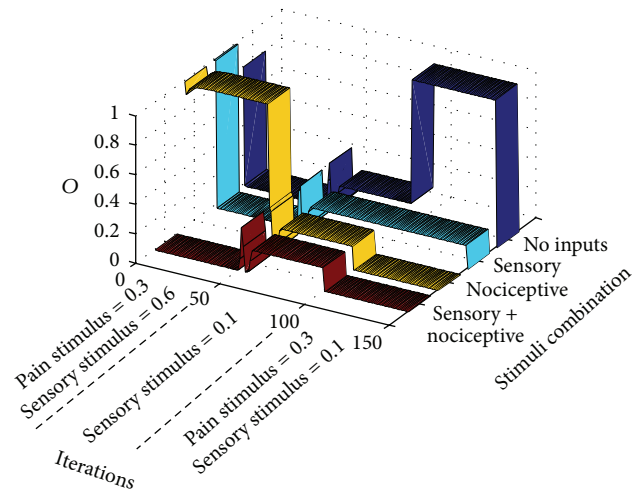

Figure 11: Modeling wind-up pain. After 50 iterations with standard training epochs, signals from mechanoreceptors become weak but repetitive, without any other type of stimulation. This situation is modeled from iterations 50 to 100 in which the gate circuit, instead of receiving different stimuli like in previous cases, only receives a repetitive weak sensory stimulus. For understanding pain responses to other types of stimuli during the phase of repetitive weak sensory stimulation, all types of plasticity (synaptic and intrinsic) are blocked from iterations 100 to 150 (as done in previous example). As can be seen, after a prolonged weak sensory stimulation, the circuit relays a pain output in the case of no stimulation (between periods of weak sensory stimulation).

wind-up pain. Readers can confer that parameters of Figure 12(b) allow phantom pain only in the case of no inputs to the gate (Figure 7(c)).

The versatility of pain responses obtained by the computational model is a consequence of the vertical symmetry of the proposed gate architecture (Figure 1(b)) in which all afferents to the circuit are excitatory. For the gate circuit, there is no way to differentiate a nociceptive or a sensory afferent. The only difference is that the spiking rate from mechanoreceptors is higher than from nociceptors due to the lower mechanoreceptors firing threshold and to the absence of a myelin sheath in nociceptors. When mechanoreceptor intensity (normalized spiking rate) is weak, as in demyelinating syndromes, the gate circuit is, some way, "deceived" and its dynamics become the same as if the sensory input was a nociceptive input.

The chart of Figure 13 represents an attempt to characterize the "standard" and "nonstandard" *modus operandi* of the gate circuit concerning the intensity of mechanoreceptor and nociceptive inputs. The sensory input intensity (the x coordinate) represents the normalized mechanoreceptor spiking rate measured at the mechanoreceptor axon terminal whereas the y-coordinate represents the normalized nociceptive spiking rate measured at the nociceptive terminal. The normalization is performed by dividing the spiking rate in a certain axon terminal by the highest possible spiking rate in any of the two axon terminals.

By exploring Figure 13, we can see that the diagonal is the place where sensory and nociceptive intensities are equal. Along the diagonal, and due to the symmetry of the circuit, it is not possible for the circuit to establish a difference between sensory and nociceptive inputs. From the point of view of neurons in the gate circuit, the two inputs are equivalent.

Below the diagonal of Figure 13, sensory inputs are more intense than nociceptive ones so that a standard type of stimulation is possible in this region.

Above the diagonal, sensory signals are weaker than nociceptive signals. Demyelinating syndromes like multiple scleroses and Guillain-Barré syndrome can reduce the rate of mechanoreceptor signals, thereby producing such situation. In these demyelinating syndromes, the network can misinterpret incoming signals so that the weaker mechanoreceptor input is treated like a nociceptive one, thereby generating a pain signal from CT neurons in a condition called dysesthesia.

We must emphasize that Figure 13 only shows two of the at least 8 initial parameters that influence the final setpoint of the circuit in which parameters stabilize and a pain condition is established. Besides the two inputs' value, the other six parameters are the value of the four modifiable synaptic weights, w, and the value of the firing threshold, t, of the two neurons of the circuit.

Other nonstandard pain conditions are depicted in the chart: like wind-up pain that is produced, according to the computational model, when a continuous weak stimulation is delivered to a subject and is manifested by pain sensations in the intervals without stimuli similar to dysesthesia (see Section 3.2.5). Phantom pain is an extreme case of wind-up pain in which sensory and nociceptive inputs are zero

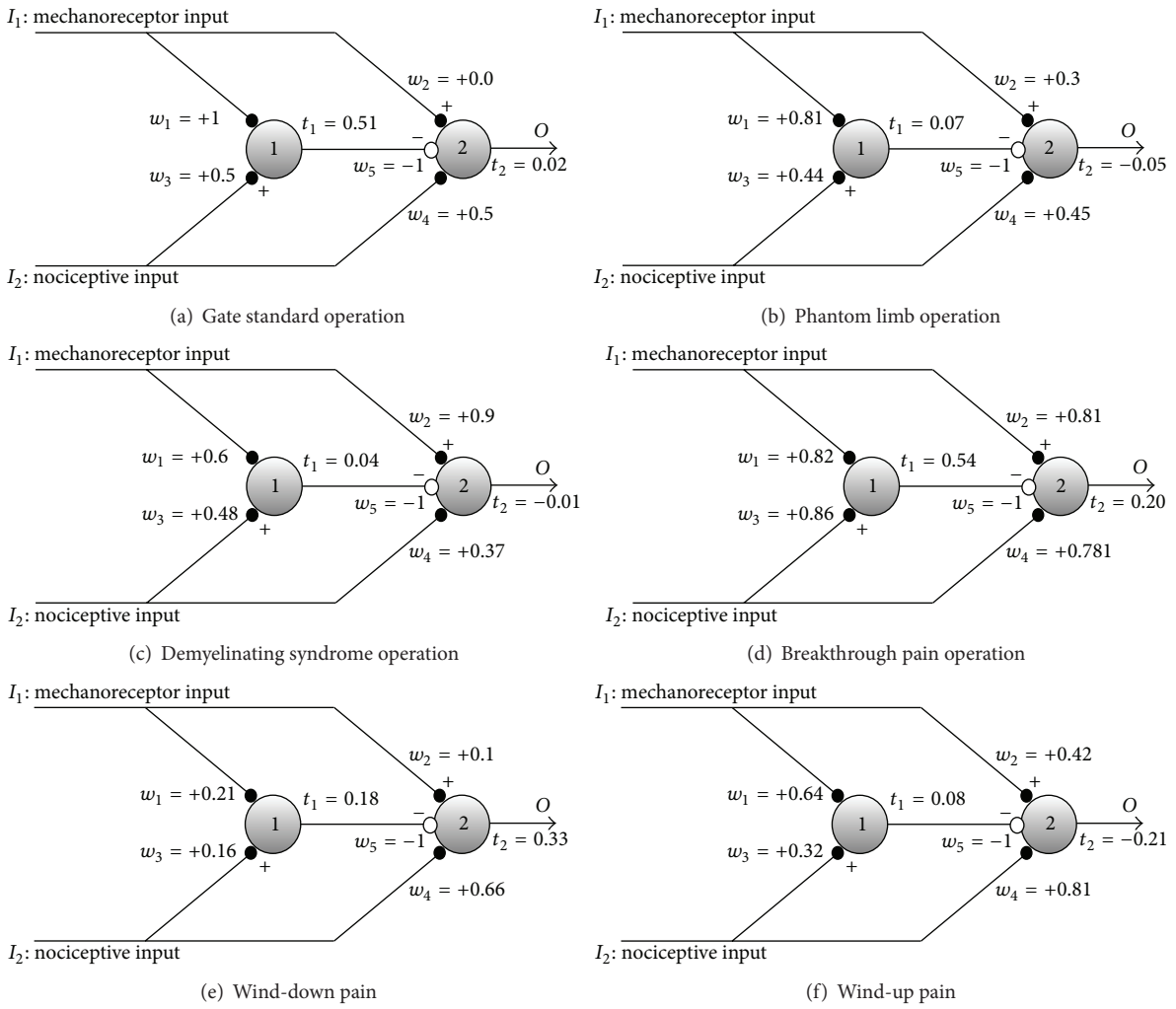

Figure 12: Synaptic weights and firing threshold values when the gate circuit arrives to stability for the different cases previously explained. When placing the different type of inputs in the gate circuit, neuron 2 response is according to the type of response expected in each case. In the case of graph (b), we considered the parameters of gate circuit that only produces phantom pain when no inputs at all enter the gate (see Figure 7(c)).

(see Section 3.2.1). According to the model, wind-down pain takes place when either very intense sensory or nociceptive stimuli are delivered. One interesting case that was not tested in previous sections is the hypothetical situation in the right upper corner of the chart where intense nociceptive and sensory stimuli are delivered simultaneously and continuously. Although the gate usually mediates a wind-down phenomenon (as shown in Figure 14), unpredictable behaviors also take place because the diagonal is the main feature in this region of the chart.

Chart of Figure 13 is far from being final. Future research will surely contribute to improve this chart. In this paper, we trained the gate circuit with very specific combinations of sensory and nociceptive inputs. For the chart to be complete, a continuous sequence of sensory and nociceptive stimuli should be input to the gate. With each stimulus, little disturbances can be applied for gathering statistic measurements in order to study other aspects of gate circuit dynamics like stability and robustness.

This paper research shows that pain conditions are the result of a dynamic adjustment of circuit parameters in the presence of different type of stimulation that are external and/or derived from internal conditions like axon conductivity in demyelinating syndromes. We showed that the interplay between synaptic and intrinsic plasticity is necessary for the circuit to settle down in stability points that allow standard and nonstandard gate operations.

5. Conclusions

In this paper, we present a parsimonious computational model of the gate circuit that is able to account for a large number of different pain conditions. When compared with the Melzack and Wall gate circuit, our model only considers strictly excitatory afferents to the gate. However, the pain conditions modelled by this simpler architecture are numerous: it models normal gate functioning, phantom limb pain condition, wind-up and wind-down pain, breakthrough

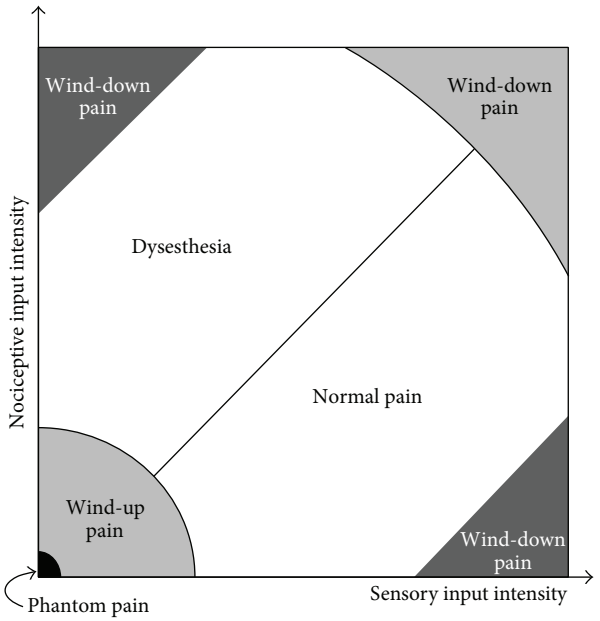

Figure 13: Different pain conditions for the different combinations of sensory and mechanoreceptor inputs according to the results of the gate circuit computer model. When the sensory input intensity (normalized firing rate) is higher than the nociceptive input intensity (below the diagonal), the circuit behaves in a "normal pain" mode. Above the diagonal, nociceptive input intensity is higher than the sensory input intensity. In this condition, the parameters of the gate circuit evolve so that pain is triggered in abnormal situations generating dysesthesia. When sensory and/or nociceptive inputs are very low, the gate circuit parameters evolve to produce wind-up pain. Phantom pain is included in this case as an extreme situation. Finally, when either nociceptive or mechanoreceptor stimulus is extremely high, wind-down pain is produced (see Figure 14).

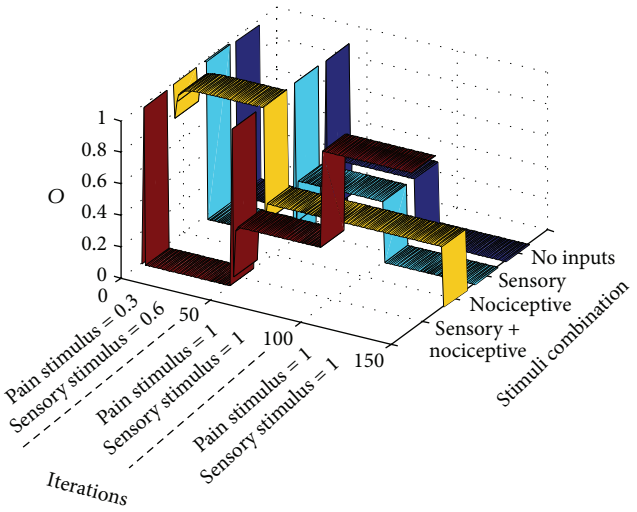

Figure 14: Modelling the hypothetical situation where, after a period of standard stimulation, gate circuit inputs are both very intense as from iteration 50 to iteration 100. After iteration 100, the four different combinations of nociceptive/sensory inputs are presented to the circuit. In the present case, as in Figures 10 and 11 cases, plasticity is blocked from iterations 100 to 150, in order to analyze the response of the circuit. As can be noticed, pain response is only intense when both sensory and nociceptive inputs are intense and are simultaneously applied. When only a nociceptive intense input is applied, the pain response is moderate. No pain response is obtained in the remaining cases.

pain, and demyelinating syndromes like Guillain-Barré and multiple sclerosis. Two very simple equations allow the adaptation of synaptic weights (4) and firing thresholds (5) when different input patterns are delivered to the circuit. In the case of standard gate operation, modelled synaptic weights and firing thresholds values converge to very specific values independently of their starting values. The obtained parameters allow the same normal operation of the real gate circuit. When stimulation is not standard, due to external or internal factors, like demyelination syndromes, modelled synaptic weights and thresholds spontaneously settle down in stability points that give rise to precisely the same non-standard pain conditions associated with the nonstandard type of stimulation. For example, intense constant stimuli produce pain reduction in the model like in real wind-down pain; weak constant sensorial stimuli produce growing pain in the model like in real wind-up pain; weakening of mechanoreceptor inputs produces abnormal pain (allodynia) in the model like in real demyelinating syndromes; and null inputs produce abnormal pain sensations (dysesthesia) like in phantom pain.

Our work opens a door in which computational models can be useful for treating pain syndromes: for relieving pain, it is possible to plan a strategy involving plasticity blockers or plasticity enhancers, together with stimulation schedules. This plan can be initially tested in a computer environment so that a personalized strategy can be planned depending on the subject's pain condition.

Conflict of Interests

The authors declare that they have no financial relation or conflict of interests with any third party mentioned in this paper or any other person or organization that would have any interests in the subject discussed in this paper.

References

[1] R. Melzack and P. D. Wall, "Pain mechanisms: a new theory," *Science*, vol. 150, no. 3699, pp. 971–979, 1965.

[2] P. D. Wall, "The gate control theory of pain mechanisms. A re-examination and re-statement," *Brain*, vol. 101, no. 1, pp. 1–18, 1978.

[3] P. W. Nathan and P. Rudge, "Testing the gate-control theory of pain in man," *Journal of Neurology, Neurosurgery and Psychiatry*, vol. 37, no. 12, pp. 1366–1372, 1974.

[4] P. W. Nathan, "The gate control theory of pain: a critical review," *Brain*, vol. 99, no. 1, pp. 123–158, 1976.

[5] N. S. Desai, L. C. Rutherford, and G. G. Turrigiano, "Plasticity in the intrinsic excitability of cortical pyramidal neurons," *Nature Neuroscience*, vol. 2, no. 6, pp. 515–520, 1999.

[6] G. G. Turrigiano, "Homeostatic plasticity in neuronal networks: the more things change, the more they stay the same," *Trends in Neurosciences*, vol. 22, no. 5, pp. 221–227, 1999.

[7] J. Sandkühler, "Models and mechanisms of hyperalgesia and allodynia," *Physiological Reviews*, vol. 89, no. 2, pp. 707–758, 2009.

[8] A. Artola, S. Bröcher, and W. Singer, "Different voltage-dependent thresholds for inducing long-term depression and long-term potentiation in slices of rat visual cortex," *Nature*, vol. 347, no. 6288, pp. 69–72, 1990.

[9] C. J. Woolf and S. W. N. Thompson, "The induction and maintenance of central sensitization is dependent on *N*-methyl-D-aspartic acid receptor activation; implications for the treatment of post-injury pain hypersensitivity states," *Pain*, vol. 44, no. 3, pp. 293–299, 1991.

[10] H. Baba, T. P. Doubell, K. A. Moore, and C. J. Woolf, "Silent NMDA receptor-mediated synapses are developmentally regulated in the dorsal horn of the rat spinal cord," *Journal of Neurophysiology*, vol. 83, no. 2, pp. 955–962, 2000.

[11] C. J. Woolf and M. W. Salter, "Neuronal plasticity: increasing the gain in pain," *Science*, vol. 288, no. 5472, pp. 1765–1768, 2000.

[12] A. J. Todd, "Neuronal circuitry for pain processing in the dorsal horn," *Nature Reviews Neuroscience*, vol. 11, no. 12, pp. 823–836, 2010.

[13] J.-L. Gaiarsa, O. Caillard, and Y. Ben-Ari, "Long-term plasticity at GABAergic and glycinergic synapses: mechanisms and functional significance," *Trends in Neurosciences*, vol. 25, no. 11, pp. 564–570, 2002.

[14] A. Compston, "The 150th anniversary of the first depiction of the lesions of multiple sclerosis," *Journal of Neurology, Neurosurgery and Psychiatry*, vol. 51, no. 10, pp. 1249–1252, 1988.

[15] J.-B. Landry, "Note sur la paralysie ascendante aiguë," *Gazette Hebdomadaire de Médecine et de Chirurgie*, vol. 6, pp. 472–488, 1859.

[16] F. J. R. Peláez and D. Andina, "Do biological synapses perform probabilistic computations?" *Neurocomputing*, vol. 114, pp. 24–31, 2013.

[17] R. S. F. Feldman, "Current theories and treatments related to phantom limb pain," *Orthotics and Prosthetics*, vol. 35, no. 3, pp. 26–30, 1981.

[18] A. Vaso, H.-M. Adahan, A. Gjika et al., "Peripheral nervous system origin of phantom limb pain," *Pain*, vol. 155, no. 7, pp. 1384–1391, 2014.

[19] B. Pentland and S. M. Donald, "Pain in the Guillain-Barre syndrome: a clinical review," *Pain*, vol. 59, no. 2, pp. 159–164, 1994.

[20] D. B. Clifford and J. L. Trotter, "Pain in multiple sclerosis," *Archives of Neurology*, vol. 41, no. 12, pp. 1270–1272, 1984.

[21] R. K. Portenoy and N. A. Hagen, "Breakthrough pain: definition, prevalence and characteristics," *Pain*, vol. 41, no. 3, pp. 273–281, 1990.

[22] R. K. Portenoy, K. Forbes, D. Lussier, and G. Hanks, "Difficult pain problems: an integrated approach," in *Oxford Textbook of Palliative Medicine*, D. Doyle, G. Hanks, N. Cherny, and K. Calman, Eds., pp. 438–458, Oxford University Press, Oxford, UK, 3rd edition, 2004.

[23] S. Mercadante, P. Ferrera, L. Di Emidio, E. Arcuri, and W. Tirelli, "When the progression of disease lowers opioid requirement in cancer patients," *Clinical Journal of Pain*, vol. 26, no. 1, pp. 56–57, 2010.

Hindawi Publishing Corporation
Neural Plasticity
Volume 2016, Article ID 1682972, 9 pages
http://dx.doi.org/10.1155/2016/1682972

Research Article

TRPV1 and PLC Participate in Histamine H4 Receptor-Induced Itch

Tunyu Jian,[1] Niuniu Yang,[1] Yan Yang,[1] Chan Zhu,[1] Xiaolin Yuan,[1] Guang Yu,[1] Changming Wang,[1] Zhongli Wang,[1] Hao Shi,[1] Min Tang,[1] Qian He,[1] Lei Lan,[2] Guanyi Wu,[1,3] and Zongxiang Tang[1]

[1]*College of Basic Medicine, Nanjing University of Chinese Medicine, 138 Xianlin Road, Nanjing 210023, China*
[2]*College of Life Science, Nanjing Normal University, Nanjing 210046, China*
[3]*College of Basic Medicine, Guangxi University of Chinese Medicine, 13 Wuhe Road, Nanning 530200, China*

Correspondence should be addressed to Guanyi Wu; w5gy1@126.com and Zongxiang Tang; zongxiangtang1@163.com

Received 15 May 2015; Revised 31 August 2015; Accepted 3 September 2015

Academic Editor: Feng Wei

Histamine H4 receptor has been confirmed to play a role in evoking peripheral pruritus. However, the ionic and intracellular signaling mechanism of activation of H4 receptor on the dorsal root ganglion (DRG) neurons is still unknown. By using cell culture and calcium imaging, we studied the underlying mechanism of activation of H4 receptor on the DRG neuron. Immepip dihydrobromide (immepip)—a histamine H4 receptor special agonist under cutaneous injection—obviously induced itch behavior of mice. Immepip-induced scratching behavior could be blocked by TRPV1 antagonist AMG9810 and PLC pathway inhibitor U73122. Application of immepip (8.3–50 μM) could also induce a dose-dependent increase in intracellular Ca^{2+} ($[Ca^{2+}]_i$) of DRG neurons. We found that 77.8% of the immepip-sensitized DRG neurons respond to the TRPV1 selective agonist capsaicin. U73122 could inhibit immepip-induced Ca^{2+} responses. In addition, immepip-induced $[Ca^{2+}]_i$ increase could be blocked by ruthenium red, capsazepine, and AMG9810; however it could not be blocked by TRPA1 antagonist HC-030031. These results indicate that TRPV1 but not TRPA1 is the important ion channel to induce the DRG neurons' responses in the downstream signaling pathway of histamine H4 receptor and suggest that TRPV1 may be involved in the mechanism of histamine-induced itch response by H4 receptor activation.

1. Introduction

Acute and chronic itch (pruritus) is an unpleasant sensation that elicits the desire or reflex to scratch. It was first defined by Samuel Hafenreffer, a German physician [1]. Pruritus is a common clinical symptom that can accompany skin or systemic diseases, for example, atopic eczema, atopic contact dermatitis, kidney failure, and liver cirrhosis [2]. Pruritogens including amines, proteases, and cytokines have been implicated in the induction of itch such as thymic stromal lymphopoietic protein (TSLP) [3], histamine [4], 5-HT [5], Ser-Leu-Ile-Gly-Arg-Leu (SLIGRL) [6], substance P [7], and IL-31 [8].

Histamine is one of the best-known endogenous mediators for the induction of itch. It is known that histamine receptors, which are found and cloned a class of G protein-coupled receptor so far, can be classified into four referred to as H1–4 [9]. H4 receptor is a new histamine receptor identified in 2000 [10]. Interestingly, some studies have implicated the H4 receptors' involvement in mediating pruritus in mice [11–13]. The intradermally injected H4 receptors agonist 4-methylhistamine could induce itch in mice [12]. In addition, immunohistochemistry and single RT-PCR studies have shown that H4 receptors are expressed in the DRG neurons of humans and rats, and their mRNA have been found in the sensory neuron [14, 15]. Furthermore, the H4 receptor agonist excites the mouse DRG neuron by increasing intracellular free calcium [14]. However, the mechanism of the H4 receptor in DRG neurons—a cluster of nerve cell bodies of peripheral sensory formation including itch—is not yet fully understood. Thus, in the present study, by using cell culture and calcium imaging, we investigated the response

properties of DRG neurons by activated histamine H4 receptor downstream signaling pathways and the pruritogens' mechanism of H4 receptor-induction. The results show that the response of DRG by activated H4 receptor was mediated by opening TRPV1 after the stimulated PLC pathway.

2. Materials and Methods

2.1. Animals and Cultures of Dissociated DRG Neurons. Four-week-old C57BL/6 mice of either sex were deeply anaesthetized with isoflurane and then exsanguinated. The spinal cord was exposed and DRG from all spinal levels were dissected. Isolated ganglia were collected in a cold culture medium containing the following: 90% DMEM-F/12, 10% fetal bovine serum, 100 μg/mL Streptomycin, and 100 U/mL penicillin (Gibco, USA). Ganglia were washed three times with culture medium and enzymatically digested in dispase (5 mg/mL, Gibco, USA) and collagenase type I (1 mg/mL, Gibco, USA) dissolved in Ca^{2+} and Mg^{2+}-free Hank's buffered salt solution (HBSS, Gibco, USA) for 30 min at 37°C, as described previously [16, 17]. DRG cells were dissociated by trituration using fire-polished Pasteur pipettes of decreasing tip pore size. Cells were centrifuged at 1200 rpm for 5 min and resuspended in the culture medium, plated on glass cover slips pretreated with 0.5 mg/mL poly-D-lysine (Sigma) and 10 μg/mL laminin (Sigma). Cells were incubated at 37°C in an incubator (95% O_2 + 5% CO_2 gas mixture) for 3 h and then flooded with additional culture medium and further incubated at 37°C. Experiments were performed within the next 24 h.

2.2. Calcium Imaging. Culture cells on cover slips were loaded with 2 μmol/L fura 2-acetomethoxy ester (Molecular Probes) supplemented with 0.01% Pluronic F-127 (wt/vol) for 40 min in the dark at 37°C. After a three-time wash with HBSS, the cells were imaged by a microscope (Olympus, Japan), and a high-speed continuously scanning monochromatic light source (Polychrome V; Till Photonics, Gräfelfing, Germany) was used for excitation at 340 and 380 nm to detect intracellular free calcium concentration ($[Ca^{2+}]_i$). Fluorescence intensities at both wavelengths (F340 and F380) were measured every 1–5 s, and images were obtained using PC-based software (C-imaging systems; Hamamatsu Photonic). Test compounds (agonist or antagonist inhibitor) were applied to these cells on the cover glass during scanning. The solution for Ca^{2+} imaging in cultured DRG neurons contained 140 mM NaCl, 5 mM KCl, 1 mM $CaCl_2$, 2 mM $MgCl_2$, 10 mM Na-HEPES, and 10 mM glucose (pH 7.3). All graphs displaying fura-2 ratios were normalized to the baseline ratio F_{340}/F_{380} = (Ratio)/(Ratio$_{t=0}$). All data were expressed as means ± SEM. Student's t-test was employed for statistical analysis of the data and P values of <0.05 were considered significant.

3. Results

To test the potential role of H4 receptor in the DRG neurons, we first investigated the effects of H4 agonist immepip dihydrobromide (immepip) and histamine to $[Ca^{2+}]_i$ in dissociated DRG neurons. We applied 50 μM immepip and histamine to the dissociated DRG neurons in a chamber perfusion solution, according to previous studies [14]. Of the 2,305 DRG neuron cultures, 74 (74/2305, 3.21%) showed a remarkable increase of $[Ca^{2+}]_i$ evoked by H4 agonist immepip; the remaining cells (96.79%) had no response (Figures 1(a) and 1(b)). All these response-neurons to immepip were small-to-medium-sized cells (Figure 1(d)). The number of cells responding did not increase when a high dose of immepip was applied. The immepip-induced increases of $[Ca^{2+}]_i$ responses on DRG neurons were in a concentration-dependent manner. By using 8.3, 16.6, and 50 μM immepip, the increased $[Ca^{2+}]_i$ were 0.22 ± 0.03 (N = 5), 0.24 ± 0.04 (N = 5), and 0.36±0.05 (N = 5), respectively (Figure 1(c)). To reveal the relationship between the histamine and H4 agonist immepip on the DRG neurons, in some cases, we perfused the DRG neurons with immepip and histamine. All immepip-activated neurons are the histamine-activated neurons (Figures 1(d)–1(i)). As shown in Figures 1(d)–1(i), immepip only induced Ca^{2+} response on neuron 2, but histamine induced Ca^{2+} response on both neuron 1 and neuron 2 (Figures 1(g), 1(h), and 1(i)). To test whether the immepip is a selective agonist of H4 receptor on the DRG neurons, we investigated the blocked effects of H4 antagonist JNJ7777120 on the immepip-induced response in dissociated DRG neurons. The results show that H4 antagonist JNJ7777120 totally blocked the immepip-induced Ca^{2+} change (N = 7) (Figure 2).

It has long been known that most of the neurons' responses to histamine increase in $[Ca^{2+}]_i$ by application of capsaicin [4]; therefore, to determine more precisely whether immepip-activated neurons also respond to the TRPV1 highly selective agonist capsaicin, we examined the response of cells by the capsaicin-followed immepip. The results indicate that 77.8% (18 of 20) of the neurons that respond to immepip (50 μM) could be activated by application of capsaicin (1 μM) (Figure 3). These results suggest that TRPV1 may be a potential candidate downstream ion channel for activation of H4 receptor on DRG neurons.

To clarify that G protein is involved in the excitatory effect of H4 agonist immepip on DRG neurons, we tested whether a G protein selective antagonist could block the excitation of immepip-induced response. In 14 detected neurons, N-ethylmaleimide (NEM, 10 μM), a selective G protein blocker [18], blocked the increase in $[Ca^{2+}]_i$ of immepip-induced response in DRG neurons. $[Ca^{2+}]_i$ of the DRG neurons increased 21.7% (N = 14) by perfusion with immepip. Immepip-induced elevation $[Ca^{2+}]_i$ of DRG neurons was abolished by preincubated with NEM (Figures 4(a) and 4(b)). In addition, NEM could not block the increase in $[Ca^{2+}]_i$ of DRG neuron by application of capsaicin (Figure 4(a)). These results indicate that G protein is involved in the H4 agonist immepip-induced excitatory effect.

To determine whether the PLC pathway mediates the neuronal excitation by immepip, a PLC-selective blocker was applied. The results revealed that 10 μM of U73122 could remarkably reduce the increase in $[Ca^{2+}]_i$ of DRG neurons by application of immepip (0.30 ± 0.05 versus 0.08 ± 0.03, paired

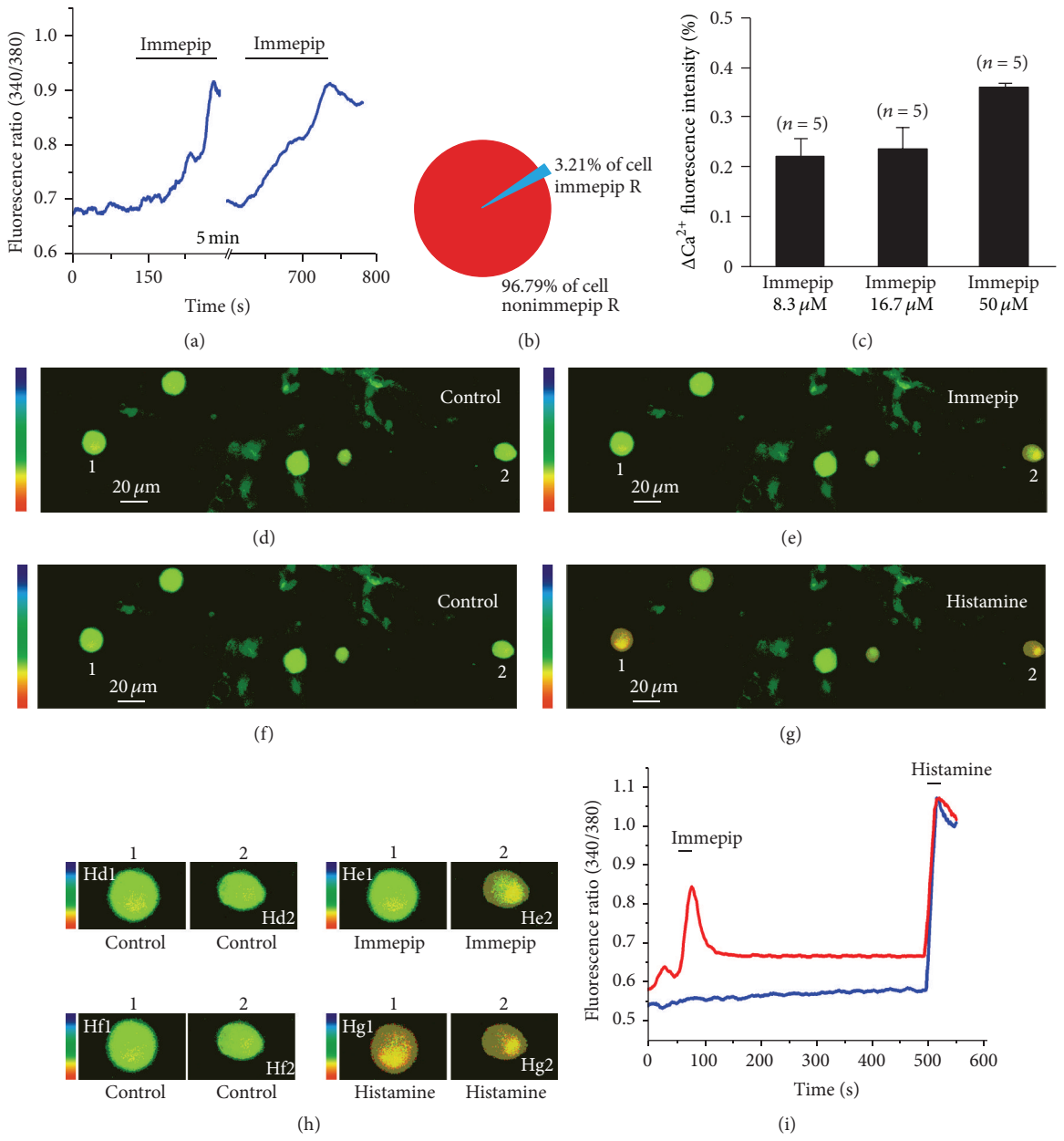

Figure 1: H4 receptor agonist immepip induced an increase in $[Ca^{2+}]_i$ of the DRG neuron. (a) Representative traces of DRG response to H4 agonist 50 μM immepip twice in 5 min interval. (b) Venn diagram of cell shows the proportion of immepip-response DRG neuron in total test neurons. (c) Histograms show that the DRG neuron exhibited a concentration-dependent increase in $[Ca^{2+}]_i$ response to 8.3, 16.7, and 50 μM immepip stimulation. (d, e, f, and g) Representative neurons response to 50 μM immepip and 50 μM histamine, (d) control, (e) neuron 2 increase in $[Ca^{2+}]_i$ by application of immepip, (f) washout, and (g) neurons 1 and 2 increase in $[Ca^{2+}]_i$ by application histamine. (h) Magnified neuron images of the same neurons in (d–g). Images of Hd1, Hd2 were magnified from neurons 1 and 2 in (d); images of He1, He2 were magnified from neurons 1 and 2 in (e); images of Hf1, Hf2 were magnified from neurons 1 and 2 in (f); images of Hg1, Hg2 were magnified from neurons 1 and 2 in (g). (i) Traces of DRG neurons 1 and 2 from (d–g) response to immepip and histamine; the data show both neuron 1 and neuron 2 respond to histamine (blue line), but only neuron 2 responds to immepip (red line).

t-test, $P < 0.05$, and $N = 10$) (Figures 4(c) and 4(d)). These results suggest that immepip induces an increase in $[Ca^{2+}]_i$ of DRG neurons by stimulating the PLC pathway.

To reveal whether the TRP channel is involved in an excitation action of immepip-induced response on the DRG neurons, we perfused neurons with ACSF containing the TRP channel blocker. As can be seen in Figure 4(e), the results show that a TRP channel antagonist ruthenium red (10 μM), which is known to block TRPV1 and TRPA1, inhibits the increase in $[Ca^{2+}]_i$ of DRG neurons by an immepip-induced response ($[Ca^{2+}]_i$ decrease from 0.29 ± 0.08 to 0.076 ± 0.04, Figure 4(f)). In addition, 10 μM of HC-030031, a highly

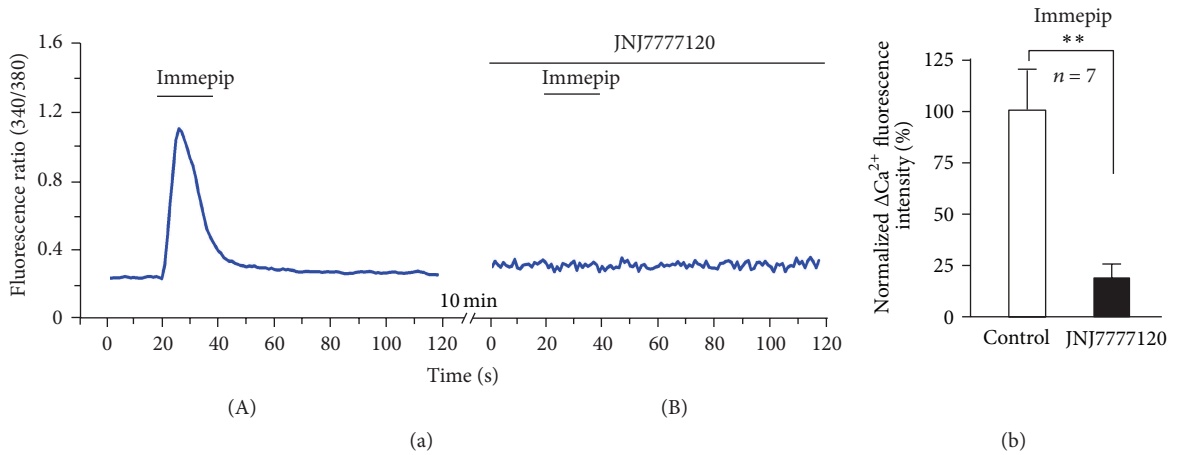

FIGURE 2: Immepip is a selective agonist of H4 receptor on the DRG neurons. (a) H4 antagonist JNJ7777120 (1 μM) totally blocked the immepip (50 μM)-induced increase in $[Ca^{2+}]_i$ ($N = 7$). (b) Normalized ΔCa^{2+} fluorescence intensity (%) of the responsive neurons. $^{**}P < 0.05$.

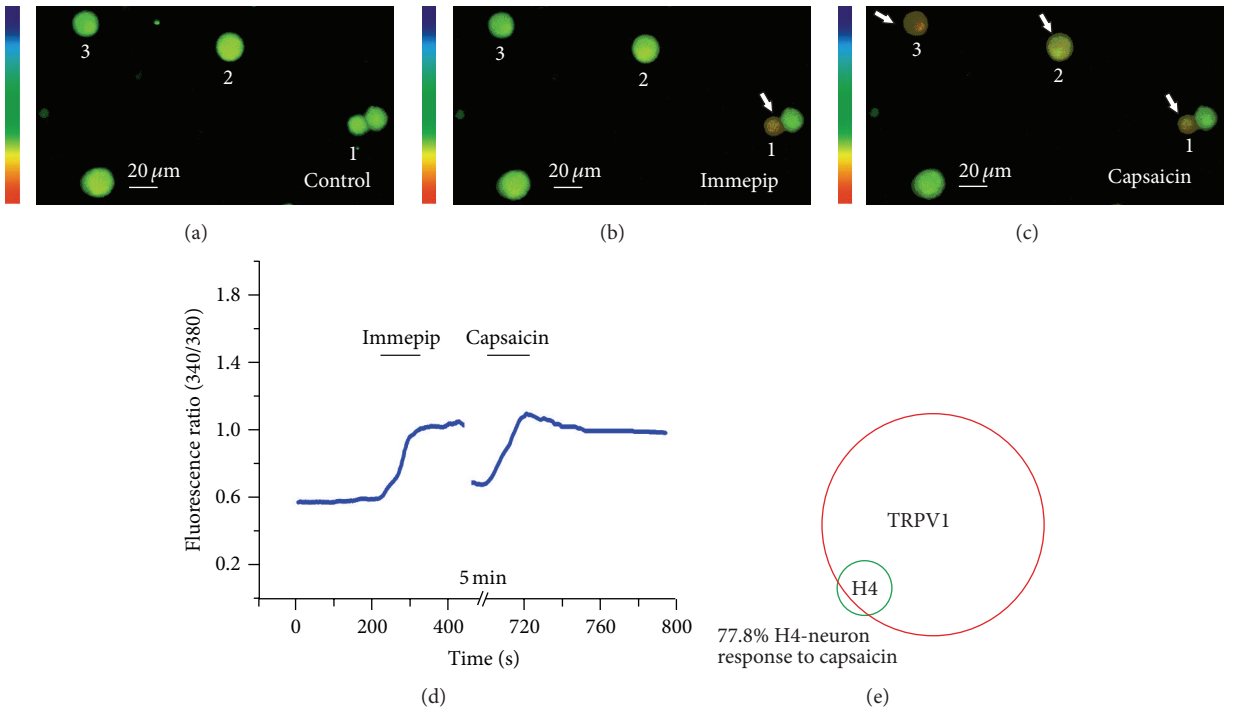

FIGURE 3: Immepip-sensitive DRG neuron responds to capsaicin. (a) Control, (b) immepip-induced increase in $[Ca^{2+}]_i$ of DRG neuron 1. (c) Capsaicin-induced increase in $[Ca^{2+}]_i$ of DRG neurons 1, 2, and 3. (d) Representative traces of another DRG response to immepip (50 μM) and capsaicin (1 μM). (e) Venn diagram showing relative proportion of immepip-sensitive DRG neuron responsive to capsaicin.

selective TRPA1 antagonist, could not block the immepip-induced calcium influx (0.28 ± 0.05 versus 0.35 ± 0.07, paired t-test, $P = 0.3168$, and $N = 5$) (Figures 4(g) and 4(h)). These results indicate that TRPV1 but not TRPA1 is involved in the H4 receptor-mediated effect on the DRG neurons. Furthermore, capsazepine, a highly selective TRPV1 antagonist, could significantly inhibit the immepip-induced excitation on DRG neurons (0.38 ± 0.13 versus 0.09 ± 0.01, paired t-test, $P < 0.05$, and $N = 5$) (Figures 5(a) and 5(b)). We also applied a typical TRPV1 antagonist, AMG9810, to test whether the TRPV1 was involved in the immepip-induced response. Immepip- and capsaicin-induced excitation were inhibited by AMG9810 in the same neurons (Figures 5(c), 5(d), and 5(e)).

To confirm the scratching effect of immepip on the histamine H4 receptor-mediated itch, the scratching bouts were counted for 30 minutes after the topical subcutaneous injection of immepip (100 μmol, 100 μL/site) into the nape of

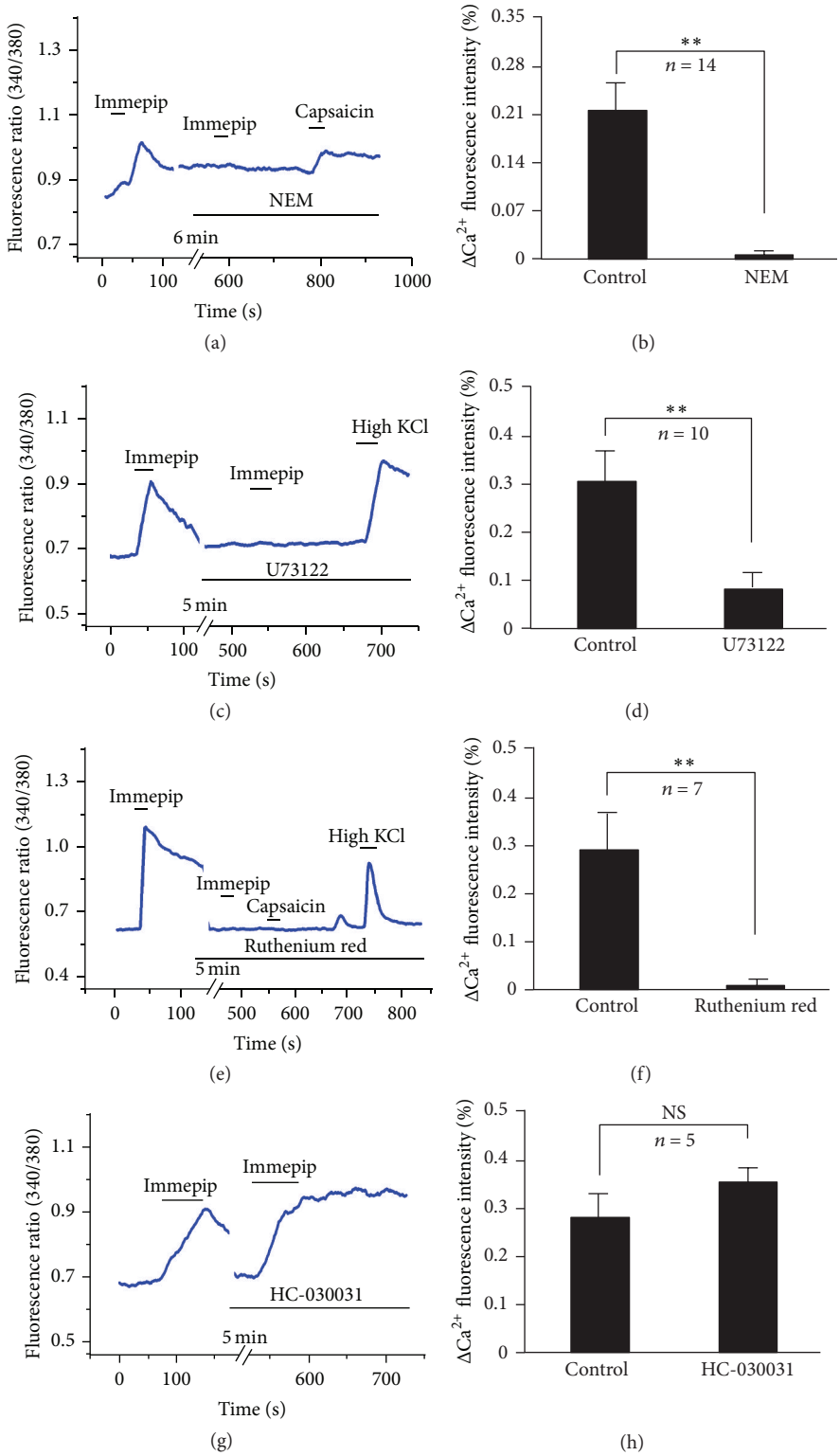

Figure 4: The effects of G protein, PLC, and TRP inhibitor on the immepip-induced increase in $[Ca^{2+}]_i$ of DRG neurons. (a, c, and e) G protein inhibitor NEM ($N = 14$), PLC inhibitor U73122 ($N = 10$), and TRP channels antagonist ruthenium red ($N = 7$) blocked the immepip-induced increase in $[Ca^{2+}]_i$, but TRPA1 antagonist HC-030031 ($N = 7$) could not block the immepip-induced increase in $[Ca^{2+}]_i$ (g). (b, d, f, and h) Mean changes (Δ) R (340/380) of the responsive neurons. $^{**}P < 0.05$.

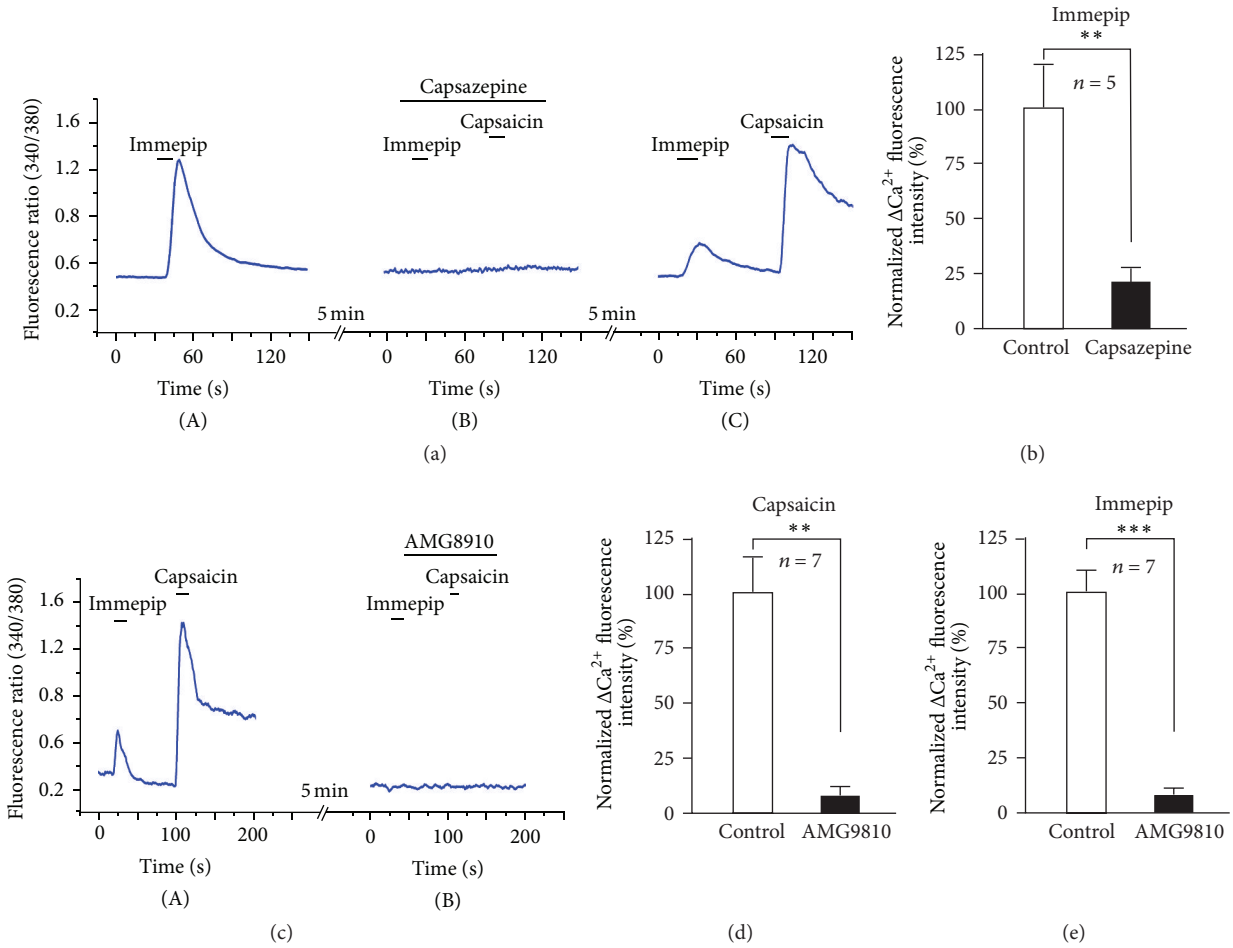

FIGURE 5: The effects of TRPV1 antagonist capsazepine on the immepip-induced increase in $[Ca^{2+}]_i$ of DRG neurons. (a) H4 agonist immepip (50 μM) and TRPV1 agonist capsaicin (1 μM)-evoked increase in $[Ca^{2+}]_i$ were evidently inhibited by TRPV1 antagonist capsazepine (1 μM) ($N = 5$), after washout of capsazepine, the DRG neuron recovery response to immepip and capsaicin. (c) Immepip (50 μM) and TRPV1 agonist capsaicin (1 μM)-evoked increase in $[Ca^{2+}]_i$ were also obviously blocked by TRPV1 typical antagonist AMG9810 (5 μM) ($N = 7$). (b, d, and e) Normalized ΔCa^{2+} fluorescence intensity (%) of the responsive neurons in the different blockers ($^{**}P < 0.01$, $^{***}P < 0.001$).

the mouse neck. The results show that the immepip induced obvious scratching behavior (96 ± 11 versus 5 ± 1, paired t-test, $P < 0.001$, and $N = 6$) (Figure 6(a)). Furthermore, after pretreatment with a typical TRPV1 antagonist, AMG9810, the scratching bouts of the immepip-induced response (98 ± 12, $N = 9$) were significantly blocked (23 ± 3, paired t-test, $P < 0.001$, and $N = 9$) (Figure 6(b)). The immepip-induced scratching behavior was also inhibited by U73122. As shown in Figure 6(c), the scratching bouts of immepip decreased from 94 ± 8 to 13 ± 5 ($N = 8$, paired t-test, and $P < 0.001$).

4. Discussion

Histamine has long been a well-known endogenous pruritogen substance and was richly predominant in peripheral mast cell and basophile granulocytes [2]. H4 receptor is a recently found histamine receptor and is a seven-transmembrane G protein coupled receptor expressed mainly in peripheral bone marrow eosinophils and mast cells [10, 19]. Although there have been extensive studies in recent years about the H4 receptor function in histamine-dependent itch in animal behavior models [11–14], the ionic mechanism and downstream signal pathway of activation of H4 receptor on DRG neuron are still unclear. In the present study, we have revealed that TRPV1 and PLC—but not TRPA1—were involved in the immepip-induced calcium influx on DRG neurons by activation of H4 receptor, demonstrating more cellular details of histamine H4 receptor in sensory neurons.

Phospholipase C (PLC) plays a key role in the signaling pathway links of GPCRs to an intracellular signaling network [20]. In sensory signal transduction, PLC-mediated pathways also play an important role. For example, MrgD, a histamine-independent itch receptor, can be activated by β-alanine that couples to an endogenous calcium-activated chloride channel in *Xenopus oocytes* by the PLC pathway [21, 22]. The PLC signaling is also required for TSLP-induced itch in epithelial cell-derived atopic dermatitis [3]. PLCβ3, a PLC isoform, is required to mediate the itch sensation in response

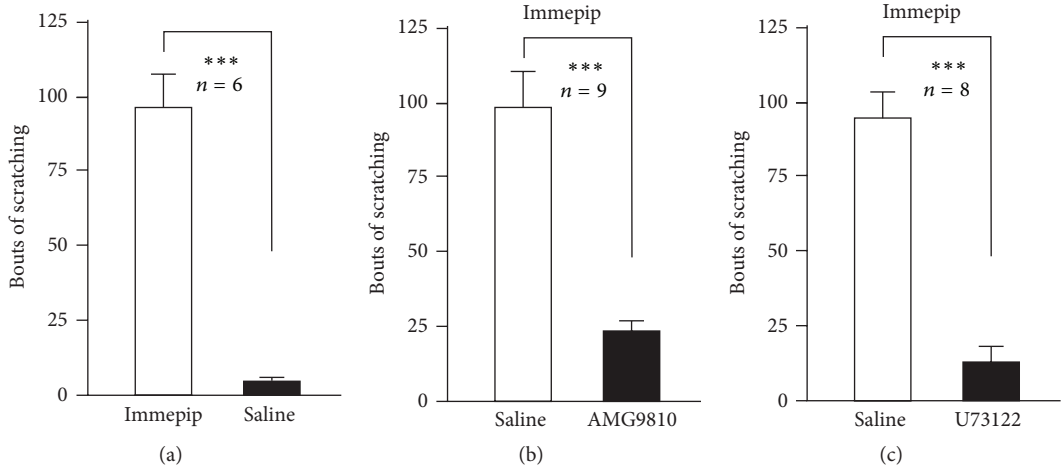

Figure 6: AMG9810 and U73122 inhibited immepip-induced scratching in mice. The histogram shows bouts of scratching by injection of immepip 100 μmol and saline 100 μL/site ($n = 6$) (a). (b) Saline (PBS) 100 μL/site or AMG9810 5 μM 100 μL/site 30 minutes pretreated before immepip subcutaneous injection. Saline (PBS) 100 μL/site or U73122 1 μM 100 μL/site 30 minutes pretreated before immepip subcutaneous injection in (c). The data are presented as mean ± SEM ($^{***}P < 0.001$).

to histamine acting on the histamine H1 receptor in C-fiber nociceptive neurons [23]. Similarly, in the present study, PLC antagonist U73122 totally blocked the immepip-induced excitation of the DRG neurons by activation of the histamine H4 receptor (Figure 4). These results suggest that the PLC pathway is involved in the histamine H4 receptor intracellular signaling of DRG neurons.

TRPV1 is a nonselective cation channel present predominantly in primary small sensory neurons and is activated by the pungency of capsaicin and acid or at temperatures over 43°C [24]. TRPV1 can also be indirectly activated by several other substances through activation on their specific receptors and by initiating various intracellular signaling pathways, such as histamine [4, 25], leukotriene B4 [26], or IL-31. TRPV1 has also been shown to be involved in histamine-induced scratching by activation of the histamine H1 receptor that can be activated by a phospholipase A2 pathway [4, 25]. But the interaction between TRPV1 and the histamine H4 receptor is still not understood. In this study, the highly selective TRPV1 antagonist capsazepine blocked the response of DRG neurons upon activation of the histamine H4 receptor. Furthermore, the TRP channel blocker, ruthenium red, can also block the response by activation of the histamine H4 receptor. The increase in $[Ca^{2+}]_i$ of DRG neurons by immepip-induced response could not be inhibited by the highly selective TRPA1 antagonist HC03003. These results indicate that TRPV1 is a functional downstream ionic channel of intracellular signaling by activation of the DRG histamine H4 receptor.

What is more, TRPV1 can be coupled to the PLC intracellular signaling pathway. First, TRPV1 currents were sensitized and activated by bradykinin, which is an inflammatory mediator, and by extracellular cations [27, 28]. Furthermore, TRPV1 can be activated by the byproduct of PLC activation, such as diacylglycerol, one of two classical second messengers of PLC [29]. TRPV1 can also be modulated by the substrates of PLC, which include the membrane phospholipid PIP2, inositol 1,4,5-trisphosphate (IP3), and diacylglycerol. They could dually modulate the sensitization and desensitization of the TRPV1 channel [30]. In this study, PLC and TRPV1 may be jointly involved in the excitation of DRG neurons by the activation of histamine H4 receptor. More studies need to be conducted to ascertain how the downstream byproduct of PLC activates TRPV1.

In summary, by activation of the histamine H4 receptor on mouse DRG neurons, immepip induced an increase in $[Ca^{2+}]_i$ via the intracellular PLC signaling pathway and TRPV1 but not TRPA1. By activation of the histamine H4 receptor, histamine may directly modulate the sensation from endogenous and exogenous mediators [31–33]. Considering that histamine is a well-known and definite itch causing substance [34–36], the histamine H4 receptor may constitute a critical part of histamine-induced itch in peripherals. It is presumed that the function of the histamine H4 receptor on the DRG neurons will help us clearly understand the mechanisms of histamine-dependent itch.

Conflict of Interests

The authors declare that there is no conflict of interests regarding the publication of this paper.

Authors' Contribution

Tunyu Jian and Niuniu Yang contributed equally to this work.

Acknowledgments

This work was supported by grants to Zongxiang Tang (31271181, 31328012), Guanyi Wu (31400950), and Xiaolin Yuan (81403407) from the NSFC, by the Nature Science Foundation of Jiangsu Province to Guanyi Wu (BK20130953), and

by the Administration of Traditional Chinese Medicine of Jiangsu Province Nanjing University of Traditional Chinese Medicine and Graduate Research and Innovation Projects in Jiangsu Province (LZ130953, LZ13020, 12XZR02, and CXLX12-0580), from the project funded by the Priority Academic Program Development of Jiangsu Higher Education Institutions (PAPD), sponsored by "Qing Lan Project" in Jiangsu Province, and from the Jiangsu Collaborative Innovation Center of Traditional Chinese Medicine (TCM) Prevention and Treatment of Tumor, Nanjing University of Chinese Medicine, Nanjing 210023, China.

References

[1] A. Ikoma, M. Steinhoff, S. Ständer, G. Yosipovitch, and M. Schmelz, "The neurobiology of itch," *Nature Reviews Neuroscience*, vol. 7, no. 7, pp. 535–547, 2006.

[2] D. M. Bautista, S. R. Wilson, and M. A. Hoon, "Why we scratch an itch: the molecules, cells and circuits of itch," *Nature Neuroscience*, vol. 17, no. 2, pp. 175–182, 2014.

[3] S. R. Wilson, L. Thé, L. M. Batia et al., "The epithelial cell-derived atopic dermatitis cytokine TSLP activates neurons to induce itch," *Cell*, vol. 155, no. 2, pp. 285–295, 2013.

[4] W.-S. Shim, M.-H. Tak, M.-H. Lee et al., "TRPV1 mediates histamine-induced itching via the activation of phospholipase A2 and 12-lipoxygenase," *The Journal of Neuroscience*, vol. 27, no. 9, pp. 2331–2337, 2007.

[5] H. Nojima and E. Carstens, "5-hydroxytryptamine (5-HT)2 receptor involvement in acute 5-HT-evoked scratching but not in allergic pruritus induced by dinitrofluorobenzene in rats," *The Journal of Pharmacology and Experimental Therapeutics*, vol. 306, no. 1, pp. 245–252, 2003.

[6] S. G. Shimada, K. A. Shimada, and J. G. Collins, "Scratching behavior in mice induced by the proteinase-activated receptor-2 agonist, SLIGRL-NH2," *European Journal of Pharmacology*, vol. 530, no. 3, pp. 281–283, 2006.

[7] T. Andoh, T. Nagasawa, M. Satoh, and Y. Kuraishi, "Substance P induction of itch-associated response mediated by cutaneous NK1 tachykinin receptors in mice," *The Journal of Pharmacology and Experimental Therapeutics*, vol. 286, no. 3, pp. 1140–1145, 1998.

[8] F. Cevikbas, X. Wang, T. Akiyama et al., "A sensory neuron-expressed IL-31 receptor mediates T helper cell-dependent itch: involvement of TRPV1 and TRPA1," *The Journal of Allergy and Clinical Immunology*, vol. 133, no. 2, pp. 448.e7–460.e7, 2014.

[9] W.-S. Shim and U. Oh, "Histamine-induced itch and its relationship with pain," *Molecular Pain*, vol. 4, article no. 29, 2008.

[10] R. Leurs, P. L. Chazot, F. C. Shenton, H. D. Lim, and I. J. P. De Esch, "Molecular and biochemical pharmacology of the histamine H4 receptor," *British Journal of Pharmacology*, vol. 157, no. 1, pp. 14–23, 2009.

[11] J. K. Bell, D. S. McQueen, and J. L. Rees, "Involvement of histamine H_4 and H_1 receptors in scratching induced by histamine receptor agonists in BalbC mice," *British Journal of Pharmacology*, vol. 142, no. 2, pp. 374–380, 2004.

[12] P. J. Dunford, K. N. Williams, P. J. Desai, L. Karlsson, D. McQueen, and R. L. Thurmond, "Histamine H_4 receptor antagonists are superior to traditional antihistamines in the attenuation of experimental pruritus," *The Journal of Allergy and Clinical Immunology*, vol. 119, no. 1, pp. 176–183, 2007.

[13] J. M. Cowden, M. Zhang, P. J. Dunford, and R. L. Thurmond, "The histamine H4 receptor mediates inflammation and pruritus in Th2-dependent dermal inflammation," *Journal of Investigative Dermatology*, vol. 130, no. 4, pp. 1023–1033, 2010.

[14] K. Rossbach, C. Nassenstein, M. Gschwandtner et al., "Histamine H 1, H 3 and H 4 receptors are involved in pruritus," *Neuroscience*, vol. 190, pp. 89–102, 2011.

[15] M. I. Strakhova, A. L. Nikkel, A. M. Manelli et al., "Localization of histamine H_4 receptors in the central nervous system of human and rat," *Brain Research*, vol. 1250, pp. 41–48, 2009.

[16] A. Y. Kim, Z. Tang, Q. Liu et al., "Pirt, a phosphoinositide-binding protein, functions as a regulatory subunit of TRPV1," *Cell*, vol. 133, no. 3, pp. 475–485, 2008.

[17] Q. Liu, Z. Tang, L. Surdenikova et al., "Sensory neuron-specific GPCR Mrgprs are itch receptors mediating chloroquine-induced pruritus," *Cell*, vol. 139, no. 7, pp. 1353–1365, 2009.

[18] M. S. Shapiro, L. P. Wollmuth, and B. Hille, "Modulation of Ca^{2+} channels by PTX-sensitive G-proteins is blocked by N-ethylmaleimide in rat sympathetic neurons," *The Journal of Neuroscience*, vol. 14, no. 11, pp. 7109–7116, 1994.

[19] M. Nakaya, N. Takeuchi, and K. Kondo, "Immunohistochemical localization of histamine receptor subtypes in human inferior turbinates," *The Annals of Otology, Rhinology, and Laryngology*, vol. 113, no. 7, pp. 552–557, 2004.

[20] M. J. Marinissen and J. S. Gutkind, "G-protein-coupled receptors and signaling networks: emerging paradigms," *Trends in Pharmacological Sciences*, vol. 22, no. 7, pp. 368–376, 2001.

[21] Q. Liu, P. Sikand, C. Ma et al., "Mechanisms of itch evoked by beta-alanine," *The Journal of Neuroscience*, vol. 32, no. 42, pp. 14532–14537, 2012.

[22] R.-G. Zhuo, X.-Y. Ma, P.-L. Zhou et al., "Mas-related G protein-coupled receptor D is coupled to endogenous calcium-activated chloride channel in *Xenopus oocytes*," *Journal of Physiology and Biochemistry*, vol. 70, no. 1, pp. 185–191, 2014.

[23] S.-K. Han, V. Mancino, and M. I. Simon, "Phospholipase Cβ 3 mediates the scratching response activated by the histamine H1 receptor on C-fiber nociceptive neurons," *Neuron*, vol. 52, no. 4, pp. 691–703, 2006.

[24] M. J. Caterina, M. A. Schumacher, M. Tominaga, T. A. Rosen, J. D. Levine, and D. Julius, "The capsaicin receptor: a heat-activated ion channel in the pain pathway," *Nature*, vol. 389, no. 6653, pp. 816–824, 1997.

[25] B. M. Kim, S. H. Lee, W. S. Shim, and U. Oh, "Histamine-induced Ca^{2+} influx via the PLA_2/lipoxygenase/TRPV1 pathway in rat sensory neurons," *Neuroscience Letters*, vol. 361, no. 1–3, pp. 159–162, 2004.

[26] E. S. Fernandes, C. T. Vong, S. Quek et al., "Superoxide generation and leukocyte accumulation: key elements in the mediation of leukotriene B_4-induced itch by transient receptor potential ankyrin 1 and transient receptor potential vanilloid 1," *The FASEB Journal*, vol. 27, no. 4, pp. 1664–1673, 2013.

[27] L. S. Premkumar and G. P. Ahern, "Induction of vanilloid receptor channel activity by protein kinase C," *Nature*, vol. 408, no. 6815, pp. 985–990, 2000.

[28] G. P. Ahern, I. M. Brooks, R. L. Miyares, and X.-B. Wang, "Extracellular cations sensitize and gate capsaicin receptor TRPV1 modulating pain signaling," *The Journal of Neuroscience*, vol. 25, no. 21, pp. 5109–5116, 2005.

[29] D. H. Woo, S. J. Jung, M. H. Zhu et al., "Direct activation of transient receptor potential vanilloid 1(TRPV1) by diacylglycerol (DAG)," *Molecular Pain*, vol. 4, article 42, 2008.

[30] T. Rohacs, B. Thyagarajan, and V. Lukacs, "Phospholipase C mediated modulation of TRPV1 channels," *Molecular Neurobiology*, vol. 37, no. 2-3, pp. 153–163, 2008.

[31] T. Bíró, B. I. Tóth, R. Marincsák, N. Dobrosi, T. Géczy, and R. Paus, "TRP channels as novel players in the pathogenesis and therapy of itch," *Biochimica et Biophysica Acta: Molecular Basis of Disease*, vol. 1772, no. 8, pp. 1004–1021, 2007.

[32] T. Liu and R.-R. Ji, "New insights into the mechanisms of itch: are pain and itch controlled by distinct mechanisms?" *Pflügers Archiv*, vol. 465, no. 12, pp. 1671–1685, 2013.

[33] F. E. R. Simons and K. J. Simons, "Histamine and H_1-antihistamines: celebrating a century of progress," *The Journal of Allergy and Clinical Immunology*, vol. 128, no. 6, pp. 1139–1150.e4, 2011.

[34] T. Akiyama and E. Carstens, "Neural processing of itch," *Neuroscience*, vol. 250, pp. 697–71, 2013.

[35] S. Davidson and G. J. Giesler, "The multiple pathways for itch and their interactions with pain," *Trends in Neurosciences*, vol. 33, no. 12, pp. 550–558, 2010.

[36] A. E. Kremer, J. Feramisco, P. W. Reeh, U. Beuers, and R. P. J. Oude Elferink, "Receptors, cells and circuits involved in pruritus of systemic disorders," *Biochimica et Biophysica Acta*, vol. 1842, no. 7, pp. 869–892, 2014.

Hindawi Publishing Corporation
Neural Plasticity
Volume 2015, Article ID 394820, 16 pages
http://dx.doi.org/10.1155/2015/394820

Research Article

Activation of the Mammalian Target of Rapamycin in the Rostral Ventromedial Medulla Contributes to the Maintenance of Nerve Injury-Induced Neuropathic Pain in Rat

Jian Wang,[1] Da-Yun Feng,[2] Zhi-Hua Li,[3] Ban Feng,[1] Han Zhang,[1] Ting Zhang,[1] Tao Chen,[1] and Yun-Qing Li[1,4]

[1]*Department of Anatomy and K. K. Leung Brain Research Centre, Fourth Military Medical University, Xi'an 710000, China*
[2]*Department of Neurosurgery, Tangdu Hospital, Fourth Military Medical University, Xi'an 710000, China*
[3]*Basic Medical College, Zhengzhou University, Zhengzhou 450001, China*
[4]*Collaborative Innovation Center for Brain Science, Fudan University, Shanghai 200032, China*

Correspondence should be addressed to Yun-Qing Li; deptanat@fmmu.edu.cn

Received 11 May 2015; Accepted 6 July 2015

Academic Editor: Yun Guan

The mammalian target of rapamycin (mTOR), a serine-threonine protein kinase, integrates extracellular signals, thereby modulating several physiological and pathological processes, including pain. Previous studies have suggested that rapamycin (an mTOR inhibitor) can attenuate nociceptive behaviors in many pain models, most likely at the spinal cord level. However, the mechanisms of mTOR at the supraspinal level, particularly at the level of the rostral ventromedial medulla (RVM), remain unclear. Thus, the aim of this study was to elucidate the role of mTOR in the RVM, a key relay region for the descending pain control pathway, under neuropathic pain conditions. Phosphorylated mTOR was mainly expressed in serotonergic spinally projecting neurons and was significantly increased in the RVM after spared nerve injury- (SNI-) induced neuropathic pain. Moreover, in SNI rat brain slices, rapamycin infusion both decreased the amplitude instead of the frequency of spontaneous excitatory postsynaptic currents and reduced the numbers of action potentials in serotonergic neurons. Finally, intra-RVM microinjection of rapamycin effectively alleviated established mechanical allodynia but failed to affect the development of neuropathic pain. In conclusion, our data provide strong evidence for the role of mTOR in the RVM in nerve injury-induced neuropathic pain, indicating a novel mechanism of mTOR inhibitor-induced analgesia.

1. Introduction

The rostral ventromedial medulla (RVM) is an important relay region that contributes to the descending pain control pathway from the periaqueductal gray (PAG) to the superficial laminae (laminae I and II) of the spinal cord [1, 2]. It is well known that the RVM is closely linked to long-lasting activation of descending control circuits that involve descending facilitation, which significantly contributes to the development of persistent pain induced by tissue and nerve injury [3]. Although many studies have focused on this region, the cellular and molecular mechanisms of descending pain facilitation control remain poorly understood.

Due to the role of the descending pain facilitation pathway, several types of injuries, such as tissue and nerve injury, often become chronic and persistent [4], eventually leading to neuropathic pain. The neuropathic pain impairs quality of life and imposes high societal costs. To date, significant progress has been made in basic and clinical studies; however, the currently available therapies for neuropathic pain remain inadequate, and the search continues not only for improved treatments but also for novel targets.

The mammalian target of rapamycin (mTOR), a conserved serine-threonine protein kinase that is inhibited by the effective clinical immunosuppressant rapamycin, regulates several intracellular processes in response to various

extracellular signals and thereby modulates mRNA translation. Thus, mTOR plays a critical role in the modulation of long-term plasticity and memory processes [5–7]. Activation of the mTOR complex with the protein raptor (mTORC1) promotes the phosphorylation of mTOR downstream targets, including eukaryotic initiation factor 4E-binding protein (4E-BP1/2) and S6 kinase (S6K), which can further lead to local protein synthesis. It has been reported that deletion of either the 4E-BP1/2 or the S6K gene in mice results in deficits in synaptic plasticity and long-term memory [8, 9]. Moreover, phosphorylated mTOR (p-mTOR), which is the activated form, is upregulated in the peripheral nervous system as well as at the spinal cord level in several pain models [10–15]. Inhibition of spinal cord mTOR by intrathecal administration has proven to be effective in alleviating the nociceptive behaviors of animals under pain conditions [10, 11, 16, 17]. Synaptic plasticity changes in chronic pain conditions can occur not only at the spinal cord level but also at the supraspinal level, including the RVM. Therefore, considering the important role of the RVM in descending pain facilitation, targeting mTOR in the RVM might be a promising way to combat pain.

Because serotoninergic (5-HTergic) neurons are the primary constitutive element in the RVM and can send projections to the superficial spinal dorsal horn (SDH) [18–20], we thus hypothesize that 5-HTergic spinally projecting neurons in the RVM contain mTOR, the activation of which could in turn increase the excitability of the 5-HTergic neurons and thus may potently potentiate the descending facilitation pain control pathway and exaggerate neuropathic pain conditions.

Accordingly, we used a spared nerve injury (SNI) model to evaluate the role of mTOR in the RVM in neuropathic pain in rats.

2. Materials and Methods

2.1. Animals. Adult male Sprague-Dawley (SD) rats (weighing 250–290 g) were used in the present study. The Ethics Committee for Animal Experiments of the Fourth Military Medical University (Xi'an, China) approved the animal experiments (permit number: 10071). All procedures were in agreement with the IASP guidelines [21]. Efforts were made to minimize the number of animals used and their suffering.

2.2. Establishment of SNI Model. The SNI surgery was performed as reported previously [22, 23]. Briefly, rats were anesthetized with pentobarbital (45 mg/kg, *i.p.*), and three terminal branches of the sciatic nerve were exposed by direct incision of the skin and a section of the biceps femoris muscle in the left thigh. The tibial and common peroneal branches were carefully tight-ligated with 5-0 silk sutures and sectioned distal to the ligation, removing 2–4 mm of the distal nerve stump. Muscle and skin were closed in two layers. The surgical procedures for the sham-operated group were identical to those for the SNI group, except that the nerves were not lesioned.

2.3. Behavioral Tests. Mechanical allodynia, as a behavioral sign of SNI-induced neuropathic pain, was assessed by measuring the 50% paw withdrawal threshold (PWT) as described previously [24]. The 50% PWT in response to a series of ascending von Frey filaments (Stoelting, Kiel, WI, USA) was determined by the up-and-down method [25]. Von Frey force was delivered perpendicularly to the plantar surface of the hind paw for 2 to 3 seconds. An abrupt withdrawal of the hind paw during stimulation was recorded as a positive response. The 50% PWT was calculated using the following formula: 50% PWT $= 10^{[Xf+k\delta]}$. Mechanical allodynia was assessed by measuring the 50% PWT of the ipsilateral hind paw in SNI- or sham-operated rats.

Thermal hyperalgesia of the hind paws was tested as described in a previous report [26]. A radiant heat source was focused onto the plantar surface of the hind paw. Measurements of the paw withdrawal latency (PWL) were obtained using a timer that was started by the activation of the heat source and stopped when withdrawal of the paw was detected with a photodetector. Three measurements of the PWL were taken for each hind paw and were averaged as the result of each test session. The ipsilateral hind paw was tested with intervals of more than 5 min between consecutive tests.

2.4. Neuronal Tract Tracing. Fluoro-gold (FG) was used as a retrograde tracer to label the RVM neurons that project to the SDH. The procedures for FG injection were essentially the same as in our previous studies [20, 27]. Briefly, after exposing the lumbar cord, 0.1 μL of a 4% solution of FG (Fluorochrome, Denver, CO, USA) dissolved in 0.9% saline was stereotaxically injected into the left side of the lumbar dorsal horn with a microsyringe attached to a glass micropipette by pressure injection. Due to the transportation period of the tracer, the rats were allowed to recover and survive for 7 days.

After perfusion, the brains and spinal cords of the rats were cut into sections. The sections were used to evaluate the FG injection sites in the SDH as well as the distribution patterns of the retrogradely FG-labeled neurons in the RVM under an epifluorescence microscope (BX-60; Olympus, Tokyo, Japan) using an appropriate filter for FG (excitation 350–395 nm; emission 430 nm).

2.5. Cannula Implantation and Microinjection into the RVM. After the rats were anesthetized with pentobarbital (45 mg/kg, *i.p.*), a 26-gauge stainless steel guide cannula was stereotaxically implanted into a site above the RVM (10.52 mm posterior to bregma, 0 mm lateral from the midline, and 10.20 mm beneath the surface of the skull). The rats were given one week to recover after cannula implantation. Intra-RVM microinjections were delivered via a 33-gauge injector needle cannula that was lowered 0.5 mm deeper into the brainstem than the guide cannula. The microinjection apparatus consisted of a Hamilton syringe (10 μL) connected to an injector (33-gauge) by a thin polyethylene tube and a motorized syringe pump. Rapamycin (250 μM/1 μL, dissolved in a saline/DMSO mix comprising 25% DMSO, Tocris Bioscience, Minneapolis, MN, USA), the specific inhibitor for mTOR, was infused into the RVM at a rate of 0.1 μL/min; an equivalent volume of 25% DMSO was used as a vehicle. After injection, the microinjection needle was left in place for at least 2 min. The injection sites were verified at the end of all of the experiments by Nissl staining, and injection sites

outside the RVM region were excluded from the study. The total number of rats showing successful implantation in the target was 28.

These rats were randomly divided into two groups designed for different purposes, as shown in Figure 6(c): Group 1: to investigate whether rapamycin could influence the induction stage of SNI-induced neuropathic pain, behavioral tests were performed before the first drug or vehicle injection, followed by SNI (Pre-SNI), and 30 min after the second injection on day 1 after SNI (SNI-D1) (Figure 6(c), top) and Group 2: behavioral tests were performed before SNI (Pre-SNI), 6 days after SNI (SNI-D6), and 30 min after drug or vehicle injection on day 7 after SNI (SNI-D7) for the purpose of demonstrating the effect of rapamycin on the maintenance stage of SNI-induced neuropathic pain (Figure 6(c), bottom).

2.6. Immunofluorescent Histochemical Staining. The rats were transcardially perfused with 150 mL of 0.01 M phosphate-buffered saline (PBS, pH 7.4), followed by 500 mL of 4% paraformaldehyde in 0.1 M phosphate buffer (PB, pH 7.4). The brainstems and/or spinal cords were transversely sliced into 25 mm thick coronal sections using a freezing microtome (CM1950, Leica, Heidelberg, Germany).

Double-immunofluorescence staining for p-mTOR/NeuN, p-mTOR/FG, or p-mTOR/5-HT was performed. All the antisera used here are shown in Table 1. The sections were sequentially incubated at room temperature with primary antisera in 0.01 M PBS containing 5% normal donkey serum (NDS), 0.3% Triton X-100, 0.05% NaN_3, and 0.25% carrageenan (PBS-NDS, pH 7.4) for 24 h. Then, the sections were incubated with fluorescein-labeled IgG (secondary antisera) for 6 h. A negative control experiment, in which the primary antisera were omitted, and a peptide competition assay were both carried out. No immunopositive products were detected.

After the immunofluorescence histochemical staining, the sections were observed and images were captured using a confocal laser-scanning microscope (CLSM, FV1000, Olympus). Digital images were captured using FLUOVIEW software (Olympus).

Micrographs of 10–12 sections per rat, which were 150 μm apart within bregma −9.30 to −11.60 mm, were analyzed for p-mTOR expression. Using ImageJ software, the RVM area, including the nucleus raphe magnus (RMg) and the nucleus reticularis gigantocellularis pars α, was outlined based on the Nissl staining. The p-mTOR-positive cells within the area were counted manually by an observer blinded to the treatment conditions. The same counting method was used to evaluate the coexpression of 5-HT/p-mTOR as well as that of p-mTOR/FG within the RVM. Cells with visible green cytoplasmic staining represent 5-HTergic or FG-labeled cells, while red staining represents p-mTOR-positive cells; thus, cells with 5-HT or FG double-labeling with p-mTOR appear yellow.

2.7. Brain Slice Preparation. The rats were decapitated, and brain slices (400 mm) containing the RVM were cut at 0°C with a vibratome (VT1200s, Leica) in a sucrose cutting solution containing the following (in mM): KCl 2.5, NaH_2PO_4 1.2, $NaHCO_3$ 26, sucrose 252, $MgSO_4{\cdot}7H_2O$ 6, $CaCl_2$ 0.5, and glucose 10, bubbled with 95% O_2/5% CO_2 (pH 7.4). For the electrophysiology studies, the brain slices were transferred to a submerged recovery chamber with oxygenated artificial cerebrospinal fluid (ACSF) containing the following (in mM): NaCl 124, KCl 2.5, $MgSO_4{\cdot}7H_2O$ 2, NaH_2PO_4 1, $NaHCO_3$ 25, $CaCl_2$ 2, and glucose 37 for 2 hours at room temperature before recording. For the biochemical experiments, the slices were slowly brought to a final temperature of 30°C in ACSF gassed with 95% O_2/5% CO_2 and incubated for at least 1 hour before the experiments. The brain slices were treated with rapamycin (250 μM) and vehicle for 30 min. Subsequently, the RVM regions were microdissected and snap-frozen over dry ice.

2.8. Western Blot Assay. Following the standard western blot protocol, rats were anesthetized with an overdose of pentobarbital (60 mg/kg, *i.p.*), and the RVM regions were carefully dissected and harvested for western blotting. To obtain total protein extracts, the tissues were lysed in 300 μL lysis buffer containing 10 mM Tris, 150 mM NaCl, 1% Triton X-100, 0.5% NP-40, and 1 mM EDTA at pH 7.4. The samples were adequately mixed at a 100 : 1 (v/v) ratio of protease inhibitor cocktail and phosphatase inhibitor cocktail (Roche, Tucson, AZ, USA). The procedures for the *in vitro*-infused brain slices were similar to those of the tissue protocols. The samples were stored at −80°C for western blot analysis. Then, 30 μg of cell lysis material (quantitatively measured using the BCA protein assay; Thermo Scientific, Rockford, IL, USA) was resolved by sodium dodecyl sulfate-polyacrylamide gel electrophoresis (SDS-PAGE) and transferred to PVDF membranes (Immobilon-P, Millipore). After blocking in nonfat milk for 1 h, the membranes were incubated overnight at 4°C with the following primary antibodies: rabbit anti-mTOR (1 : 1000, Cell Signaling Technology); rabbit anti-p-mTOR (1 : 1000, Cell Signaling Technology); rabbit anti-S6K (1 : 1000, Cell Signaling Technology); rabbit anti-p-S6K (1 : 1000, Cell Signaling Technology); and mouse anti-β-actin (1 : 5000, Sigma, St. Louis, MO, USA). The immunoblots were then reacted with the corresponding horseradish peroxidase-(HRP-) conjugated secondary antibodies (anti-rabbit 1 : 5000, anti-mouse 1 : 5000; Amersham Pharmacia Biotech, Piscataway, NJ, USA). All of the reactions were detected by the enhanced chemiluminescence (ECL) detection method (Amersham) and exposure to film. The scanned images were quantified and analyzed with ImageJ software. Target protein levels were normalized against β-actin levels and expressed as fold changes relative to the naïve control group.

2.9. Electrophysiology. Neurons in the RVM region were targeted for recording using an upright microscope equipped with Zeiss (Oberkochen, Germany) infrared-differential interference contrast (IR-DIC) optics, a 40× water-immersion objective, and a video-imaging camera. The patch pipette was filled with intracellular solution containing the following (in mM): K-gluconate 130, NaCl 5, KCl 15, EGTA 0.4, HEPES 10, Mg-ATP 4, and Tris-GTP 0.2, pH 7.25–7.35, with an osmotic pressure of 290–300 mOsm/L.

Table 1: Antisera used in each group.

Group	Primary antisera	Secondary antisera
p-mTOR/NeuN	Rabbit anti-p-mTOR (1 : 200, Cell Signaling Technology, Danvers, MA, USA) Mouse anti-NeuN (1 : 500, Millipore, Temecula, CA, USA)	Alexa 594 donkey anti-rabbit (1 : 500, Invitrogen, Camarillo, CA, USA) Alexa 488 donkey anti-mouse (1 : 500, Invitrogen)
p-mTOR/FG	Rabbit anti-p-mTOR (1 : 200, Cell Signaling Technology) Guinea pig anti-FG (1 : 200, Protos Biotech, New York, NY, USA)	Alexa 594 donkey anti-rabbit (1 : 500, Invitrogen) Alexa 488 donkey anti-guinea pig (1 : 500, Invitrogen)
p-mTOR/5-HT	Rabbit anti-p-mTOR (1 : 200, Cell Signaling Technology) Goat anti-5-HT (1 : 500, Immunostar, Hudson, WI, USA)	Alexa 594 donkey anti-rabbit (1 : 500, Invitrogen) Alexa 488 donkey anti-goat (1 : 500, Invitrogen)

The pipette resistance, as measured in the bath, was typically 4±0.5 MΩ. The voltage was held at −60 mV, and neurons were given at least 3 min to stabilize before data were collected. Spontaneous discharge and the number of action potentials were used to investigate SNI-induced changes in neuronal excitability in the RVM. The initial access resistance was 15–30 MΩ and was monitored throughout the experiment. Data were discarded if the access resistance changed by >15% during the experiment. Data were filtered at 1 kHz and digitized at 10 kHz.

2.9.1. Spontaneous Discharge. The excitatory postsynaptic currents (EPSCs) of the RVM 5-HTergic neurons, which are mediated by AMPA receptors [28], were voltage-clamped and recorded at −60 mV with an Axon 700B amplifier (Molecular Devices, Sunnyvale, CA, USA) after blocking GABAergic transmission by picrotoxin (100 mM, Sigma), a $GABA_A$ receptor antagonist.

2.9.2. Spike Number. The membrane excitability of the recorded neurons was measured in current-clamp mode by determining the number of action potentials elicited by intracellular injection of 0, 10, 20, 30, 40, 50, and 60 pA depolarizing currents for 400 ms. The spike number was determined to estimate the influence of rapamycin on the recorded neurons.

In all cases, biocytin (0.5%) was introduced into the intracellular solution to identify the morphological properties of the recorded neurons. After recording, the brain slices were immediately fixed in 4% paraformaldehyde in 0.1 M PB for 4 h at room temperature. Then, sections were rinsed with 3% hydrogen peroxide in 0.01 M PBS for 30 min. After thorough washing with PBS, the tissue was incubated with a goat anti-5-HT (1 : 500, Immunostar) antibody in PBS-NDS (pH 7.4) for 24 h, followed by incubation with Alexa 594 avidin D (1 : 1000, Invitrogen) and Alexa 488 donkey anti-goat (1 : 500, Invitrogen) antibodies in PBS for 6 h at room temperature. The sections were then observed, and images were captured with a confocal microscope (Olympus).

2.10. Statistical Analysis. Statistical data were calculated using GraphPad Prism 5 software. The results are expressed as the mean ± SEM. Two-way ANOVA with Bonferroni multiple comparisons tests or one-way ANOVA with Tukey's multiple comparisons post hoc tests were used for between-groups comparisons (e.g., the western blot data with surgery and drug administration as main effects). Student's paired *t*-test was used to analyze the differences between two groups (e.g., the difference in the numbers of p-mTOR-positive cells between the SNI-induced neuropathic pain group and the sham group). P values < 0.05 were considered significant.

3. Results

3.1. Spared Nerve Injury Produced Significant Mechanical Allodynia rather than Thermal Hyperalgesia in Rats. Spared nerve injury (SNI) produced increased nociceptive responses to innocuous mechanical stimulation (mechanical allodynia) of the ipsilateral hind paw in rats from as early as post-SNI operation day 1, and this effect was maintained for at least 2 weeks (Figure 1(a)). However, SNI had no impact on the latency of withdrawal to the radiant heat stimulus (no thermal hyperalgesia) (Figure 1(b)). In fact, our present data are consistent with a previous report demonstrating that the low mechanical threshold induced by SNI could persist even for 9 weeks after surgery, but there was no reported decrease in the hind paw withdrawal latency to the radiant heat stimulus [23].

3.2. p-mTOR Was Exclusively Expressed in Neurons within the RVM. By using double-immunofluorescence staining, we found that the activated form of mTOR, p-mTOR, was expressed in the RVM, and it was exclusively expressed by neurons based on the observation that p-mTOR was almost completely colocalized with NeuN, a marker for neurons, in rats in both the sham (Figures 2(a)–2(c)) and post-SNI day 7 groups (Figures 2(d)–2(f)).

3.3. The mTOR Signaling Pathway in the RVM Was Significantly Activated after SNI. We observed that the number of p-mTOR-positive neurons was significantly increased in the RVM on day 7 after SNI compared to the sham group (Figures 2(a), 2(d), and 2(f)), indicating that activation of mTOR in the RVM may contribute to SNI-induced neuropathic pain.

It has been reported that S6K, a main downstream substrate for mTOR, is involved in several intracellular processes, including neuronal plasticity and long-term memory [17]. Therefore, we used western blot analysis to further evaluate the mTOR signaling pathway, including mTOR and S6K, in the RVM after SNI. Compared with naïve control rats, the expression of both phosphorylated mTOR and phosphorylated S6K (p-mTOR and p-S6K) was not significantly altered in the sham rats (Figures 2(h), 2(i), and 2(k)). As indicated in Figure 2(h), p-mTOR and p-S6K were significantly elevated

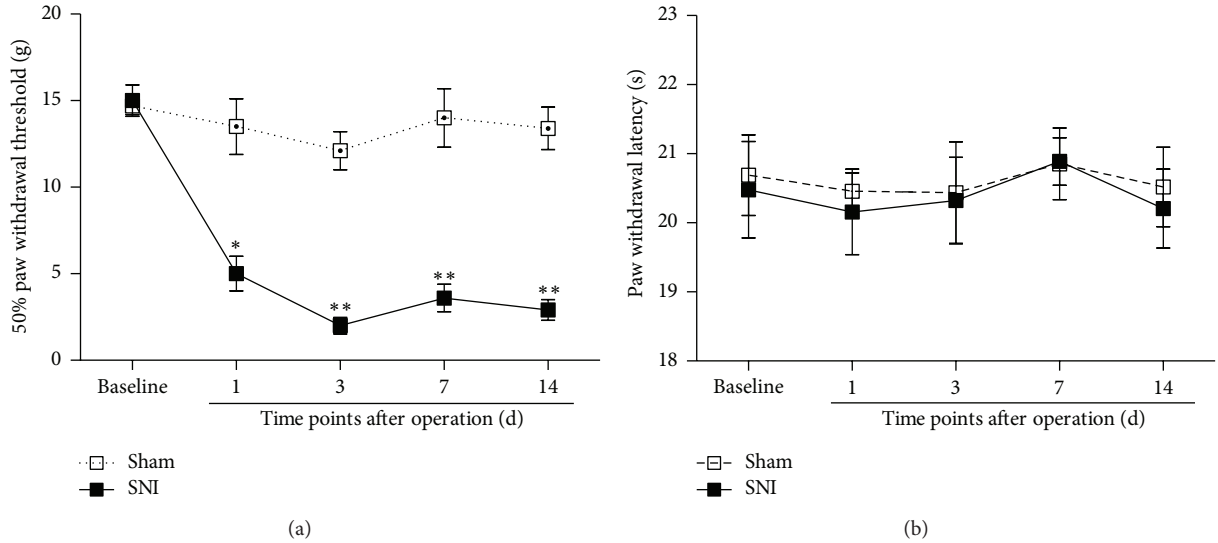

Figure 1: SNI produced significant mechanical allodynia but no thermal hyperalgesia in rats. (a) The 50% paw withdrawal threshold assessed by von Frey filaments was significantly lower after the SNI surgery ($n = 8$) compared to the sham ($n = 8$) group. Mechanical allodynia was obvious at day 1 and persisted for at least 2 weeks. (b) Paw withdrawal latency measured by radiant heat was not changed after the SNI surgery ($n = 8$) compared to the sham ($n = 8$) group ($^{*}P < 0.05$ and $^{**}P < 0.01$ compared to the sham control at the same time point).

in the RVM 3 days after SNI, and phosphorylation was maintained for at least 14 days compared to the control group (Figures 2(h) and 2(i); p-mTOR: SNI D3: 1.42 ± 0.25; SNI D7: 1.86 ± 0.39; SNI D14: 1.49 ± 0.28-fold of naive control, $^{*}P < 0.05$; p-S6K: SNI D3: 1.75±0.23; SNI D7: 1.96±0.57; SNI D14: 1.61 ± 0.28-fold of naïve control, $^{*}P < 0.05$, $n = 4$). The change in p-S6K was similar to that in p-mTOR, indicating that the mTOR signaling pathway in the RVM was activated by SNI 3 days after surgery. Compared with the naïve control group, p-mTOR and p-S6K expression was slightly increased, but no significant difference was detected at 1 day after SNI (Figures 2(h), 2(i), and 2(k), p-mTOR: SNI D1: 1.17 ± 0.36-fold of naïve control, $P > 0.05$; p-S6K: SNI D1: 1.14 ± 0.38-fold of naïve control, $P > 0.05$, $n = 4$). Total mTOR and S6K were not changed in any of the groups in the present study (Figures 2(h), 2(j), and 2(l)). In summary, these data suggest that the mTOR signaling pathway, including mTOR and S6K, was activated in the RVM, which might indicate new protein synthesis and could result in changes in neuroplasticity.

3.4. Most Spinally Projecting Neurons in the RVM Expressed p-mTOR. Injections of FG into the lumbar SDH (Figure 3(a) and 3(b)) resulted in many retrogradely labeled spinally projecting neurons in the RVM (Figure 3(d)). Although FG was injected unilaterally into the (left) lumbar SDH, 81.9% (203/248) of the retrogradely labeled spinally projecting neurons contained p-mTOR-immunoreactive (IR) staining (Figures 3(c)–3(e)), which indicates that more than three-quarters of the spinally projecting neurons in the RVM express p-mTOR.

3.5. The Upregulated p-mTOR Was Mainly Colocalized with 5-HTergic Neurons in the SNI Rats. Because 5-HTergic neurons have previously been shown to be involved in the descending pain control pathway, particularly those localized within the RVM, we further investigated the relationship between 5-HT and p-mTOR. Our immunofluorescence staining results showed that a majority of the p-mTOR-IR neurons contained 5-HT (Figures 4(a)–4(f)). The number of 5-HTergic neurons was slightly increased within the RVM in the SNI rats, but no statistical significance was detected compared to the sham control group (25.52 ± 5.13 per section in the SNI D7 group *versus* 20.8±4.02 in the sham control group, $n = 3$ rats/group, $P > 0.05$). Interestingly, 5-HT-positive p-mTOR-IR neurons were remarkably increased in the RVM 7 days after SNI compared to sham rats (Figure 4(g)). In contrast, 5-HT-negative p-mTOR-IR neurons were not significantly altered 7 days after SNI (Figure 4(h)). These results indicate that SNI-induced neuropathic pain caused a substantial upregulation of p-mTOR, which primarily occurred in 5-HTergic neurons in the RVM.

3.6. Infusion of Rapamycin Rapidly Decreased the Upregulation of p-mTOR and p-S6K in the RVM in Brain Slices In Vitro. As reported previously, rapamycin is a specific and effective inhibitor of mTOR. To investigate the inhibitory effect of rapamycin *in vitro*, we incubated brain slices containing the RVM with rapamycin (250 μM) for 30 min. Thereafter, the RVM region was collected and assessed by western blotting. We found that SNI significantly increased the expression of both p-mTOR and its downstream substrate p-S6K (Figure 5(a), p-mTOR: SNI D7 + vehicle: 1.80 ± 0.48-fold of sham + vehicle, $^{*}P < 0.05$; p-S6K: SNI D7 + vehicle: 1.77 ± 0.45-fold of sham + vehicle, $n = 4$, $^{*}P < 0.05$), which is inconsistent with our tissue western blot data. Moreover, rapamycin (250 μM) significantly reversed the upregulation of p-mTOR as well as p-S6K after 30 min of drug infusion (p-mTOR: SNI D7 + rapamycin: 1.11 ± 0.27-fold of naïve control

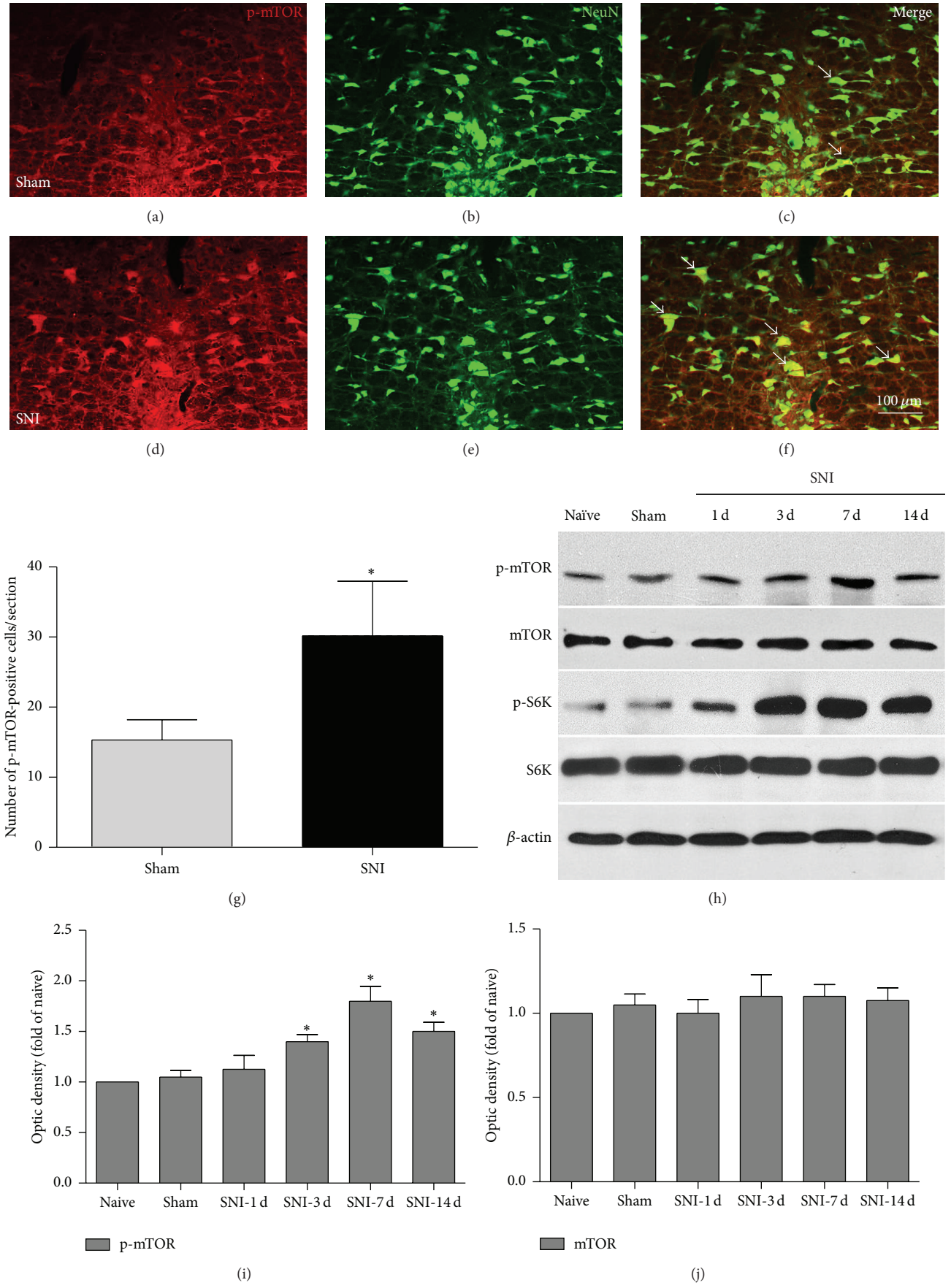

Figure 2: Continued.

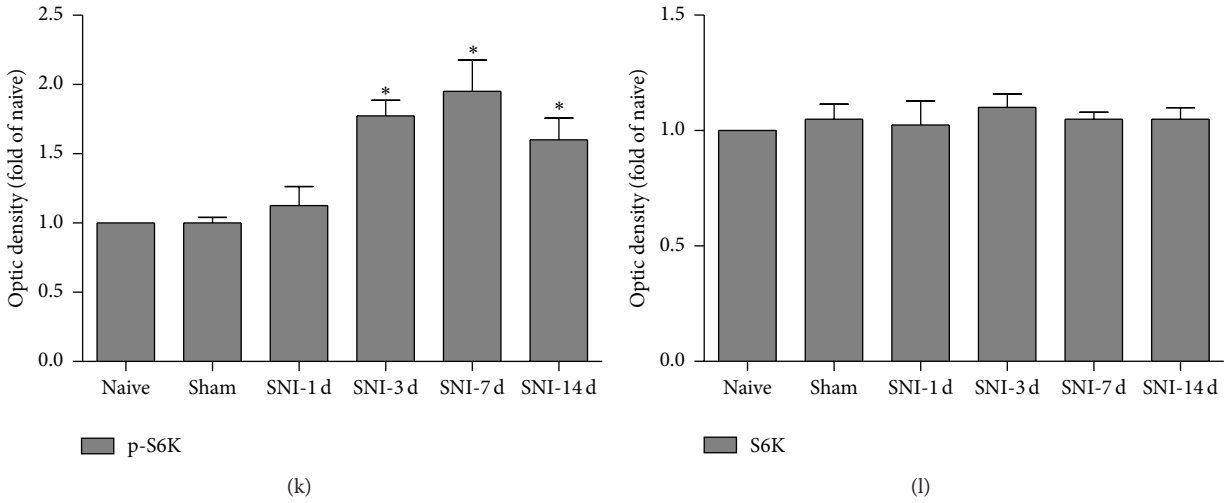

Figure 2: mTOR was remarkably activated in the RVM after SNI. (a)–(f) Double immunostaining showed that p-mTOR (red) was almost exclusively expressed in neurons (green). Single arrows indicate some typical double-labeled (yellow) cells. (a)–(g) Cell counting in the RVM shows that the number of p-mTOR-positive neurons was significantly increased 7 days after the SNI surgery ($^*P < 0.05$ compared to the sham control group). Scale bars = 100 μm. (h)–(l) The expression levels of total and phosphorylated mTOR (h, i, and j) and S6K (h, k, and l) were revealed by western blotting. Three days after SNI, phosphorylated mTOR and S6K (p-mTOR and p-S6K) in the RVM were significantly increased. Nonphosphorylated mTOR and S6K were not changed after SNI ($^*P < 0.05$ compared to the naïve control group, $n = 4$).

versus SNI D7 + vehicle: 1.80 ± 0.48-fold of naïve control, $P < 0.05$; p-S6K: SNI 7d + rapamycin: 1.17 ± 0.29-fold of naïve control *versus* SNI D7 + vehicle 1.77 ± 0.45-fold of naïve control, $n = 4$, $P < 0.05$), indicating that rapamycin could rapidly inhibit the activation of mTOR after SNI *in vitro*.

3.7. The Excitability of 5-HTergic Neurons in the RVM Was Greatly Increased in SNI Rats, and It Could Be Effectively Impaired by Rapamycin via a Postsynaptic Mechanism. To further investigate the neuronal excitability of 5-HT and the effect of rapamycin on 5-HTergic neurons in the RVM, we carried out whole-cell patch-clamp recording. A total of sixty 5-HT-positive neurons ($n = 60$) from 12 rats were identified by biocytin introduction in combination with 5-HT immunofluorescence staining (Figure 5(b)). Moreover, the membrane characteristics of 5-HTergic neurons were quite different. They showed a relatively higher membrane capacitance (Cm) and a smaller membrane resistance (Rm) compared to other small neurons in the RVM, indicating that they have a larger membrane surface and smaller electrical resistance.

We first investigated the frequency and amplitude of spontaneous excitatory postsynaptic currents (sEPSCs) in the RVM neurons. Most of the 5-HTergic neurons recorded in the RVM that were responsive to rapamycin showed increased activity. Inconsistent with previous reports [29], the frequency and amplitude of sEPSCs were significantly increased after SNI (Figures 5(c)–5(f)), which indicates that the probability of presynaptic transmitter release and the postsynaptic neuronal excitability, respectively, was elevated. Subsequently, we used rapamycin (250 μM) to evaluate whether the enhanced presynaptic and postsynaptic excitability could be reversed. We found that the amplitude (baseline, 45.26 ± 1.89 pA; rapamycin, 35.83 ± 2.58 pA. $P < 0.05$, $n = 15$, paired t-test), but not the frequency (baseline, 3.41±0.12 Hz; rapamycin, 3.29±0.33, $P > 0.05$, $n = 15$, paired t-test), of the sEPSCs was inhibited by rapamycin application in rats with SNI but not in the sham control rats (frequency: baseline, 1.22 ± 0.11 Hz; rapamycin, 1.20 ± 0.19 Hz. $P > 0.05$, $n = 15$, paired t-test; amplitude: baseline, 29.79 ± 1.80 pA; rapamycin, 28.14 ± 1.28 pA. $P > 0.05$, $n = 15$, paired t-test) (Figures 5(c)–5(f)). These results suggest that rapamycin can decrease the postsynaptic excitability of 5-HTergic neurons in the RVM after SNI.

We next compared the effects of rapamycin on the action potentials of the 5-HTergic neurons and determined that the spike number of the recorded neurons was obviously increased after SNI (Figures 5(g) and 5(h)). Rapamycin (250 μM) did not change the spike number in recorded neurons from the sham group ($F_{(1,62)} = 2.25$, $P > 0.05$, $n = 15$, two-way repeated measures ANOVA) (Figure 5(g)). However, in the presence of rapamycin, the spike number of 5-HTergic neurons in the SNI group was significantly reduced ($F_{(1,48)} = 8.56$, $P < 0.05$, $n = 15$, two-way repeated measures ANOVA) (Figure 5(h)). These results indicate that rapamycin inhibited the excitability of 5-HTergic neurons in the RVM under neuropathic pain conditions.

3.8. Microinjection of Rapamycin into the RVM Potently Alleviated Mechanical Allodynia during the Maintenance but Not the Induction of SNI-Induced Neuropathic Pain. We preliminarily investigated nociceptive behaviors in the SNI rats mentioned above. In agreement with previous reports [22], significant mechanical allodynia rather than thermal hyperalgesia was observed in the present study (Figure 1). Based on this observation, we next used mechanical PWT instead of heat PWL to assess the nociceptive behaviors.

To determine whether rapamycin could prevent the development of the induction stage of mechanical allodynia,

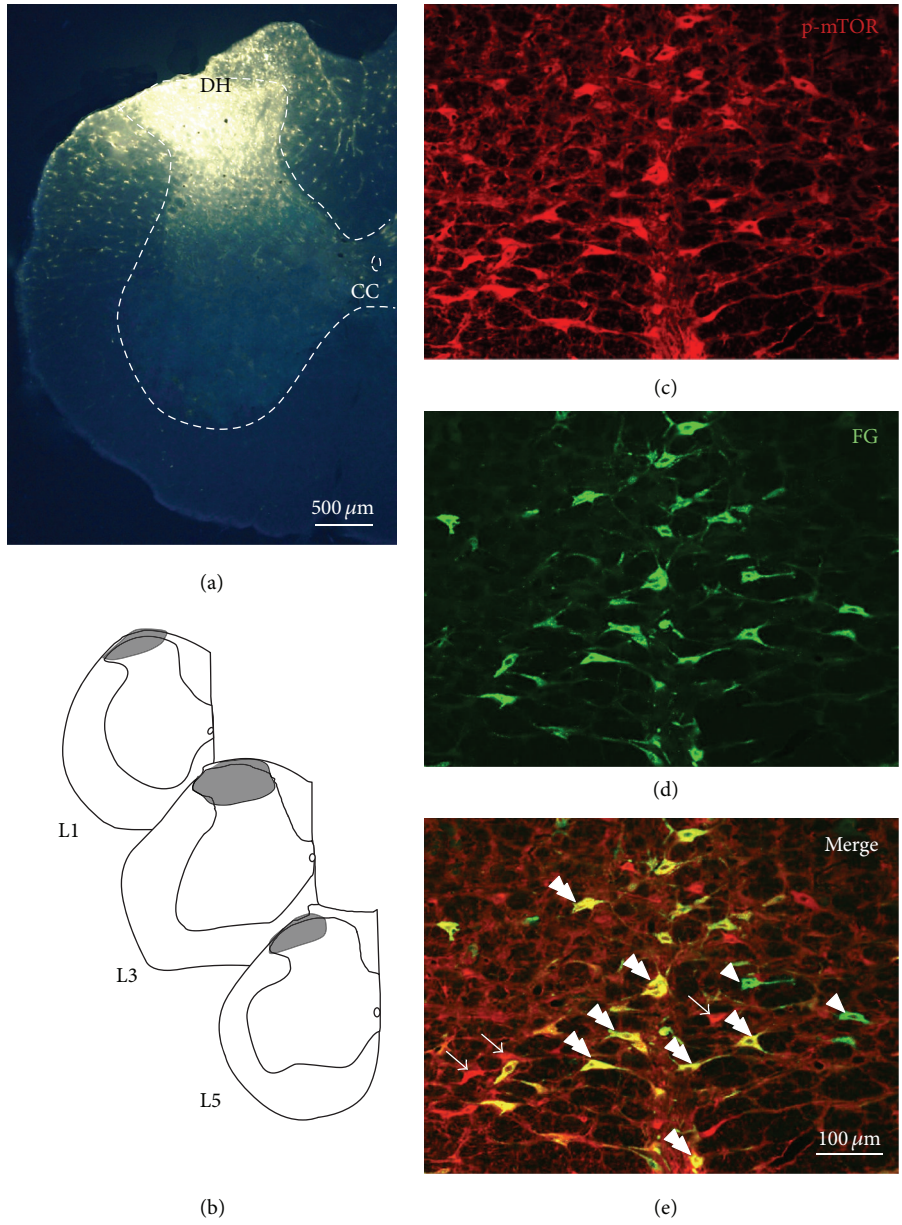

Figure 3: Most of the FG-labeled spinally projecting neurons in the RVM expressed p-mTOR. (a) Fluorescence photomicrograph showing the FG injection site in the lumbar spinal dorsal horn (SDH). (b) Camera lucida drawings show the rostrocaudal extent of the FG injection site at the different levels indicated, L1, L3, and L5. L1, L3, and L5 show the corresponding segments of the lumbar cord (DH: dorsal horn; CC: central canal). (c)–(e) Representative fluorescence photomicrographs showing p-mTOR (red) and FG (green) double-labeled neurons in the RVM. The double arrowheads indicate p-mTOR/FG double-labeled neurons (yellow), the arrowheads indicate FG single-labeled neurons, and the arrows indicate p-mTOR single-labeled neurons in the RVM. Scale bar = 500 μm in (a) and 100 μm in (e) (applied to (c)–(e)).

we microinjected rapamycin via a cannula implanted into the RVM (Figures 6(a) and 6(b)) immediately before SNI surgery and at day 1 after SNI, which was followed by behavioral testing 30 min later (Figure 6(c)). After treatment with rapamycin, the PWT in the SNI + rapamycin group showed no significant change compared to that in the SNI + vehicle control group at day 1 after SNI (Figure 6(d)), indicating that rapamycin could not alleviate the neuropathic pain induced by SNI in the induction stage. Subsequently, we investigated whether rapamycin could reverse established neuropathic pain. On day 6 after SNI, the rats demonstrated typical increased nociceptive responses to nonnoxious mechanical stimulation (Figure 6(e)). Compared with the vehicle control group, the mechanical allodynia was significantly reduced after microinjection of rapamycin into the RVM on day 7 after SNI (Figure 6(e)). Because our biochemical results showed that the amount of both p-mTOR and p-S6K was increased after SNI (Figures 2(h), 2(i), and 2(k)) and because rapamycin infusion into the brain slices could effectively reverse the upregulated level of p-mTOR and p-S6K (Figure 5(a)), we

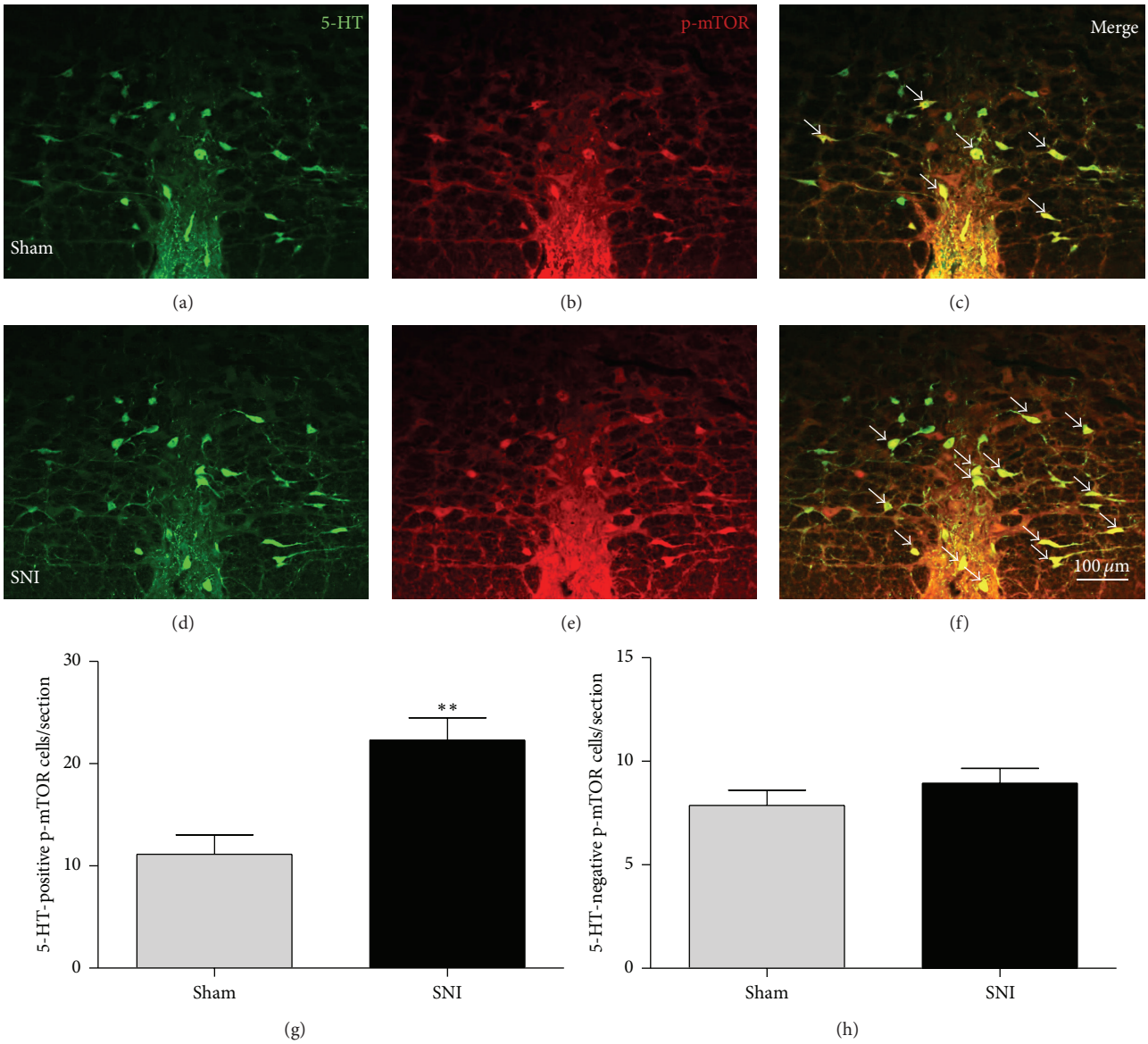

Figure 4: p-mTOR was mainly colocalized with 5-HTergic neurons in the RVM, and the number of 5-HT-positive p-mTOR neurons was significantly increased 7 days after SNI. (a)–(f) Representative fluorescence photomicrographs showing the expression of 5-HT (green) and p-mTOR (red) double-labeled neurons in the RVM in the sham control (a–c) versus the SNI 7-day group (d–f). Single arrows indicate p-mTOR/5-HT double-labeled (yellow) neurons. Scale bars = 100 μm. (g) The average number of 5-HT-positive p-mTOR neurons per section increased significantly in the SNI rats 7 days after surgery compared to the sham ($^{**}P < 0.01$). (h) In contrast, the average number of 5-HT-negative p-mTOR neurons did not change after SNI ($n = 4$ rats/group).

concluded that the effect of rapamycin in partially reversing the mechanical allodynia was exerted via inactivation of the mTOR signaling pathway, thus decreasing the excitability of 5-HTergic spinally projecting neurons in the RVM.

4. Discussion

In the current study, we provide the first demonstration of the following: (1) mTOR is expressed in the RVM region and can be activated in nerve injury-induced neuropathic pain; (2) this mTOR is largely expressed in 5-HTergic neurons, which mainly comprise the descending pain control pathway; (3) inhibition of the activated mTOR restores the overexcitability of the 5-HTergic neurons to normal; and (4) inactivation of mTOR by intra-RVM rapamycin microinjection alleviates established hyperalgesia (abolished at the maintenance stage of neuropathic pain) rather than influencing the beginning priming (induction stage) of neuropathic pain. These findings suggest that the mTOR signaling pathway in the RVM is involved in the maintenance of nerve injury-induced neuropathic pain and that inhibition of mTOR in the RVM could effectively alleviate neuropathic pain in SNI rats.

Due to the importance of the descending pain control pathway in mammals [2], many studies have been performed

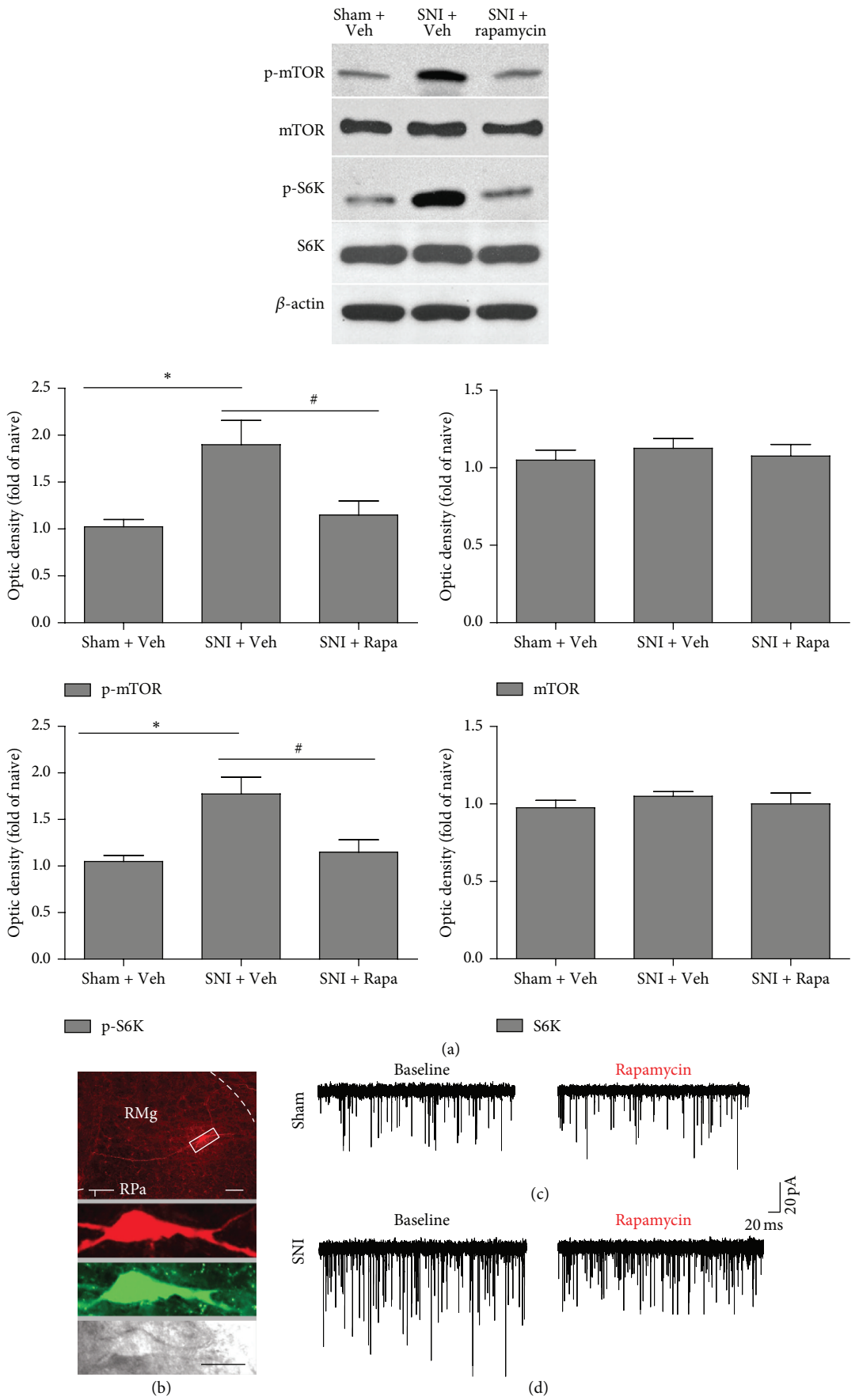

Figure 5: Continued.

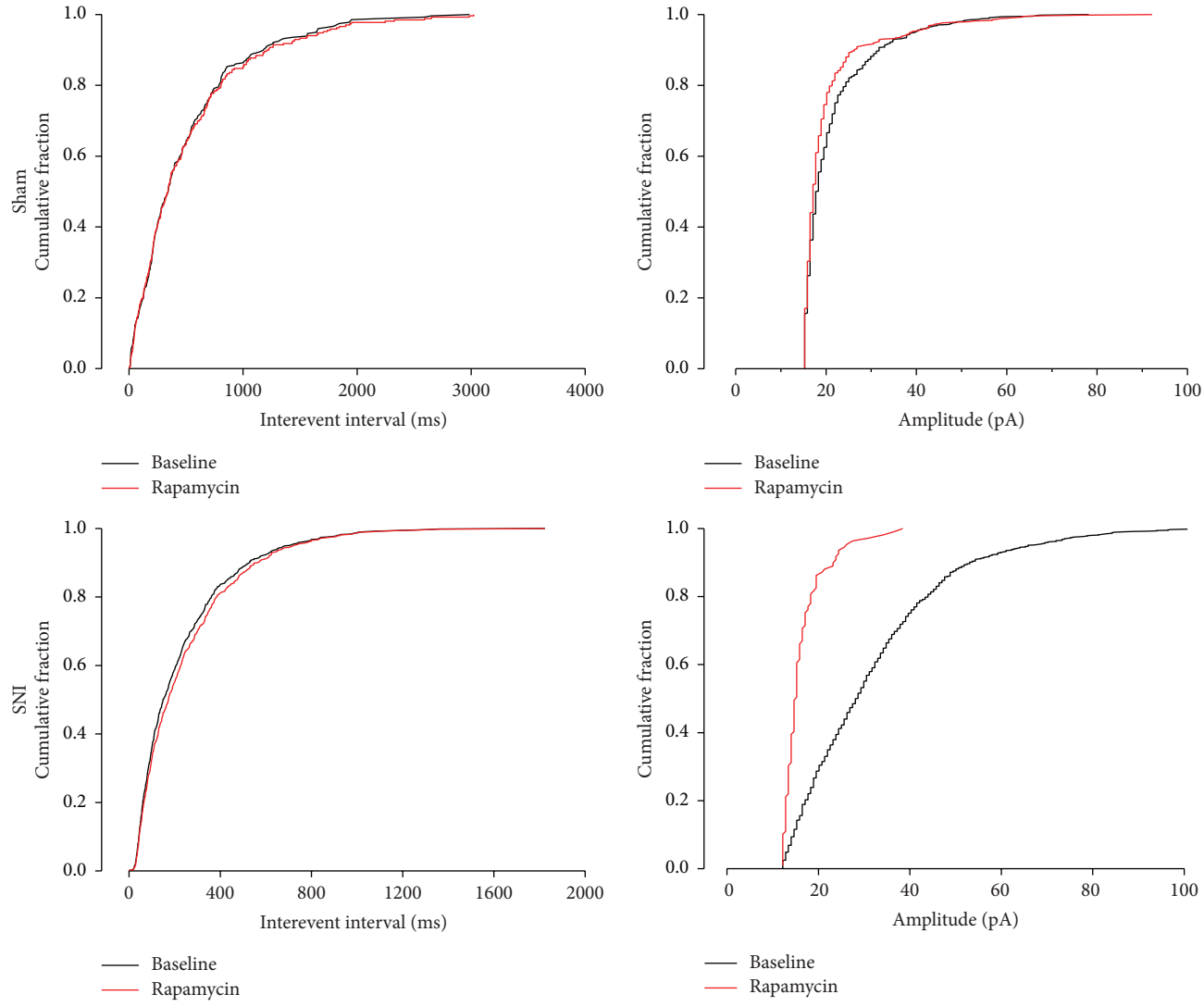

(e)

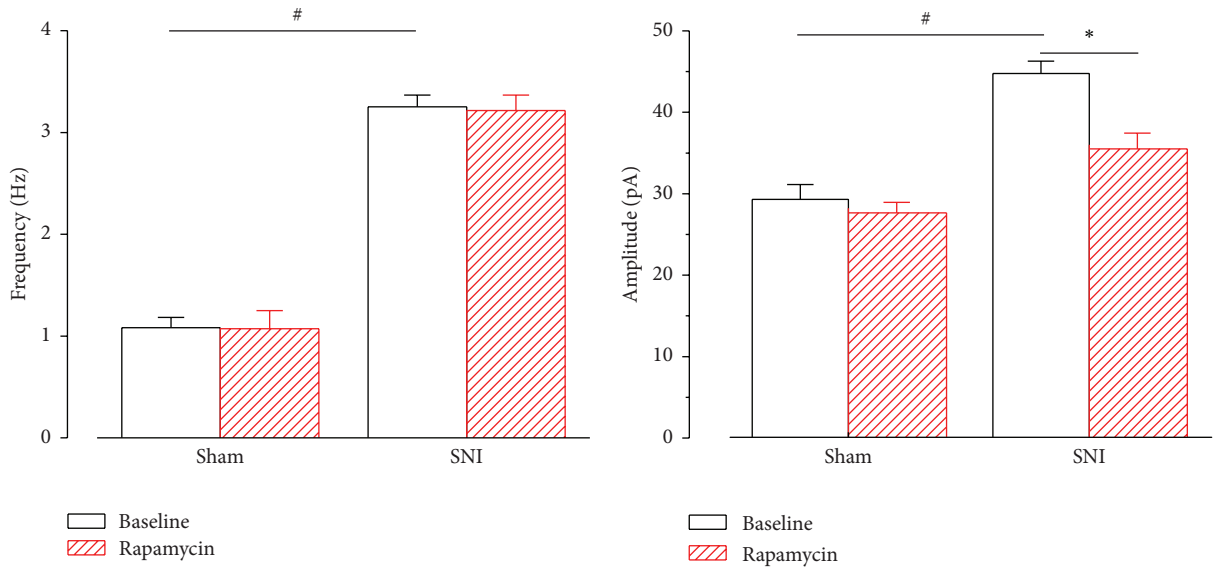

(f)

Figure 5: Continued.

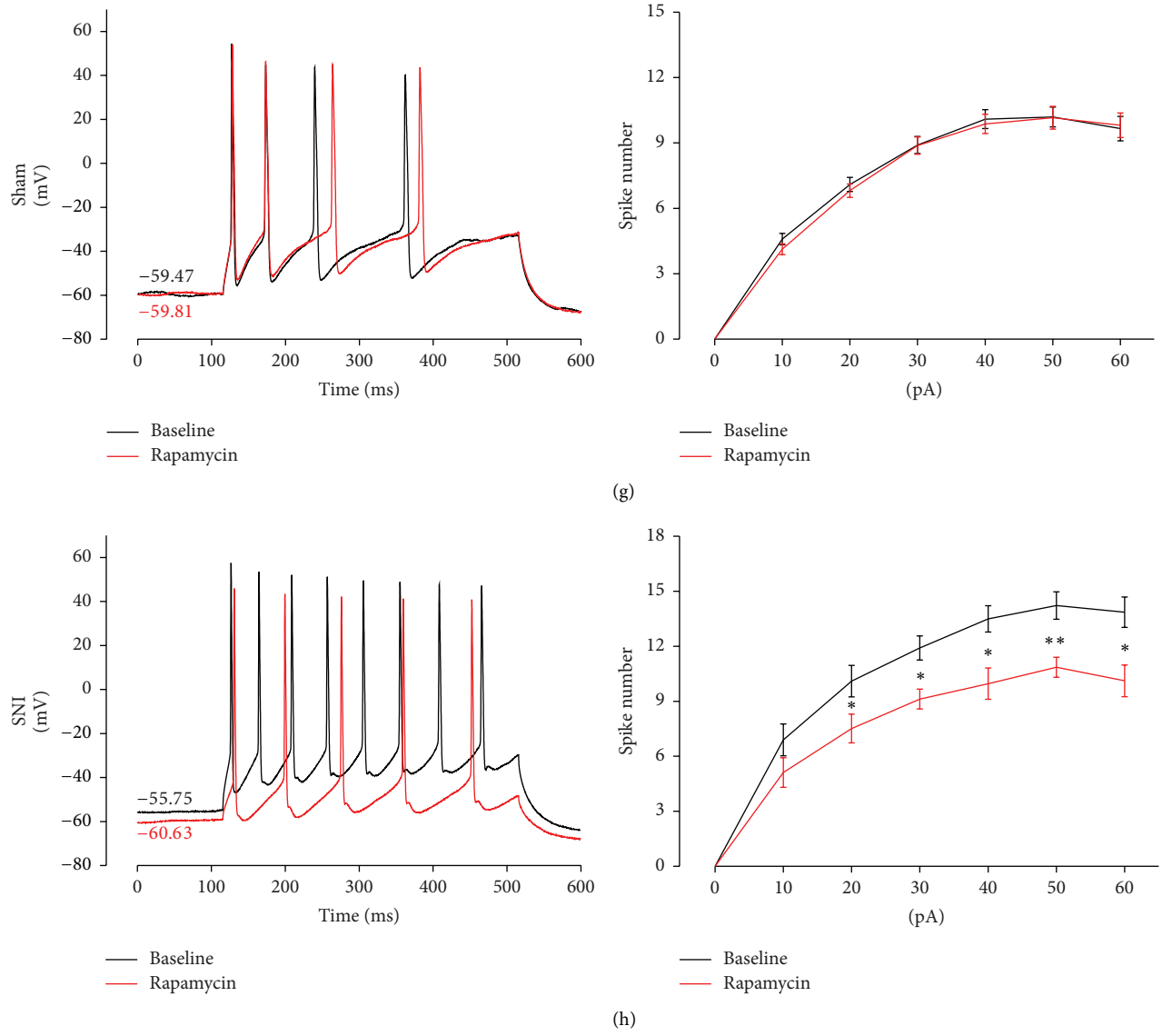

Figure 5: The neuronal excitability of 5-HTergic neurons in the RVM was significantly increased in SNI rats, which could be effectively impaired by rapamycin via a postsynaptic mechanism. (a) *In vitro* brain slice infusion revealed that rapamycin (250 μM) rapidly inhibited the activation of mTOR in SNI rats. Consistently, in the absence of rapamycin, SNI produced a significant increase in the levels of phosphorylated mTOR and S6K ($^{*}P < 0.05$ compared to the sham + vehicle group, $n = 4$). After treatment with rapamycin (250 μM) on day 7, the upregulation of p-mTOR and p-S6K levels was remarkably decreased ($^{\#}P < 0.05$ compared to the SNI + vehicle group, $n = 4$) in brain slices from SNI rats. (b) One representative whole-cell patched neuron in the RVM was injected with biocytin (labeled with Alexa 594, red). This cell also showed 5-HT immunoreactivity (Alexa 488, green). The same neuron is also pictured during whole-cell patching (RMg: raphe magnus nucleus; RPa: raphe pallidus nucleus). Scale bars = 100 μm (above) and 25 μm (below). (c)–(e) Superimposed samples and cumulative fraction results showing that rapamycin inhibited the amplitude rather than the frequency of spontaneous excitatory postsynaptic currents (sEPSCs) in the RVM 5-HTergic neurons. (c), (e) Bath application of rapamycin (250 μM) had no effect on the frequency and amplitude of the sEPSCs in rats with sham surgery. (d), (e) Rapamycin (250 μM) inhibited the frequency but not the amplitude of sEPSCs in rats with SNI. (f) Summarized results for the effects of rapamycin on sEPSCs in rats with SNI or sham surgery (*SNI *versus* sham $P < 0.05$, $n = 15$; $^{\#}$SNI + rapamycin *versus* sham + rapamycin, $P < 0.05$, $n = 15$). (g) Sample traces and average results showing that the number of action potentials (APs) in a train induced by the injection of step currents (400 ms, 0–60 pA) was not affected by rapamycin in the sham group ($n = 15$, $P > 0.05$, two-way repeated measures ANOVA). (h) Sample traces and average results showing that the number of APs in a train induced by the injection of step currents (400 ms, 0–60 pA) was significantly reduced by rapamycin in the SNI group ($n = 15$, $P < 0.05$, two-way repeated measures ANOVA). The Holm-Sidak post hoc test indicated that rapamycin decreased the spike number when currents of 20 ($t = 2.50$, $^{*}P < 0.05$), 30 ($t = 2.62$, $^{*}P < 0.05$), 40 ($t = 2.34$, $^{*}P < 0.05$), 50 ($t = 3.34$, $^{**}P < 0.01$), and 60 pA ($t = 2.57$, $^{*}P < 0.05$) were applied. It is worth noting that the resting membrane potential (RMP) was slightly hyperpolarized and that the amplitude of spikes was also slightly decreased in the SNI group.

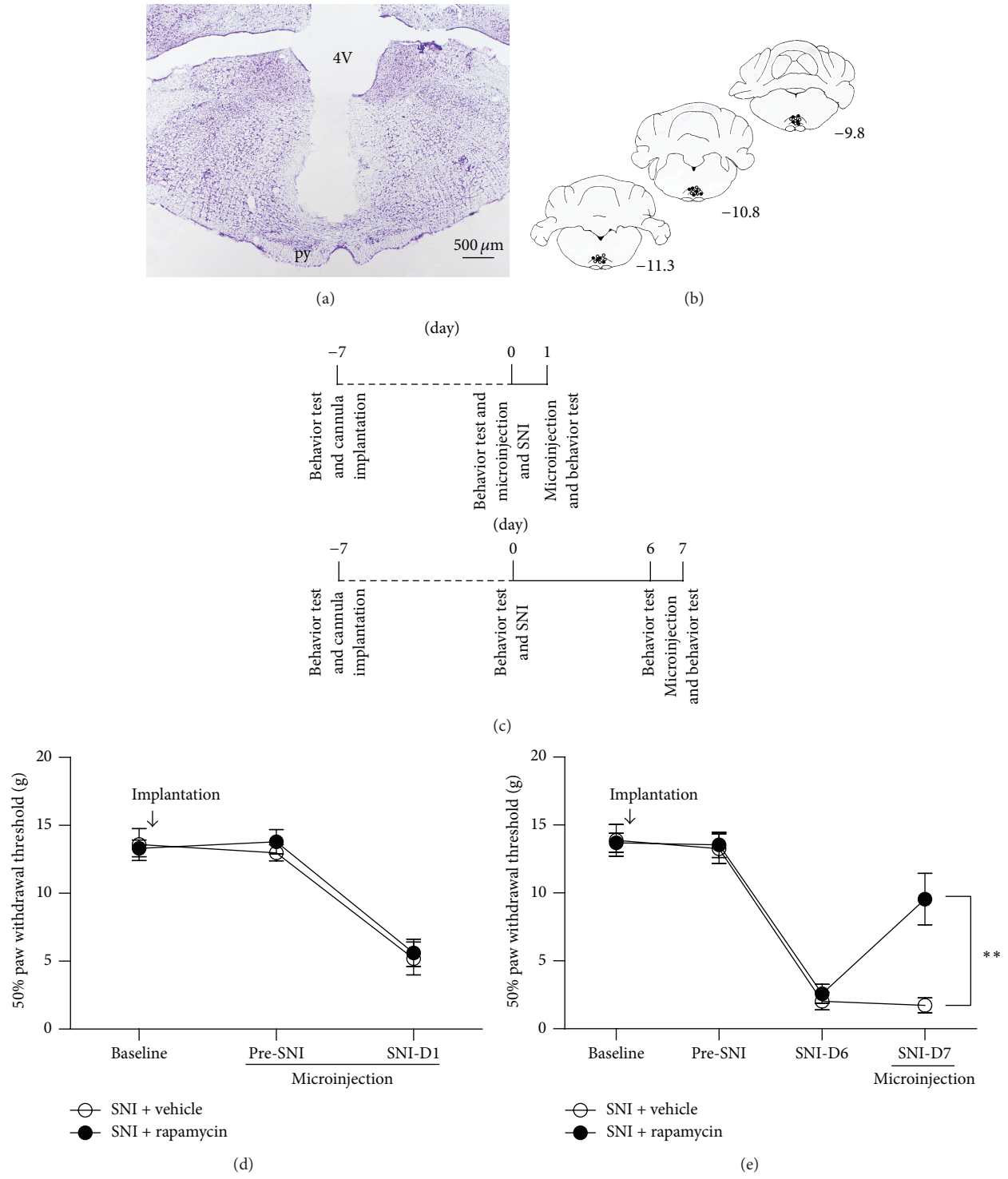

Figure 6: Intra-RVM microinjection of the mTOR inhibitor rapamycin (250 μM) partially reversed established mechanical allodynia (maintenance stage) but showed no effect on the induction stage of SNI-induced neuropathic pain in rats. (a) Representative Nissl-stained section showing injection sites within the RVM (4V: 4th ventricle; py: pyramidal tract). Scale bar = 500 μm. (b) Camera lucida drawings showing the cannula tip placements in rats injected with rapamycin (black circles, $n = 14$) or vehicle (white circles, $n = 14$) in the RVM. The numbers correspond to the distance in millimeters (mm) posterior to bregma in the brain. (c) Experimental schedule. The behavioral tests, cannula implantation, microinjection, and SNI surgery were performed as indicated in the schedule. (d) Intra-RVM microinjection of rapamycin (250 μM) before SNI (Pre-SNI) and 1 day after SNI (SNI-D1) could not alleviate mechanical allodynia 30 min after the SNI-D1 injection compared to vehicle injection ($n = 7$ rats/group). (e) Microinjection of rapamycin (250 μM) into the RVM 30 min before the behavioral test significantly reduced mechanical allodynia at 7 days after SNI (SNI-D7) compared to vehicle injection ($^{**}P < 0.01$, $n = 7$ rats/group).

to elucidate the mechanisms underlying this critical pathway. It has been demonstrated that blockade of RVM activity with lidocaine produced conditioned place preference (CPP), which is linked to pain relief, in nerve injury models, indicating that descending pain facilitation pathways modulate injury-induced spontaneous tonic pain [30]. Wei et al. [3] have reported that selectively depleting functional 5-HT phenotypes in RVM neurons with shRNA interference (RNAi) of tryptophan hydroxylase-2 (Tph-2, the rate-limiting enzyme in the synthesis of neuronal 5-HT) attenuated tissue or nerve injury-induced allodynia and hyperalgesia. This finding provides strong evidence that descending 5-HT from the RVM is an important contributor to pain facilitation during the development of persistent pain. Recently, by taking advantage of optogenetic methods, optogenetic stimulation in Tph2-channelrhodopsin 2 (ChR2) transgenic mice was shown to decrease both mechanical and thermal pain thresholds [31]. However, in contrast, several studies showed the opposite results [32–35], that 5-HT from the RVM is important for the descending inhibitory pathway. These controversial arguments regarding whether RVM 5-HT plays a facilitatory or inhibitory role might be explained by the different subtypes of 5-HT receptors located in the SDH, according to the reports. For example, 5-HT_3 receptors are reported to mediate descending facilitation and to contribute to pain hypersensitivity [36], whereas the activation of 5-HT_2 receptors can potentiate glycine release in the SDH to inhibit pain transmission [35]. In addition, a previous study also provided evidence that, under conditions of experimental pain, activation of 5-HT_7 receptors leads to antinociceptive effects in the spinal cord [37]. In the present study, we found that 5-HTergic neurons were slightly, although not significantly, increased after nerve injury. However, the excitability of these 5-HTergic neurons was elevated after SNI (Figure 5). Rapamycin could effectively inhibit 5-HT overexcitability and thus attenuate hyperalgesia (Figure 6), which indicates that 5-HT in the RVM is probably involved in the descending pain facilitation pathway under nerve injury-induced neuropathic pain conditions.

mTOR has been extensively studied in tumors [38], cardiovascular diseases [39], and neurodegenerative disorders [40, 41]. Recently, emerging evidence has indicated that mTOR plays a role in pain processing, and it is becoming clear that mTOR is important in the regulation of nociception, at both the peripheral and spinal cord levels [10–17]. To date, however, no report has investigated mTOR at the supraspinal level and its role in nociceptive modulation. Here, we provide potent evidence that mTOR contributes to neuropathic pain by increasing the neuronal excitability of 5-HTergic neurons in the RVM, thus potentiating descending pain facilitation.

mTOR regulates protein translation through multiple factors. 4E-BP1/2 and S6K are involved in the regulation of cell physiology through the modulation of protein synthesis [42]. 4E-BP1/2 inhibits the interaction of the cap-binding translation initiation factor eIF4E with other elongation factors, which is a key regulatory process in translation. mTOR-mediated phosphorylation of 4E-BP1/2 releases this inhibition, allowing translation initiation to proceed. S6K-mediated phosphorylation of S6 promotes the unwinding and initiation of translation of a subgroup of mRNAs called 5′-terminal oligopyrimidine tract (TOP) mRNAs. TOP mRNAs encode ribosomal proteins and elongation factors 1a and 2, which are important in translational control [43]. In the present study, we detected that p-mTOR and p-S6K levels were significantly elevated in the RVM after SNI (Figure 2), which suggests that mTOR-mediated protein translation and synthesis are increased. The upregulated p-mTOR was mainly coexpressed with 5-HT (Figure 4). In contrast, the number of 5-HTergic neurons was slightly increased within the RVM in the SNI rats, but no statistical significance was detected compared to the sham control group. Therefore, the synthesis of 5-HT in the RVM may not obviously increase. However, by using whole-cell patch recording, we found that the 5-HTergic neurons were overexcited, with significant increases in the amplitude and frequency of sEPSCs as well as the number of action potentials (Figure 5). In addition, rapamycin inhibited only the amplitude and not the frequency of sEPSCs (Figure 5); we thus propose that the postsynaptic overexcitability of the 5-HTergic neurons, which primarily depends on an increase in glutamate receptors, is mainly due to the activation of mTOR. It has been reported that mTOR signaling can potentiate the insertion of AMPA (α-amino-3-hydroxy-5-methyl-4-isoxazole-propionic acid) receptors into the postsynaptic membrane and lead to long-term potentiation (LTP) [44, 45]. Thus, the data collected from our immunofluorescence staining and electrophysiology are consistent with previous reports and suggest that the activation of mTOR might lead to an increase in AMPA receptors and their insertion into the postsynaptic membrane, resulting in the elevated neuronal excitability of the 5-HTergic neurons in the RVM.

As an effective immunosuppressant, rapamycin is widely used to prevent transplant rejection. Chronic treatment of patients with mTOR inhibitors is associated with an increased incidence of pain [46, 47], including the possible development of complex regional pain syndrome (CRPS) [48, 49]. Other animal studies have also reported similar results [50, 51]. These conflicting results might be due to the following reasons: (1) the drug concentration of rapamycin or its analogues was not the same as in the other reports in which the inhibition of mTOR produces antinociception; (2) long-term treatment might lead to feedback activation of other pronociceptive signal proteins or molecules; and (3) intrathecal administration of rapamycin (at the spinal cord level) might play a very complicated role in pain transmission with unknown mechanisms.

The present study used intra-RVM, instead of intrathecal, administration of rapamycin (250 μM, 30 min before the behavioral tests), and this treatment remarkably attenuated the nociceptive behaviors induced by SNI (Figure 6). Moreover, intra-RVM rapamycin treatment was effective on day 7 after SNI (the maintenance stage of neuropathic pain) but not on day 1 after SNI (the induction stage). The behavioral pharmacological data suggest that inhibition of mTOR in the RVM at the late phase (maintenance stage) of neuropathic pain might be effective, even though pain has already been well established. By contrast, inhibition of mTOR in the RVM had no effect on the development (induction stage) of

neuropathic pain. All of these results are consistent with our biochemical data showing that RVM p-mTOR was not greatly enhanced at day 1 but showed a significant increase at 7 days after SNI (Figure 2).

Combining our current results with previous findings, we conclude that the specific inhibition of mTOR by rapamycin in the RVM is a promising avenue for the management of neuropathic pain. This effect probably occurs via deactivation of 5-HTergic spinally projecting neurons in the RVM, which are required for descending pain facilitation. Nonetheless, the present study also has some limitations. Due to the lack of a specific mTOR activator, reverse experiments involving the activation of mTOR in the RVM, which should produce or enhance nociception, are difficult to achieve. Moreover, optogenetic methods as well as transgenic animals should be further introduced to confirm the role of mTOR in the RVM, not only in neuropathic pain but also in inflammatory pain.

5. Conclusion

Through the deactivation of 5-HTergic spinally projecting neurons in the RVM and thus the weakening of descending pain facilitation, specific targeting of the activation of mTOR in the RVM is a promising avenue for the management of neuropathic pain.

Conflict of Interests

The authors have declared that no conflict of interests exists.

Authors' Contribution

Jian Wang, Da-Yun Feng, Zhi-Hua Li, and Ban Feng contributed equally to this work.

Acknowledgments

This work was supported by grants from the National Natural Science Foundation of China (Grant no. 81371239 to Yun-Qing Li) and Natural Science Basic Research Plan in Shaanxi Province of China (Grant no. 2012JM4040 to Ting Zhang).

References

[1] M. M. Morgan, K. L. Whittier, D. M. Hegarty, and S. A. Aicher, "Periaqueductal gray neurons project to spinally projecting GABAergic neurons in the rostral ventromedial medulla," *Pain*, vol. 140, no. 2, pp. 376–386, 2008.

[2] M. J. Millan, "Descending control of pain," *Progress in Neurobiology*, vol. 66, no. 6, pp. 355–474, 2002.

[3] F. Wei, R. Dubner, S. Zou et al., "Molecular depletion of descending serotonin unmasks its novel facilitatory role in the development of persistent pain," *Journal of Neuroscience*, vol. 30, no. 25, pp. 8624–8636, 2010.

[4] A. I. Basbaum, D. M. Bautista, G. Scherrer, and D. Julius, "Cellular and molecular mechanisms of pain," *Cell*, vol. 139, no. 2, pp. 267–284, 2009.

[5] M. Costa-Mattioli, W. S. Sossin, E. Klann, and N. Sonenberg, "Translational control of long-lasting synaptic plasticity and memory," *Neuron*, vol. 61, no. 1, pp. 10–26, 2009.

[6] V. Briz, G. Zhu, Y. Wang et al., "Activity-dependent rapid local RhoA synthesis is required for hippocampal synaptic plasticity," *The Journal of Neuroscience*, vol. 35, no. 5, pp. 2269–2282, 2015.

[7] T. T. Gipson and M. V. Johnston, "Plasticity and mTOR: towards restoration of impaired synaptic plasticity in mTOR-related neurogenetic disorders," *Neural Plasticity*, vol. 2012, Article ID 486402, 10 pages, 2012.

[8] J. L. Banko, F. Poulin, L. Hou, C. T. DeMaria, N. Sonenberg, and E. Klann, "The translation repressor 4E-BP2 is critical for eIF4F complex formation, synaptic plasticity, and memory in the hippocampus," *The Journal of Neuroscience*, vol. 25, no. 42, pp. 9581–9590, 2005.

[9] M. D. Antion, M. Merhav, C. A. Hoeffer et al., "Removal of S6K1 and S6K2 leads to divergent alterations in learning, memory, and synaptic plasticity," *Learning & Memory*, vol. 15, no. 1, pp. 29–38, 2008.

[10] S. M. Géranton, L. Jiménez-Díaz, C. Torsney et al., "A rapamycin-sensitive signaling pathway is essential for the full expression of persistent pain states," *The Journal of Neuroscience*, vol. 29, no. 47, pp. 15017–15027, 2009.

[11] E. Norsted Gregory, S. Codeluppi, J. A. Gregory, J. Steinauer, and C. I. Svensson, "Mammalian target of rapamycin in spinal cord neurons mediates hypersensitivity induced by peripheral inflammation," *Neuroscience*, vol. 169, no. 3, pp. 1392–1402, 2010.

[12] Q. Xu, B. Fitzsimmons, J. Steinauer et al., "Spinal phosphinositide 3-kinase-Akt-mammalian target of rapamycin signaling cascades in inflammation-induced hyperalgesia," *The Journal of Neuroscience*, vol. 31, no. 6, pp. 2113–2124, 2011.

[13] I. Obara, K. K. Tochiki, S. M. Géranton et al., "Systemic inhibition of the mammalian target of rapamycin (mTOR) pathway reduces neuropathic pain in mice," *Pain*, vol. 152, no. 11, pp. 2582–2595, 2011.

[14] M.-H. Shih, S.-C. Kao, W. Wang, M. Yaster, and Y.-X. Tao, "Spinal cord NMDA receptor-mediated activation of mammalian target of rapamycin is required for the development and maintenance of bone cancer-induced pain hypersensitivities in rats," *The Journal of Pain*, vol. 13, no. 4, pp. 338–349, 2012.

[15] W. Zhang, X.-F. Sun, J.-H. Bo et al., "Activation of mTOR in the spinal cord is required for pain hypersensitivity induced by chronic constriction injury in mice," *Pharmacology Biochemistry and Behavior*, vol. 111, pp. 64–70, 2013.

[16] C. O. Asante, V. C. Wallace, and A. H. Dickenson, "Formalin-induced behavioural hypersensitivity and neuronal hyperexcitability are mediated by rapid protein synthesis at the spinal level," *Molecular Pain*, vol. 5, article 27, 2009.

[17] L. Lisi, P. Aceto, P. Navarra, and C. Dello Russo, "mTOR kinase: a possible pharmacological target in the management of chronic pain," *BioMed Research International*, vol. 2015, Article ID 394257, 13 pages, 2015.

[18] J. M. Braz and A. I. Basbaum, "Genetically expressed transneuronal tracer reveals direct and indirect serotonergic descending control circuits," *The Journal of Comparative Neurology*, vol. 507, no. 6, pp. 1990–2003, 2008.

[19] T. Chen, X.-L. Wang, J. Qu et al., "Neurokinin-1 receptor-expressing neurons that contain serotonin and gamma-aminobutyric acid in the rat rostroventromedial medulla are involved in pain processing," *The Journal of Pain*, vol. 14, no. 8, pp. 778–792, 2013.

[20] J. Wang, H. Zhang, Y.-P. Feng et al., "Morphological evidence for a neurotensinergic periaqueductal gray-rostral ventromedial medulla-spinal dorsal horn descending pathway in rat," *Frontiers in Neuroanatomy*, vol. 8, article 112, 2014.

[21] M. Zimmermann, "Ethical guidelines for investigations of experimental pain in conscious animals," *Pain*, vol. 16, no. 2, pp. 109–110, 1983.

[22] A.-F. Bourquin, M. Süveges, M. Pertin et al., "Assessment and analysis of mechanical allodynia-like behavior induced by spared nerve injury (SNI) in the mouse," *Pain*, vol. 122, no. 1-2, pp. 14e1–14e14, 2006.

[23] I. Decosterd and C. J. Woolf, "Spared nerve injury: an animal model of persistent peripheral neuropathic pain," *Pain*, vol. 87, no. 2, pp. 149–158, 2000.

[24] S.-J. Geng, F.-F. Liao, W.-H. Dang et al., "Contribution of the spinal cord BDNF to the development of neuropathic pain by activation of the NR2B-containing NMDA receptors in rats with spinal nerve ligation," *Experimental Neurology*, vol. 222, no. 2, pp. 256–266, 2010.

[25] S. R. Chaplan, F. W. Bach, J. W. Pogrel, J. M. Chung, and T. L. Yaksh, "Quantitative assessment of tactile allodynia in the rat paw," *Journal of Neuroscience Methods*, vol. 53, no. 1, pp. 55–63, 1994.

[26] X. H. Zhao, Y. Q. Zhao, C. Zhu et al., "Different analgesic effects of intrathecal endomorphin-2 on thermal hyperalgesia and evoked inflammatory pain in ovariectomized rats," *Pain Physician*, vol. 18, no. 2, pp. 195–205, 2015.

[27] Y.-L. Dong, W. Wang, H. Li et al., "Neurochemical properties of the synapses in the pathways of orofacial nociceptive reflexes," *PLoS ONE*, vol. 7, no. 3, Article ID e34435, 2012.

[28] L. K. Crawford, C. P. Craige, and S. G. Beck, "Increased intrinsic excitability of lateral wing serotonin neurons of the dorsal raphe: a mechanism for selective activation in stress circuits," *Journal of Neurophysiology*, vol. 103, no. 5, pp. 2652–2663, 2010.

[29] Z. Z. Pan, M. W. Wessendorf, and J. T. Williams, "Modulation by serotonin of the neurons in rat nucleus raphe magnus in vitro," *Neuroscience*, vol. 54, no. 2, pp. 421–429, 1993.

[30] T. King, L. Vera-Portocarrero, T. Gutierrez et al., "Unmasking the tonic-aversive state in neuropathic pain," *Nature Neuroscience*, vol. 12, no. 11, pp. 1364–1366, 2009.

[31] Y. Cai, W. Wang, Y. Hou, and Z. Z. Pan, "Optogenetic activation of brainstem serotonergic neurons induces persistent pain sensitization," *Molecular Pain*, vol. 10, no. 1, article 70, 2014.

[32] S. Sounvoravong, M. N. Nakashima, M. Wada, and K. Nakashima, "Decrease in serotonin concentration in raphe magnus nucleus and attenuation of morphine analgesia in two mice models of neuropathic pain," *European Journal of Pharmacology*, vol. 484, no. 2-3, pp. 217–223, 2004.

[33] F.-Y. Liu, X.-X. Qu, X. Ding et al., "Decrease in the descending inhibitory 5-HT system in rats with spinal nerve ligation," *Brain Research*, vol. 1330, pp. 45–60, 2010.

[34] S. Hagiwara, H. Iwasaka, N. Takeshima, and T. Noguchi, "Mechanisms of analgesic action of pulsed radiofrequency on adjuvant-induced pain in the rat: roles of descending adrenergic and serotonergic systems," *European Journal of Pain*, vol. 13, no. 3, pp. 249–252, 2009.

[35] H. Li, J.-F. Kang, and Y.-Q. Li, "Serotonin potentiation of glycine-activated whole-cell currents in the superficial laminae neurons of the rat spinal dorsal horn is mediated by protein kinase C," *Brain Research Bulletin*, vol. 58, no. 6, pp. 593–600, 2002.

[36] W. Guo, K. Miyoshi, R. Dubner et al., "Spinal 5-HT3 receptors mediate descending facilitation and contribute to behavioral hypersensitivity via a reciprocal neuron-glial signaling cascade," *Molecular Pain*, vol. 10, article 35, 2014.

[37] A. Brenchat, D. Zamanillo, M. Hamon, L. Romero, and J. M. Vela, "Role of peripheral versus spinal 5-HT(7) receptors in the modulation of pain undersensitizing conditions.," *European Journal of Pain*, vol. 16, no. 1, pp. 72–81, 2012.

[38] D. A. Fruman and C. Rommel, "PI3K and cancer: lessons, challenges and opportunities," *Nature Reviews Drug Discovery*, vol. 13, no. 2, pp. 140–156, 2014.

[39] S. Sciarretta, M. Volpe, and J. Sadoshima, "Mammalian target of rapamycin signaling in cardiac physiology and disease," *Circulation Research*, vol. 114, no. 3, pp. 549–564, 2014.

[40] S. Ghavami, S. Shojaei, B. Yeganeh et al., "Autophagy and apoptosis dysfunction in neurodegenerative disorders," *Progress in Neurobiology*, vol. 112, pp. 24–49, 2014.

[41] F. Pilar-Cuéllar, R. Vidal, A. Díaz et al., "Neural plasticity and proliferation in the generation of antidepressant effects: hippocampal implication," *Neural Plasticity*, vol. 2013, Article ID 537265, 21 pages, 2013.

[42] J. Jaworski and M. Sheng, "The growing role of mTOR in neuronal development and plasticity," *Molecular Neurobiology*, vol. 34, no. 3, pp. 205–219, 2006.

[43] X. M. Ma and J. Blenis, "Molecular mechanisms of mTOR-mediated translational control," *Nature Reviews Molecular Cell Biology*, vol. 10, no. 5, pp. 307–318, 2009.

[44] M. Cammalleri, R. Lütjens, F. Berton et al., "Time-restricted role for dendritic activation of the mTOR-p70S6K pathway in the induction of late-phase long-term potentiation in the CA1," *Proceedings of the National Academy of Sciences of the United States of America*, vol. 100, no. 2, pp. 14368–14373, 2003.

[45] R. M. S. Weragoda, E. Ferrer, and E. T. Walters, "Memory-like alterations in Aplysia axons after nerve injury or localized depolarization," *Journal of Neuroscience*, vol. 24, no. 46, pp. 10393–10401, 2004.

[46] K. Budde, T. Becker, W. Arns et al., "Everolimus-based, calcineurin-inhibitor-free regimen in recipients of de-novo kidney transplants: an open-label, randomised, controlled trial," *The Lancet*, vol. 377, no. 9782, pp. 837–847, 2011.

[47] F. X. McCormack, Y. Inoue, J. Moss et al., "Efficacy and safety of sirolimus in lymphangioleiomyomatosis," *The New England Journal of Medicine*, vol. 364, no. 17, pp. 1595–1606, 2011.

[48] M. G. Molina, F. Diekmann, D. Burgos et al., "Sympathetic dystrophy associated with sirolimus therapy," *Transplantation*, vol. 85, no. 2, pp. 290–292, 2008.

[49] T. E. Witzig, S. M. Geyer, I. Ghobrial et al., "Phase II trial of single-agent temsirolimus (CCI-779) for relapsed mantle cell lymphoma," *Journal of Clinical Oncology*, vol. 23, no. 23, pp. 5347–5356, 2005.

[50] O. K. Melemedjian, A. Khoutorsky, R. E. Sorge et al., "mTORC1 inhibition induces pain via IRS-1-dependent feedback activation of ERK," *Pain*, vol. 154, no. 7, pp. 1080–1091, 2013.

[51] M. Gao, X. Yan, and H.-R. Weng, "Inhibition of glycogen synthase kinase 3beta activity with lithium prevents and attenuates paclitaxel-induced neuropathic pain," *Neuroscience*, vol. 254, pp. 301–311, 2013.

Hindawi Publishing Corporation
Neural Plasticity
Volume 2015, Article ID 453170, 11 pages
http://dx.doi.org/10.1155/2015/453170

Research Article

Huperzine A Alleviates Mechanical Allodynia but Not Spontaneous Pain via Muscarinic Acetylcholine Receptors in Mice

Zhen-Xing Zuo,[1,2] Yong-Jie Wang,[2] Li Liu,[3] Yiner Wang,[3] Shu-Hao Mei,[3] Zhi-Hui Feng,[2] Maode Wang,[1] and Xiang-Yao Li[3]

[1]*Department of Neurosurgery, First Affiliated Hospital, Medical College, Xi'an Jiaotong University, Xi'an, Shaanxi 710061, China*
[2]*Center for Mitochondrial Biology and Medicine, The Key Laboratory of Biomedical Information Engineering of Ministry of Education, School of Life Science and Technology and Frontier Institute of Science and Technology, Xi'an Jiaotong University, Xi'an 710049, China*
[3]*Institute of Neuroscience and Collaborative Innovation Center for Brain Science, School of Medicine, Zhejiang University, Hangzhou, Zhejiang 310058, China*

Correspondence should be addressed to Maode Wang; maodewang@163.com and Xiang-Yao Li; leexiangyao@gmail.com

Received 31 March 2015; Revised 13 September 2015; Accepted 14 September 2015

Academic Editor: James M. Wyss

Chronic pain is a major health issue and most patients suffer from spontaneous pain. Previous studies suggest that Huperzine A (Hup A), an alkaloid isolated from the Chinese herb *Huperzia serrata*, is a potent analgesic with few side effects. However, whether it alleviates spontaneous pain is unclear. We evaluated the effects of Hup A on spontaneous pain in mice using the conditioned place preference (CPP) behavioral assay and found that application of Hup A attenuated the mechanical allodynia induced by peripheral nerve injury or inflammation. This effect was blocked by atropine. However, clonidine but not Hup A induced preference for the drug-paired chamber in CPP. The same effects occurred when Hup A was infused into the anterior cingulate cortex. Furthermore, ambenonium chloride, a competitive inhibitor of acetylcholinesterase, also increased the paw-withdrawal threshold but failed to induce place preference in CPP. Therefore, our data suggest that acetylcholinesterase in both the peripheral and central nervous systems is involved in the regulation of mechanical allodynia but not the spontaneous pain.

1. Introduction

Chronic pain affects 15–18% of the population [1]. As well as allodynia, hyperalgesia, and spontaneous pain, patients with chronic pain also present with cognitive impairment, emotional change, insomnia, and mood disorders [2]. Currently, analgesic drugs are used primarily to treat pain [3] but limited effects are a major issue for clinical management [4]. Therefore, finding new drugs is important for the treatment of chronic pain.

Herbal medicines are a potential source of analgesic drugs. The use of herbal medicines has long history, and the analgesic effects of several of them have been evaluated by using extracts or isolated compounds [5]. Among these, Huperzine A (Hup A), an alkaloid isolated from a Chinese club-moss, has received much attention due to its potent and selective inhibition of acetylcholinesterase [6–10], and its analgesic effects have been evaluated in both normal animals and models of spinal cord injury (Table 1) [11–13]. Spontaneous pain, which occurs without stimulation, has been reported to affect ~96% of chronic pain patients [14], and this is the primary target of clinical pain management [15, 16]. However, whether Hup A affects spontaneous pain is not clear. Therefore, we designed the current study to evaluate the analgesic effects of Hup A on spontaneous pain using the conditioned place preference (CPP) behavioral assay [17].

2. Materials and Methods

2.1. Animals. Male C57B L/6 mice aged 8–10 weeks (20–35 g) were housed four or five per cage at constant room temperature (25 ± 1°C) and relative humidity (60 ± 5%) under

Table 1

Application method	Species, strain	Pain model	Behavioral paradigm	Effects	Reference
i.t.	Rat	Formalin	Thermal escape test, formalin test	Escape latency (+), flinching (−)	[13]
i.p.	Mouse	Normal	Hot-plate test	Licking latency (+)	[11]
i.t. or i.p.	Rat (SD)	Static compression	Von Frey assay	Hindpaw-withdrawal threshold (+)	[12]

i.t., intrathecal; i.p., intraperitoneal; SD, Sprague-Dawley.

a 12 h light/dark schedule (lights on 07.00–19.00), with food and water available *ad libitum*. Before the behavioral tests, the mice were allowed to adapt to laboratory conditions for about one week and to habituate to the testing situation for at least 15 min before experiments. To induce inflammatory pain, 10 μL of 50% complete Freund's adjuvant (CFA; Sigma, St. Louis, MO) was injected subcutaneously into the plantar surface of the left hindpaw. The Animal Care and Use Committee of Zhejiang University approved all of the mouse protocols.

2.2. Common Peroneal Nerve (CPN) Model. The CPN ligation model of neuropathic pain was generated as described previously [18, 19]. Briefly, mice were anesthetized with isoflurane (1–3%, as needed). The left CPN between the anterior and posterior muscle groups was slowly ligated with chromic gut suture 5-0 (Ethicon, Blue Ash, USA) until the appearance of twitching of the digits. The skin was sutured using 5-0 silk and cleaned with povidone iodine. Sham surgery was conducted in the same manner but the nerve was not ligated. Animals were kept in a normal cage after surgery. The mice were used for behavioral tests on postsurgical days 3–14.

2.3. Mechanical Allodynia Test. On the experimental day, the von Frey behavioral test was performed according to the up–down algorithm described by Dixon [20]. To determine reflex responses evoked by mechanical stimuli, animals were placed on a raised mesh grid and covered with a clear plastic box for containment. Calibrated von Frey filaments were applied to the middle of the plantar surface of each paw until the filament bent. Brisk withdrawal or paw flinching was considered a positive response. Lifting of the paw due to normal locomotor behavior was ignored. In the absence of a response, the filament of next greater force was applied. Following a response, the filament of the next lower force was applied. The tactile stimulus producing a 50% likelihood of a withdrawal response was calculated and treated as the paw-withdrawal threshold (PWT). The PWTs of mice were normalized by the PWTs tested before the sham or nerve-injury operations.

2.4. Cannulation and Microinjection. The cannula surgery and microinjection were performed as described previously [19]. Briefly, mice were anesthetized with isoflurane (1–3%, as needed) in 100% oxygen at 0.5 L/min via face-mask. The scalp was shaved and cleaned with iodine (Triadine, Shanghai, China) and alcohol. The head was fixed into an adapter mounted on a stereotaxic frame (model 962; Kopf, California, USA) and AKWA Tears (Akorn, Buffalo Grove, IL, USA) were applied to the eyes. An incision was made over the skull and the surface was exposed. Two small holes were drilled above the anterior cingulate cortex (ACC), and the dura was gently reflected. Guide cannulas were placed 0.7 mm anterior to bregma, 0.3 mm lateral to the midline, and 0.75 mm ventral to the surface of the skull. For microinjection, each mouse was restrained in a plastic cone (Braintree Scientific, Braintree, USA), and a small hole was cut in the plastic overlying the microinjection guides. Each dummy cannula was removed, and a microinjection cannula was inserted into each guide. A 30-gauge injection cannula was inserted to a depth 0.7 mm deeper than each guide. Huperzine A (0.5 μL, 0.01 μg/μL) was delivered at 0.5 μL/min using a syringe driven by an infusion pump (Harvard Apparatus, Inc., South Natick, MA). The volume delivered was confirmed by watching the movement of the meniscus in a length of calibrated polyethylene tubing (PE10, Braintree Scientific, Braintree, USA). After delivery to one side of the brain, the cannula was left in place for 1 min to prevent solution from flowing back up the guide. The cannula was then retracted and inserted into the opposite side of the brain. Ten minutes after microinjection, the mice were given the mechanical allodynia test.

2.5. Conditioned Place Preference (CPP) Test. The CPP test was adapted from the paradigm established by King et al. in adult rats [17, 21]. Briefly, mice were preconditioned for three days, starting 3 days after CPN ligation, and the chamber preference was evaluated on preconditioned day 3. A single trail conditioning was performed as below: the following day (day 7 after CPN), mice received the appropriate control (i.e., vehicle) paired with a randomly chosen chamber in the morning, and the appropriate drug paired with the other chamber 4 h later (in the afternoon). Chamber pairings were counterbalanced. Twenty hours after the afternoon pairing, mice were placed in the CPP box with access to all chambers and their behavior recorded for 15 min was analyzed for chamber preference. The preference time was calculated as the time spent in the drug-paired chamber minus the time spent in the saline-paired chamber.

The multitrial conditioning was performed as follows: preconditioning to an automated 3-chamber CPP box was performed across 3 days, starting 1 day after CFA injection. All animals are exposed to the environment with full access to all chambers across 30 min each day. On day 3, behavior was recorded for 15 min and analyzed to verify absence of preconditioning chamber preference. Animals spending more than 80% (time spent > 720 sec) or less than 20% (time spent < 120) of the total time in a chamber were eliminated from further testing. Following the preconditioning phase,

mice underwent conditioning across 6 days with alternating treatment-chamber pairings. Mice received vehicle- (e.g., saline-) chamber pairing on odd days and Hup A-chamber pairing on even days. Mice were placed in the paired chamber with no access to the other chamber immediately following vehicle or drug. Drug and chamber pairing were counterbalanced. On test day animals were placed into the neutral chamber and had access to all chambers during the 15 min observation period, during which time spent in each of the chambers was recorded.

2.6. Novel Object Recognition Test. The novel object recognition test was adapted from the paradigm reported by Leger et al. [22]. Briefly, mice were put into a plastic box (40 cm × 40 cm × 40 cm) to habituate for 5 min. Twenty-four hours later, two identical bottles were placed 10 cm from two corners of the box, and mice were allowed to explore them for 5 min. Twenty-four hours later, one of the bottles was replaced by a new bottle with a different shape and mice were again allowed to explore freely for 5 min, and the times spent exploring the old and new bottles were recorded. The discrimination index was calculated as the difference between the times spent with the new and old bottles.

2.7. Acetylcholinesterase (AChE) Activity. The AChE activity was determined using an assay kit and following the manufacturer's recommendations (MAK119; Sigma, St. Louis, USA). Briefly, 0.1 mg/kg Hup A was injected intraperitoneally into mice after 3 days of CPN ligation, and the ACCs were sampled after 0, 0.5, 2, and 6 h. The AChE activity was normalized to the 0 h injection group.

2.8. Data Analysis. SigmaPlot 11.0 was used to plot and fit the data. Statistical comparisons were made using Student's *t*-test, the paired *t*-test, and one-way or two-way repeat measure ANOVA (Two-way RM ANOVA); the Student-Newmann-Keuls (SNK) or Tukey's test was used for *post hoc* comparisons. All data are presented as the mean SEM. In all cases, $P < 0.05$ was considered statistically significant.

3. Results

3.1. Analgesic Effects of Hup A on Mechanical Allodynia under Chronic Pain Conditions. Yu et al. reported that Hup A attenuates the mechanical allodynia induced by static intrathecal compression [12], suggesting that Hup A is a good candidate pain-killer. Here we used the CPN ligation model, which causes little impairment of motor function [18], to further evaluate the analgesic effects of Hup A on neuropathic pain. The PWT was tested before and three days after CPN ligation, and the ligation significantly decreased it (sham versus nerve injury, $n = 7$ per group, Tukey's test, $P < 0.001$; Figure 1(a)). A low dose of Hup A (0.02 mg/kg and 0.075 mg/kg, i.p.; Figures 1(a) and 1(b)) did not change the PWT, while a higher dose (0.1 mg/kg and 0.15 mg/kg) increased the PWTs of mice with nerve injury to normal levels at 0.5 h after injection. The hypersensitivity returned 2 h after injection (Tukey's test, $P < 0.001$; Figures 1(c) and 1(d)). While Hup A at 0.2 mg/Kg increased the PWTs of mice from both the sham and nerve-injury groups, the analgesic effect lasted for >2 h (sham versus nerve injury, Tukey's test, $P > 0.05$; Figure 1(e)). To investigate whether muscarinic acetylcholine receptors (mAChRs) are involved in the analgesic effects of Hup A, atropine (1 mg/kg), an antagonist of mAChRs, was injected first, and Hup A (0.1 mg/kg) was injected 0.5 h later. Under these conditions, atropine blocked the effects of Hup A on the PWTs (sham versus nerve injury, Tukey's test, $P < 0.001$; Figure 1(c)), suggesting that mAChRs are involved in the regulation of mechanical allodynia. Similar to previous reports [12], our data suggest that Hup A alleviates mechanical allodynia.

To investigate whether Hup A has an analgesic effect on chronic inflammatory pain, we injected CFA into the left hindpaw, and this decreased the PWTs one day after injection (Baseline: saline versus CFA, Tukey's test, $P > 0.05$; after injection: Tukey's test, $P < 0.01$; Figure 1(f)). Injection of Hup A (0.1 mg/kg, i.p.) increased the PWTs to the control level (saline versusCFA, Tukey's test, $P > 0.05$), and this effect did not last for 2 h (saline versus CFA, Tukey's test, $P < 0.05$). Similarly, injection of atropine (1 mg/kg, i.p.) blocked the effect of Hup A on the PWTs (atropine + Hup A, saline versus CFA, Tukey's test, $P < 0.001$). Therefore, our data suggested that Hup A alleviates the mechanical allodynia of neuropathic and chronic inflammatory pain via mAChRs.

3.2. Effects of Hup A on Spontaneous Pain. Spontaneous pain is one of the major pathological phenomena of chronic pain [15, 16]. Here, we used the CPP assay [17] to evaluate the effects of Hup A on spontaneous pain. The mice did not show place preference in the preconditioning test (Figure 2(a)), and the injection of clonidine (0.5 mg/Kg, i.p.) into the nerve-injured mice induced a preference for the drug-paired chamber ($n = 6$, $P < 0.05$; Figure 2(b)), suggesting the presence of spontaneous pain induced by CPN ligation. But Hup A (0.1 mg/Kg and 0.15 mg/kg) did not induce place preference in nerve-injured mice (Figure 2(b)). However, the effects of clonidine were markedly different from those of Hup A (groups: $F_{2;33} = 11.79$, $P < 0.01$, two-way repeated measures ANOVA, $n = 6$ for Hup A 0.1 mg/kg and clonidine group, $n = 5$ for Hup A 0.15 mg/kg; Figure 2(b)). The preference time for clonidine also differed from that of Hup A (one-way ANOVA, $F_{2;16} = 8.50$, $P < 0.01$, $n = 6$ for Hup 0.1, clonidine group, $n = 5$ for Hup 0.15, Figure 2(c)). These data suggested that Hup A at the dosage of 0.1 mg/kg and 0.15 mg/kg does not alleviate spontaneous pain in mice with CPN ligation.

Peripheral inflammation may induce spontaneous pain, so we used the same behavioral paradigm to test the effects of Hup A on ongoing pain. Similarly, clonidine (i.p.) increased the time spent in the drug-paired chamber (saline-paired versus clonidine-paired, $n = 9$, $P < 0.05$; Figures 2(d) and 2(e)), while Hup A (0.1 mg/Kg) did not show any effect (Figures 2(d) and 2(e)). The preference time for clonidine also differed from that of Hup A ($F_{2;28} = 5.13$, $P < 0.05$, one-way ANOVA; Figure 2(f)). To further confirm these results, a multitrial conditioning was employed, in which mice received Hup A for several times, and the multiple application of Hup A still did not induce place preference

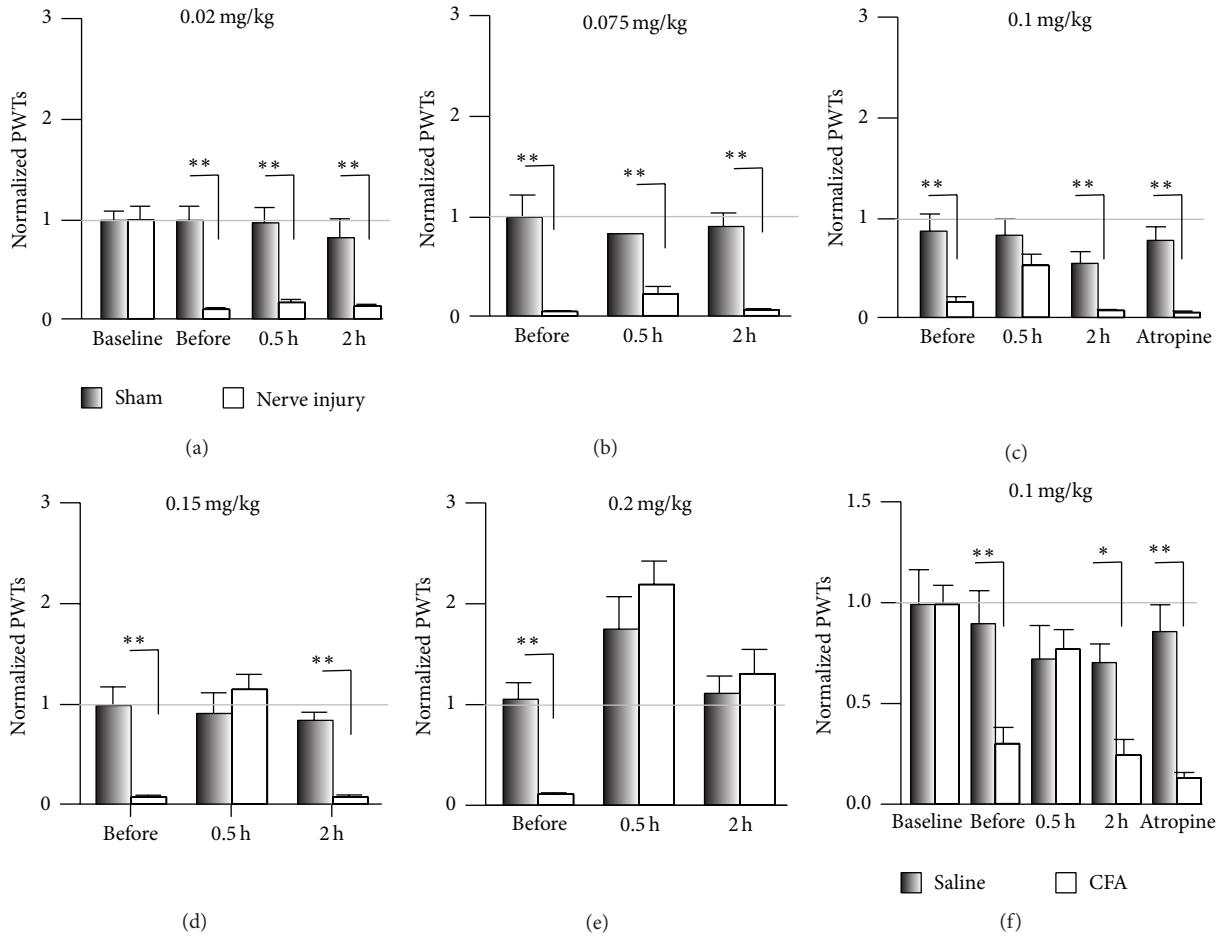

Figure 1: Systemic injection of Hup A raised the PWT in nerve-injured mice. (a) Hup A at 0.02 mg/kg had no effect on the PWTs in the sham and nerve-injury groups (two-way repeated measures ANOVA, sham versus injury: $F_{1;55} = 50.04$, $P < 0.01$; treatments: $F_{3;55} = 8.17$, $P < 0.01$, $n = 7$ per group, $^{**}P < 0.01$ under Tukey's test). (b) Hup A at 0.075 mg/kg had no effect on the PWTs in the sham and nerve-injury groups (two-way repeated measures ANOVA, sham versus injury: $F_{1;32} = 227.45$, $P < 0.01$; treatments: $F_{2;32} = 0.08$, $P > 0.01$, $n = 5$ for sham, $n = 6$ for CPN, $^{**}P < 0.01$ under Tukey's test). (c) Hup A at 0.1 mg/kg increased the PWTs in the nerve-injury group, but not in the sham group, and this effect was blocked by atropine (two-way RM ANOVA, sham versus injury: $F_{1;69} = 14.60$, $P < 0.01$; treatments: $F_{4;69} = 20.13$, $P < 0.01$, $n = 7$ per group, $^{**}P < 0.01$ under Tukey's test). (d) Hup A at 0.15 mg/kg raised the PWTs in the nerve-injury group, but not in the sham group (two-way RM ANOVA, sham versus injury: $F_{1;29} = 29.91$, $P < 0.01$; treatments: $F_{2;29} = 9.18$, $P < 0.01$, $n = 5$ per group, $^{**}P < 0.01$ under Tukey's test). (e) Increasing the dose of Hup A to 0.2 mg/kg raised the PWTs in both groups, and the analgesic effects lasted >2 h (two-way RM ANOVA, sham versus injury: $F_{1;41} = 0.29$, $P > 0.05$; treatments: $F_{2;41} = 23.17$, $P < 0.01$, $n = 7$ per group, $^{**}P < 0.01$ under SNK test). (f) Hup A at 0.1 mg/kg increased the PWTs in the CFA injection group, but not in the saline group, and this effect was blocked by atropine (two-way RM ANOVA, saline versus CFA: $F_{1;94} = 13.24$, $P < 0.01$; treatments: $F_{4;94} = 6.89$, $P < 0.01$, saline, $n = 10$; CFA, $n = 9$, $^{*}P < 0.05$; $^{**}P < 0.01$ under Tukey's test). "Baseline" indicates the PWTs before operation. "Before" indicates PWTs before intraperitoneal drug injection.

(Figures 2(g)–2(i)). Therefore our data suggested that Hup A has no effect on the spontaneous pain induced by peripheral inflammation.

3.3. Ambenonium Chloride Has No Effect on Spontaneous Pain. Since both peripheral and central sensitization are involved in the regulation of chronic pain [23], Hup A applied systemically may alleviate the mechanical allodynia by inhibiting AChE [24] in the peripheral nerve system. To test this, we investigated the analgesic effects of ambenonium chloride, a competitive AChE inhibitor that does not pass through the blood-brain barrier (BBB) [25, 26]. Ambenonium at 0.01 mg/kg (i.p.) had no effect on the PWTs (Figure 3(a)), while it increased them in the nerve-injury group at 0.05 mg/kg (Figure 3(b)) and in both groups at 0.1 mg/kg (Figure 3(c)). We therefore used ambenonium at 0.05 mg/kg to investigate the involvement of AChE in the regulation of spontaneous pain. The mice did not show a preference for the ambenonium-paired chamber in CPP (Figures 3(d)–3(f)), and no difference was detected in the preference time between the sham and nerve-injury groups (Figure 3(f)), suggesting that ambenonium has no effect on spontaneous pain. Therefore, inhibiting AChE in the peripheral nervous system alleviates evoked pain but not spontaneous pain.

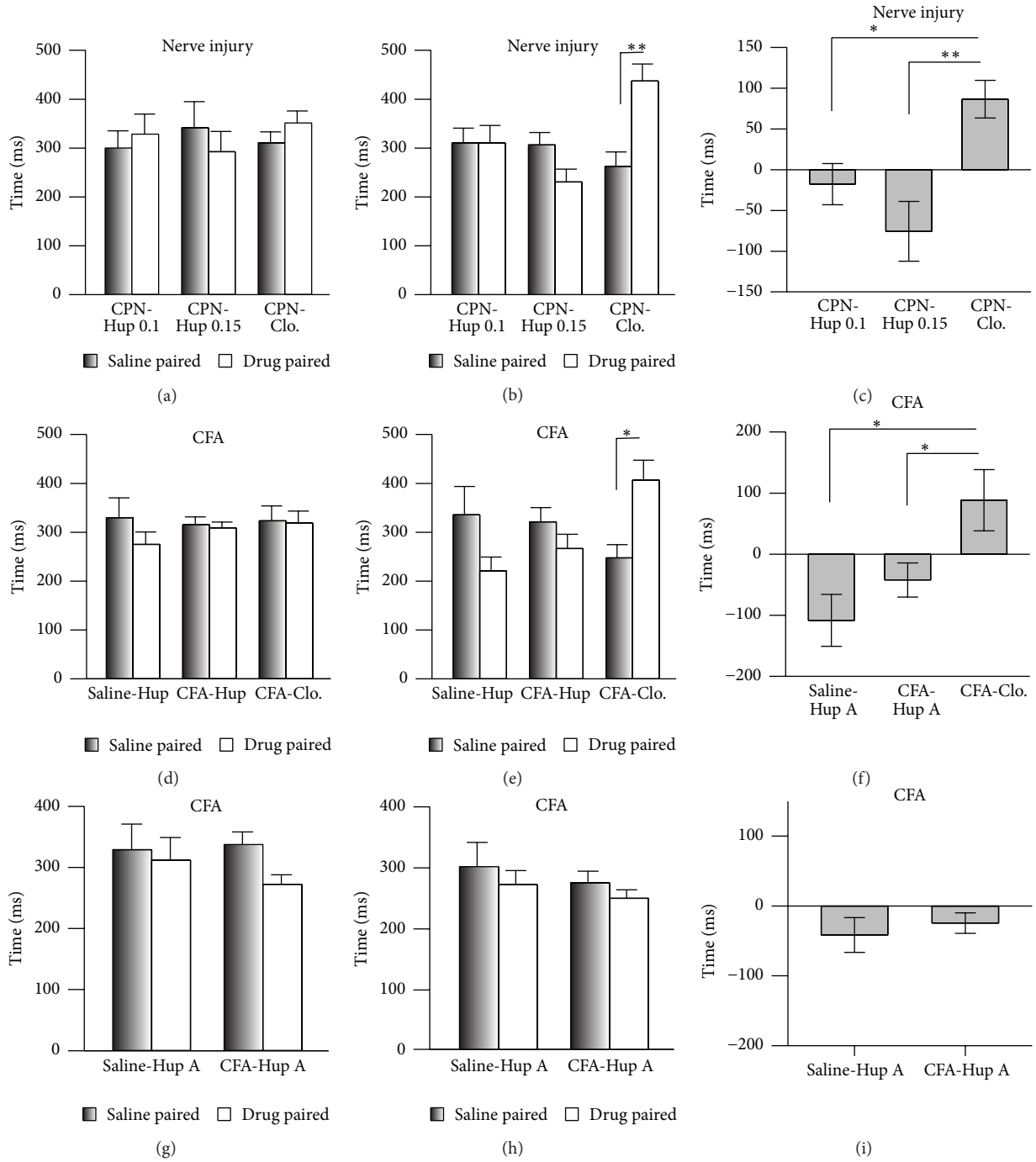

Figure 2: Systemic injection of clonidine but not Hup A alleviated spontaneous neuropathic pain as assessed in the CPP test. (a) Times spent in the chambers during the preconditioning period (two-way RM ANOVA, groups: $F_{2;33} = 1.30$, $P > 0.05$; saline versus drug: $F_{1;33} = 0.03$, $P > 0.05$, $n = 6$ for Hup 0.1, clonidine group, $n = 5$ for Hup 0.15). (b) Clonidine but not Hup A (0.1 mg/kg and 0.15 mg/kg) induced preference for the drug-paired chamber (two-way RM ANOVA, groups: $F_{2;33} = 11.79$, $P < 0.01$; saline versus drug: $F_{1;33} = 0.98$, $P > 0.05$, $n = 6$ for Hup 0.1, clonidine group, $n = 5$ for Hup 0.15, $^{*}P < 0.01$ under SNK test). (c) Preference times induced by Hup A and clonidine in mice with nerve injury (one-way ANOVA, $F_{2;16} = 8.50$, $P < 0.01$, $n = 6$ for Hup 0.1, clonidine group, $n = 5$ for Hup 0.15, $^{*}P < 0.05$ under SNK test). (d) Time spent by mice in the chambers in the saline- and CFA-injected groups during the preconditioning period (two-way RM ANOVA, groups: $F_{2;57} = 0.54$, $P > 0.05$; saline versus drug: $F_{1;57} = 0.82$,$P > 0.05$, $n = 5$ for saline-Hup A, $n = 16$ for CFA-Hup A, $n = 9$ for CFA-Clo.). (e) Clonidine but not Hup A induced preference for the drug-paired chamber by CFA-injected mice (two-way RM ANOVA, groups: $F_{2;57} = 3.34$, $P = 0.05$; saline versus drug: $F_{1;57} = 0.01$, $P > 0.05$, $n = 5$ for saline-Hup A, $n = 16$ for CFA-Hup A, and $n = 9$ for CFA-Clo.; $^{*}P < 0.05$ under SNK test). (f) Preference times of mice with CFA injection induced by Hup A and clonidine (one-way ANOVA, $F_{2;28} = 5.13$, $P < 0.05$, $^{*}P < 0.05$ under SNK test). (g) Time spent by mice in the chambers in the saline- and CFA-injected groups during the preconditioning period for multitrial conditioning (two-way RM ANOVA, groups: $F_{1;29} = 0.86$, $P > 0.05$; saline versus drug: $F_{1;29} = 1.15$, $P > 0.05$, $n = 7$ for saline-Hup A, $n = 8$ for CFA-Hup A). (h) Hup A (0.1 mg/kg) did not induce preference for the drug-paired chamber by CFA-injected mice in the multitrial conditioning (two-way RM ANOVA, groups: $F_{1;29} = 1.43$, $P > 0.05$; saline versus drug: $F_{1;29} = 0.93$, $P > 0.05$, $n = 7$ for saline-Hup A, $n = 8$ for CFA-Hup A). (i) Preference times of mice with CFA injection induced by Hup A in the multitrial conditioning (t-test, $P > 0.05$).

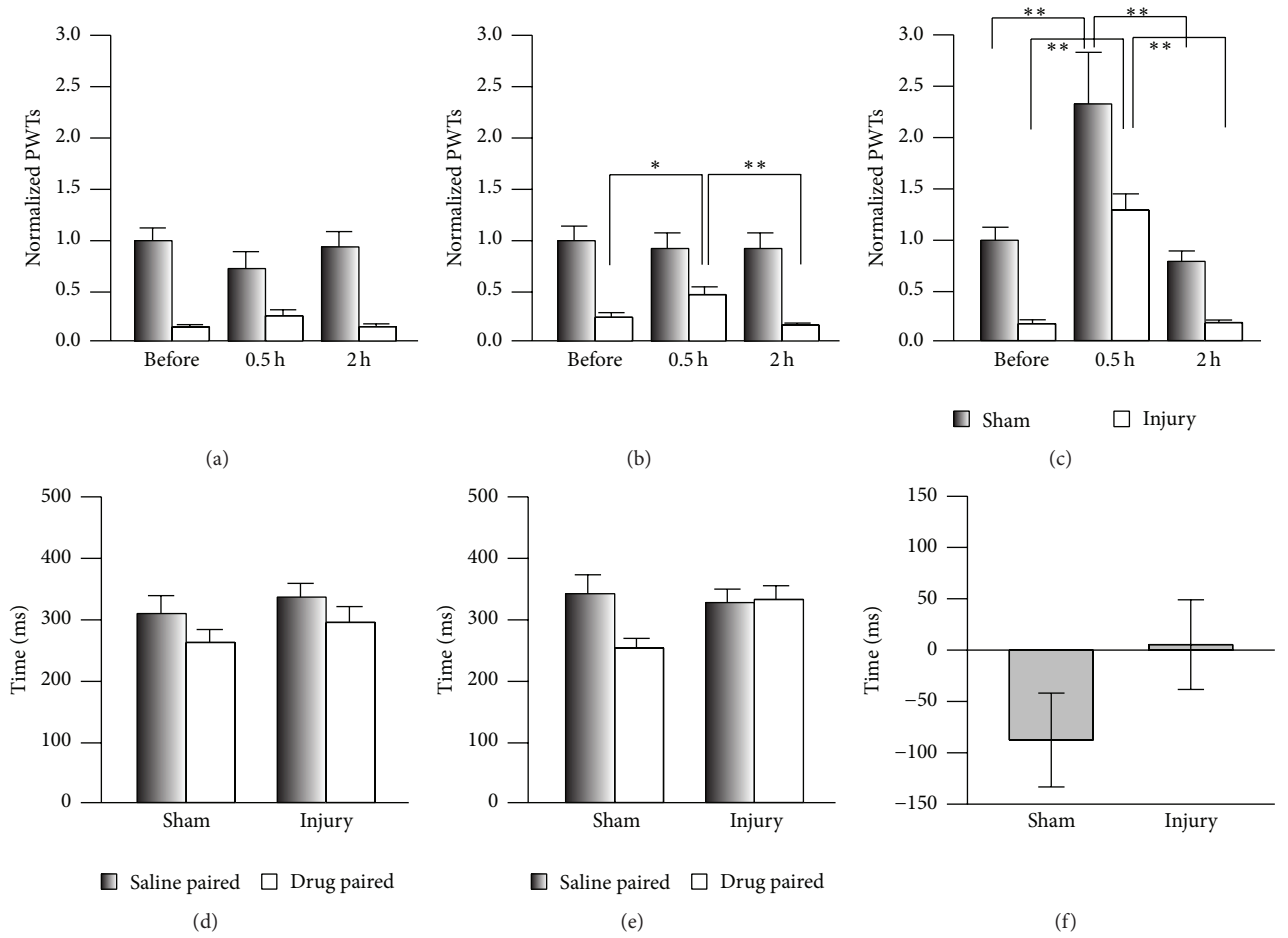

Figure 3: Application of ambenonium chloride had no effect on spontaneous pain. (a) Ambenonium at 0.01 mg/kg had no effect on the PWTs of the sham and nerve-injury groups (two-way RM ANOVA, sham versus injury: $F_{1;35} = 30.45$, $P < 0.01$; treatments: $F_{2;35} = 0.59$, $P > 0.05$, $n = 6$ per group). (b) Ambenonium at 0.05 mg/kg increased the PWTs of the nerve-injury group (two-way RM ANOVA, sham versus injury: $F_{1;41} = 27.52$, $P < 0.01$; treatments: $F_{2;41} = 2.94$, $P > 0.05$, $n = 6$ for sham, $n = 8$ for injury; $^{*}P < 0.05$ and $^{**}P < 0.01$ under SNK test). (c) Increasing the dose of ambenonium to 0.1 mg/kg raised the PWTs in both groups (two-way RM ANOVA, sham versus injury: $F_{1;32} = 28.57$, $P < 0.01$; treatments: $F_{2;32} = 22.42$, $P < 0.01$, $^{**}P < 0.01$ under Tukey's test). (d) Time spent in the chambers during the CPP preconditioning period (two-way RM ANOVA, sham versus injury: $F_{1;43} = 4.21$, $P > 0.05$; saline versus drug: $F_{1;43} = 1.76$, $P > 0.05$, $n = 9$ for sham group, $n = 13$ for injury group). (e) Ambenonium at 0.05 mg/kg did not induce preference for the drug-paired chamber in the CPP test (two-way RM ANOVA, sham versus injury: $F_{1;43} = 11.57$, $P < 0.05$; saline versus drug: $F_{1;43} = 1.61$, $P > 0.05$, $n = 9$ for sham group, $n = 13$ for injury group). (f) No difference in the preference time induced by ambenonium at 0.05 mg/kg was detected in the CPP test (t-test, $P > 0.05$, $n = 9$ for sham group, $n = 13$ for injury group).

3.4. Analgesic Effects of Hup A in the Anterior Cingulate Cortex. Although it has been reported that Hup A passes through the BBB, whether the AChE in the central nervous system is decreased by Hup A was unclear. The ACC is important in the maintenance of chronic pain [19, 21]. We first evaluated the expression levels of AChE on day 1 (D1) and day 3 (D3) after CPN ligation and found that in the nerve-injury group it increased to 2.63 ± 0.34 and 2.83 ± 0.31 times that of the sham group, respectively ($n = 5$ per group, Figure 4(a)). Similarly, the activities of AChEs at D3 increased to 1.47 ± 0.19 times that of the Sham group, and Hup A (0.1 mg/kg) decreased them to the level of the sham group at 0.5 h after injection (0.81 ± 0.04, $n = 4$) and 2 h (0.82 ± 0.06, $n = 4$, one-way ANOVA, $F_{3;26} = 5.81$, $P < 0.01$, Figure 4(b)). These data suggested that the systemic injection of Hup A decreases the activities of AChE in the ACC.

We further infused Hup A into the ACC (0.005 μg/0.5 μL/side) (Figure 4(c)). This markedly increased the PWTs in both sham and nerve-injured mice (sham: before versus Hup A, $P < 0.01$; nerve injury: before versus Hup A, $P < 0.01$, $n = 5$ for both groups), while this effect was blocked by atropine (i.p., sham versus nerve injury, $P < 0.001$; Figure 4(d)), suggesting the involvement of cingulate mAChRs in pain regulation. While infusion of Hup A into the ACC did not induce place preference, mice in both of the sham (paired t-test, $P > 0.05$, $n = 4$/group) and nerve-injury groups (paired t-test, $P > 0.05$, $n = 4$/group) spent equal times in the chambers during preconditioning (Figure 4(e)). Furthermore, when Hup A was infused, the mice did not show a preference for the drug-paired chamber (two-way RM ANOVA, Figure 4(f)). Also, no difference was detected between the sham and nerve-injury groups in the preference

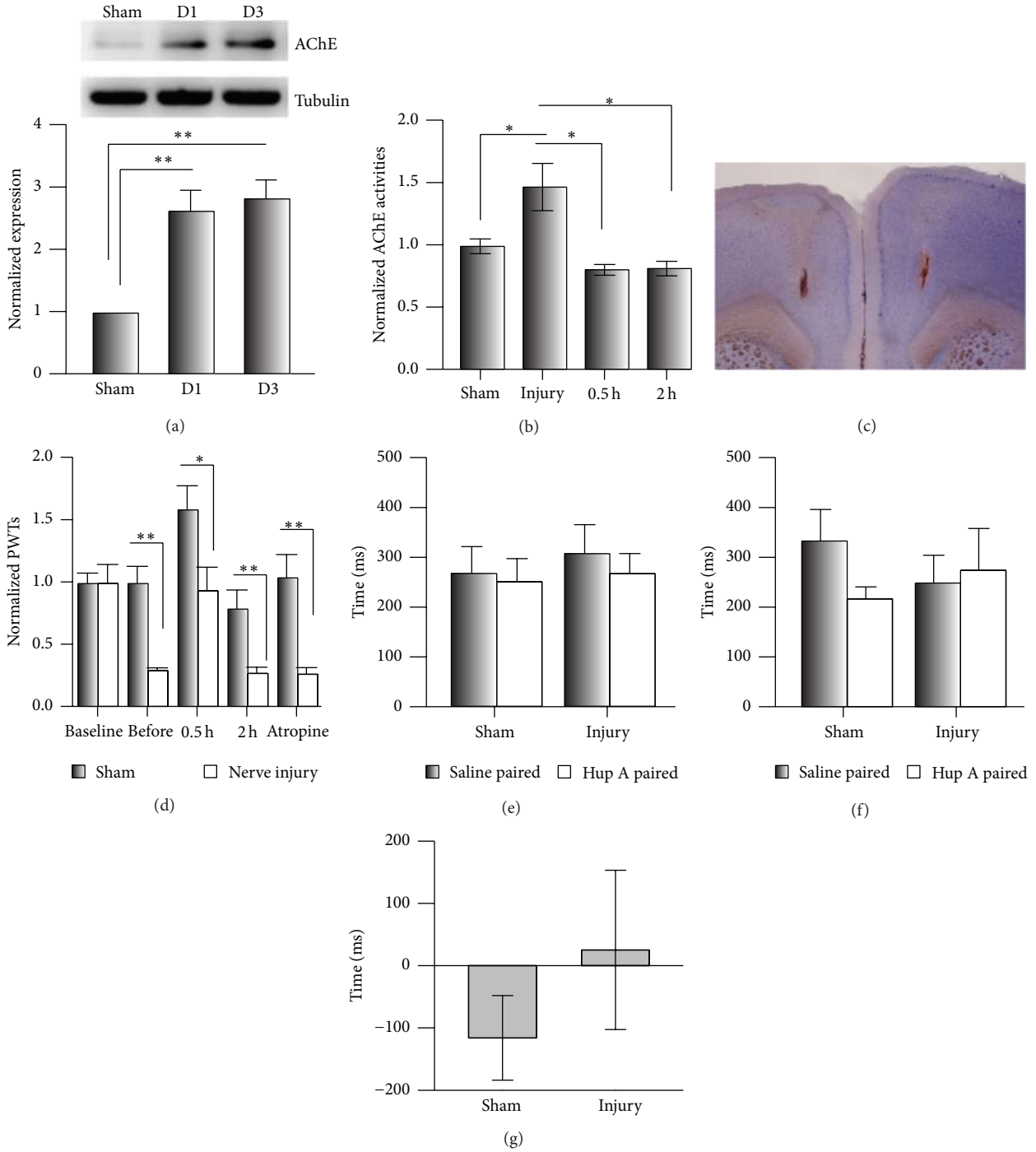

Figure 4: Infusion of Hup A into the anterior cingulate cortex did not alleviate spontaneous neuropathic pain. (a) The expression levels of AChE in the ACC were increased by the nerve injury (one-way ANOVA, $F_{2;14} = 14.64$, $P < 0.01$; $n = 5$ per group, $^{**}P < 0.05$ under SNK test). (b) The AChE activity in the ACC of mice with nerve injury was increased, and this was inhibited by Hup A at 0.1 mg/kg, i.p. (one-way ANOVA, $F_{3;26} = 5.81$, $P < 0.01$; $n = 10$ for sham group, $n = 9$ for injury, $n = 4$ for 0.5 h group and 2 h group, $^{*}P < 0.05$ under SNK test). (c) An example showing the injection site in the ACC of hematoxylin and eosin stained brain section. (d) Infusion of Hup A into the ACC increased PWTs in the sham and nerve-injury groups, and atropine blocked this analgesic effect (two-way RM ANOVA, sham versus injury: $F_{1;49} = 14.89$, $P < 0.01$; treatments: $F_{4;49} = 15.93$, $P < 0.01$, $n = 5$ per group, $^{**}P < 0.01$ under Tukey's test). (e) Time spent in the chambers during the preconditioning period of the CPP test (two-way RM ANOVA, sham versus injury: $F_{1;15} = 0.39$, $P > 0.05$; saline versus drug: $F_{1;15} = 0.27$, $P > 0.05$, $n = 4$ per group). (f) Infusion of Hup A into the ACC did not induce a preference for the drug-paired chamber in the CPP test (two-way RM ANOVA, sham versus injury: $F_{1;15} = 0.09$, $P > 0.05$; saline versus drug: $F_{1;15} = 0.40$, $P > 0.05$, $n = 4$ per group). (g) No change occurred in the preference time induced by Hup A in the CPP (t-test, $P > 0.05$).

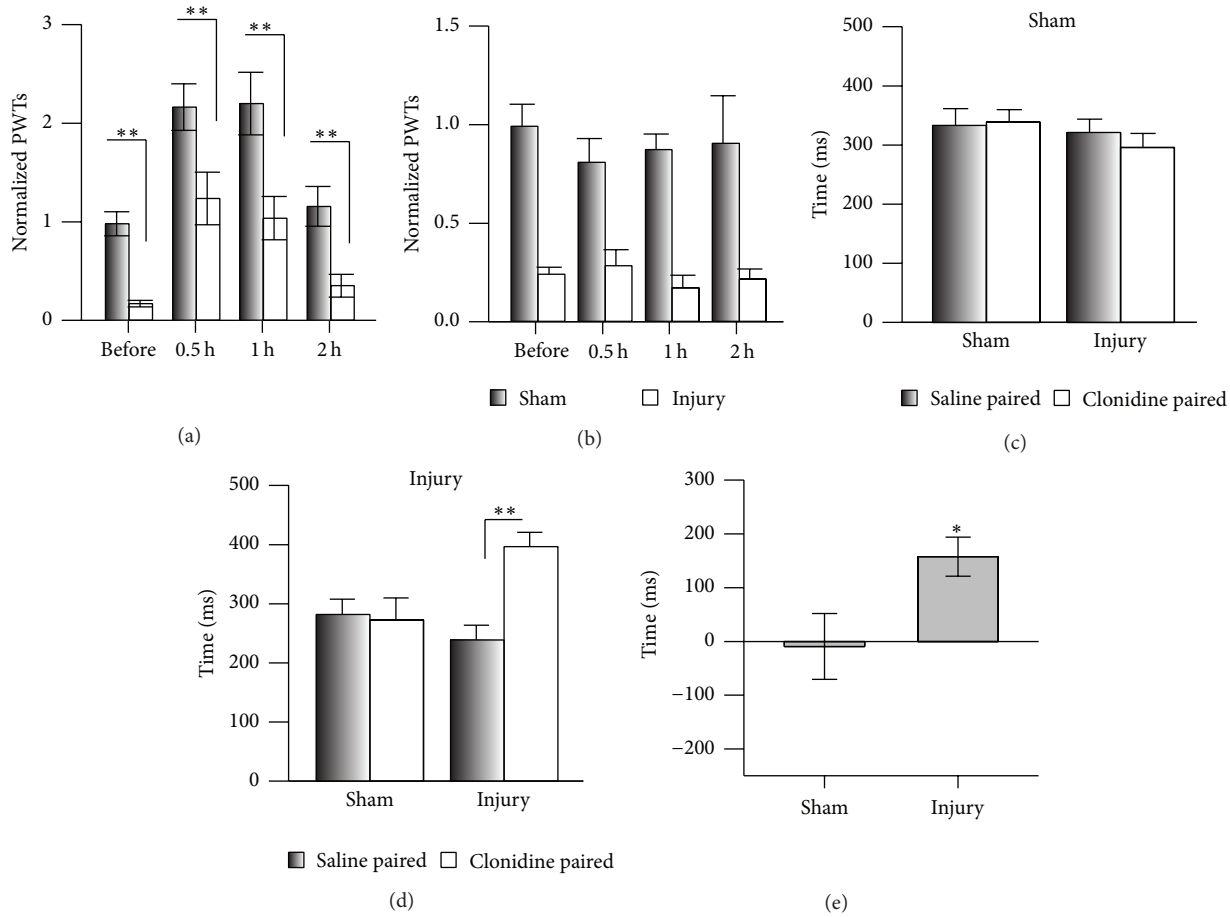

Figure 5: Infusion of clonidine into the anterior cingulate cortex alleviated spontaneous neuropathic pain. (a) Infusion of clonidine into the ACC increased the PWTs in the sham and nerve-injury groups (two-way RM ANOVA, sham versus injury: $F_{1;63} = 21.12$, $P < 0.01$; treatments: $F_{3;63} = 23.13$, $P < 0.01$, $n = 7$ for sham, $n = 9$ for injury, $^{**}P < 0.01$ under Tukey's test). (b) Infusion of saline into the ACC had no effect on the PWTs (two-way RM ANOVA, sham versus injury: $F_{1;39} = 44.54$, $P < 0.01$; treatments: $F_{3;39} = 0.29$, $P > 0.01$, $n = 5$ per group). (c) Time spent in the chambers during the preconditioning period in the CPP test (two-way RM ANOVA, sham versus injury: $F_{1;31} = 3.54$, $P > 0.05$; saline versus drug: $F_{1;31} = 0.10$, $P > 0.05$, $n = 8$ per group). (d) Infusion of clonidine into the ACC induced a preference for the drug-paired chamber in the CPP test (two-way RM ANOVA, sham versus injury: $F_{1;31} = 4.13$, $P = 0.06$; saline versus drug: $F_{1;31} = 4.06$, $P > 0.05$, $n = 8$ per group, $^{**}P < 0.01$ under Tukey's test). (e) Hup A changed the preference time in the CPP test (t-test, $n = 8$ per group $^{*}P < 0.05$).

time (t-test, $P > 0.05$; Figure 4(g)). Our data suggested that AChE in the ACC is involved in the regulation of mechanical allodynia, but not spontaneous pain.

To exclude the possibility that the infusion damaged the ACC, which could lead to the negative performance of mice in the CPP, we infused clonidine (4 μg/0.5 μL/side) into the ACC and evaluated its analgesic effects on both PWT and CPP. Clonidine increased the PWTs in both sham and nerve-injured mice (two-way RM ANOVA, Figure 5(a)), while saline had no effect (Figure 5(b)). Similarly, the clonidine did not induce a clear preference on the sham mice (two-way RM ANOVA, Figure 5(c)), while a clear preference for the clonidine-paired chamber was evident on the injury mice (two-way RM ANOVA, Figure 5(d)), and the sham and nerve-injury groups were similar in the preference times due to the big variation of sham group (sham versus injury, t-test, $P > 0.05$, Figure 5(e)). Therefore, clonidine infused into the ACC attenuates both mechanical allodynia and spontaneous pain.

3.5. Effects of Clonidine and Hup A on Learning. Learning is involved in the performance of CPP, so the failure of Hup A to affect CPP may have been due to impaired learning. We therefore examined this possibility using the novel object recognition task. After 5 min habituation, two identical bottles (1 and 2) were put into symmetrical locations in the box, and the mice were allowed to explore them freely for 5 min, when they spent almost the same time exploring each bottle (two-way RM ANOVA, $F_{2;43} = 1.86$, $P > 0.05$, $n = 7$ for both control and clonidine groups, $n = 8$ for the Hup A group; Figure 6(a)). To avoid motor impairment during the training phase, the Hup A or clonidine was injected (i.p.) immediately after training. One bottle (#2) was replaced by a new one (#3) 24 h after training, and

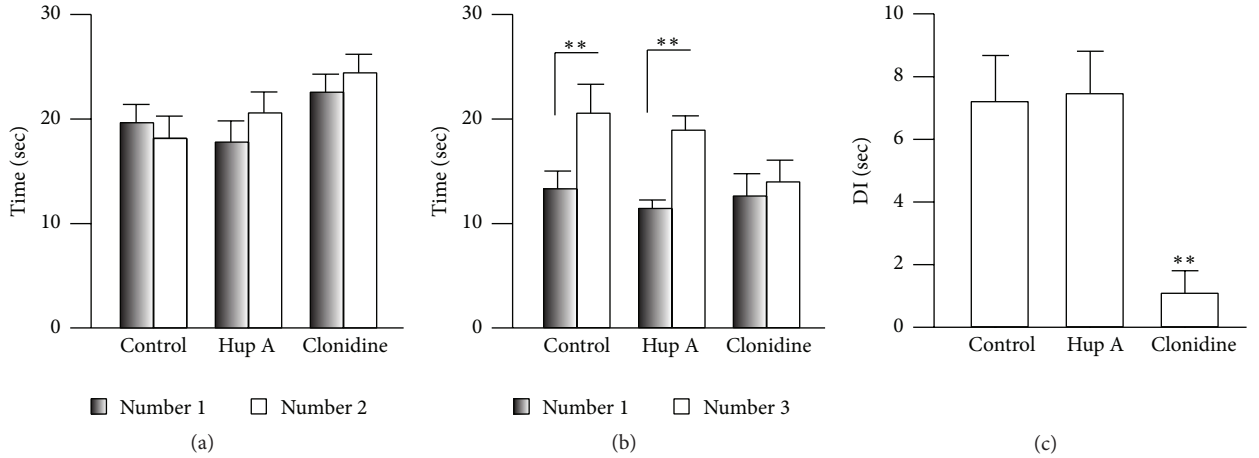

Figure 6: Hup A did not affect learning in mice. (a) Exploration times for the two identical bottles in each group (two-way RM ANOVA, objects: $F_{1;43} = 2.19$, $P > 0.05$; groups: $F_{1;43} = 1.86$, $P > 0.05$, $n = 7$ for control and clonidine group, $n = 8$ for Hup A group). (b) The control and Hup A groups spent more time exploring the novel object (two-way RM ANOVA, objects: $F_{1;43} = 1.04$, $P > 0.05$; groups: $F_{1;43} = 51.05$, $P < 0.01$, $n = 7$ for control and clonidine group, $n = 8$ for Hup A group, $^{**}P < 0.01$ under SNK test). (c) The discrimination index did not differ between the control and Hup A groups (one-way ANOVA, $F_{2;21} = 7.10$, $P < 0.01$; $^{*}P < 0.05$ under SNK test). DI indicates discrimination index.

the times spent exploring the familiar (#1) and novel bottles (#3) were recorded. Surprisingly, the mice injected with Hup A (0.1 mg/kg) showed a clear preference for the novel bottle (#1: 11.61 ± 0.82 sec; #3: 19.12 ± 1.36 sec; Figure 6(b)), similar to the control group (#1: 13.49 ± 1.70 sec; #3: 20.74 ± 2.77 sec), but the clonidine group did not show a preference (#1: 12.82 ± 2.12 sec; #3: 14.15 ± 2.10 sec). And a significant difference was detected between the control (7.25 ± 1.48, $n = 7$) and clonidine groups (0.06 ± 0.03, $n = 7$, $P < 0.05$ versus control), but not the Hup A group (7.51 ± 1.35, $n = 8$, $P > 0.05$ versus control) on the discrimination index (one-way ANOVA, $F_{2;21} = 7.10$; $P < 0.01$, Figure 6(c)). These data suggested that the application of Hup A has no effect on learning in mice.

4. Discussion

In the current study, we evaluated the analgesic effects of Hup A on both mechanical allodynia and spontaneous pain in mice. Our data showed that although mechanical allodynia was significantly attenuated, spontaneous pain did not change when Hup A was injected systemically or infused locally into the ACC. Furthermore, we found that Hup A did not impair learning in the novel object recognition task. Ambenonium chloride, an inhibitor of AChE, had effects similar to Hup A. Our data therefore suggest that mAChRs are involved in the regulation of stimulation-evoked pain but not spontaneous pain.

4.1. Analgesic Effects of Hup A on Evoked Pain. The data from our study agrees with the previous report [12] that Hup A attenuates mechanical allodynia, a form of evoked pain induced by nerve injury. However, unlike that report, in which only rats with nerve injury were used [12], here we evaluated the analgesic effects of Hup A on mice with sham treatment or CPN ligation, and our data suggested that Hup A at 0.1 mg/kg (i.p.) is the appropriate dose for chronic pain management, because higher doses such as 0.2 mg/kg raised the PWTs of the mice in the sham group. The antinociceptive action of Hup A has also been evaluated using the hot-plate test in normal mice, which showed that Hup A at 70 μg/kg increases the response latency [11]. This dose of Hup A is lower than that used in the current study and may be due to the different strain [27]. Furthermore, we showed for the first time that Hup A increased the PWTs of mice with peripheral inflammation. Therefore, our data suggested that Hup A alleviates the mechanical allodynia induced by both peripheral inflammation and nerve injury.

4.2. Effects of Hup A on Spontaneous Pain. Hup A evidently had no effect on spontaneous pain. The presence of spontaneous pain has been reported and evaluated using the CPP behavioral assay [17]. In our study, mice with nerve injury or peripheral inflammation did not show a preference for the Hup A-paired chamber, suggesting that spontaneous pain does not change. This was not due to the experimental design, because clonidine in the ACC did induce a preference for the drug-paired chamber in the nerve-injured mice [17]. Also, Hup A did not affect performance in the novel object-recognition behavioral paradigm, suggesting that the learning in mice is normal when Hup A is administered. It has been proposed that the reward system is involved in CPP [28]. We did find that mechanical allodynia was attenuated by Hup A, and the activity of AChE in the ACC was inhibited by Hup A (i.p.), which excluded the possibility that Hup A had no effect on the central nervous system. It is possible that the aversive state induced by nerve injury was not changed by Hup A, so mice did not show a preference for the drug-paired chamber. Whether the mAChR system is involved in regulating the reward system needs further study.

It has been shown that intrathecal Hup A increases the thermal escape latency and decreases flinching behavior in

rats in the formalin test, which suggests that Hup A affects thermal allodynia and spontaneous pain [11]. However, it must be noted that flinching in the formalin test in that study was observed for several hours after injection, while, in our system, the spontaneous pain was evaluated several days after nerve injury or CFA injection, so the mechanisms mediating the spontaneous pain in the two models may be quite different.

4.3. AChE in Both the Peripheral and Central Nervous Systems Is Involved in the Regulation of Chronic Pain. Our data showed that the analgesic effect of Hup A was blocked by atropine, suggesting that the activity of mAChRs has a role in the regulation of evoked pain (Figure 1(b)). Hup A at 0.1 mg/kg only increased the PWTs of mice with nerve injury, but not the sham group, suggesting that mice with nerve injury are more sensitive to Hup A than the sham group, and this may be due to the increased AChEs under chronic pain conditions (Figure 4(a)). Since ambenonium chloride cannot pass through the BBB [25, 26], its analgesic effects suggest that peripheral AChE is involved in the hypersensitivity, while not ruling out its involvement in the central nervous system, since we also found that the activity of AChE in the ACC was inhibited by intraperitoneal Hup A, and Hup A infusion did change the hypersensitivity in both the sham and nerve-injury groups. Therefore, our data suggested that AChE in both the peripheral and central nervous systems is involved in the regulation of evoked pain.

4.4. Evoked Pain and Spontaneous Pain May Be Mediated by Different Mechanisms. The results of clinical studies and behavioral observations suggest that evoked and spontaneous pain are mediated by different mechanisms. Clinical studies have shown that evoked and spontaneous pain do not always coexist [14], and it has also been found that limited damage to fibers in patients changes the sensations induced by touch and warmth but may not induce spontaneous pain [29]. Here, we found that both Hup A and ambenonium chloride only alleviated mechanical allodynia but did not induce a preference for the drug-paired chamber, suggesting that spontaneous pain did not change, and these results resemble the effects of adenosine on CPP [17]. Similar results have been reported in clinical studies using ketamine, which reduces both spontaneous pain and evoked pain, whereas lidocaine only reduces evoked pain [30]. It is quite possible that evoked and spontaneous pain are regulated by different factors, and analgesic drugs that attenuate evoked pain may fail to affect spontaneous pain. Anyway, we did not find place preference induced by Hup A, and the doses that attenuated evoked pain were not enough to alleviate spontaneous pain. Therefore, other analgesic drugs should be combined with Hup A to alleviate both pain and evoked pain in clinical trials.

Conflict of Interests

The authors declare no competing financial interests.

Authors' Contribution

Zhen-Xing Zuo and Yong-Jie Wang performed the experiments, Li Liu, Yiner Wang, and Shu-Hao Mei analyzed the data, Xiang-Yao Li, Maode Wang, and Zhi-Hui Feng designed the experiments, and Maode Wang and Xiang-Yao Li wrote the paper. Zhen-Xing Zuo and Yong-Jie Wang are equal contributors.

Acknowledgments

This study was supported by the National Program on Key Basic Research Project (973 Program) (2014CB548200), and the Natural Science Foundation of Zhejiang Province, China (LQ13C090001).

References

[1] H. A.-S. Huijer, "Chronic pain: a review," *Journal Medical Libanais*, vol. 58, no. 1, pp. 21–27, 2010.

[2] M. C. Bushnell, M. Čeko, and L. A. Low, "Cognitive and emotional control of pain and its disruption in chronic pain," *Nature Reviews Neuroscience*, vol. 14, no. 7, pp. 502–511, 2013.

[3] R. H. Dworkin, A. B. O'Connor, J. Audette et al., "Recommendations for the pharmacological management of neuropathic pain: an overview and literature update," *Mayo Clinic Proceedings*, vol. 85, no. 3, supplement, pp. S3–S14, 2010.

[4] M. J. Keenan, R. J. Martin, A. M. Raggio et al., "High-amylose resistant starch increases hormones and improves structure and function of the gastrointestinal tract: a microarray study," *Journal of Nutrigenetics and Nutrigenomics*, vol. 5, no. 1, pp. 26–44, 2012.

[5] Y. Zhang, C. Wang, L. Wang et al., "A novel analgesic isolated from a traditional Chinese medicine," *Current Biology*, vol. 24, no. 2, pp. 117–123, 2014.

[6] Z.-F. Wang, L.-L. Tang, H. Yan, Y.-J. Wang, and X.-C. Tang, "Effects of huperzine A on memory deficits and neurotrophic factors production after transient cerebral ischemia and reperfusion in mice," *Pharmacology Biochemistry and Behavior*, vol. 83, no. 4, pp. 603–611, 2006.

[7] J. Zhou, H. Y. Zhang, and X. C. Tang, "Huperzine A attenuates cognitive deficits and hippocampal neuronal damage after transient global ischemia in gerbils," *Neuroscience Letters*, vol. 313, no. 3, pp. 137–140, 2001.

[8] J. Zhou and X. C. Tang, "Huperzine A attenuates apoptosis and mitochondria-dependent caspase-3 in rat cortical neurons," *FEBS Letters*, vol. 526, no. 1–3, pp. 21–25, 2002.

[9] L. S. Wang, J. Zhou, X. M. Shao, and X. C. Tang, "Huperzine A attenuates cognitive deficits and brain injury in neonatal rats after hypoxia–ischemia," *Brain Research*, vol. 949, no. 1-2, pp. 162–170, 2002.

[10] J. N. Crawley, "Designing mouse behavioral tasks relevant to autistic-like behaviors," *Mental Retardation and Developmental Disabilities Research Reviews*, vol. 10, no. 4, pp. 248–258, 2004.

[11] N. Galeotti, C. Ghelardini, L. D. C. Mannelli, and A. Bartolini, "Antinociceptive profile of the natural cholinesterase inhibitor huperzine A," *Drug Development Research*, vol. 54, no. 1, pp. 19–26, 2001.

[12] D. Yu, D. K. Thakor, I. Han et al., "Alleviation of chronic pain following rat spinal cord compression injury with multimodal

actions of huperzine A," *Proceedings of the National Academy of Sciences of the United States of America*, vol. 110, no. 8, pp. E746–E755, 2013.

[13] P. Park, S. Schachter, and T. Yaksh, "Intrathecal Huperzine A increases thermal escape latency and decreases flinching behavior in the formalin test in rats," *Neuroscience Letters*, vol. 470, no. 1, pp. 6–9, 2010.

[14] M.-M. Backonja and B. Stacey, "Neuropathic pain symptoms relative to overall pain rating," *Journal of Pain*, vol. 5, no. 9, pp. 491–497, 2004.

[15] A. Tappe-Theodor and R. Kuner, "Studying ongoing and spontaneous pain in rodents—challenges and opportunities," *European Journal of Neuroscience*, vol. 39, no. 11, pp. 1881–1890, 2014.

[16] G. J. Bennett, "What is spontaneous pain and who has it?" *Journal of Pain*, vol. 13, no. 10, pp. 921–929, 2012.

[17] T. King, L. Vera-Portocarrero, T. Gutierrez et al., "Unmasking the tonic-aversive state in neuropathic pain," *Nature Neuroscience*, vol. 12, no. 11, pp. 1364–1366, 2009.

[18] K. I. Vadakkan, Y. H. Jia, and M. Zhuo, "A behavioral model of neuropathic pain induced by ligation of the common peroneal nerve in mice," *The Journal of Pain*, vol. 6, no. 11, pp. 747–756, 2005.

[19] X.-Y. Li, H.-G. Ko, T. Chen et al., "Alleviating neuropathic pain hypersensitivity by inhibiting PKMζ in the anterior cingulate cortex," *Science*, vol. 330, no. 6009, pp. 1400–1404, 2010.

[20] S. R. Chaplan, F. W. Bach, J. W. Pogrel, J. M. Chung, and T. L. Yaksh, "Quantitative assessment of tactile allodynia in the rat paw," *Journal of Neuroscience Methods*, vol. 53, no. 1, pp. 55–63, 1994.

[21] C. Qu, T. King, A. Okun, J. Lai, H. L. Fields, and F. Porreca, "Lesion of the rostral anterior cingulate cortex eliminates the aversiveness of spontaneous neuropathic pain following partial or complete axotomy," *Pain*, vol. 152, no. 7, pp. 1641–1648, 2011.

[22] M. Leger, A. Quiedeville, V. Bouet et al., "Object recognition test in mice," *Nature Protocols*, vol. 8, no. 12, pp. 2531–2537, 2013.

[23] C. J. Woolf and M. W. Salter, "Neuronal plasticity: increasing the gain in pain," *Science*, vol. 288, no. 5472, pp. 1765–1768, 2000.

[24] X. Gao, C. Y. Zheng, L. Yang, X. C. Tang, and H. Y. Zhang, "Huperzine A protects isolated rat brain mitochondria against beta-amyloid peptide," *Free Radical Biology and Medicine*, vol. 46, no. 11, pp. 1454–1462, 2009.

[25] M. I. Papp, S. Komoly, I. G. Szirmai, and T. Kovács, "Similarities between CSF-brain extracellular transfer and neurofibrillary tangle invasion in Alzheimer's disease," *Neurobiology of Aging*, vol. 27, no. 3, pp. 402–412, 2006.

[26] G. B. Koelle, "Histochemical demonstration of reversible anticholinesterase action at selective cellular sites in vivo," *The Journal of Pharmacology and Experimental Therapeutics*, vol. 120, no. 4, pp. 488–503, 1957.

[27] J. S. Mogil, "Animal models of pain: progress and challenges," *Nature Reviews Neuroscience*, vol. 10, no. 4, pp. 283–294, 2009.

[28] E. Navratilova and F. Porreca, "Reward and motivation in pain and pain relief," *Nature Neuroscience*, vol. 17, no. 10, pp. 1304–1312, 2014.

[29] I. P. Kleggetveit and E. Jørum, "Large and small fiber dysfunction in peripheral nerve injuries with or without spontaneous pain," *The Journal of Pain*, vol. 11, no. 12, pp. 1305–1310, 2010.

[30] H. Gottrup, F. W. Bach, G. Juhl, and T. S. Jensen, "Differential effect of ketamine and lidocaine on spontaneous and mechanical evoked pain in patients with nerve injury pain," *Anesthesiology*, vol. 104, no. 3, pp. 527–536, 2006.

Hindawi Publishing Corporation
Neural Plasticity
Volume 2015, Article ID 249756, 9 pages
http://dx.doi.org/10.1155/2015/249756

Research Article

Upregulation of EMMPRIN (OX47) in Rat Dorsal Root Ganglion Contributes to the Development of Mechanical Allodynia after Nerve Injury

Qun Wang,[1] Yanyuan Sun,[1] Yingna Ren,[1] Yandong Gao,[2] Li Tian,[1] Yang Liu,[1] Yanan Pu,[1] Xingchun Gou,[3] Yanke Chen,[4] and Yan Lu[1]

[1]*Department of Anesthesiology and Pain Management, Xijing Hospital, Fourth Military Medical University, Xi'an 710032, China*
[2]*Department of Anesthesiology, Yulin First Hospital, Yulin 710021, China*
[3]*Institute of Basic Medical Science, Xi'an Medical University, Xi'an 710021, China*
[4]*Experiment Center of Biomedical Research, School of Medicine, Xi'an Jiaotong University, Xi'an 710061, China*

Correspondence should be addressed to Yanke Chen; yankechen@126.com and Yan Lu; yanlu20008@yahoo.com

Received 28 April 2015; Revised 24 June 2015; Accepted 28 June 2015

Academic Editor: Yun Guan

Matrix metalloproteinases (MMPs) are widely implicated in inflammation and tissue remodeling associated with various neurodegenerative diseases and play an important role in nociception and allodynia. Extracellular Matrix Metalloproteinase Inducer (EMMPRIN) plays a key regulatory role for MMP activities. However, the role of EMMPRIN in the development of neuropathic pain is not clear. Western blotting, real-time quantitative RT-PCR (qRT-PCR), and immunofluorescence were performed to determine the changes of messenger RNA and protein of EMMPRIN/OX47 and their cellular localization in the rat dorsal root ganglion (DRG) after nerve injury. Paw withdrawal threshold test was examined to evaluate the pain behavior in spinal nerve ligation (SNL) model. The lentivirus containing OX47 shRNA was injected into the DRG one day before SNL. The expression level of both mRNA and protein of OX47 was markedly upregulated in ipsilateral DRG after SNL. OX47 was mainly expressed in the extracellular matrix of DRG. Administration of shRNA targeted against OX47 in vivo remarkably attenuated mechanical allodynia induced by SNL. In conclusion, peripheral nerve injury induced upregulation of OX47 in the extracellular matrix of DRG. RNA interference against OX47 significantly suppressed the expression of OX47 mRNA and the development of mechanical allodynia. The altered expression of OX47 may contribute to the development of neuropathic pain after nerve injury.

1. Introduction

Neuropathic pain caused by a lesion or disease of the somatosensory system is refractory to routine analgesic measures [1, 2]. Following nerve injury, the sensory nervous system undergoes maladaptive changes that result in neuronal hyperexcitability [3–5]. The spinal dorsal horn is a relay station in which sensory information from dorsal root ganglia (DRG) is received, integrated, and relayed to several brain regions. Multiple alterations distributed widely across the peripheral and central nervous system contribute to the development of neuropathic pain. The peripheral nervous system is subject to damage, and the alterations are evident in the DRG. Despite the fact that intensive research activity is focused on the changes of ion channels, growth factors, cytokines, and glia cells in the DRG [5], the most inchoate alterations after nerve injury are not fully identified.

Matrix metalloproteinases (MMPs) are a family of zinc-dependent endopeptidases that play crucial roles in a wide range of proteolytic processes. More than 20 members of the family were reported, such as Collagenase-1 (MMP-1), Stromelysin-1 (MMP-3), Matrilysin (MMP-7), Gelatinase A (MMP-2), Gelatinase B (MMP-9), and MT1-MMP (MMP-14) [6, 7]. Earlier studies mainly shed light on the functions of MMPs in the physiological state. Recent studies suggested that MMPs are widely implicated in inflammation and tissue remodeling associated with various neurodegenerative diseases through the cleavage of the extracellular matrix

and enhancement of cytokines, chemokines, growth factors, cell surface receptors, and cell adhesion molecules [5, 6]. Meanwhile, they are also involved in supporting regeneration and vascular remodeling processes [7–9]. When the nervous system is injured, transcription and synthesis of MMPs in several cell types will increase to promote local repair, remyelination, regeneration, and even angiogenesis [10–13]. Moreover, recent studies demonstrated that MMPs also play crucial roles in nociception and hyperalgesia [10, 14], especially in the neuropathic pain and migraine [10, 15]. MMP-9 and MMP-2 were found to be involved in the development of neuropathic pain [16].

Extracellular Matrix Metalloproteinase Inducer (EMMPRIN) plays a key regulatory role in several MMPs activities [17–19]. CD147 (human), OX47 (rat), basigin, M6 antigen, neurothelin, HT7, and gp42 are different names for EMMPRIN in different species [17–20]. Numerous studies have shown that EMMPRIN display a remarkable repertoire of biological functions, including cell growth and migration, tissue regeneration, and cell differentiation and adhesion. Excessive expression of EMMPRIN was demonstrated to increase the invasiveness of tumor cells and play a role in the pathophysiology of various disease processes [21–24], such as atherosclerosis [25], acute myocardial infarction [26, 27], and transient [28] and permanent focal cerebral ischemia [29]. In vivo study showed that altered MMP expressions of tumor stromal fibroblasts were closely correlated with the expression level of CD147 [30–32]. Relevant studies manifested that fibroblasts transfected with restructuring CD147 adenovirus vector upregulated the expressions of MMP-1 and MMP-3 [33].

The role of EMMPRIN in the development of neuropathic pain induced by nerve injury is not clear. The present study examined the expression changes of OX47 in the DRG and spinal dorsal horn in neuropathic pain condition induced by peripheral nerve injury.

2. Materials and Methods

2.1. Animals. Male Sprague-Dawley rats (200–220 g), purchased from Animal Center of Fourth Military Medical University, were housed in groups of six under the constant temperature (25 ± 1)°C and 12 h light/dark cycle with free access to food and water. Behavioral tests were conducted by an observer blind to the behavioral analysis and drug treatments. All the operating procedures, in accordance with ethical guidelines, were approved by the Animal Care Committee.

2.2. Spinal Nerve Ligation (SNL) Model. All animals were deeply anesthetized with sodium pentobarbital (40 mg/kg) by intraperitoneal injection. Then the L5 spinal nerve ligation (SNL) surgery was conducted as previously described [34]. Briefly, the L5 spinal nerve was isolated through the removal of spinal transverse process. Subsequently, the L5 nerve was tightly ligated with 5-0 silk thread twice in 0.3 cm interval. Then, the incision was sutured layer by layer. After the surgery, all animals were transmitted to feeding room, where they were closely monitored to recover from the operation. Control surgery was subjected to the same procedure except for the ligation of L5 spinal nerve.

2.3. Behavioral Analysis. All behavioral tests were performed by a blinded observer. Rats were placed individually in cages (30 cm × 30 cm × 30 cm) with a wire mesh bottom (1 cm × 1 cm × 1 cm) and fully habituated three times prior to the assessment of paw withdrawal mechanical threshold (PWMT) with a frequency of one hour every day. One day before the SNL surgery, the baseline of PWMT was measured. One day after surgery, the PWMT was measured again to exclude the unsuccessful model (motor dysfunction or pain threshold value did not decrease obviously) followed by measurement at different postoperative days (1 d, 3 d, 7 d, 14 d, and 21 d). After acclimatization (30 min), mechanical nociceptive thresholds were determined by paw withdrawal to stimulation of the glabrous surface of the paw. Calibrated von Frey filaments (Stoelting, 1, 1.5, 2, 4, 6, 8.3, 11.1, 16.5, and 26 g) were applied with enough force to cause buckling of the filament. If rats appeared to shake the foot, lick foot, or show withdrawal behavior within 5 s, then it was defined as positive reaction. At the same force, the measurement was repeated 5 times at intervals of 5 minutes. Once more than sixty percent of measurement appeared as positive reaction, the minimal force was determined as the paw withdrawal mechanical threshold.

2.4. Western Blotting. Rats were transcardially perfused with 0.1 M PBS after deep anesthesia with sodium pentobarbital. The L5 DRGs and spinal cord segments were then rapidly removed, followed by being homogenized in a RIPA lysis buffer (Beyotime Inc., Nantong, China) containing a proteinase inhibitors phenylmethanesulfonyl fluoride (PMSF, 1 mM) (Beyotime Inc., Nantong, China). Protein concentrations were measured by the BCA Assay (Pierce Biotechnology) and 15 μg proteins were loaded, separated on a 12% SDS-PAGE, and transferred to polyvinylidene difluoride membranes (PVDF). The PVDF membranes were subsequently immunoblotted with the appropriate primary antibodies including mouse monoclonal antibody to OX47 (1 : 500, Santa Cruz Biotech, US) and anti-rat actin mouse monoclonal antibody (20 μg/mL, Chemicon International, Inc.). After being extensively washed, the membranes were incubated with a horseradish peroxidase-conjugated goat anti-mouse secondary antibody (Zhongshanqinqiao, Beijing, China). Signals were detected by an ECL kit (Pierce Biotechnology) according to the manufacturer's instructions.

2.5. Real-Time Quantitative RT-PCR (qRT-PCR). Total RNA were extracted from tissues by Trizol (Invitrogen, US). cDNA was synthesized by superscript first strand synthesis kit (Invitrogen, US) according to the manufacturer's standard protocol. Then, OX47 and glyceraldehyde-3-phosphate dehydrogenase (GAPDH) mRNA expression levels were measured by Mini-Opticon real-time PCR detection system (Bio-Rad, Hercules, CA, USA) in SYBR Green master mix (Takara, Otsu, Japan) according to a standard protocol. Finally, all data were analyzed by Opticon Monitor software (version 3.1; Bio-Rad). All primers were synthesized by the Shanghai

Sangon Biological Engineering Technology and Services Co. Ltd. (Shanghai, China). The sequences of PCR primers are listed:

OX47:

5′-GTTTGTGAAGCTGATCTGCAAG-3′

5′-ACAGCTCAGGCGTGGATATAAT-3′

GAPDH:

5′-GGCAAGTTCAATGGCACAGT-3′

5′-TGGTGAAGACGCCAGTAGACTC-3′

2.6. Immunofluorescence Chemistry. The rats were deeply anesthetized with sodium pentobarbital (40 mg/kg) and perfused through the ascending aorta with saline followed by 4% paraformaldehyde. The L5 spinal cord and dorsal root ganglion were postfixed with the same fixative for 2 h and then cryoprotected in a solution of 20% sucrose in 1% phosphate buffer (pH 7.4) overnight at room temperature. The serial coronal sections (40 μm) were cut by a cryostat microtome (CM1900, Leica, Germany). In double labeling experiments, all sections were blocked with 2% goat serum and incubated overnight at 4°C with mouse monoclonal antibody to OX47 (1 : 500, Santa Cruz Biotech, US), polyclonal rabbit anti-glial fibrillary acidic protein (1 : 1000, DAKO, US), anti-Collagen IV (1 : 1000, Sigma, US), and anti-Laminin (1 : 1000, Sigma, US). Subsequently, the slices were washed with 0.01% PBS three times and incubated with the respective Cy3-conjugated or FITC-conjugated (1 : 1000, Sigma, US) secondary antibody for 30 minutes in the dark at room temperature. Negative controls were conducted by omitting the primary antibodies during the immunostaining. After immunostaining, sections were mounted with 50% glycerol and covered with coverslips. Eventually, the sections were observed by using a laser scanning confocal microscope (Olympus FV1000, Tokyo, Japan). Images were adjusted by the FV10-ASW 3.1 Viewer software.

2.7. Construction of shRNA Lentiviral Vector. The lentiviral vector pMAGic 4.1 (SunBio Inc., Shanghai, China) was used to generate short hairpin RNA (shRNA) specific for rat EMMPRIN (OX-47). Four different regions of OX47 mRNA (gene ID NM 001109882) were selected as the RNAi target sites, namely, 394–412 bp, 756–774 bp, 900–918 bp, and 1206–1220 bp. Another pair of oligonucleotides (designated as shRNA-control) encoding a nonspecific shRNA, a negative control, was also synthesized. These oligonucleotides were annealed and subcloned into the Age I and EcoR I restriction endonuclease sites of pMAGic 4.1 lentiviral vector (SunBio, Shanghai, China), which included the green fluorescent protein (GFP) tag. All of the constructed vectors were confirmed by DNA sequencing.

HEK293 cells and MADB106 mammary adenocarcinoma cells were cultured in medium containing RPMI 1640 (Gibco, BRL Life Technologies, Karlsruhe, Germany) with 10% foetal bovine serum (FBS, Gibco) at 37°C under a mixture of 95% air and 5% CO2. HEK293 cells were cotransfected with these lentiviral vectors together with packaged plasmid pMD2.G (Addgene plasmid # 12259) and psPAX2 (Addgene plasmid # 12260) by Lipofectamine 2000 (Invitrogen, Carlsbad, CA, USA) according to the manufacturer's instructions. Forty-eight hours post transfection, harvested MADB106 cells were then infected with 1 mL of viral stock containing 5 μg/mL polybrene and enhanced infection solution (Eni.S) for 48 h. Then this medium was replaced by normal culture medium. The interference efficiency was verified by quantitative qRT-PCR. The shRNA oligonucleotides with maximum effect (75%) of silencing for OX47 were listed below:

5′-CCGGGGACACAGGCACTTATGAATTCA-AGAGATTCATAAGTGCCTGTGTCCTTTTTTg-3′

5′-AATTCAAAAAAGGACACAGGCACTTAT-GAATCTCTTGAATTCATAAGTGCCTGTGTCC-3′

2.8. Injection of Lentivirions. Lentivirions expressing either GFP or shRNA against OX47 were injected into DRG in vivo using a published method modified version [35]. Briefly, lentiviral preparations (1×10^9 transfection units per mL) were diluted with 20% mannitol in a ratio of 1 : 1 and injected unilaterally into L5 DRGs (6 μL per DRG, or 3×10^6 transfection units per DRG) in deeply anesthetized condition. At second day after viral infection, rats were subjected to SNL as described above. Mechanical hyperalgesia was measured by a von Frey monofilament. Rats were sacrificed on 7–22 days after SNL; then the L4-L5 DRGs were rapidly isolated and subjected to Western blot analysis for OX47 and β-actin.

2.9. Statistics. Student's t-test or analysis of variance (ANOVA) for random measures was performed followed by post hoc Fisher's test to determine statistically significant differences. Statistical significance was taken at $P < 0.05$. All data were presented as mean ± SEM.

3. Results

3.1. The Expression of OX47 Was Exclusively Upregulated in DRG after SNL. qRT-PCR and Western blot were used to assess the changes of OX47 expression in DRG and spinal cord after SNL. OX47 molecules include glycosylated (MW 56–72 kD) and nonglycosylated (MW 25 kD) forms. The expression level of both mRNA (Figure 1(a)) and protein (Figures 2(a) and 2(c)) of OX47 in the ipsilateral (SNL) L5 DRG was significantly increased compared to the contralateral side. Particularly, the nonglycosylated OX47 with 25 kD was exceptionally enhanced. The increased expression of mRNA and protein occurred from the first day after SNL, reached the peak at the fourteenth day, and was maintained at a relatively stable level for at least 21 days (Figures 1(a) and 2(c)). However, the expression level of both mRNA (Figure 1(b)) and protein (Figure 2(b)) of OX47 in the spinal dorsal horn showed no significant difference between the ipsilateral and contralateral sides. In line with the mRNA expression, only the glycosylated rather than nonglycosylated OX47 was detected with low level expression in Western

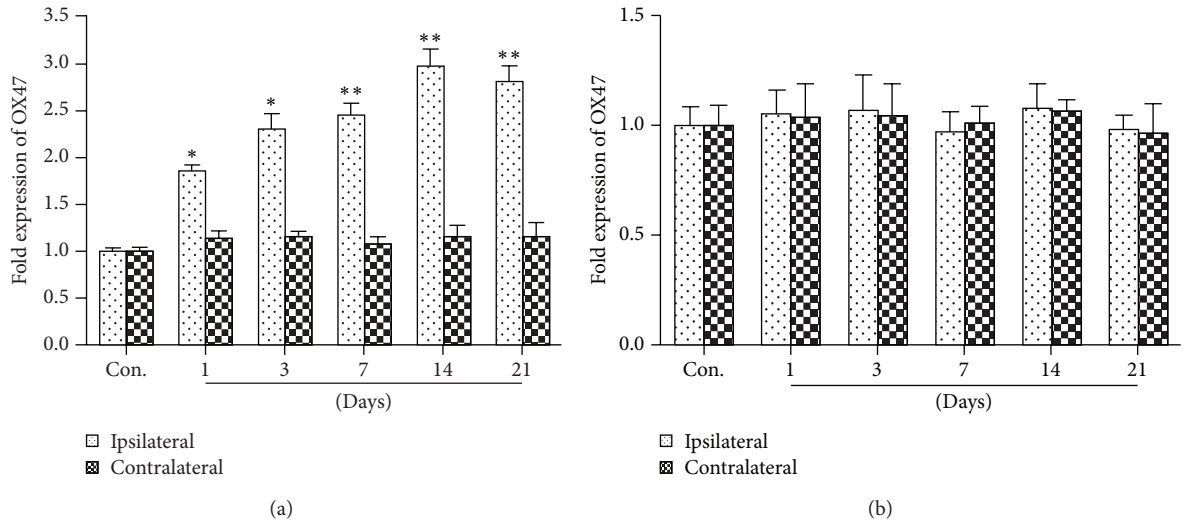

Figure 1: Upregulation of OX47 mRNA in the DRG after spinal nerve ligation (SNL). (a) The expression level of OX47 mRNA in DRGs of control and SNL group. mRNA levels were determined by real-time quantitative RT-PCR (qRT-PCR). Nerve injury induced a significant upregulation of OX47 mRNA expression at ipsilateral DRG. $n = 8$ per group. $^{*}P < 0.05$, $^{**}P < 0.01$. (b) The expression level of OX47 mRNA in spinal cord of control and SNL group. There are no significant differences between the ipsilateral and contralateral spinal cord. $n = 8$ per group. $P > 0.05$.

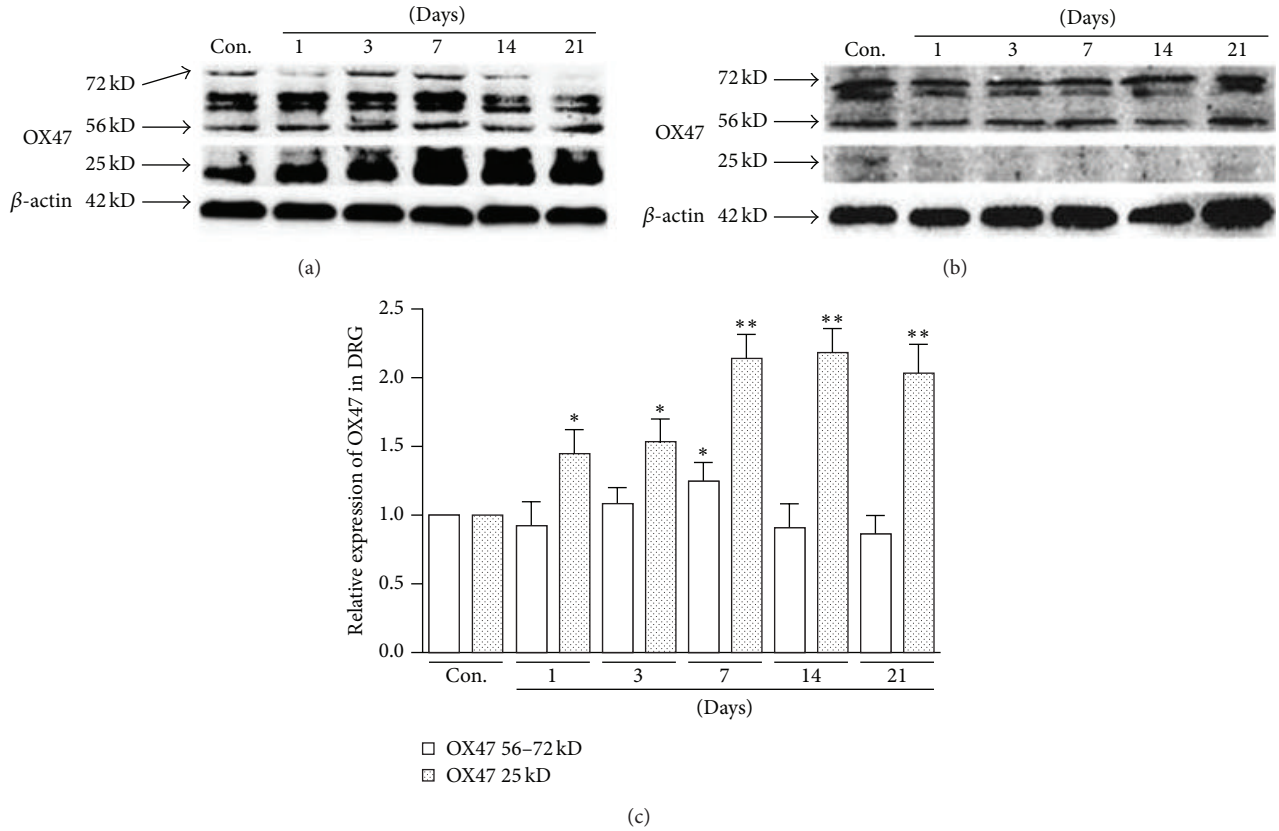

Figure 2: Upregulation of OX47 protein in the DRG after spinal nerve ligation (SNL). (a) The expression level of OX47 protein in DRGs of control and SNL group. Protein levels were determined by Western blotting. Note that the nonglycosylated OX47 (25 kd) protein expression was increased from the first day after SNL. (b) The expression level of OX47 protein in spinal cord of control and SNL group. Note that only glycosylated protein was detected with low level. (c) Statistical data indicated that the increased expression of OX47 protein in DRG occurred from the first day after SNL, reached the peak at the fourteenth day, and was maintained at a relatively stable level for at least 21 days. $n = 6$ per group. $^{*}P < 0.05$, $^{**}P < 0.01$.

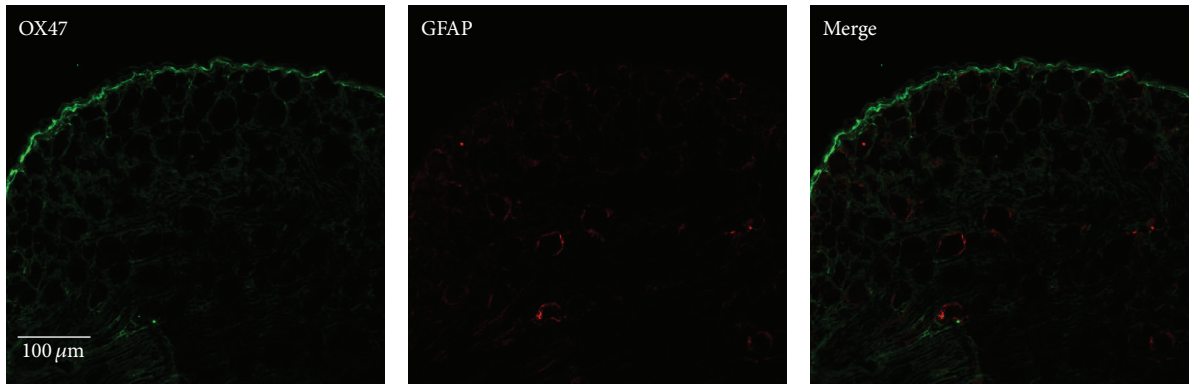

Figure 3: Double-labeled immunostaining of OX47 with GFAP in naïve DRG. Representative confocal microscopy shows the immunoreactivity (green) for OX47 and GFAP (red).

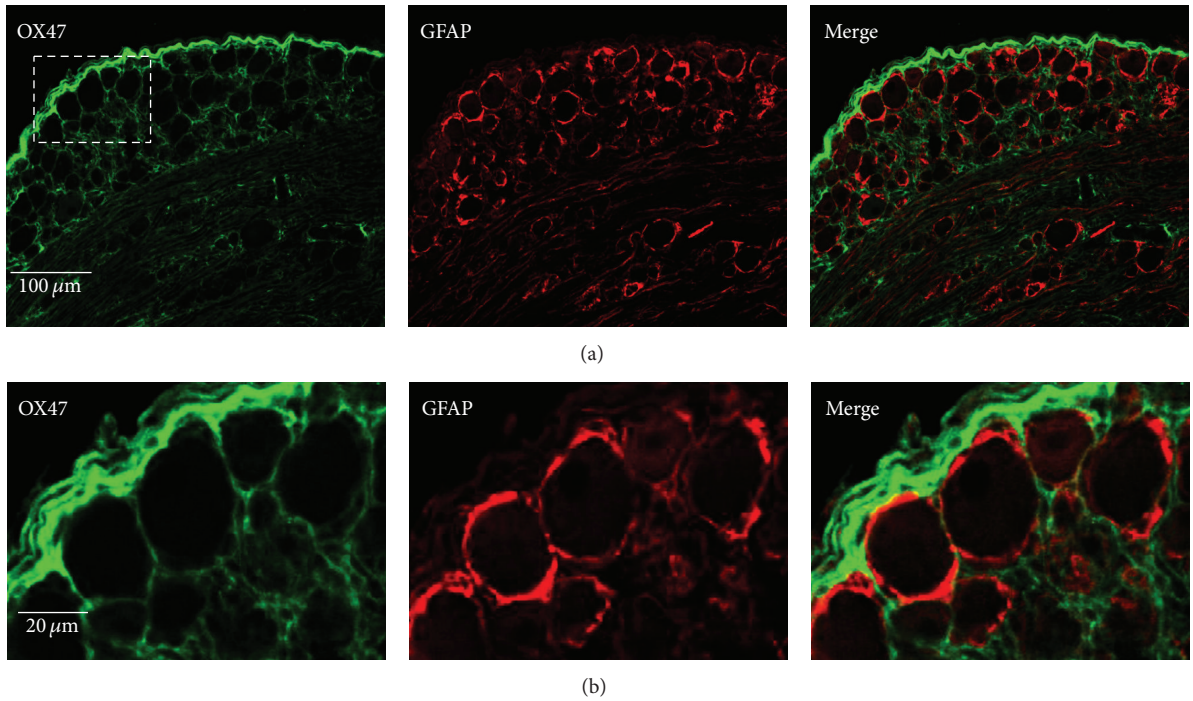

Figure 4: Double-labeled immunostaining of OX47 with GFAP in DRG 3 days after SNL. (a) Representative confocal microscopy shows that OX47 immunoreactivity was mainly detected in the extracellular matrix around DRG neurons and partially overlapped with flattened SGCs positive for GFAP. (b) Higher magnification of selected area in (a).

blotting (Figure 2(b)). Taken together, these data indicated that peripheral nerve injury significantly augmented the expression of EMMPRIN in spinal DRG.

3.2. OX47 Was Mainly Expressed in the Extracellular Matrix of DRG. To further characterize the cellular localization of OX47 in DRG, we carried out double-labeled immunostaining of OX47 with glial fibrillary acidic protein (GFAP), a marker of astrocyte (satellite glial cell in DRG). In the naïve rat, both OX47 and GFAP were expressed at a low level (Figure 3). Three days after SNL, the activated satellite glial cells (SGCs) encircled and surrounded large-, medium-, and small-sized DRG neurons (Figure 4). OX47 immunoreactivity was mainly detected in the extracellular matrix around DRG neurons and partially overlapped with flattened SGCs positive for GFAP (Figure 4). Clearly, OX47 immunoreactivity was not colocalized with DRG neurons.

Collagen IV and Laminin are major components of the extracellular matrix. We next performed double labeling of OX47 with Collagen IV and Laminin. Indeed, OX47 immunoreactivity was overlapped with Collagen IV in DRG's capsule and extracellular matrix (Figure 5(a)), while the Laminin immunoreactivity was mainly colocalized with OX47 in DRG's capsule (Figure 5(b)). Overall, the colocalization with Collagen IV, SGCs, and Laminin suggested that

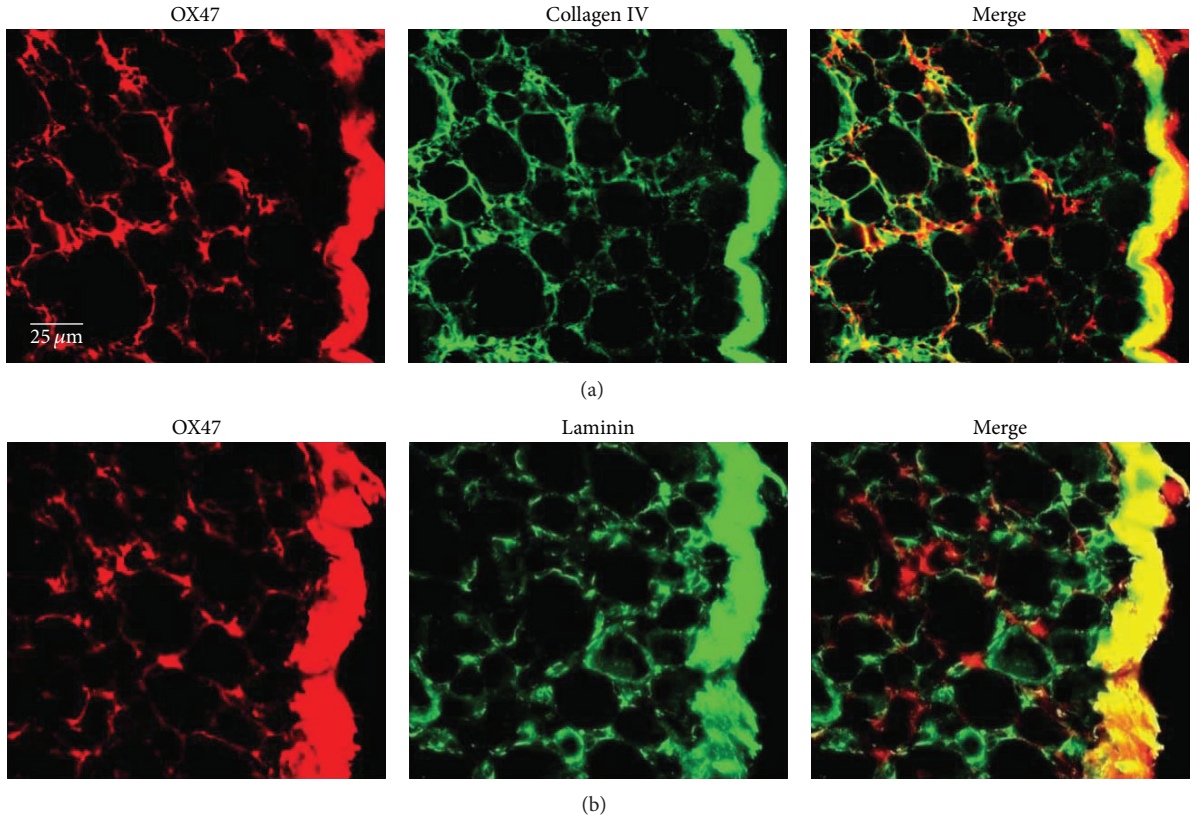

Figure 5: Double-labeled immunostaining of OX47 with Collagen IV and Laminin in DRG. (a) OX47 positive labeling was colocalized with Collagen IV in DRG's capsule and extracellular matrix. (b) OX47 was mainly colocalized with Laminin in DRG's capsule.

OX47 was mainly expressed in the extracellular matrix of DRG.

3.3. Pretreatment with OX47 shRNA Markedly Attenuated the Development of Mechanical Allodynia. To further shed light on the functional role of OX47 in neuropathic pain condition, we constructed a shRNA lentiviral vector and completed packaging the lentivirus. Seven days after injection of the shRNA into DRG, the expression of OX47 mRNA in the DRG was significantly suppressed (Figure 6(a)). In contrast to the OX47 shRNA, the control RNA did not significantly alter the OX47 mRNA expression. We next assessed the effect of OX47 shRNA in the SNL model. Pretreatment of OX47 shRNA significantly increased the paw withdrawal threshold as compared with control RNA-treated animals and thus attenuated the mechanical allodynia as expected (Figure 6(b)). These data indicated that pretreatment with OX47 shRNA markedly attenuated the development of mechanical allodynia after nerve injury.

4. Discussion

The present study provided evidence that upregulation of EMMPRIN in the dorsal root ganglion was involved in the development of mechanical allodynia after nerve injury. Firstly, the expression of EMMPRIN mRNA and protein was apparently increased in DRG after SNL, which is consistent with the notion that DRG neurons undergo significant plastic changes in neuropathic pain conditions [36]. Secondly, EMMPRIN was colocalized with Collagen IV, Laminin-1, and SGCs, indicating that EMMPRIN was mainly expressed in the extracellular matrix of DRG. DRG neurons were surrounded by the flattened SGCs and basal laminae of the extracellular matrix [37, 38]. The basal lamina consists of various types of molecules including type IV Collagen, Laminins, entactin/nidogen, and heparan sulfate proteoglycans [39–41]. SGCs are linked to each other by adherent gap junctions [37] and contain several ion channels, receptors, and adhesion molecules [38]. Following peripheral nerve injury, SGCs underwent changes in cell number, structure, and function [38, 42–45]. Several reports demonstrated that GFAP expression was upregulated in SGCs after SNL [46–48]. The MMP-2 was also upregulated in SGCs after SNL [16]. The upregulation of EMMPRIN in extracellular matrix suggested that nerve injury induced significant changes of molecular content in extracellular matrix surrounding the neuron-SGC units. Finally, administration of the EMMPRIN shRNA significantly suppressed mechanical allodynia induced by spinal nerve injury.

It was well accepted that the "Neuron-Glia-Neuron" positive feedback loop leads to the generation and maintenance of neuropathic pain. After nerve injury, proinflammatory cytokines such as IL-6, IL-1β, and TNF-α were released from activated glial cells in DRG, whereby these factors led to

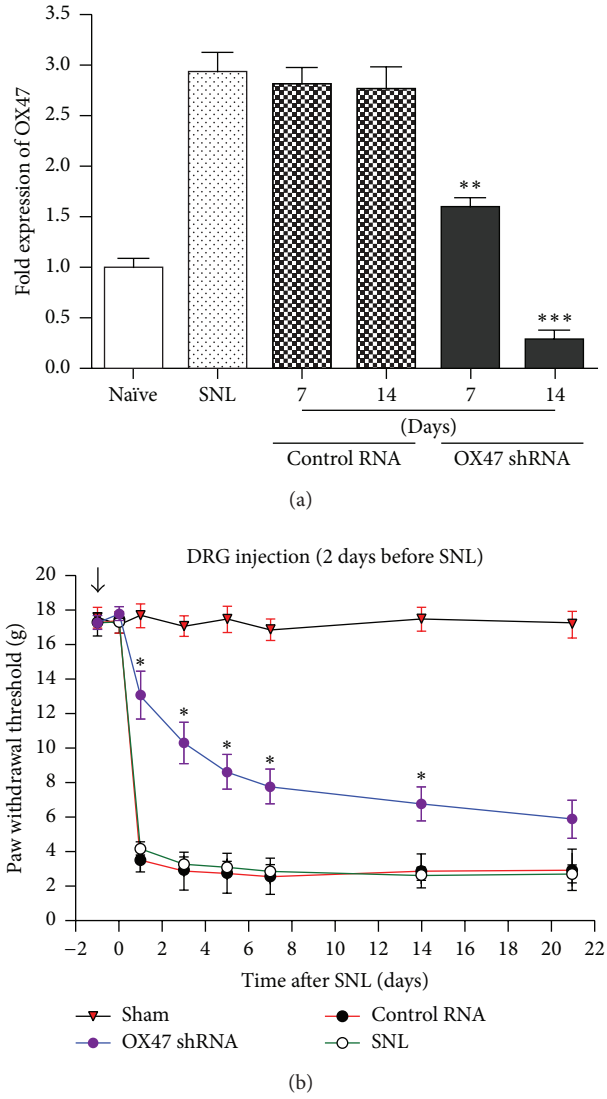

Figure 6: DRG injection of OX47 shRNA markedly attenuated the development of mechanical allodynia. (a) OX47 mRNA expression in DRG of control RNA and OX47 shRNA group. Data show that OX47 shRNA obviously decreased the mRNA expression in the 7 d and 14 d after SNL. $n = 5$ per group. $^{**}P < 0.01$, $^{***}P < 0.001$. (b) Increased paw withdrawal threshold after OX47 shRNA injection. Note that mechanical allodynia was remarkably attenuated in rats infected with lentivirus containing shRNA of OX47. $n = 7$ per time point. $^{*}P < 0.05$ compared to nonsilencing control shRNA (nonspecific scrambled shRNA).

peripheral sensitization by enhancing excitability of DRG neurons [16, 49–53]. The present study suggested that the extracellular matrix may be also involved in the development of neuropathic pain; that is, the formation of "Extracellular Matrix-Glia-Neuron" interactive network may be involved in the development of neuropathic pain. EMMPRIN, the crucial component of extracellular matrix within DRG, may potentially become a novel target for the treatment of neuropathic pain. Inhibition of EMMPRIN may provide a hopeful therapeutic approach for curing neuropathic pain.

In conclusion, peripheral nerve injury induced upregulation of OX47 in the extracellular matrix of DRG. RNA interference against OX47 significantly suppressed the expression of OX47 mRNA and the development of mechanical allodynia. The altered expression of OX47 may contribute to the development of neuropathic pain after nerve injury. Further research is needed to explore which signal pathway EMMPRIN mainly affects during the development of neuropathic pain.

Conflict of Interests

The authors declare that there is no conflict of interests regarding the publication of this paper.

Authors' Contribution

Qun Wang, Yanyuan Sun, and Yingna Ren contributed equally to this work.

Acknowledgment

This work was supported by the National Natural Science Foundation of China (81471139 and 81020108020 to Yan Lu; 81101744 to Yanke Chen; 81471140 to Yanyuan Sun).

References

[1] R.-D. Treede, T. S. Jensen, J. N. Campbell et al., "Neuropathic pain: redefinition and a grading system for clinical and research purposes," *Neurology*, vol. 70, no. 18, pp. 1630–1635, 2008.

[2] M. Haanpää, N. Attal, M. Backonja et al., "NeuPSIG guidelines on neuropathic pain assessment," *Pain*, vol. 152, no. 1, pp. 14–27, 2011.

[3] A. I. Basbaum, D. M. Bautista, G. Scherrer, and D. Julius, "Cellular and molecular mechanisms of pain," *Cell*, vol. 139, no. 2, pp. 267–284, 2009.

[4] S. A. Prescott, Q. Ma, and Y. De Koninck, "Normal and abnormal coding of somatosensory stimuli causing pain," *Nature Neuroscience*, vol. 17, no. 2, pp. 183–191, 2014.

[5] M. Costigan, J. Scholz, and C. J. Woolf, "Neuropathic pain: a maladaptive response of the nervous system to damage," *Annual Review of Neuroscience*, vol. 32, pp. 1–32, 2009.

[6] A. Page-McCaw, A. J. Ewald, and Z. Werb, "Matrix metalloproteinases and the regulation of tissue remodelling," *Nature Reviews Molecular Cell Biology*, vol. 8, no. 3, pp. 221–233, 2007.

[7] W. C. Parks, C. L. Wilson, and Y. S. López-Boado, "Matrix metalloproteinases as modulators of inflammation and innate immunity," *Nature Reviews Immunology*, vol. 4, no. 8, pp. 617–629, 2004.

[8] G. A. Rosenberg, "Matrix metalloproteinases in neuroinflammation," *Glia*, vol. 39, no. 3, pp. 279–291, 2002.

[9] X. Wang, J. Jung, M. Asahi et al., "Effects of matrix metalloproteinase-9 gene knock-out on morphological and motor outcomes after traumatic brain injury," *Journal of Neuroscience*, vol. 20, no. 18, pp. 7037–7042, 2000.

[10] S. E. Lakhan and M. Avramut, "Matrix metalloproteinases in neuropathic pain and migraine: friends, enemies, and therapeutic targets," *Pain Research and Treatment*, vol. 2012, Article ID 952906, 10 pages, 2012.

[11] V. W. Yong, C. A. Krekoski, P. A. Forsyth, R. Bell, and D. R. Edwards, "Matrix and diseases of the CNS," *Trends in Neurosciences*, vol. 21, no. 2, pp. 75–80, 1998.

[12] B.-Q. Zhao, E. Tejima, and E. H. Lo, "Neurovascular proteases in brain injury, hemorrhage and remodeling after stroke," *Stroke*, vol. 38, no. 2, pp. 748–752, 2007.

[13] B.-Q. Zhao, S. Wang, H.-Y. Kim et al., "Role of matrix metalloproteinases in delayed cortical responses after stroke," *Nature Medicine*, vol. 12, no. 4, pp. 441–445, 2006.

[14] M. M. Ahmed, K. C. King, S. M. Pearce, M. A. Ramsey, G. S. Miranpuri, and D. K. Resnick, "Novel targets for Spinal Cord Injury related neuropathic pain," *Annals of Neurosciences*, vol. 18, no. 4, pp. 162–167, 2011.

[15] R.-R. Ji, Z.-Z. Xu, X. Wang, and E. H. Lo, "Matrix metalloprotease regulation of neuropathic pain," *Trends in Pharmacological Sciences*, vol. 30, no. 7, pp. 336–340, 2009.

[16] Y. Kawasaki, Z.-Z. Xu, X. Wang et al., "Distinct roles of matrix metalloproteases in the early- and late-phase development of neuropathic pain," *Nature Medicine*, vol. 14, no. 3, pp. 331–336, 2008.

[17] J. Sun and M. E. Hemler, "Regulation of MMP-1 and MMP-2 production through CD147/extracellular matrix metalloproteinase inducer interactions," *Cancer Research*, vol. 61, no. 5, pp. 2276–2281, 2001.

[18] S. Caudroy, M. Polette, B. Nawrocki-Raby et al., "EMMPRIN-mediated MMP regulation in tumor and endothelial cells," *Clinical and Experimental Metastasis*, vol. 19, no. 8, pp. 697–702, 2002.

[19] K. Nabeshima, H. Iwasaki, K. Koga, H. Hojo, J. Suzumiya, and M. Kikuchi, "Emmprin (basigin/CD147): matrix metalloproteinase modulator and multifunctional cell recognition molecule that plays a critical role in cancer progression," *Pathology International*, vol. 56, no. 7, pp. 359–367, 2006.

[20] H. Seulberger, C. M. Unger, and W. Risau, "HT7, Neurothelin, Basigin, gp42 and OX-47—many names for one developmentally regulated immuno-globulin-like surface glycoprotein on blood-brain barrier endothelium, epithelial tissue barriers and neurons," *Neuroscience Letters*, vol. 140, no. 1, pp. 93–97, 1992.

[21] T. Kanekura, X. Chen, and T. Kanzaki, "Basigin (CD147) is expressed on melanoma cells and induces tumor cell invasion by stimulating production of matrix metalloproteinases by fibroblasts," *International Journal of Cancer*, vol. 99, no. 4, pp. 520–528, 2002.

[22] T. Muramatsu and T. Miyauchi, "Basigin (CD147): a multifunctional transmembrane protein involved in reproduction, neural function, inflammation and tumor invasion," *Histology and Histopathology*, vol. 18, no. 3, pp. 981–987, 2003.

[23] P. Zhu, N. Lu, Z.-G. Shi et al., "CD147 overexpression on synoviocytes in rheumatoid arthritis enhances matrix metalloproteinase production and invasiveness of synoviocytes," *Arthritis Research and Therapy*, vol. 8, no. 2, article R44, 2006.

[24] P. Zhu, J. Ding, J. Zhou, W.-J. Dong, C.-M. Fan, and Z.-N. Chen, "Expression of CD147 on monocytes/macrophages in rheumatoid arthritis: its potential role in monocyte accumulation and matrix metalloproteinase production," *Arthritis Research & Therapy*, vol. 7, no. 5, pp. R1023–1033, 2005.

[25] E. Y. Choi, D. Kim, B. K. Hong et al., "Upregulation of extracellular matrix metalloproteinase inducer (EMMPRIN) and gelatinases in human atherosclerosis infected with *Chlamydia pneumoniae*: the potential role of *Chlamydia pneumoniae* infection in the progression of atherosclerosis," *Experimental and Molecular Medicine*, vol. 34, no. 6, pp. 391–400, 2002.

[26] R. Nie, S. Xie, B. Du, X. Liu, B. Deng, and J. Wang, "Extracellular matrix metalloproteinase inducer (EMMPRIN) is increased in human left ventricle after acute myocardial infarction," *Archives of Medical Research*, vol. 40, no. 7, pp. 605–611, 2009.

[27] N. G. Kounis, G. N. Kounis, G. Almpanis, A. Mazarakis, and C. Koutsojannis, "Extracellular matrix metalloproteinase inducer (EMMPRIN), acute myocardial infarction and the Kounis syndrome," *Archives of Medical Research*, vol. 41, no. 2, pp. 149–150, 2010.

[28] D. Burggraf, M. Liebetrau, H. K. Martens et al., "Matrix metalloproteinase induction by EMMPRIN in experimental focal cerebral ischemia," *European Journal of Neuroscience*, vol. 22, no. 1, pp. 273–277, 2005.

[29] W. Zhu, S. Khachi, Q. Hao et al., "Upregulation of EMMPRIN after permanent focal cerebral ischemia," *Neurochemistry International*, vol. 52, no. 6, pp. 1086–1091, 2008.

[30] S. Caudroy, M. Polette, J.-M. Tournier et al., "Expression of the extracellular matrix metalloproteinase inducer (EMMPRIN) and the matrix metalloproteinase-2 in bronchopulmonary and breast lesions," *Journal of Histochemistry and Cytochemistry*, vol. 47, no. 12, pp. 1575–1580, 1999.

[31] K. Dalberg, E. Eriksson, U. Enberg, M. Kjellman, and M. Bäckdahl, "Gelatinase A, membrane type 1 matrix metalloproteinase, and extracellular matrix metalloproteinase inducer mRNA expression: correlation with invasive growth of breast cancer," *World Journal of Surgery*, vol. 24, no. 3, pp. 334–340, 2000.

[32] C. Thorns, A. C. Feller, and H. Merz, "EMMPRIN (CD 174) is expressed in Hodgkin's lymphoma and anaplastic large cell lymphoma. An immunohistochemical study of 60 cases," *Anticancer Research*, vol. 22, no. 4, pp. 1983–1986, 2002.

[33] R. Li, L. Huang, H. Guo, and B. P. Toole, "Basigin (murine EMMPRIN) stimulates matrix metalloproteinase production by fibroblasts," *Journal of Cellular Physiology*, vol. 186, no. 3, pp. 371–379, 2001.

[34] S. H. Kim and J. M. Chung, "An experimental model for peripheral neuropathy produced by segmental spinal nerve ligation in the rat," *Pain*, vol. 50, no. 3, pp. 355–363, 1992.

[35] M. Glatzel, E. Flechsig, B. Navarro et al., "Adenoviral and adeno-associated viral transfer of genes to the peripheral nervous system," *Proceedings of the National Academy of Sciences of the United States of America*, vol. 97, no. 1, pp. 442–447, 2000.

[36] A. J. Man, J. K. Leach, and P. Bannerman, "Redirection of neurite outgrowth by coupling chondroitin sulfate proteoglycans to polymer membranes," *Annals of Biomedical Engineering*, vol. 42, no. 6, pp. 1271–1281, 2014.

[37] E. Pannese, "The satellite cells of the sensory ganglia," *Advances in Anatomy, Embryology, and Cell Biology*, vol. 65, pp. 1–111, 1981.

[38] M. Hanani, "Satellite glial cells in sensory ganglia: from form to function," *Brain Research Reviews*, vol. 48, no. 3, pp. 457–476, 2005.

[39] R. Timpl, "Macromolecular organization of basement membranes," *Current Opinion in Cell Biology*, vol. 8, no. 5, pp. 618–624, 1996.

[40] A. C. Erickson and J. R. Couchman, "Still more complexity in mammalian basement membranes," *Journal of Histochemistry and Cytochemistry*, vol. 48, no. 10, pp. 1291–1306, 2000.

[41] P. Dubový, R. Jančálek, and I. Klusáková, "A heterogeneous immunofluorescence staining for laminin-1 and related basal lamina molecules in the dorsal root ganglia following constriction nerve injury," *Histochemistry and Cell Biology*, vol. 125, no. 6, pp. 671–680, 2006.

[42] P. S. Cherkas, T.-Y. Huang, T. Pannicke, M. Tal, A. Reichenbach, and M. Hanani, "The effects of axotomy on neurons and satellite glial cells in mouse trigeminal ganglion," *Pain*, vol. 110, no. 1-2, pp. 290–298, 2004.

[43] T. Y. Huang, M. Hanani, M. Ledda, S. De Palo, and E. Pannese, "Aging is associated with an increase in dye coupling and in gap junction number in satellite glial cells of murine dorsal root ganglia," *Neuroscience*, vol. 137, no. 4, pp. 1185–1192, 2006.

[44] T.-Y. Huang and M. Hanani, "Morphological and electrophysiological changes in mouse dorsal root ganglia after partial colonic obstruction," *The American Journal of Physiology—Gastrointestinal and Liver Physiology*, vol. 289, no. 4, pp. G670–G678, 2005.

[45] P. T. Ohara, J.-P. Vit, A. Bhargava et al., "Gliopathic pain: when satellite glial cells go bad," *Neuroscientist*, vol. 15, no. 5, pp. 450–463, 2009.

[46] F.-Y. Liu, Y.-N. Sun, F.-T. Wang et al., "Activation of satellite glial cells in lumbar dorsal root ganglia contributes to neuropathic pain after spinal nerve ligation," *Brain Research*, vol. 1427, pp. 65–77, 2012.

[47] W. Xie, J. A. Strong, and J.-M. Zhang, "Early blockade of injured primary sensory afferents reduces glial cell activation in two rat neuropathic pain models," *Neuroscience*, vol. 160, no. 4, pp. 847–857, 2009.

[48] M. Takeda, T. Tanimoto, J. Kadoi et al., "Enhanced excitability of nociceptive trigeminal ganglion neurons by satellite glial cytokine following peripheral inflammation," *Pain*, vol. 129, no. 1-2, pp. 155–166, 2007.

[49] M. Schäfers, D. H. Lee, D. Brors, T. L. Yaksh, and L. S. Sorkin, "Increased sensitivity of injured and adjacent uninjured rat primary sensory neurons to exogenous tumor necrosis factor-alpha after spinal nerve ligation," *Journal of Neuroscience*, vol. 23, no. 7, pp. 3028–3038, 2003.

[50] C. Sommer and M. Kress, "Recent findings on how proinflammatory cytokines cause pain: peripheral mechanisms in inflammatory and neuropathic hyperalgesia," *Neuroscience Letters*, vol. 361, no. 1–3, pp. 184–187, 2004.

[51] E. D. Milligan and L. R. Watkins, "Pathological and protective roles of glia in chronic pain," *Nature Reviews Neuroscience*, vol. 10, no. 1, pp. 23–36, 2009.

[52] J. Scholz and C. J. Woolf, "The neuropathic pain triad: neurons, immune cells and glia," *Nature Neuroscience*, vol. 10, no. 11, pp. 1361–1368, 2007.

[53] L. R. Watkins, E. D. Milligan, and S. F. Maier, "Glial activation: a driving force for pathological pain," *Trends in Neurosciences*, vol. 24, no. 8, pp. 450–455, 2001.

Hindawi Publishing Corporation
Neural Plasticity
Volume 2015, Article ID 752782, 14 pages
http://dx.doi.org/10.1155/2015/752782

Research Article

A Novel Nitronyl Nitroxide with Salicylic Acid Framework Attenuates Pain Hypersensitivity and Ectopic Neuronal Discharges in Radicular Low Back Pain

Wen-Juan Han,[1] Lei Chen,[2] Hai-Bo Wang,[3] Xiang-Zeng Liu,[4] San-Jue Hu,[1] Xiao-Li Sun,[2] and Ceng Luo[1]

[1]*Institute of Neuroscience, Fourth Military Medical University, Xi'an 710032, China*
[2]*Department of Pharmacy, Xijing Hospital, Fourth Military Medical University, Xi'an 710032, China*
[3]*School of Pharmacy, Fourth Military Medical University, Xi'an 710032, China*
[4]*Class 2013, School of Clinical Medicine, Fourth Military Medical University, Xi'an 710032, China*

Correspondence should be addressed to Xiao-Li Sun; xiaolis@fmmu.edu.cn and Ceng Luo; luoceng@fmmu.edu.cn

Received 22 December 2014; Revised 31 March 2015; Accepted 7 April 2015

Academic Editor: Yun Guan

Evidence has accumulated that reactive oxygen species and inflammation play crucial roles in the development of chronic pain, including radicular low back pain. Nonsteroid anti-inflammatory drugs (NSAIDs), for example, salicylic acid, aspirin, provided analgesic effects in various types of pain. However, long-term use of these drugs causes unwanted side effects, which limits their implication. Stable nitronyl (NIT) nitroxide radicals have been extensively studied as a unique and interesting class of new antioxidants for protection against oxidative damage. The present study synthesized a novel NIT nitroxide radical with salicylic acid framework (SANR) to provide synergistic effect of both antioxidation and antiinflammation. We demonstrated for the first time that both acute and repeated SANR treatment exerted dramatic analgesic effect in radicular low back pain mimicked by chronic compression of dorsal root ganglion in rats. This analgesic potency was more potent than that produced by classical NSAIDs aspirin and traditional nitroxide radical Tempol alone. Furthermore, SANR-induced behavioral analgesia is found to be mediated, at least in partial, by a reduction of ectopic spontaneous discharges in injured DRG neurons. Therefore, the synthesized NIT nitroxide radical coupling with salicylic acid framework may represent a novel potential therapeutic candidate for treatment of chronic pain, including radicular low back pain.

1. Introduction

Radicular low back pain represents a frequent and poorly understood medical problem. It is a major cause of disability and higher health care costs in the world. This clinical condition often results from vertebral injuries, intervertebral disc herniation, intervertebral foramen stenosis, or other disorders affecting the dorsal root ganglion (DRG) or its near nerve root. So far, to reveal the underlying mechanism of radicular low back pain, a number of preclinical models have been developed that attempt to mimic the above known causes of low back pain [1, 2]. Amongst those, chronic compression of the dorsal root ganglion (CCD) model in rodents displayed dramatic pain hypersensitivity such as mechanical hypersensitivity (hyperalgesia and allodynia) and thermal hyperalgesia that mimic the pain symptom observed in low back pain patients [1–6]. Although epidural steroid injection and surgical intervention have been used both clinically and experimentally in many cases, radicular low back pain remains a common chronic pain condition that is sometimes refractory to current treatment modalities [7, 8]. Therefore, development of new therapeutics is helpful and in urgent need towards the treatment of radicular low back pain.

Much evidence has accumulated that reactive oxygen species (ROS) play an important role in the development of chronic pain [9, 10]. Various ROS scavengers and antioxidants provided analgesic effects in animal models of inflammatory and neuropathic pain [9, 11–15]. In recent years, nitroxide

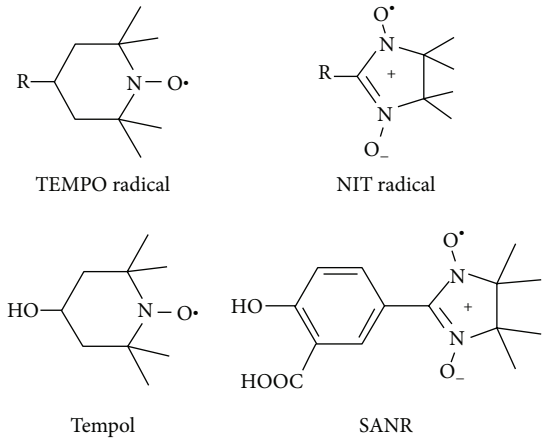

Figure 1: Structure of SANR and other nitroxide radicals. Structure of TEMPO, α-nitronyl (NIT) group radicals, Tempol, and SANR.

radicals have been extensively studied as a unique and interesting class of antioxidants to protect against ionizing radiation [16], ischemia/reperfusion injury [17], neurodegenerative diseases [18, 19], and chronic pain [9, 11–14]. Some nitroxide radicals, for example, amifostine, are being used in clinical practice [20]. Unlike other antioxidants that act in a sacrificial mode, nitroxide radicals act as self-replenishing antioxidants in a catalytic manner. The TEMPO and α-nitronyl (NIT) groups are the two major kinds of nitroxide radicals (Figure 1). Tempol (4-hydroxy-2,2,6,6-tetramethylpiper-idine-N-oxyl), a kind of TEMPO, is found to alleviate pain in various experimental pain models [12–15, 21]. Compared with Tempol, NIT group nitroxide radicals have an extensive distribution of unpaired spin density. As such, much attention has been levied towards the development of this kind of new NIT nitroxyl radicals. However, whether NIT group NRs possess antinociceptive action has remained elusive.

In addition to reactive oxygen species, inflammatory processes are thought to play key roles in radicular low back pain (please see Strong et al. [1] for review). Attenuation of pain behaviors by nonsteroidal anti-inflammatory drugs (NSAIDs) has been demonstrated in various rodent back pain models [22–26]. However, long-term use of NSAIDs causes unwanted gastrointestinal and cardiovascular side effects, which limits its broader applications. Herein, we have for the first time synthesized a novel NIT nitroxide radical with salicylic acid framework (SANR) exerting the beneficial effects of both the NSAIDs and the antioxidants (Figure 1). We demonstrated that both acute and long-term systemic administration of SANR attenuated the mechanical hypersensitivity and thermal hyperalgesia observed in an experimental model of CCD rats. Furthermore, SANR provided more pain relief than either traditional nitroxide compound Tempol or NSAIDs aspirin alone.

Evidence has accumulated that abnormal spontaneous discharges of primary afferent sensory neurons may contribute to radicular low back pain [3, 4]. We therefore investigated whether SANR produced analgesia by inhibition of spontaneous discharges of primary afferent sensory neurons in CCD rats. Our results revealed that SANR produced a marked depression of spontaneous discharges of primary afferent A fibers in CCD rats in a dose-dependent manner. When compared to the same concentration of Tempol or aspirin, SANR exhibited a much stronger analgesic effect. Taken together, these findings clearly suggest that synthesis of new NIT nitroxyl radical with salicylic acid framework may represent a potential new candidate for the treatment of radicular low back pain.

2. Materials and Methods

2.1. Synthesis of SANR. 2,3-Bis(hydroxyl amino)-2,3-dimethylbutane was prepared by the published method. All other chemical reagents were purchased from the Beijing OuHe Chemical Limited Company (Beijing, China). The other chemical reagents were used without further purification. High resolution mass spectroscopy (HRMS) was carried out on a Varian 7.0T ESI-FTICR-MS (Varian, USA). Elemental analyses were carried out using a PerkinElmer analyser model 240C (PerkinElmer, America).

A solution of 5-formyl-2-hydroxybenzoic acid (1.66 g, 10 mmol) and 2,3-bi (hydroxyl amino)-2,3-dimethylbutane (1.48 g, 10 mmol) in methanol (25 mL) was heated under reflux for 18 h. After the reaction, the methanol was removed and the residue was suspended in 100 mL CH_2Cl_2, aqueous $NaIO_4$ (2.14 g, 10 mmol in 50 mL) was added dropwise over a period of 10 min at 0°C, and the mixture was stirred for a further 20 min at 0°C. The organic phase was separated, and the aqueous phase was extracted with CH_2Cl_2 (3 × 20 mL). The combined organic layers were dried over anhydrous Na_2SO_4. The deep blue solution was then evaporated. The crude product was purified by column chromatography on silica gel using absolute ether/ethyl acetate/(1 : 1) as eluent, giving a deep blue solid product 1. Yield 21.4%. MS (*m/z*): 294.10 $[M+H]^+$; Anal. Calcd for $C_{14}H_{17}N_2O_5$: C, 57.33; H, 5.84; N, 9.55%, Found: C, 57.35; H, 5.81; N, 9.67%.

2.2. Animals and CCD Models. Adult Sprague-Dawley rats weighing 200–250 g were subjected to CCD surgery. All experimental protocols were approved by the Institutional Animal Use and Protection Committee, Fourth Military Medical University. All the testing was carried out in accordance with the approved guidelines. The CCD model was prepared as described previously [3]. Briefly, under anesthesia (sodium pentobarbital, 40 mg/kg, i.p.), the transverse process and intervertebral foramen at L5 on left side were exposed. A L-shaped stainless steel rod was inserted into foramen to produce a steady compression on the ganglia. After the rods were in place, the muscle and skin layers were sutured with administration of about 200 mg antibiotics.

2.3. Behavioral Tests. Behavioral testing was carried out in habituated mice by an observer blinded to the identity of the groups. As previously described [27, 28], mechanical sensitivity was tested with manual application of von Frey hairs (North Coast) to the plantar surface of hindpaw. Each filament was applied 10 times and the paw withdrawal

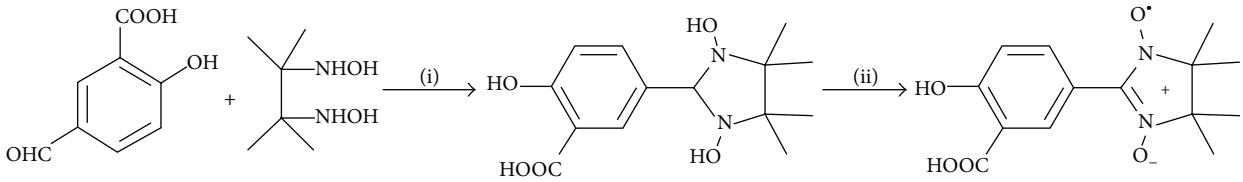

Figure 2: Synthesis of SANR. A scheme showing the synthetic route of SANR. Reagents and conditions: (i) MeOH, r.t.; (ii) $NaIO_4$, CH_2Cl_2, 0°C.

response frequency (the percentage of positive responses to the stimulus) was recorded. The force of a particular filament required to elicit 50% frequency of paw withdrawal was expressed as the mechanical threshold. Thermal sensitivity was tested by application of infrared heat to the plantar surface of hindpaw and the response latency was measured from an automated device readout (IITC Life Science).

Mice were evaluated for their motor coordination using the rotarod test. After training sessions, mice were placed on an accelerating rod. The latency for the rat to fall off the rod and the speed of rod at this time were recorded and a mean latency and speed for the 4 trials were calculated. The acceleration was from 2 to 60 r.p.m. over a 180 s period.

2.4. Extracellular Recording of DRG Single Unit Fiber Activities. Activities of single unit DRG A-fibers were recorded 3–8 days after the CCD surgery. Under sodium pentobarbital anesthesia (40 mg/kg, i.p.), laminectomy was performed at the L1-L2 and L4-L5 levels, and two small pools were formed at the exposure regions, separately. In the L4-L5 pool the stainless steel rod was removed. The spinal nerve was transected 7–10 mm distal to the DRG so that the discharge activities of the dorsal root fibers would originate primarily from the DRG region and not from peripheral sensory terminals. During recording, L4-L5 pool (drug pool) was filled with warm ACSF (35–37°C) containing (in mM): NaCl 150, KCl 5, $CaCl_2$ 2, $MgCl_2$ 1, D-glucose 10, and HEPES 10, with the pH adjusted to 7.4, and L1-L2 pool (recording pool) was filled with warm paraffin oil (35–37°C). Under a microscope, a microfilament (15–30 μm in diameter) presumably including up to a few nerve fibers was teased from the dorsal root. The proximal end was placed on a fine platinum electrode (29 μm in diameter) for electrophysiological recording of DRG single fiber activities. The firing patterns of a single fiber were displayed on a memory oscilloscope (VC-11, Japan) and recorded via an A/D board to a computer hard drive and stored for offline analysis. Unit activities with identical wave forms were selected as single fiber activities as previously described [3, 29].

Aspirin was dissolved in dimethyl sulfoxide (DMSO) as a stock solution and kept frozen; it was diluted in ACSF before the experiments. Tempol and SANR were dissolved in ACSF, respectively, before the experiments. Single unit discharges were recorded in the presence and absence of these three drugs or vehicle for at least another 5 min. Inhibition rate in discharge were calculated as (maximal discharge rate after drug using − baseline rate)/baseline rate × 100% [30].

2.5. Statistical Analysis. All data are expressed as mean ± S.E.M. Analysis of variance (ANOVA) for random measures was carried out, followed by either a post hoc Fisher's test or Dunnett's test. $P < 0.05$ was considered significant.

3. Results

3.1. Synthesis of SANR. The compound SANR was synthesized according to Ullman's procedure as shown in Figure 2. According to Ullman's pioneering work, any aldehydes may give rise to NIT nitroxides [31]. Followed by condensation of 5-formyl-2-hydroxybenzoic acid with 2,3-bis(hydroxyl amino)-2,3-dimethyl butane in methanol solution at room temperature, stable white solids 1,3-dihydroxyimidazolidine were rapidly obtained [32]. One of the key steps in the synthesis of NIT nitroxide radicals is the oxidation of 1,3-dihydroxyimidazolidines. We chose the aqueous of $NaIO_4$ as oxidant to oxidize the 1,3-dihydroxyimidazolidine to obtain the final target compound SANR in yield of 21%.

3.2. Development of Mechanical Hypersensitivity and Thermal Hyperalgesia in Rats Subjected to Chronic Compression of DRG (CCD). Following chronic compression of L5 DRG (CCD), the rats appeared in good health and did not show any signs of autotomy throughout the study. Sensitivity of CCD rats to mechanical and thermal stimuli was tested at different time points after operation. Compared to sham controls, CCD rats developed bilateral mechanical hypersensitivity (allodynia and hyperalgesia), which was manifested as a significant decrease in response threshold to von Frey hairs application to the bilateral hindpaws (Figures 3(a) and 3(b), $n = 10$, $P < 0.05$ at all time points). This mechanical hypersensitivity appeared on the 1st day after compression, persisting over the entire experimental period. In parallel, a dramatic drop in response latency to noxious plantar heat stimuli, reflecting thermal hyperalgesia, was found in bilateral hindpaws of CCD rats (Figures 3(c) and 3(d), $n = 10$, $P < 0.05$ at all time points). Therefore, it can be inferred that rats with chronic compression of L5 DRGs develop strong mechanical hypersensitivity and thermal hyperalgesia, which is consistent with previous reports in rodents [3–5].

3.3. Acute Administration of SANR Attenuates Mechanical Hypersensitivity and Thermal Hyperalgesia in CCD Rats. To investigate the acute effect of SANR on the pain hypersensitivity observed in CCD rats, we administered SANR via intraperitoneal (i.p.) injection once at 3 d after operation when mechanical and thermal hyperalgesia was completely

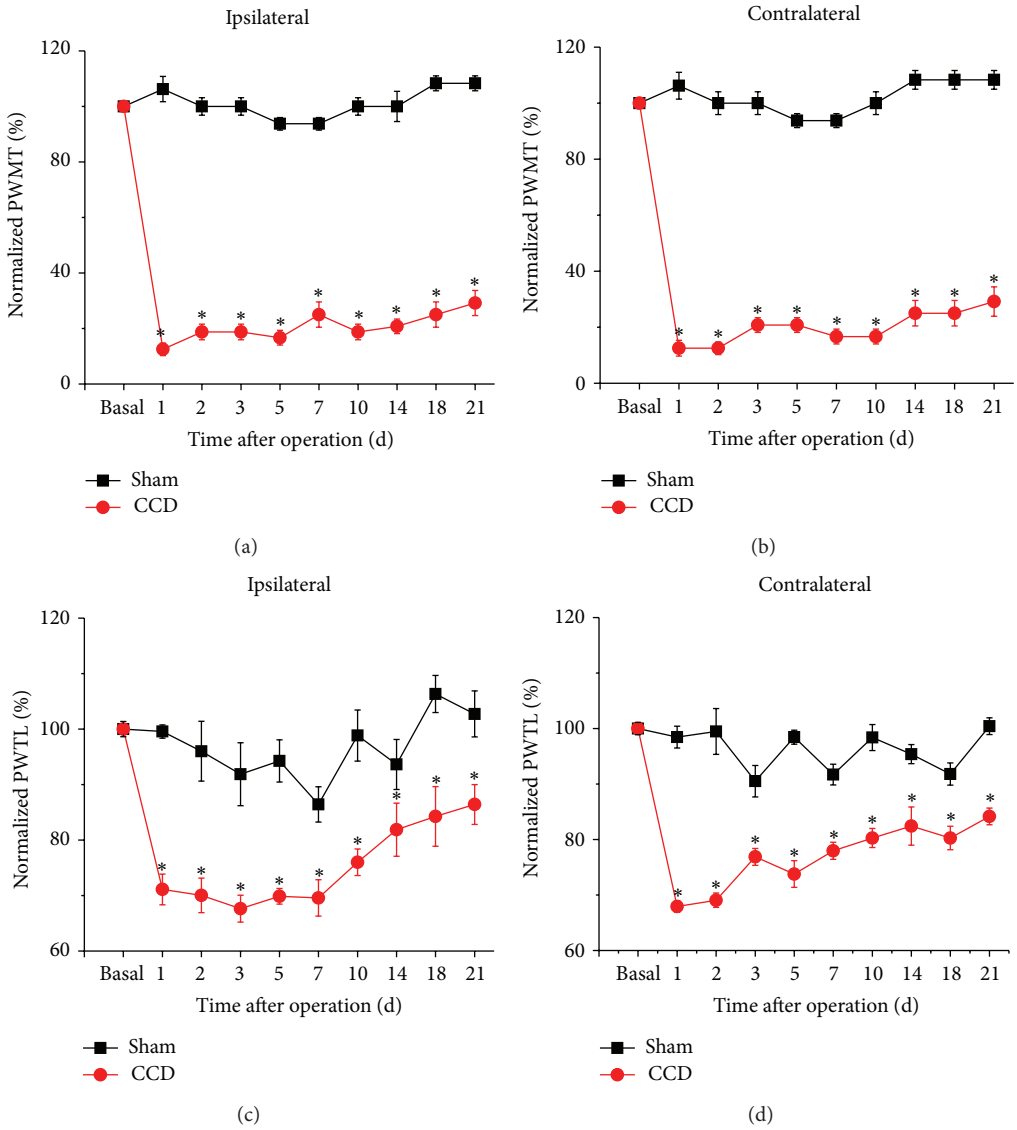

Figure 3: Development of mechanical hypersensitivity and thermal hyperalgesia following chronic compression of DRG (CCD) in rats. (a-b) Mechanical hypersensitivity developed in CCD rats but not in sham controls for both ipsilateral (a) and contralateral hindpaws (b). Note that paw withdrawal mechanical threshold (PWMT) to von Frey hairs decreased dramatically from the 1st day following chronic compression of L5 DRG ($n = 10$; $P < 0.05$). (c-d) Thermal hyperalgesia was observed by measuring paw withdrawal thermal latency (PWTL) to radiant heat in CCD rats and sham controls for both ipsilateral (c) and contralateral hindpaws (d). Note that PWTL significantly decreased in CCD rats ($n = 10$; $P < 0.05$) but not in sham group ($n = 10$; $P > 0.05$) with a similar time course with mechanical hypersensitivity. All data are expressed as mean ± S.E.M.

developed. As shown in Figure 4(a), acute administration of SANR (54, 180, 540 μmol/kg body weight) dose-dependently elevated the mechanical threshold to von Frey hairs in ipsilateral paw as compared to predrug level, reflecting as attenuation of mechanical hypersensitivity (Figure 4(a), $n = 10$). This antinociceptive effect started from 1 h after drug administration, persisting over the test period, namely, 24 h after SANR delivery. Dose-response curve at 7 h after drug was fitted to a Hill equation, which yielded an IC50 of 506.5 ± 14.6 μmol/kg for SANR in attenuation of mechanical hypersensitivity (Figure 4(b)). Similarly, CCD-induced ipsilateral thermal hyperalgesia was dramatically reduced by acute SANR in a dose-dependent manner with a similar time course, as measured by a prolongation of response latency to radiant heat stimuli compared to predrug level (Figure 4(c), $n = 10$). The dose-response curve revealed an IC50 of 119.9 ± 4.1 μmol/kg for SANR in inhibition of thermal hyperalgesia (Figure 4(d)). In contrast, i.p. vehicle did not alter the magnitude of CCD-induced mechanical hypersensitivity and thermal hyperalgesia (Figures 4(a) and 4(c), $n = 10$, $P > 0.05$). In addition, motor coordination was not altered by systemic SANR administration (180 μmol/kg, i.p.), as compared to vehicle group (Figures 4(e) and 4(f), $P > 0.05$, $n = 6$).

We then further compared the analgesic potency of SANR with the same dosing regimen of traditional nitroxide

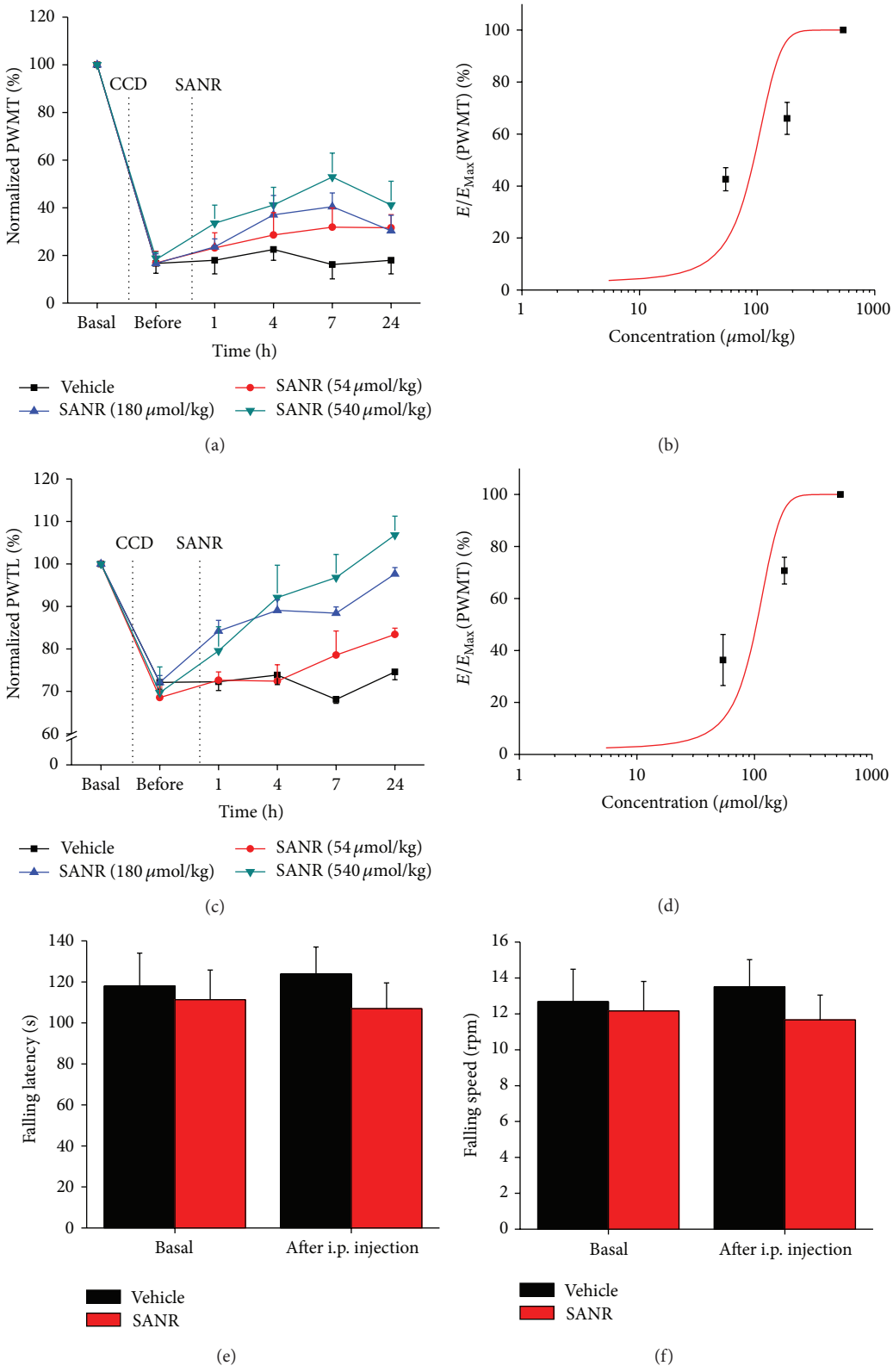

Figure 4: (a, b) Intraperitoneal (i.p.) administration of SANR (54, 180, and 540 μmol/kg body weight) attenuated mechanical hypersensitivity (a) and thermal hyperalgesia (c) induced by chronic compression of lumbar DRG in a dose-dependent manner ($n = 10$). Concentration-response curves of SANR at 7 h after drug delivery on mechanical hypersensitivity (b) and thermal hyperalgesia (d) are shown, respectively. (e, f) Motor coordination was not altered by systemic SANR (180 μmol/kg, i.p.). Quantitative analysis showing that i.p. SANR did not affect the latency (e) and speed (f) for rats falling from the accelerating rod, as compared to vehicle group ($n = 6$ for each group, $P > 0.05$). All data are expressed as mean ± S.E.M.

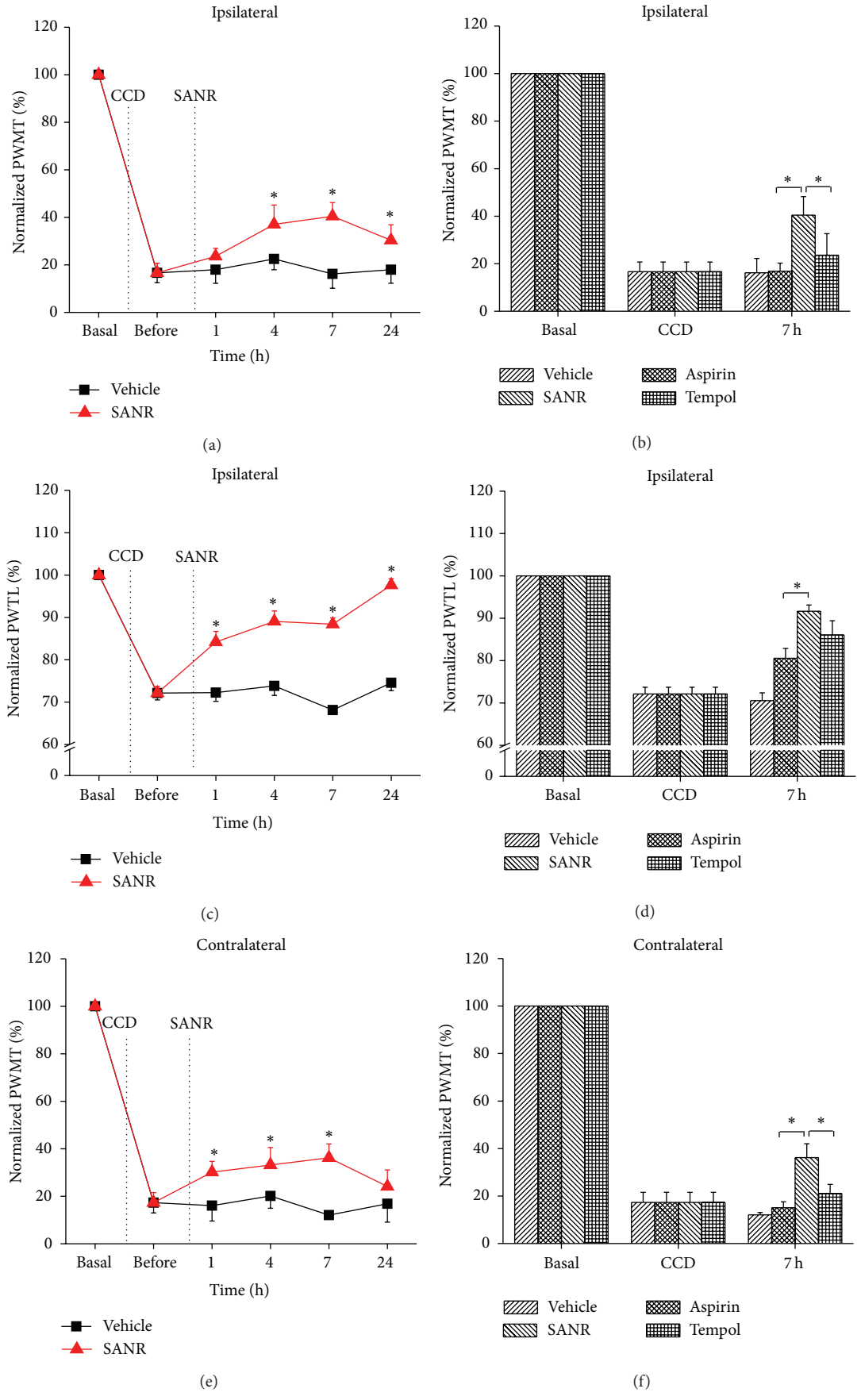

Figure 5: Continued.

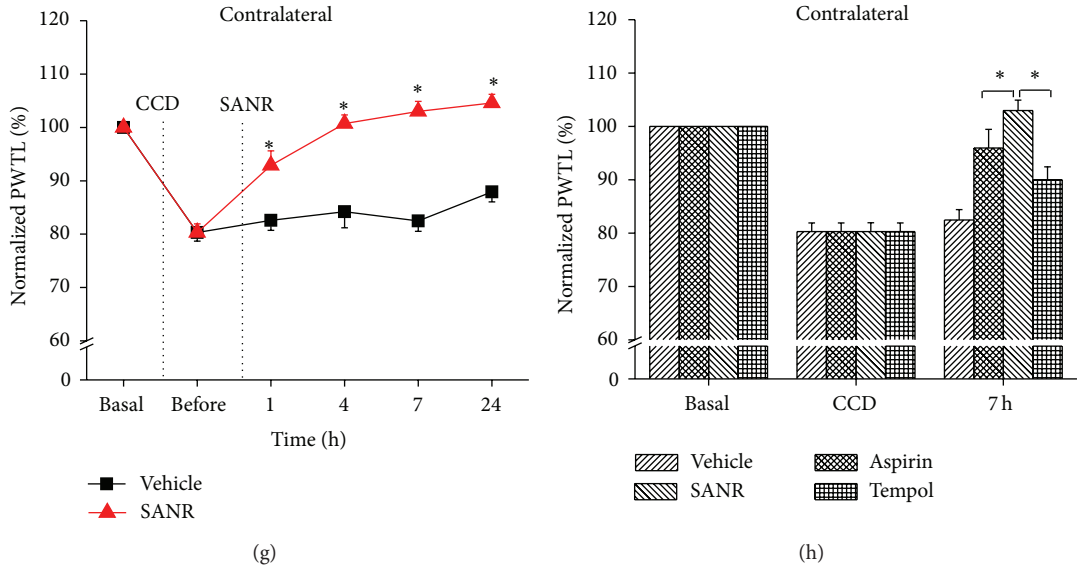

Figure 5: Acute treatment of SANR produces antinociceptive effect on CCD-induced mechanical hypersensitivity and thermal hyperalgesia in bilateral hindpaws, which is more potent than parent nitroxide moiety Tempol and parent NSAIDs moiety aspirin. (a, c) Time course of mechanical hypersensitivity (a) and thermal hyperalgesia (c) in ipsilateral hindpaw of CCD rats before and after i.p. SANR (180 μmol/kg) (red) and vehicle treatment (black). Note that ipsilateral mechanical and thermal hyperalgesia was attenuated significantly by SANR. (b, d) Comparison of analgesic potency in ipsilateral mechanical (b) and thermal hyperalgesia (d) produced by the same concentration of SANR, Tempol, and aspirin. Note that SANR showed significantly stronger effect than Tempol and aspirin. (e, g) Contralateral mechanical hypersensitivity (e) and thermal hyperalgesia (g) was reduced by acute SANR as well. (f, h) Comparison of the efficacy by SANR with Tempol and aspirin in inhibiting mechanical (f) and thermal hyperalgesia (h). All data are expressed as mean ± S.E.M. $^*P < 0.05$.

compound Tempol and classical NSAIDs aspirin alone. As shown in Figure 5(a), SANR at dose of 180 μmol/kg significantly inhibited ipsilateral mechanical hypersensitivity. In contrast, i.p. Tempol and aspirin alone at this low concentration produced little effect on the mechanical hypersensitivity. Quantitative analysis at 7 h after drug delivery revealed that the analgesic potency by SANR was significantly higher than Tempol and aspirin alone (Figure 5(b), $P = 0.045$ versus Tempol, $P = 0.006$ versus aspirin). In parallel, SANR exerted stronger inhibition on ipsilateral thermal hyperalgesia when compared to Tempol and aspirin alone (Figures 5(c) and 5(d), $n = 10$, $P = 0.047$ versus Tempol, $P = 0.025$ versus aspirin).

In addition to prominent inhibition on ipsilateral pain hypersensitivity, acute SANR produced marked reduction of contralateral spread of mechanical hypersensitivity and thermal hyperalgesia as well (Figures 5(e) and 5(g), $n = 10$, $P < 0.05$). Similarly, SANR was found to be more efficacious on depression of both contralateral mechanical (Figure 5(f), $P = 0.044$ versus Tempol, $P = 0.032$ versus aspirin) and thermal hyperalgesia than Tempol and aspirin alone (Figure 5(h), $P = 0.018$ versus Tempol, $P = 0.046$ versus aspirin).

3.4. Repeated SANR Treatment Progressively Reverses the Development of CCD-Induced Mechanical Hypersensitivity and Thermal Hyperalgesia. We further addressed whether repeated treatment of SANR could reverse the development of CCD-induced pain hypersensitivity. To do this, we administered SANR for 21 d once daily beginning at 3 d after DRG compression. As compared to vehicle group, repeated administration of SANR progressively reversed the development of ipsilateral mechanical hypersensitivity in CCD rats (Figure 6(a), $n = 10$, $P < 0.05$ at all time points tested). In comparison with Tempol and aspirin, SANR produced more pain relief on mechanical hyperalgesia (Figure 6(b), $n = 10$ for each drug). Quantitative analysis at 18 d after drug treatment showed that the extent of reversal of mechanical hyperalgesia by SANR was significantly stronger than that of Tempol and aspirin (Figure 6(b), $P = 0.043$ versus Tempol, $P = 0.039$ versus aspirin). Similarly, progressive and complete reversal of ipsilateral thermal hyperalgesia was seen after treatment with repeated SANR (Figure 6(c), $n = 10$). Furthermore, SANR was much more efficacious than Tempol and aspirin alone (Figure 6(d), $P = 0.029$ versus Tempol, $P = 0.018$ versus aspirin).

Figures 6(e) and 6(g) show a notable depression of contralateral mechanical hypersensitivity (Figure 6(e), $n = 10$) and thermal hyperalgesia by SANR (Figure 6(g), $n = 10$). Although Tempol displayed a comparable effect on contralateral mechanical hypersensitivity with SANR when examined at 18 d after drug application (Figure 6(f), $n = 10$, $P = 0.059$), its inhibition on thermal hyperalgesia was still weaker than SANR (Figure 6(h), $n = 10$, $P = 0.036$). Aspirin was consistently weaker than SANR on attenuation of both contralateral mechanical hypersensitivity (Figure 6(f), $n = 10$, $P = 0.047$) and thermal hyperalgesia (Figure 6(h), $n = 10$, $P = 0.049$). Collectively, these behavioral results uncovered a potential therapeutic value of this newly synthesized compound SANR on the development of hyperalgesia observed in radicular low back pain.

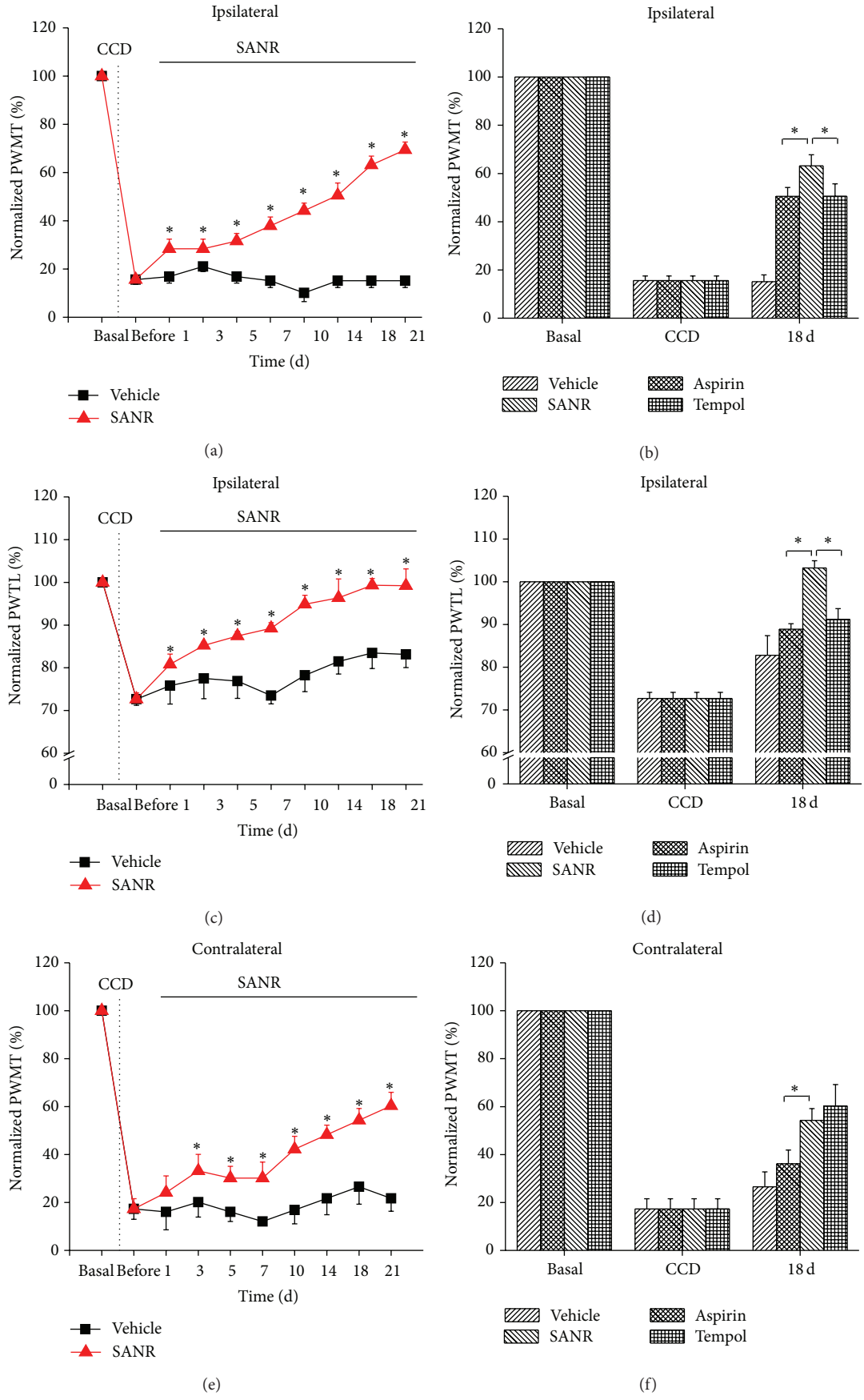

Figure 6: Continued.

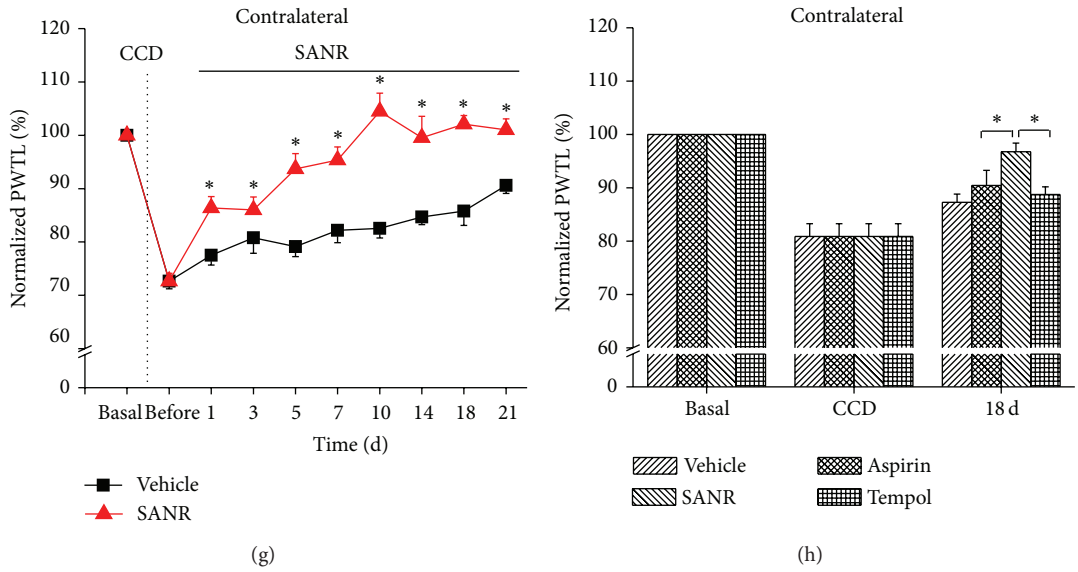

Figure 6: Repeated treatment of SANR produces antinociceptive effect on CCD-induced mechanical hypersensitivity and thermal hyperalgesia in bilateral hindpaws, which is more potent than parent nitroxide moiety Tempol and parent NSAIDs moiety aspirin. (a, c) Time course of mechanical hypersensitivity (a) and thermal hyperalgesia (c) in ipsilateral hindpaw of CCD rats before and after repeated i.p. SANR (180 μmol/kg) (red) and vehicle treatment (black). Note that ipsilateral mechanical and thermal hyperalgesia was progressively and completely reversed by SANR. (b, d) Comparison of analgesic potency in ipsilateral mechanical (b) and thermal hyperalgesia (d) produced by the same concentration of SANR, Tempol, and aspirin for 18 days. Note that SANR showed significantly stronger effect than Tempol and aspirin. (e, g) Contralateral mechanical hypersensitivity (e) and thermal hyperalgesia (g) were reduced by repeated SANR administration as well. (f, h) Comparison of the efficacy by SANR with Tempol and aspirin in inhibiting mechanical (f) and thermal hyperalgesia (h) at 18 d during continuous drug administration. All data are expressed as mean ± S.E.M. $^*P < 0.05$.

3.5. SANR Inhibits Ectopic Spontaneous Discharges in Compressed DRG Neurons. Previous studies have shown that abnormal spontaneous discharges of primary afferent sensory neurons may contribute to the development of radicular low back pain [3, 4]. We are therefore interested to know whether SANR-induced analgesia in low back pain was mediated by its suppression on ectopic spontaneous discharges in compressed DRG neurons. Single fiber recordings were employed in the dorsal roots of the injured L5 DRG derived from 27 CCD rats. Upon testing at 3–5 d after the onset of compression, we observed that primary afferent A fibers frequently exhibited ectopic spontaneous discharges (Figure 7(a), right panel). The conduction velocities were within the range of 2.5–26 m/s indicating that all the axons were myelinated. This ectopic spontaneous discharge rarely happens in control rats (Figure 7(a), left panel). Quantitative analysis showed that the mean frequency of spontaneous firing reached 16.78 ± 2.33 Hz (Figure 7(b), $n = 118$). This spontaneous activity of all the tested units can last for 2–6 h (2.28 ± 1.35 h). According to the dynamic features of interspike interval series, three different firing patterns have been previously reported in the injured lumbar A-fiber DRG neurons, which is periodic, nonperiodic (irregular), and bursting activity [3]. In our case, most patterns of spontaneous firing (59/118) observed fell into regular discharges (Figure 7(c), left panel). 37/118 were bursting activity (Figure 7(c), middle panel), and 22 out of 118 fibers displayed irregular firings (Figure 7(c), right panel).

As compared to control, superfusing SANR at a concentration of 10 mM reversibly inhibited the rate of spontaneous discharges of the primary afferent A fibers from CCD rats (see Figure 7(d) left and middle panels for original traces and Figure 7(d) right panel for frequency histogram of typical examples). When examined in a concentration range of 1–100 mM, the inhibitory rate of SANR was enhanced in magnitude with increasing concentrations, as seen in Figure 7(e). Figure 7(f) illustrates a dose-response curve for the suppressive effect of SANR on spontaneous activity (Figure 7(f), $n = 7$). The inhibitory rate averaged to be 19.4 ± 5.5%, 31.2 ± 11.6%, 43.7 ± 15.8%, 80.6 ± 5.4%, and 98.4 ± 1.5% for SANR at 1, 3, 10, 30, and 100 mM, respectively. Analysis of the curve based on the Hill plot yielded an IC_{50} of 18.8 mM for SANR (Figure 7(f)). These results indicate that SANR-induced analgesia may be at least, partially mediated by its inhibition of ectopic spontaneous activity of injured DRG neurons.

3.6. SANR Exerts Stronger Inhibition of Spontaneous Activity of Injured DRG Neurons Than Tempol and Aspirin. We further compared the efficacy of SANR with the same concentration of Tempol and aspirin alone on the ectopic spontaneous discharges in the injured DRG neurons. Three compounds were tested in the same cell. To exclude the possible influence between each other, the drug was applied in a mixed order. As shown in Figure 8(a), bath-applied aspirin at 10 mM significantly depressed the frequency of ectopic spontaneous discharges compared to control in a reversible manner (Figure 8(a), $n = 4$, $P = 0.014$). A similar effect was obtained upon Tempol (10 mM) treatment (Figure 8(a), $n = 4$, $P = 0.019$). In striking contrast,

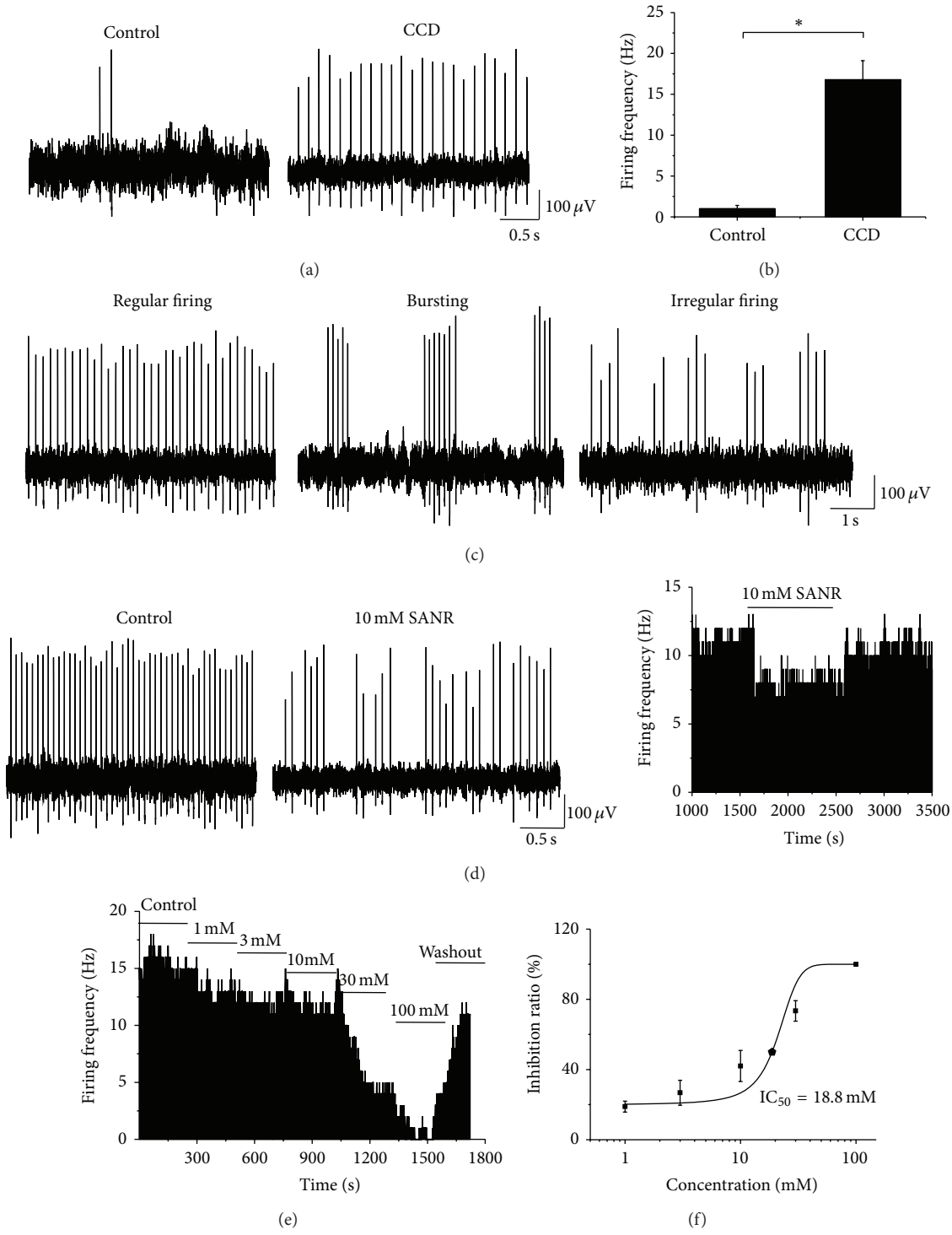

Figure 7: SANR produces dramatic inhibition on ectopic spontaneous discharges of the injured DRG neurons in CCD rats. (a) Following chronic compression of DRG, primary afferent A fibers of DRG neurons frequently exhibited ectopic spontaneous discharges (right panel); this rarely happens in sham control rats (left panel). (b) Quantitative analysis of the rate of spontaneous discharges in A-type DRG neurons derived from CCD and control rats. (c) According to the dynamic features of interspike interval series, three different firing patterns were observed, which are regular (left panel), bursting (middle panel), and irregular patterns (right panel). (d) Representative traces showing that bath application of SANR (10 mM) (middle panel) produces marked depression of spontaneous discharge rate compared to vehicle in the same cell (left panel). Frequency histogram on the same cell was shown in the right panel. (e) Frequency histogram showing a dose-dependent inhibition of ectopic spontaneous discharges by SANR in a reversible manner. (f) Analysis of the curve based on the Hill plot yielded an IC_{50} of 18.8 mM for SANR.

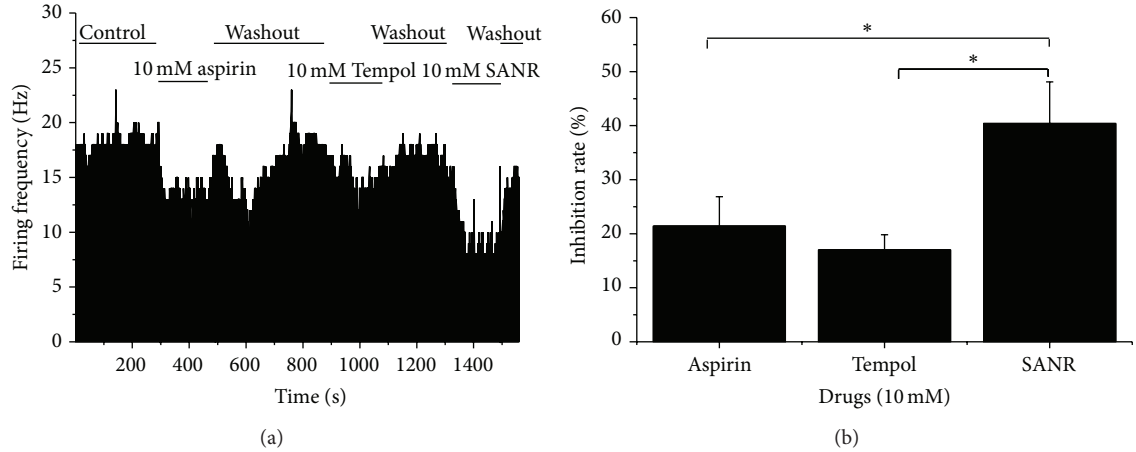

(a) (b)

Figure 8: Comparison of the inhibitory potency of SANR (10 mM) on ectopic spontaneous discharge with the same concentration of Tempol and aspirin. (a) Frequency histogram showing the inhibition of ectopic spontaneous discharge of the injured DRG neurons by SANR, Tempol, and aspirin on the same cell. (b) Quantitative analysis showing that the inhibition rate by SANR ($n = 4$) on spontaneous activity was much stronger than that by Tempol ($n = 4$, $P < 0.05$) and aspirin ($n = 4$, $P < 0.05$) alone. All data are expressed as mean ± S.E.M.

administration of SANR (10 mM) produced most potent inhibition of spontaneous activity (Figure 8(a), $n = 4$, $P = 0.013$). Quantitative analysis revealed that the averaged inhibition rate by SANR was significantly different from that by Tempol and aspirin alone (Figure 8(b), $n = 4$, $P = 0.049$ versus Tempol, $P = 0.047$ versus aspirin).

4. Discussion

Oxidative stress and inflammation have long been assumed to be involved in the development and maintenance of chronic pain [1, 9, 10]. Various antioxidants, for example, nitroxides and NSAIDs, for example, aspirin, have been shown to provide partial relief in some types of chronic pain [9, 11–15, 22–25]. However, chronic use of these drugs at high doses often causes severe unwanted side effects, which limits their broader implication. Utilizing chemical synthesis, the present study for the first time synthesized a new NIT nitroxide radical with salicylic acid framework (SANR). *In vivo* and *in vitro* results revealed that this new compound produced a remarkable antinociceptive effect in CCD-induced low back pain, which is much more potent than traditional nitroxide compound Tempol and classical NSAIDs aspirin. These results indicate that NIT nitroxide radical with salicylic acid framework might provide a new class of analgesic drug candidates.

A growing body of evidence has accumulated that stable nitroxide radicals have been studied as a unique and interesting class of antioxidants to protect again various oxidant stress including chronic pain [12–19, 21]. Stable nitroxides include two types: Tempol and NIT nitroxides. Although Tempol has been shown to exert antinociceptive effect in inflammatory and neuropathic pain [12–15, 21], whether NIT radicals protect against pain has not been fully understood. Compared with other antioxidants, NIT group nitroxides have incomparable advantages of scavenging radicals through a rapid catalytic manner. More importantly, electrochemical properties with more extensive distribution of the unpaired spin density make NIT group nitroxides more suitable for structure modification. For example, with the introduction of chirality into NIT nitroxides, a series of chiral NIT nitroxides were synthesized. These new compounds have been shown to be able to protect against radiation [33] and memory deficit [19]. These results inferred that modification of NIT nitroxides may represent a direction for the development of new therapeutic drugs against neurological disorders. However, whether NIT nitroxides and its derivatives possess analgesic effect has remained elusive. In this study, we successfully synthesized a new NIT nitroxide with salicylic acid framework with both antioxidative and anti-inflammatory action. In support of our assumption, Tempo-aspirin and Tempo-indomethacin have been recently synthesized and are found to exert anti-inflammatory and superoxide dismutase scavenging properties in A459 cells [34].

One of the most striking findings of this study is that SANR eliminated pain hypersensitivity in low back pain produced in an experimental of CCD model. Consistent with previous reports, CCD rats display not only ipsilateral but also contralateral mechanical and thermal hyperalgesia, indicating the involvement of peripheral and central sensitization [5, 35, 36]. Acute treatment with systemic SANR produced dramatic analgesic effect on bilateral mechanical hypersensitivity and thermal hyperalgesia lasting beyond 24 h. Following repeated administration of SANR, the development of bilateral pain hypersensitivity was progressively and completely reversed. This indicates that SANR may play a role in both peripheral and central sensitization induced by chronic compression. Furthermore, we compared the antihyperalgesic potency exerted by SANR with the same concentration of traditional nitroxides Tempol and classical NSAIDs aspirin alone. It was found that both acute and repeated treatment with SANR exhibited much stronger efficacy than Tempol and aspirin in expediting the recovery

of low back pain. This suggests that the addition of NIT nitroxides moiety into NSAIDs salicylic acid framework may provide the additive analgesia via synergistic anti-inflammatory and antioxidative action.

Ectopic spontaneous activity of injured DRG neurons has been implicated as a key driver of neuropathic pain including radicular low back pain [3, 4, 37]. Previous reports together with our unpublished data showed that chronic neuropathic pain is often associated with spontaneous activity in A-type DRG neurons, whereas chronic inflammatory pain mainly induces spontaneous discharges in C-type DRG neurons [3, 4, 37, 38]. Consistent with previous studies, we demonstrated that A-type DRG neurons displayed frequent spontaneous firing following chronic DRG compression [3, 4, 30]. Another striking finding of the present study is that bath applications of SANR remarkably depressed the spontaneous discharges of A-type DRG neurons caused by DRG compression in a dose-dependent manner. This inhibition can be reversed after washout of SANR. Although NSAIDs aspirin and nitroxides Tempol have been reported to exert analgesic effect in some types of neuropathic pain [9, 11, 12, 22–25], the cellular mechanisms underlying this analgesia in CCD-induced low back pain has not been studied in details. This study showed that Tempol and aspirin exhibited significant inhibition on the spontaneous firing in injured A-type DRG neurons from CCD rats as well. However, when evaluating the inhibitory rate of the same concentration of these three compounds, SANR provided the strongest analgesia, which is significant from Tempol and aspirin. It can be inferred from the above that SANR-induced analgesia in low back pain *in vivo* may be mediated, at least in partial by the depression of ectopic spontaneous activity of injured DRG neurons.

The primary mechanisms of SANR underlying the behavioral and neuronal antinociceptive actions *in vivo* and *in vitro* have remained unclear. Several mechanisms have been implicated in the antinociceptive actions of aspirin [26], including inhibition of cyclooxygenases [39, 40], NF-κB pathway [41], and acid-sensing ion channels [42] as well as activation of adenosine A2 receptors [43]. Under pathological pain states, ROS has been involved in the activation of TRP channels [44, 45], enhancement of NMDA receptor phosphorylation [46], induction of AMPA receptor trafficking to the membrane [47], and activation of MAP kinases [48]; delivery of antioxides could reverse the above changes. However, which downstream mechanisms could underlie the analgesic effect of SANR in low back pain needs to be further studied in the future.

In conclusion, the present study firstly synthesized a novel compound SANR by introducing functional moiety of NSAIDs salicylic acid into NIT nitroxides and demonstrated the dramatic analgesic effects of this newly synthesized compound in low back pain. It was further revealed that this analgesia is at least in partial mediated by a reduction of ectopic spontaneous discharges by SANR in injured DRG neurons. Therefore, synthesis of new NIT nitroxide with NSAIDs salicylic acid framework may represent a novel potential therapeutic candidate for the treatment of chronic pain, including radicular low back pain.

Conflict of Interests

The authors declare no competing financial interests.

Authors' Contribution

Wen-Juan Han, Lei Chen, and Hai-Bo Wang contributed equally to this study.

Acknowledgments

This work was supported by Natural Science Foundation of China (NSFC) grants (nos. 31171065 and 31471059), National Basic Research Program (973 Program, no. 2014CB543200), and Program for Shaanxi Province Key Research Team of Science and Technology Innovation (no. 2012 KCT-14) to Ceng Luo; National Science and Technology Support Program of China (no. 2012BAK25B00) to Hai-Bo Wang; and Natural Science Basic Research Program of Shaanxi Province (no. 2014JQ4127) to Wen-Juan Han.

References

[1] J. A. Strong, W. Xie, F. J. Bataille, and J.-M. Zhang, "Preclinical studies of low back pain," *Molecular Pain*, vol. 9, no. 1, pp. 9–17, 2013.

[2] X.-Y. Lin, J. Yang, H.-M. Li, S.-J. Hu, and J.-L. Xing, "Dorsal root ganglion compression as an animal model of sciatica and low back pain," *Neuroscience Bulletin*, vol. 28, no. 5, pp. 618–630, 2012.

[3] S.-J. Hu and J.-L. Xing, "An experimental model for chronic compression of dorsal root ganglion produced by intervertebral foramen stenosis in the rat," *Pain*, vol. 77, no. 1, pp. 15–23, 1998.

[4] X.-J. Song, S.-J. Hu, K. W. Greenquist, J.-M. Zhang, and R. H. Lamotte, "Mechanical and thermal hyperalgesia and ectopic neuronal discharge after chronic compression of dorsal root ganglia," *Journal of Neurophysiology*, vol. 82, no. 6, pp. 3347–3358, 1999.

[5] R.-G. Chen, W.-W. Kong, D.-L. Ge, C. Luo, and S.-J. Hu, "Bilateral mechanical and thermal hyperalgesia and tactile allodynia after chronic compression of dorsal root ganglion in mice," *Neuroscience Bulletin*, vol. 27, no. 4, pp. 233–240, 2011.

[6] R. Defrin, M. Devor, and S. Brill, "Tactile allodynia in patients with lumbar radicular pain (sciatica)," *Pain*, vol. 155, no. 12, pp. 2551–2559, 2014.

[7] X. Gu, S. X. Wang, L. L. Yang et al., "Time-dependent effect of epidural steroid on pain behavior induced by chronic compression of dorsal root ganglion in rats," *Brain Research*, vol. 1174, no. 1, pp. 39–46, 2007.

[8] X. P. Gu, L. Y. Peng, D. Yang et al., "The respective and interaction effects of spinal GRs and MRs on radicular pain induced by chronic compression of the dorsal root ganglion in the rat," *Brain Research*, vol. 1396, pp. 88–95, 2011.

[9] H. K. Kim, S. K. Park, J.-L. Zhou et al., "Reactive oxygen species (ROS) play an important role in a rat model of neuropathic pain," *Pain*, vol. 111, no. 1-2, pp. 116–124, 2004.

[10] W. Kallenborn-Gerhardt, K. Schröder, G. Geisslinger, and A. Schmidtko, "NOXious signaling in pain processing," *Pharmacology and Therapeutics*, vol. 137, no. 3, pp. 309–317, 2013.

[11] S. N. Hassler, K. M. Johnson, and C. E. Hulsebosch, "Reactive oxygen species and lipid peroxidation inhibitors reduce mechanical sensitivity in a chronic neuropathic pain model of spinal cord injury in rats," *Journal of Neurochemistry*, vol. 131, no. 4, pp. 413–417, 2014.

[12] M. Fidanboylu, L. A. Griffiths, and S. J. L. Flatters, "Global inhibition of reactive oxygen species (ROS) inhibits paclitaxel-induced painful peripheral neuropathy," *PLoS ONE*, vol. 6, no. 9, Article ID e25212, 2011.

[13] M. M. Khattab, "TEMPOL, a membrane-permeable radical scavenger, attenuates peroxynitrite- and superoxide anion-enhanced carrageenan-induced paw edema and hyperalgesia: a key role for superoxide anion," *European Journal of Pharmacology*, vol. 548, no. 1–3, pp. 167–173, 2006.

[14] I. Lee, H. K. Kim, J. H. Kim, K. Chung, and J. M. Chung, "The role of reactive oxygen species in capsaicin-induced mechanical hyperalgesia and in the activities of dorsal horn neurons," *Pain*, vol. 133, no. 1–3, pp. 9–17, 2007.

[15] M. Tal, "A novel antioxidant alleviates heat hyperalgesia in rats with an experimental painful peripheral neuropathy," *NeuroReport*, vol. 7, no. 8, pp. 1382–1384, 1996.

[16] S. M. Hahn, M. C. Krishna, A. M. Deluca, D. Coffin, and J. B. Mitchell, "Evaluation of the hydroxylamine tempol-H as an in vivo radioprotector," *Free Radical Biology and Medicine*, vol. 28, no. 6, pp. 953–958, 2000.

[17] D. Gelvan, P. Saltman, and S. R. Powell, "Cardiac reperfusion damage prevented by a nitroxide free radical," *Proceedings of the National Academy of Sciences of the United States of America*, vol. 88, no. 11, pp. 4680–4684, 1991.

[18] Q. Liang, A. D. Smith, S. Pan et al., "Neuroprotective effects of TEMPOL in central and peripheral nervous system models of Parkinson's disease," *Biochemical Pharmacology*, vol. 70, no. 9, pp. 1371–1381, 2005.

[19] T.-Y. Shi, D.-Q. Zhao, H.-B. Wang et al., "A new chiral pyrrolyl α-nitronyl nitroxide radical attenuates β-amyloid deposition and rescues memory deficits in a mouse model of Alzheimer disease," *Neurotherapeutics*, vol. 10, no. 2, pp. 340–353, 2013.

[20] J. R. Kouvaris, V. E. Kouloulias, and L. J. Vlahos, "Amifostine: the first selective-target and broad-spectrum radioprotector," *Oncologist*, vol. 12, no. 6, pp. 738–747, 2007.

[21] Z. Li, G. Ji, and V. Neugebauer, "Mitochondrial reactive oxygen species are activated by mGluR5 through IP3 and activate ERK and PKA to increase excitability of amygdala neurons and pain behavior," *Journal of Neuroscience*, vol. 31, no. 3, pp. 1114–1127, 2011.

[22] F. Amaya, T. A. Samad, L. Barrett, D. C. Broom, and C. J. Woolf, "Periganglionic inflammation elicits a distally radiating pain hypersensitivity by promoting COX-2 induction in the dorsal root ganglion," *Pain*, vol. 142, no. 1-2, pp. 59–67, 2009.

[23] W. Xie, J. A. Strong, D. Kim, S. Shahrestani, and J.-M. Zhang, "Bursting activity in myelinated sensory neurons plays a key role in pain behavior induced by localized inflammation of the rat sensory ganglion," *Neuroscience*, vol. 206, pp. 212–223, 2012.

[24] Z.-J. Huang, E. Hsu, H.-C. Li, A. L. Rosner, R. L. Rupert, and X.-J. Song, "Topical application of compound ibuprofen suppresses pain by inhibiting sensory neuron hyperexcitability and neuroinflammation in a rat model of intervertebral foramen inflammation," *The Journal of Pain*, vol. 12, no. 1, pp. 141–152, 2011.

[25] M. Kawakami, T. Matsumoto, H. Hashizume, K. Kuribayashi, and T. Tamaki, "Epidural injection of cyclooxygenase-2 inhibitor attenuates pain-related behavior following application of nucleus pulposus to the nerve root in the rat," *Journal of Orthopaedic Research*, vol. 20, no. 2, pp. 376–381, 2002.

[26] H. S. Smith, "Aspirin-inspired analgesia: old drug, new mechanism, sans Cox?" *Pain Physician*, vol. 15, no. 4, pp. E359–E361, 2012.

[27] C. Luo, V. Gangadharan, K. K. Bali et al., "Presynaptically localized cyclic GMP-dependent protein kinase 1 is a key determinant of spinal synaptic potentiation and pain hypersensitivity," *PLoS Biology*, vol. 10, no. 3, Article ID e1001283, 2012.

[28] W. Sun, B. Miao, X.-C. Wang et al., "Reduced conduction failure of the main axon of polymodal nociceptive C-fibres contributes to painful diabetic neuropathy in rats," *Brain*, vol. 135, part 2, pp. 359–375, 2012.

[29] S.-J. Hu, H.-J. Yang, Z. Jian et al., "Adrenergic sensitivity of neurons with non-periodic firing activity in rat injured dorsal root ganglion," *Neuroscience*, vol. 101, no. 3, pp. 689–698, 2000.

[30] S.-J. Hu, X.-J. Song, K. W. Greenquist, J.-M. Zhang, and R. H. LaMotte, "Protein kinase A modulates spontaneous activity in chronically compressed dorsal root ganglion neurons in the rat," *Pain*, vol. 94, no. 1, pp. 39–46, 2001.

[31] E. F. Ullman, J. H. Osiecki, D. G. B. Boocock, and R. Darcy, "Studies of stable free radicals. X. Nitronyl nitroxide monoradicals and biradicals as possible small molecule spin labels," *Journal of the American Chemical Society*, vol. 94, no. 20, pp. 7049–7059, 1972.

[32] X.-Y. Qin, G. Xiong, Y.-G. Sun et al., "Preparation and characterization of new chiral pyrrolyl α-nitronyl nitroxide radicals in which the imidazolyl framework was directly bound to chiral center," *Journal of Molecular Structure*, vol. 989, no. 1–3, pp. 10–19, 2011.

[33] H. Wang, Y. Jia, P. Gao et al., "Synthesis, radioprotective activity and pharmacokinetics characteristic of a new stable nitronyl nitroxyl radical-NIT2011," *Biochimie*, vol. 95, no. 8, pp. 1574–1581, 2013.

[34] W. Flores-Santana, T. Moody, W. Chen et al., "Nitroxide derivatives of non-steroidal anti-inflammatory drugs exert anti-inflammatory and superoxide dismutase scavenging properties in A459 cells," *British Journal of Pharmacology*, vol. 165, no. 4, pp. 1058–1067, 2012.

[35] N. Shenker, R. Haigh, E. Roberts, P. Mapp, N. Harris, and D. Blake, "A review of contralateral responses to a unilateral inflammatory lesion," *Rheumatology (Oxford)*, vol. 42, no. 11, pp. 1279–1286, 2003.

[36] K. A. Sluka, A. Kalra, and S. A. Moore, "Unilateral intramuscular injections of acidic saline produce a bilateral, long-lasting hyperalgesia," *Muscle & Nerve*, vol. 24, no. 1, pp. 37–46, 2001.

[37] M. Devor, "Ectopic discharge in Aβ afferents as a source of neuropathic pain," *Experimental Brain Research*, vol. 196, no. 1, pp. 115–128, 2009.

[38] X. Weng, T. Smith, J. Sathish, and L. Djouhri, "Chronic inflammatory pain is associated with increased excitability and hyperpolarization-activated current (Ih) in C- but not Aδ-nociceptors," *Pain*, vol. 153, no. 4, pp. 900–914, 2012.

[39] G. A. Higgs, S. Moncada, and J. R. Vane, "Eicosanoids in inflammation," *Annals of Clinical Research*, vol. 16, no. 5-6, pp. 178–199, 1984.

[40] J. Clària and C. N. Serhan, "Aspirin triggers previously undescribed bioactive eicosanoids by human endothelial cell-leukocyte interactions," *Proceedings of the National Academy of Sciences of the United States of America*, vol. 92, no. 21, pp. 9475–9479, 1995.

[41] M.-J. Yin, Y. Yamamoto, and R. B. Gaynor, "The anti-inflammatory agents aspirin and salicylate inhibit the activity of I(kappa)B kinase-beta," *Nature*, vol. 396, no. 6706, pp. 77–80, 1998.

[42] W. Wang, S.-D. Ye, K.-Q. Zhou, L.-M. Wu, and Y.-N. Huang, "High doses of salicylate and aspirin are inhibitory on acid-sensing ion channels and protective against acidosis-induced neuronal injury in the rat cortical neuron," *Journal of Neuroscience Research*, vol. 90, no. 1, pp. 267–277, 2012.

[43] B. N. Cronstein, M. C. Montesinos, and G. Weissmann, "Sites of action for future therapy: an adenosine-dependent mechanism by which aspirin retains its antiinflammatory activity in cyclooxygenase-2 and NFkappaB knockout mice," *Osteoarthritis and Cartilage*, vol. 7, no. 4, pp. 361–363, 1999.

[44] D. Kozai, N. Ogawa, and Y. Mori, "Redox regulation of transient receptor potential channels," *Antioxidants & Redox Signaling*, vol. 21, no. 6, pp. 971–986, 2014.

[45] N. Nishio, W. Taniguchi, Y. K. Sugimura et al., "Reactive oxygen species enhance excitatory synaptic transmission in rat spinal dorsal horn neurons by activating TRPA1 and TRPV1 channels," *Neuroscience*, vol. 247, pp. 201–212, 2013.

[46] X. Gao, H. K. Kim, J. M. Chung, and K. Chung, "Reactive oxygen species (ROS) are involved in enhancement of NMDA-receptor phosphorylation in animal models of pain," *Pain*, vol. 131, no. 3, pp. 262–271, 2007.

[47] D. Z. Lee, J. M. Chung, K. Chung, and M.-G. Kang, "Reactive oxygen species (ROS) modulate AMPA receptor phosphorylation and cell-surface localization in concert with pain-related behavior," *Pain*, vol. 153, no. 9, pp. 1905–1915, 2012.

[48] Y. Son, S. Kim, H.-T. Chung, and H.-O. Pae, "Reactive oxygen species in the activation of MAP kinases," *Methods in Enzymology*, vol. 528, pp. 27–48, 2013.